MAJOR AND TRACE ELEMENT CHEMICAL COMPOSITION OF GAHNITE FROM GRANITIC PEGMATITES AND A METAMORPHOSED MASSIVE SULFIDE DEPOSIT: SIGNIFICANCE FOR PEGMATITE FRACTIONATION AND DISCRIMINATION BETWEEN Li-RICH AND Li-POOR PEGMATITES

by

Jason Anthony Yonts

July, 2014

Director of Thesis: Dr. Adriana Heimann

Major Department: Geological Sciences

Rare-element granitic pegmatites are common hosts to economic deposits of rare metals, including Li, Ta, and rare-earth elements, which are increasing in economic importance due to advancing technology. Gahnite ($ZnAl_2O_4$) occurs as an accessory mineral in metamorphosed massive sulfide deposits (MMSDs) and some rare-element granitic pegmatites, including those with rare-metal mineralization, but detailed chemical studies of gahnite in these rocks are very scarce. In this study, gahnite from twenty-four granitic pegmatites and the Broken Hill-type Nine Mile MMSD, Australia, was analyzed for major and trace element chemical compositions to determine the relative degree of evolution of the pegmatites and identify chemical differences between Li-rich and Li-poor pegmatites and between these and MMSDs.

In the spinel ternary diagram in terms of mol % gahnite (Ghn), hercynite (Hc), and spinel (Spl) end-members, the compositions of gahnite from the pegmatites fall within the previously defined pegmatite field and are given by: $Ghn_{70.63\text{-}98.48}Hc_{0.95\text{-}28.61}Spl_{0.00\text{-}4.52}$. Gahnite from the Nine Mile deposit ($Ghn_{55.62\text{-}76.06}Hc_{17.47\text{-}37.34}Spl_{3.81\text{-}10.73}$) falls within the MMSD field characterized by compositions that reach higher Mg and lower Zn contents compared to gahnite from granitic pegmatites. Gahnite from the LCT (lithium, cesium, tantalum) family, rare-element class, beryl-columbite-phosphate subtype and LCT family, muscovite-rare element class, Li subclass granitic

pegmatites of the Comechingones (Blanca Dora, Juan Román, Magdalena, La Ona, and Sin Nombre pegmatites) and Conlara (Nancy pegmatite) pegmatite districts, Pampean Pegmatite Province, Argentina, was analyzed in detail. The chemical composition of gahnite from these pegmatites is defined by the ranges $Ghn_{78.49\text{-}90.35}Hc_{9.07\text{-}20.52}Spl_{0.25\text{-}3.37}$. Gahnite from the Nancy pegmatite has higher Mg and Mn contents than gahnite from the Comechingones pegmatites. Chemical zoning within gahnite crystals is characterized by an increase in Zn (~2.8 wt.% ZnO) and a decrease in Fe (~2.6 wt.% FeO) from core to rim, reflecting the evolution of the pegmatite melt via simple fractional crystallization. Plots of molecular Fe *vs.* Zn and Fe+Mg *vs.* Zn+Mn and Zn/Fe ratios in gahnite display the diadochy and the relative degree of fractionation of the pegmatites. The Zn/Fe ratios range from 3.82 to 9.96. Based on all these parameters, the relative degree of evolution of the pegmatites increases in the order: Sin Nombre → Magdalena → Juan Román → Blanca Dora → Nancy → La Ona. This order is consistent with mineralogical evidence and indicates that the composition of gahnite in granitic pegmatites can effectively be used to determine the relative degree of evolution of pegmatite melts.

The trace elements present in gahnite are first-series transition metals (Ti, V, Cr, Co, Ni, and Cu), as well as Mn, Li, Ga, Cd, Sn, and Pb. Gahnite in the Nine Mile deposit reaches higher Ti, V, Cr, Co, Ni, and Pb and lower Mn, Li, Ga, Sn, and Cu contents than gahnite from granitic pegmatites. Gahnite from highly evolved granitic pegmatites of the Borborema Pegmatite Province, Brazil, has the highest Cu (up to 68 ppm), Mn (up to 8,819 ppm), Li (up to 376 ppm) and Zn (up to 43 wt.% ZnO) contents and these compositions may be good indicators of Li-rich pegmatites. This study shows that the major and trace element chemistry of gahnite in granitic pegmatites may be used to understand relative pegmatite evolution and to distinguish pegmatites that contain Li-mineralization from barren pegmatites.

MAJOR AND TRACE ELEMENT CHEMICAL COMPOSITION OF GAHNITE FROM GRANITIC PEGMATITES AND A METAMORPHOSED MASSIVE SULFIDE DEPOSIT: SIGNIFICANCE FOR PEGMATITE FRACTIONATION AND DISCRIMINATION BETWEEN Li-RICH AND Li-POOR PEGMATITES

A Thesis

Presented To the Faculty of the Department of Geological Sciences

East Carolina University

In Partial Fulfillment of the Requirements for the Degree

Master of Science in Geology

by

Jason Anthony Yonts

July, 2014

MAJOR AND TRACE ELEMENT CHEMICAL COMPOSITION OF GAHNITE FROM GRANITIC PEGMATITES AND A METAMORPHOSED MASSIVE SULFIDE DEPOSIT: SIGNIFICANCE FOR PEGMATITE FRACTIONATION AND DISCRIMINATION BETWEEN Li-RICH AND Li-POOR PEGMATITES

by

Jason A. Yonts

APPROVED BY:

DIRECTOR OF THESIS: _____
(Dr. Adriana Heimann, PhD)

COMMITTEE MEMBER: _____
(Dr. Terri L. Woods, PhD)

COMMITTEE MEMBER: _____
(Dr. Eric M. Horsman, PhD)

COMMITTEE MEMBER: _____
(Dr. Michael A. Wise, PhD)

CHAIR OF THE DEPARTMENT OF GEOLOGICAL SCIENCES: _____
(Dr. Stephen J. Culver, PhD, DSc.)

DEAN OF THE GRADUATE SCHOOL: _____
(Dr. Paul J. Gemperline, PhD)

ACKNOWLEDGEMENTS

I would like to first thank my advisor, Dr. Adriana Heimann, for all of her help, support, and encouragement on this thesis project. I would also like to thank my other committee members, Drs. Eric Horsman, Terri Woods, and Michael Wise for all of their advice and knowledge on this project.

Thank you to Tom Fink at East Carolina University Biology Department for help with SEM-EDS analysis and Nick Foster at Fayetteville State University for help with the EMP analysis. Alan Koenig at the USGS Denver LA-ICP-MS laboratory is thanked for help overseeing LA-ICP-MS analysis and providing advice for data interpretations. Thank you also to Michael Wise for providing expertise and helping to answer question about pegmatites. Also thanks to David London of the University of Oklahoma for providing expertise about pegmatites and to Miguel Galliski for providing samples of gahnite and information and assistance about pegmatites from Argentina. Samples of gahnite were also graciously provided by Dwight Soares, Adam Szuszkiewicz, Mike Wise, Wolf Leyh, the Smithsonian Institution in Washington, D.C., and George Harlow and Jamie Newman from the American Museum of Natural History, N.Y.

Funding for this project was provided by the USGS Mineral Resources External Research Program (award G10AP00051) and the Thomas Harriot College of Arts and Sciences at East Carolina University and Research and Graduate Studies to Dr. Adriana Heimann. I thank the Society of Economic Geologists Hugh E. McKinstry Student Fund and Grant-in-Aid of Research from Sigma Xi, The Scientific Research Society, for providing funding for this project. I would also like to acknowledge funding from the East Carolina University Department of Geological

Sciences and the Geological Society of America (GSA) student travel grant to attend and present my thesis research at the southeastern GSA conference in Blacksburg, VA.

Finally, I would like to thank friends and family. Thank you to David Szynal, Erica Serna, Heather Lancaster, Leatha Moretz, and Katie Cummings for helping me in many ways during the last two years. I would have given up this endeavor if not for their moral support. Special thanks are due to my parents, Kay and James Yonts, and wife Megan Yonts for all of their love, support, and encouragement over the years making this chapter in my life possible.

TABLE OF CONTENTS

LIST OF TABLES

CHAPTER 1

CHAPTER 2

LIST OF FIGURES

CHAPTER 1

CHAPTER 2

CHAPTER 1

THE COMPOSITION OF GAHNITE FROM THE COMECHINGONES AND CONLARA PEGMATITE DISTRICTS, PAMPEAN PEGMATITE PROVINCE, ARGENTINA: IMPLICATIONS FOR PEGMATITE FRACTIONATION

Jason A. Yonts[1], Adriana Heimann[1*], and Miguel A. Galliski[2]

For Canadian Mineralogist

[1] Department of Geological Sciences, East Carolina University, 101 Graham Building, Greenville, NC 27858, USA

[2] IANIGLA, CCT MENDOZA-CONICET, Avda. Adrián Ruiz Leal s/n, Parque General San Martín, 5500, Mendoza, Argentina

* Corresponding author: A. Heimann, heimanna@ecu.edu.

ABSTRACT

Gahnite ($ZnAl_2O_4$) from the LCT family, rare-element class, beryl-columbite-phosphate subtype and LCT family, muscovite rare-element class, Li subclass granitic pegmatites of the Comechingones (Blanca Dora, Juan Román, Magdalena, La Ona, and Sin Nombre pegmatites) and Conlara (Nancy pegmatite) pegmatite districts was analyzed in detail. Based on the molecular proportions of end-member compositions (gahnite, hercynite, and spinel), gahnite from these pegmatite districts are defined by the ranges $Ghn_{78.49\text{-}90.35}Hc_{9.07\text{-}20.52}Spl_{0.25\text{-}3.37}$. The compositions define two clusters of data, both of which fall within the previously defined field for granitic pegmatites, with gahnite from the Nancy pegmatite having higher Mg and Mn contents than gahnite from the pegmatites of the Comechingones pegmatite district. Chemical zoning in gahnite crystals is characterized by an increase in Zn (~2.8 wt.% ZnO) and a decrease in Fe (~2.6 wt.% FeO) from core to rim, reflecting the evolution of the pegmatite melt via simple fractional crystallization. Other crystals show a complex zoning pattern with only a clear trend near the rim. A plot of molecular Fe *vs*. Zn was used to display the diadochy and evaluate the degree of evolution of gahnite because the degree of fractionation of a pegmatite can potentially be determined by the Zn/Fe ratio of gahnite. A plot of molecular Fe+Mg *vs.* Zn+Mn better displays the substitutions within the gahnite crystal structure showing that Zn and Mn are inversely correlated with Fe and Mg. Based on the Zn/Fe ratios and Fe+Mg and Zn+Mn of gahnite, the relative degree of evolution of the pegmatites increases in the approximate order: Sin Nombre → Magdalena → Juan Román → Blanca Dora → Nancy → La Ona. This is consistent with mineralogical evidence and indicates that the composition of gahnite in granitic pegmatites can effectively be used to determine the relative degree of evolution of pegmatite melts.

1.1 INTRODUCTION

Gahnite ($ZnAl_2O_4$), the zinc end-member of the spinel group of minerals, is found as an accessory mineral in aluminous metasedimentary rocks, metabauxites, skarns, marbles, metamorphosed massive sulfide deposits, quartz veins, granites, and granitic pegmatites (Spry and Scott, 1986a; Heimann et al., 2005). In granitic pegmatites it occurs most commonly in metasomatic replacement bodies, fracture fillings, and intermediate zones (e.g., Černý and Hawthorne, 1982; Soares et al., 2007). Gahnite in granitic pegmatites is known to occur with and contain inclusions of quartz, albite, muscovite, tourmaline, garnet, beryl, zircon, columbite, and nigerite, and occasionally sphalerite (e.g., Eskola, 1914; Černý and Hawthorne, 1982; Jackson, 1982; Neiva and Champness, 1997; Zhaolin et al., 1999a; Szuszkiewicz and Łobos, 2004; Soares et al., 2007).

Gahnite occurs as an accessory mineral in the lithium, cesium, tantalum (LCT) family, rare-element class, beryl-columbite-phosphate subtype and LCT family muscovite rare-element class, Li subclass granitic pegmatites (based on Černý and Ercit, 2005, and Černý et al., 2012 classification) of the Comechingones and Conlara pegmatite districts of the large Pampean Pegmatite Province (PPP), Argentina (e.g., Galliski, 1994). The Comechingones and Conlara pegmatite districts are economically important and have produced large amounts of beryl, mica, K-feldspar, quartz, Ta ore minerals, Li minerals, and Bi minerals since 1930 (Galliski and Černý, 2006; Galliski, 2009).

The chemical composition of gahnite in granitic pegmatites has been used in a few cases to determine the degree of evolution of the pegmatite melt (Batchelor and Kinnaird, 1984; Soares et al., 2007). Even though gahnite was reported in the Comechingones and Conlara pegmatite districts, chemical studies of the mineral have not been previously undertaken. With the

exception of two studies, one of columbite-tantalite from the Comechingones district and one on bobfergusonite from the Nancy pegmatite (Tait et al., 2004; Galliski and Černý, 2006) chemical analyses of other minerals are yet to be performed. In this study we present the major element composition of gahnite from granitic pegmatites from the Comechingones (Blanca Dora, Juan Román, Magdalena, La Ona, and Sin Nombre pegmatites) and Conlara (Nancy pegmatite) pegmatite districts of the PPP, Argentina. The aim of this study is to determine the compositional variations of gahnite from these pegmatites at the scale of pegmatite district, single pegmatite body, and single crystal in order to advance our understanding of the chemical characteristics and relative evolution of the magmatic-hydrothermal fluids that lead to the formation of the various pegmatites.

1.2 SAMPLING AND ANALYTICAL METHODS

Samples of gahnite were collected from granitic pegmatites from the Comechingones (Blanca Dora, Juan Román, Magdalena, La Ona, and Sin Nombre pegmatites) and Conlara (Nancy pegmatite) pegmatite districts in the Córdoba and San Luis Provinces of central and northwestern Argentina. Polished thick-sections (200 μm) were made from mineral separates and larger specimens of granitic pegmatite samples collected in the field and were used to conduct petrographic analysis, scanning electron microscope with energy-dispersive X-ray spectroscopy (SEM-EDS) analysis, and electron microprobe (EMP) analysis. Petrographic analysis was conducted using Olympus BX51 and BX41 dual reflected/transmitted light microscopes housed in the Department of Geological Sciences at East Carolina University (ECU) to determine the mineralogy and identify areas for SEM and EMP analysis based on the characteristics of each gahnite sample (e.g., crystal size, shape, and presence of inclusions). The

SEM-EDS analysis was performed using an FEI Quanta 200 Mark 1 SEM interfaced with an Oxford Inca X-act X-ray energy dispersive microanalysis elemental detector housed in the Department of Biology at ECU to obtain images and qualitative estimates of the composition of unknown minerals. Operating conditions were an accelerating voltage of 20 kV, a beam current of 20 nA, and a beam diameter of 5 – 6 micrometers. Electron microprobe analysis was conducted at Fayetteville State University using a JEOL JXA 8530F Hyperprobe electron microprobe. Operating conditions were an accelerating voltage of 20 kV, a beam current of 10 nA, and a beam diameter of 3 and 10 micrometers. Standards used for these analyses included Astimex almandine garnet (Si, Mg, Fe), bustamite (Ca, Mn), sanidine (K), synthetic chromium oxide (Cr), synthetic rutile (Ti), and Smithsonian gahnite (Al, Zn). Transects and individual spot analyses were conducted to check for core to rim variations. A total of 239 analyses were obtained from 10 crystals.

1.3 GEOLOGIC SETTING

The Pampean Pegmatite Province (PPP), Argentina, is one of the largest pegmatite provinces in South America with an approximate area of ~800 km by ~200 km (Galliski and Černý, 2006). The development of the PPP took place from the Neoproterozoic to the Paleozoic during two main orogenic cycles, the Pampean (~550 Ma - ~510 Ma) and Famatinian (~500 Ma - ~435 Ma) (Sims et al., 1998; Schwartz et al., 2008; Galliski, 2009; Drobe et al., 2011). The pegmatites of the PPP formed during three main times: during the Pampean orogeny, early in the Famatinian orogeny, and post-Famatinian orogeny (Otamendi et al., 2004; Galliski and Černý, 2006). The events resulted in pegmatites of the rare-element class of the LCT family, muscovite-rare-element class, and muscovite class (Galliski et al., 2011) (based on the

classification scheme of Černý and Ercit, 2005, and Černý et al., 2012). Several of these pegmatites are economically important and have produced 25,000 tonnes (t) of beryl, 45 t of Ta ore minerals, 1,000 t of Li-bearing minerals, 20 t of bismuth minerals, 40,000 t of mica, 500,000 t of K-feldspar, and 500,000 t of quartz since 1930 (Galliski and Černý, 2006; Galliski, 2009).

The Pampean- and Famatinian-age pegmatites have been divided into districts and include the Centenario, Ambato, Valle Fértil, Alta Gracia, Cerro Blanco, El Quemado, Quilmes, Calchaquí, Ancasti, Sierra Brava, Conlara, Totoral, La Estanzuela, Altautina, Comechingones, El Portezuelo, Velasco, Punilla, and Potrerillos districts (Galliski and Černý, 2006; Schwartz et al., 2008; Galliski, 2009; Galliski et al., 2011; Galliski and Sfragulla, 2014). The studied gahnite is derived from pegmatites that are part of the Conlara and Comechingones pegmatite districts, as defined and characterized by Galliski (1994, 1999a, b), in the Eastern Sierras Pampeanas located between the Archaean-Paleoproterozoic craton to the east and the Grenville Cuyania-Precordillera terrane to the west (Siegesmund et al., 2010). Below we describe the two pegmatite districts, including location, origin, and host rocks, as well as the individual pegmatites. A summary of the characteristics of the pegmatites is presented in Table 1.

1.3.1 Conlara Pegmatite District

The Conlara pegmatite district is located in the northern portion of the Sierra de San Luis (Fig. 1; Galliski, 1999b; Galliski et al., 2011). The pegmatites of this district possibly formed from partial melting of the Puncoviscana Formation during the Famatinian orogenic event (Galliski, 1999b, 2009, Galliski et al., 2011; Drobe et al., 2011). This formation grades from very-low grade to low-grade metasedimentary rocks in the northern region to medium-to-high metamorphic grade gneisses and migmatites towards the southern region (Zimmerman, 2005;

Galliski, 2009; Drobe et al., 2011; Adams et al., 2011). As a result, the original pegmatite melts were peraluminous low-Ca calcalkaline with high large-ion lithophile element (LILE) and volatile (especially B and P) contents (Galliski, 2009). These pegmatite melts intruded into crystalline basement rocks dominated by the complex Abukuma-type metamorphic belt of the Conlara Metamorphic Complex (Galliski, 1999b). This belt is composed of medium metamorphic grade quartz-mica schists (Martínez and Galliski, 2011), biotite tonalitic gneisses, and rare amphibolites (Galliski, 1999b).

Many pegmatites in the district have been classified into different groups based on geographic location (Galliski, 1999b). Pegmatites located at the southern end of the district are classified as beryl-rich granitic pegmatites and pegmatites of the north to northwest are lithium-rich pegmatites (Galliski, 1999b). Several pegmatites of the district have alteration zones (e.g., tourmalinization, muscovitization, and silicification) that generally reach several centimeters into the country rocks (Galliski, 1999b). The general mineralogy of the pegmatites in the province includes K-feldspar, albite, quartz, and muscovite, accessory spodumene, amblygonite ($(LiAl(PO_4)(F))$), beryl, columbite ($(Mn,Fe)(Nb,Ta)_2O_6$), and gahnite, and rare lithiophilite ($LiMnPO_4$) and bismuthinite (Bi_2S_3) (Galliski, 1999b).

1.3.1.1 Nancy Pegmatite

The Nancy pegmatite is a poorly evolved LCT family, rare-element class, beryl-columbite-phosphate subtype pegmatite that intruded into medium-grade gray gneisses of the Conlara Metamorphic Complex (448 - 420 Ma) (Tait et al., 2004; Steenken et al., 2004, 2006, 2008, 2010). It has a tabular shape, it is discordant, has an average width of 7 m but varies from 4 m in the south to 28 m in the north, and is exposed for 140 m (Tait et al., 2004). The pegmatite

has a well-defined internal zonation consisting of border, wall, and intermediate zones, and a quartz core (Tait et al., 2004). A 2-3 mm thick muscovite layer is present along the contact with the host rock and a similar layer divides the border and wall zones (Tait et al., 2004). The wall zone is generally 10-cm thick and contains K-feldspar, fine-grained quartz, and minor albite and muscovite (Tait et al., 2004). The intermediate zone is divided from the wall zone by a massive milky-quartz layer and consists of K-feldspar, albite, quartz, muscovite, gahnite, beryl, and columbite (Tait et al., 2004). Gahnite occurs as isolated crystals surrounded by fine-grained quartz, feldspar, and muscovite. The K-feldspar is partially albitized and intergrown with coarse-grained quartz and 10-cm wide muscovite books. Tait et al. (2004) also described garnet as a common accessory mineral residing as inclusions within K-feldspar and albite in the intermediate zone. The quartz core is not continuous throughout the pegmatite body and, where present, is composed of coarse-grained milky quartz. Phosphate nodules (up to 50 x 30 x 20 cm) can be found throughout the pegmatite consisting of very dark green to black bobfergusonite ($Na_2Mn_5FeAl(PO_4)_6$), Mn-rich apatite and Mn-rich wyllieite ($(Na,Ca,Mn)(Mn,Fe)(Fe,Mg)Al(PO_4)_3$), minor quartz, sphalerite, and pyrite, and secondary limonite and hematite (Tait et al., 2004).

1.3.2 Comechingones Pegmatite District

The Comechingones pegmatite district has an approximate area of 800 km^2 (Demartis et al., 2010) and is located in the northern end of the Sierra de los Comechingones of the Sierras de Córdoba, Argentina (Fig. 1; Galliski, 1999a; Drobe et al., 2010; Siegesmund et al., 2010; Morteani et al., 2012). Granitic pegmatites of the district were formed by extreme magmatic differentiation of S (+I)-type granitoids and emplaced in basement gneisses, amphibolites,

cordieritic migmatites, limestones, and scarce serpentinites during the Pampean orogeny (~580 Ma - ~510 Ma) (Sims et al., 1998; Galliski, 1999b, 2009; Galliski and Černý, 2006; Demartis et al., 2011; Drobe et al., 2011).

The studied pegmatites from the Comechingones district include the Sin Nombre, Juan Román, La Ona, Blanca Dora, and Magdalena pegmatites. These pegmatites belong to the LCT family, rare-element class, beryl-columbite-phosphate subtype and to the LCT family, muscovite-rare element class, Li subclass of granitic pegmatites (Hub, 1994, 1995; Galliski, 1999a, 2009; Demartis et al., 2012). Many of the pegmatites were exploited for beryl, muscovite, columbite, and uranium and have significant reserves of beryl, muscovite, feldspar, and quartz (Galliski, 1999a, 2009). The Magdalena pegmatite is one of the most exploited for the production of beryl in the Comechingones pegmatite district (Galliski, 1999a). Based on mineralogy, the geochemical evolution of the pegmatites ranges from the poorly evolved Magdalena pegmatite to the most evolved La Ona pegmatite (Galliski and Černý, 2006; Galliski and Sfragulla, 2014).

The Sin Nombre, Juan Román, La Ona, and Blanca Dora pegmatites intruded into augen-gneisses while the Magdalena pegmatite intruded into cordieritic migmatites (Galliski and Černý, 2006). The pegmatites are tabular in shape, range from 5 to 40 m in thickness, and are concordant to slightly discordant, except for the subhorizontal Magdalena pegmatite (Galliski and Sfragulla, 2014). They range from 200 m (Magdalena) to 1,000 m (La Ona) in length. The lengths of the remaining pegmatites of the Comechingones district are 209 m for Sin Nombre, 240 m for Juan Román, and 300 m for Blanca Dora. Commonly well-developed zonation includes a border, wall, intermediate, and quartz core zones, and minor replacement bodies (Galliski, 1999a; Galliski and Sfragulla, 2014). Albite, K-feldspar, quartz, and muscovite, with

accessory beryl, tourmaline, garnet, columbite, apatite, uraninite, triplite, gahnite, allanite, epidote, pyrite, and chalcopyrite comprise the general mineralogy of the Comechingones pegmatites (Galliski, 1999a; Galliski and Černý, 2006; Galliski and Sfragulla, 2014). Secondary uranium-lead minerals (masuyite ($Pb[(UO_2)_3O_3(OH)_2]\cdot 3(H_2O)$), fourmarierite ($Pb(UO_2)_4O_3(OH)_4\bullet 4(H_2O)$), and vandendriesscheite ($Pb(UO_2)_{10}O_6(OH)_{11}\bullet 11(H_2O)$)), uranium-phosphate minerals (autunite ($Ca(UO_2)_2(PO_4)_2\bullet 10\text{-}12(H_2O)$) and meta-autunite ($Ca(UO_2)_2(PO_4)_2\bullet 2\text{-}6(H_2O)$)), uranophane ($Ca(UO_2)_2SiO_3(OH)_2\bullet 5(H_2O)$), malachite, pyrolusite (MnO_2), and phosphosiderite ($FePO_4\bullet 2(H_2O)$) have been identified within granitic pegmatites of the district (Galliski, 1999a). The majority of the accessory minerals are concentrated in the core edges and intermediate zone of the pegmatites. Gahnite is located in the core edges partially replaced or covered with muscovite.

1.4 CHARACTERISTICS OF GAHNITE

Gahnite from the Conlara and Comechingones districts occurs as ‘emerald’ green to slightly bluish-green crystals commonly associated with muscovite and less commonly with quartz and microcline (Fig. 2). The gahnite crystals range in size from 0.2 mm to 20 mm. The contacts between gahnite, quartz, and feldspar are sharp and do not display alteration or reaction. However, the contact between gahnite and muscovite appears to be an alteration shown by an irregular and broken-up contact (Fig. 2D, E). The muscovite crystals are rich in inclusions consisting of gahnite, quartz, and opaque Fe oxides.

The studied gahnite crystals are crossed by numerous fractures, occasionally exhibiting minor weathering characterized by a yellow-brown staining within the fractures (Fig. 2A, D). Abundant inclusions are present along structurally controlled planes and concentrated in masses

(Fig. 2A, C, F). Gahnite from the Sin Nombre and La Ona pegmatites contains sparse inclusions consisting of quartz and two-phase fluid inclusions of liquid and gas (Fig. 2B, E). Gahnite from the Magdalena, Nancy, and Blanca Dora pegmatites has abundant tiny inclusions of quartz, muscovite, and two-phase fluid inclusions of liquid and gas scattered throughout the crystals (Fig. 2C, D, F). These inclusions appear to be dispersed randomly with areas of high concentration forming dark areas and anastomosing lines (Figs. 2, 3).

1.5 GAHNITE CHEMISTRY

Gahnite from all the pegmatites has the following chemical compositional ranges: 34.6 - 39.7 wt.% ZnO, 4.8 - 9.0 wt.% FeO, and 0.05 - 0.7 wt.% MgO. Gahnite compositions are expressed and plotted in terms of the corresponding spinel end members in mol % of gahnite (Ghn), hercynite (Hc), and spinel (Spl) and are defined by the ranges $Ghn_{78.49\text{-}90.35}Hc_{9.07\text{-}20.52}Spl_{0.25\text{-}3.37}$ (Fig. 4A; Table 2). Gahnite from the La Ona pegmatite has the highest Zn contents and a compositional range expressed by $Ghn_{82.59\text{-}90.35}Hc_{9.07\text{-}16.74}Spl_{0.26\text{-}0.83}$, while gahnite from the Magdalena pegmatite has the lowest Zn and highest Fe contents and its compositional variation is defined by $Ghn_{78.49\text{-}86.29}Hc_{13.15\text{-}20.52}Spl_{0.45\text{-}1.65}$. Gahnite compositions in the remaining pegmatites are defined by $Ghn_{79.55\text{-}84.84}Hc_{14.75\text{-}19.69}Spl_{0.33\text{-}1.10}$ for the Juan Román pegmatite, $Ghn_{80.90\text{-}88.26}Hc_{11.05\text{-}18.36}Spl_{0.67\text{-}1.34}$ for the Blanca Dora pegmatite, $Ghn_{79.80\text{-}82.58}Hc_{16.71\text{-}19.11}Spl_{0.25\text{-}1.35}$ for the Sin Nombre pegmatite, and $Ghn_{84.12\text{-}86.24}Hc_{10.96\text{-}13.68}Spl_{2.18\text{-}3.37}$ for the Nancy pegmatite.

Gahnite in the Nancy pegmatite, from the Conlara pegmatite district, has higher Mg contents than gahnite from the Comechingones pegmatite district, ranging from 2.18 to 3.37 mol % spinel end member, and this is reflected in the ternary diagram by the shift towards the spinel corner. Gahnite from the Comechingones district is characterized by low Mg contents, reaching values up to 1.65 mol % spinel in the La Ona pegmatite (Fig. 4A). Gahnite from the Nancy

pegmatite and the Comechingones pegmatites also contains small amounts of Mn (Fig. 4B; Table 2). Gahnite compositions in terms of mol % of the gahnite (Ghn), combined hercynite and spinel (Hc+Spl), and galaxite (Glx) end members are defined by the ranges $Ghn_{77.41-89.50}Hc+Spl_{9.56-21.21}Glx_{0.67-2.35}$ (Fig. 4B; Table 2). The compositions of gahnite from pegmatites of the Comechingones pegmatite district are defined by $Ghn_{77.41-89.50}Hc+Spl_{9.56-21.21}Glx_{0.67-1.89}$. The composition of gahnite from the Nancy pegmatite of the Conlara pegmatite district is expressed by $Ghn_{82.50-84.21}Hc+Spl_{13.44-15.58}Glx_{1.74-2.35}$. In terms of wt.%, the MnO contents range from 0.68 to 0.92 wt.% MnO in the Nancy pegmatite and from 0.26 to 0.74 wt.% MnO in the Comechingones pegmatites. In the ternary diagram, it can be seen that the Mn content of gahnite from the Comechingones district does not vary among the pegmatites and that it is higher in the Nancy pegmatite (Fig. 4B).

A plot of molecular (Fe+Mg)/Al *vs.* (Zn+Mn)/Al provides evidence for the diadochy within the gahnite crystal structure (Batchelor and Kinnaird, 1984; Fig. 5). The data are expected to plot in a linear trend having a slope of -1 if diadochy is fully complete between Zn and Mn with Fe and Mg. However, gahnite compositions from these pegmatites plot in small clusters. In this diagram, gahnite from the Nancy pegmatite plots with the gahnite from the Comechingones pegmatite district, overlapping gahnite compositions from the La Ona pegmatite. The composition of gahnite from the La Ona pegmatite is defined by (Zn+Mn)/Al ratios of 0.44±0.02 and (Fe+Mg)/Al of 0.09±0.02. Gahnite compositions from the Sin Nombre, Juan Román, and Magdalena pegmatites overlap and have lower average (Zn+Mn)/Al values (~0.41±0.02) than gahnite from the Nancy, La Ona, and Blanca Dora pegmatites and slightly higher average (Fe+Mg)/Al values (~0.10±0.01) than gahnite from the Nancy and La Ona pegmatites. Gahnite from the Blanca Dora pegmatite has intermediate (Zn+Mn)/Al values

(~0.42) and the highest (Fe+Mg)/Al values (up to 0.10) of all gahnite analyzed from these pegmatites (Fig. 5).

1.6 DISCUSSION

Gahnite has been known to occur in granitic pegmatites since the 1800s. One of the first published descriptions of gahnite from granitic pegmatites was from a pegmatite near Träskböle in Perniö, Finland (Eskola, 1914). A few studies of the occurrence of gahnite in granitic pegmatites began to appear in Europe and North America during the mid-1900s (e.g., Pehram, 1948; von Knorring and Dearnley, 1960). It was not until the 1980s and 90s that detailed chemical studies of gahnite in granitic pegmatites emerged (e.g., Jackson, 1982; Batchelor and Kinnaird, 1984; Spry and Scott, 1986b; Alfonso et al., 1995; Morris et al., 1997; Neiva and Champness, 1997; Zhaolin et al., 1999a). These studies improved our understanding of the conditions required for the formation of gahnite in granitic pegmatites. The information gained from these studies and others were used to aid in the understanding of the occurrence and compositions of gahnite from the granitic pegmatites of the Conlara and Comechingones pegmatite districts, Argentina, analyzed in this study, and this is discussed below. First, we discuss the formation of gahnite and its occurrence in granitic pegmatites in the context of a review of other worldwide occurrences. Then, we consider the composition of gahnite from the Argentina pegmatites and present the implications for relative pegmatite evolution. We also discuss the significance of the chemical zoning in gahnite crystals for melt evolution.

1.6.1 Gahnite formation and occurrence

In granitic pegmatites, gahnite and sphalerite are the main Zn-bearing minerals (Černý and Hawthorne, 1982). Their crystallization is controlled by the activity of the S in the melts and for gahnite, the availability of Zn and Al (Černý and Hawthorne, 1982). Sphalerite is likely to form in sulfide-rich pegmatite melts while gahnite forms in sulfide-poor pegmatite melts (Černý and Hawthorne, 1982). The pegmatites studied from the Comechingones pegmatite district do not contain sulfide minerals and the chemistry of the melts resulted in the crystallization of gahnite rather than sphalerite. The Nancy pegmatite from the Conlara pegmatite district hosts minor sulfide minerals in the form of sphalerite in phosphate nodules and may represent a melt of higher S content compared with the Comechingones pegmatite melts. This higher content of S could be explained by compositional differences between pegmatite melts as well as different host rocks than those for the pegmatites of the Comechingones pegmatite district. The pegmatites from the Comechingones pegmatite district are hosted in augen-gneisses and cordierite migmatites of the Guacha Corral Shear Zone while the Nancy pegmatite from the Conlara pegmatite district is hosted in medium-grade gneiss of the Conlara Metamorphic Complex. The presence of sulfides and the host rock difference are also reflected in the higher Mg and Mn content in gahnite from the Nancy pegmatite compared with gahnite from pegmatites of the Comechingones district (see Section 1.6.2 below for elaboration).

Gahnite is a peraluminous mineral and will form in granitic pegmatites when there is excess Al and available Zn (Clarke, 1981; Černý and Hawthorne, 1982; Morris et al., 1997). Feldspars are typically the first aluminosilicates to crystallize in granitic pegmatites. If excess Al_2O_3 is available following their crystallization, other aluminous minerals may form, such as garnet, muscovite, and gahnite (von Knorring and Dearnley, 1960; Clarke, 1981; Černý and

Hawthorne, 1982; Hess, 1989). Based on an extensive compilation done for this study, the occurrence of gahnite was reported in only one granitic pegmatite of the NYF (niobium, yttrium, fluorine) family that corresponds to a rare-element class, euxenite suptype pegmatite from the Topsham district, Maine (Yatsevitch, 1934; Spry and Scott, 1986b; Wise and Francis, 1992). Therefore, in contrast to LCT pegmatites, those of the NYF family tend to be metaluminous and do not commonly have available Al_2O_3 to form gahnite.

Gahnite from the Nancy pegmatite and the Comechingones district pegmatites is in contact with muscovite, quartz, and microcline. Quartz and microcline crystals do not contain inclusions of gahnite but a few inclusions of quartz were observed in gahnite. Muscovite has small inclusions of gahnite and gahnite has small inclusions of muscovite near the edges of the crystals. Based on the inclusion relationships, gahnite likely formed after microcline and simultaneously with muscovite. However, muscovite inclusions in gahnite and gahnite inclusions in muscovite may be the result of muscovitization of gahnite, in which case gahnite most likely formed prior to muscovite. Quartz is known to form throughout the entire crystallization of the pegmatite melt. The most likely order of mineral formation is: quartz – microcline – gahnite – muscovite.

1.6.2 The chemistry of gahnite and relative evolution of the Argentina pegmatites

In the ternary diagram in terms of gahnite-spinel-hercynite end-members, the composition of gahnite in granitic pegmatites from Argentina falls within the field for gahnite in granitic pegmatites defined by Spry and Scott (1986a) (Fig. 6). These chemical compositions yielded two distinct clusters of data, one for the Nancy pegmatite and another one for the pegmatites of the Comechingones district (Figs. 4A, 6). In most cases, the concentration of Mg

and Mn are typically low or absent in gahnite from granitic pegmatites, since other minerals (e.g., biotite, tourmaline, garnet) incorporate Mg and Mn before the crystallization of gahnite (e.g., Tulloch, 1981). It would be expected that the elevated contents of Mg and Mn in gahnite from the Nancy pegmatite would also be reflected in the accessory mineralogy of the host pegmatite. The presence of Mn-rich apatite, bobfergusonite ($Na_2Mn_5Fe^{3+}Al(PO_4)_6$), and Mn-rich wyllieite ($(Na,Ca,Mn)(Mn,Fe)(Fe,Mg)Al(PO_4)_3$) in the Nancy pegmatite (Tait et al., 2004) suggests that its pegmatite melt had elevated Mn contents during the formation of gahnite. These minerals are absent in the pegmatites of the Comechingones district, suggesting that the melts likely had lower Mn contents than that of the Nancy pegmatite, and this is also reflected in the composition of gahnite.

The elevated Mg content in gahnite from the Nancy pegmatite can be explained by several alternative or combined factors. First, the Nancy pegmatite and the Comechingones pegmatites are hosted by different rocks, and they could have provided additional Mg to the Nancy pegmatite melt via assimilation of Mg-bearing assemblages. However, the occurrence of Mg-bearing assemblages in the host rocks of the Nancy pegmatite is unknown. Alternatively, the melts were different and higher in Mg than those of the Comechingones pegmatites due to a different source, and this resulted in higher Mg contents in gahnite and other minerals. Another factor that could determine the high Mg content in gahnite is the lower abundance of other Mg-bearing minerals such as garnet and tourmaline and/or a lower Mg content in these minerals. In fact, the Nancy pegmatite lacks tourmaline (Tait et al., 2012), a mineral whose early crystallization commonly depletes the pegmatite melts in Mg, and this can explain the high Mg content in gahnite in this pegmatite. Finally, a likely explanation for the relatively high Mg content in gahnite from the Nancy pegmatite is the combination of the presence of sphalerite in

these rocks and its absence in the pegmatites from the Comechingones district and the lack of tourmaline in the Nancy pegmatite. If sphalerite crystallized early in the pegmatite, or at the same time as gahnite in a nearby location, it could have depleted the pegmatite melt in Zn, relatively, preventing gahnite from incorporating more Zn and allowing for more Mg into its structure due to the absence of other Mg-bearing phases. Whatever their origin, elevated Mg and Mn contents in the Nancy pegmatite melt allowed gahnite to incorporate relatively high amounts of these elements into its structure compared to the other pegmatites. However, due to the limited chemical information available for other minerals, the elevated Mg content in gahnite from the Nancy pegmatite cannot be explained satisfactorily until more mineral-chemical studies are conducted.

The variation of Zn/Fe ratios in gahnite can be used to infer the relative degree of evolution of the pegmatite, in which Zn increases with fractionation (Fig. 4A; Batchelor and Kinnaird, 1984; Soares et al., 2007). Gahnite compositions in pegmatites of the Comechingones pegmatite district do not differ in Mg or Mn contents but do so in the relative amount of Zn and Fe, so these elements are useful indicators of evolution. Gahnite from the La Ona pegmatite exhibits the highest Zn contents ($Ghn_{82.59-90.35}Hc_{9.07-16.74}Spl_{0.26-0.83}$; Fig. 4). Based on the mineralogy and mineral chemistry (i.e., feldspars), the degree of evolution of the pegmatites generally increases towards the south of the district (Demartis et al., 2012; Galliski and Sfragulla, 2014). The La Ona and Juan Román pegmatites are located in the southern portion of the district and are part of the same group (Co. Las Ovejas; Table 1) but their gahnite does not reflect the same degree of evolution. The La Ona pegmatite is considered the most evolved pegmatite of the district and contains Be (beryl), Nb (columbite), phosphates, and uranium minerals, the last one not found in the Juan Román pegmatite (Hub, 1994; Galliski, 1999a;

Galliski and Sfragulla, 2014; Table 1). The fact that gahnite from the La Ona pegmatite displays the highest Zn content is consistent with it being the most evolved pegmatite based on mineralogy. Similarly high Zn contents would be expected in gahnite from the Juan Román pegmatite based on geographic location. However, gahnite from this pegmatite has slightly lower Zn contents than that from the La Ona pegmatite. This is likely due to subtle chemical differences in the original pegmatite melt, and this prevented gahnite from incorporating high amounts of Zn in gahnite from the Juan Román pegmatite.

The Magdalena, Sin Nombre, and Blanca Dora pegmatites are located further to the north than the La Ona and Juan Román pegmatites in the Comechingones pegmatite district and based on their mineralogy they are generally considered less evolved than the pegmatites to the south (Hub, 1994; Galliski, 1999a; Demartis et al., 2012; Galliski and Sfragulla, 2014), which is reflected in the composition of gahnite. The Sin Nombre pegmatite contains garnet, beryl, tourmaline (schorl), apatite, and autunite as accessory minerals and is considered the least evolved pegmatite. The Magdalena and Blanca Dora pegmatites, as well as the Juan Román pegmatite, have fluorapatite and columbite, and the latter mineral is absent in the Sin Nombre pegmatite. Because the Magdalena and Juan Román pegmatites have similar mineralogy, they are expected to have similar gahnite compositions, and their compositions in fact overlap (Figs. 4, 5). Gahnite from the Magdalena pegmatite has the lowest Zn contents (34.64 wt.% ZnO; 78.49 mol % gahnite end-member), but overall they are similar as those in gahnite from the Juan Román and Sin Nombre pegmatites. However, gahnite from the Juan Román and Magdalena pegmatites reaches higher Zn contents than that from the Sin Nombre pegmatite, which indicates a higher degree of evolution for the former pegmatites compared with the latter, and this is consistent with the mineralogical evidence presented above. The lowest Zn contents in gahnite

from the Blanca Dora pegmatite are higher than those in gahnite from the Juan Román, Magdalena, and Sin Nombre pegmatites and reach the middle of the compositional field of gahnite from Argentina reflecting an intermediate degree of evolution. Therefore, based on the Zn content of gahnite and mineralogy, the order of increasing melt evolution for the Comechingones pegmatites is: Sin Nombre → Magdalena → Juan Román → Blanca Dora → La Ona. We note here that the pegmatites do not belong to the same group and not all are comagmatic. Therefore, the interpretation of the relative degree of evolution inferred from the composition of gahnite is not meant to speak of a single melt that evolved to form the various pegmatites.

The plot of molecular (Fe+Mg)/Al *vs.* (Zn+Mn)/Al in gahnite has been used to understand the substitution mechanism involving Zn, Fe^{2+}, Mn, and Mg, as well as the degree of evolution of the pegmatites (Figs. 5, 7; Batchelor and Kinnaird, 1984; Tindle and Breaks, 1998; Soares et al., 2007). In this plot, gahnite compositions also fall within the field defined by Batchelor and Kinnaird (1984) for igneous gahnite (Fig. 5). The data are expected to plot in a linear trend having a slope of -1 in perfect diadochy conditions (Batchelor and Kinnaird, 1984). However, this plot does not adequately display the diadochy of gahnite from the Argentina pegmatites (Fig. 7) and the best fit of a line through the data has an R^2 of 0.92 and a slope of -1.12. This behavior makes it hard to visualize the relative degree of evolution of the pegmatites. Therefore, the compositions and substitutions were further investigated. First, the compositions of gahnite from Argentina pegmatites studied here and previously published compositions of gahnite in granitic pegmatites worldwide were plotted together in this diagram to define the compositional field of gahnite in granitic pegmatites, which is shown in Figure 7, and to determine if gahnite from Argentina falls along the same linear trend (Fig. 7; Table 3). All

previously published compositions of gahnite in granitic pegmatites define an $R^2 = 0.86$ and a slope = -0.99. The compositions of gahnite from Argentina plot in the middle of the overall gahnite compositional field, with similarity to gahnite from the Separation Rapids, Canada (Tindle and Breaks, 1998), Lord Hill, Maine (Spry and Scott, 1986b), and Topsham, Maine (Spry and Scott, 1986b) pegmatites. This relatively low R^2 for the Argentina data, and the even lower value for all the gahnite data may be attributed to substitutions taking place in the gahnite structure other than the ones considered in this diagram, or the use of Al as a normalizing agent, and this is investigated below with alternative parameters for the Argentina gahnite.

Since Mn and Mg are low to absent in gahnite from the pegmatites of the Comechingones district and do not vary much among samples, a plot of molecular Fe^{2+} *vs.* Zn was used to better display the diadochy of gahnite and evaluate the relative degree of evolution of the pegmatite melts (Fig. 8). Gahnite from the Comechingones pegmatite district plots along a line with $R^2 = 0.97$ and slope = -1.04. Gahnite from the Nancy pegmatite does not follow the same linear trend and defines a different array that falls below (lower Fe for a given Zn content) the data of gahnite from the Comechingones pegmatites. The Nancy data define a line with $R^2 = 0.68$ and slope = -0.62, both much lower than that for the other data. This may be the result of gahnite from the Nancy pegmatite being the only analyzed pegmatite from the Conlara pegmatite district and that there are less data to define the correlation. What is more important is that this low correlation between Fe and Zn in gahnite from the Nancy pegmatite reflects the higher Mn and Mg contents in this gahnite compared with the other gahnite analyzed (Fig. 8).

The Zn/Fe^{2+} ratio of gahnite also provided information about the relative degree of evolution of the pegmatites investigated (Fig. 8; Table 2). The average Zn/Fe ratios in gahnite from the pegmatites of the Comechingones district decrease in the order La Ona (6.245) →

Blanca Dora (5.213) → Sin Nombre (4.609) → Magdalena (4.592) → Juan Román (4.584). Based on the highest Zn/Fe ratios among gahnite from the Comechingones pegmatites, which have very low to absent Mn and Mg contents, the La Ona pegmatite reflects the most evolved melts, which is consistent with the highest Zn contents and the mineralogical evidence mentioned above. Similarly, the Sin Nombre and Magdalena pegmatites are interpreted as the least evolved pegmatites of the district based on the location of gahnite in the Zn *vs.* Fe diagram, which is also consistent with Zn contents in gahnite and mineralogical evidence. However, gahnite from the Juan Román pegmatite has a compositional range from low to intermediate Zn contents and the lowest average Zn/Fe ratios, but based on the pegmatite mineralogy it is more evolved than the Magdalena and Sin Nombre pegmatites. Because the compositional variation in gahnite from the Juan Román pegmatite reaches higher Zn and lower Fe contents than gahnite in the Sin Nombre pegmatite, the former pegmatite is interpreted as more evolved, which points to the fact that Zn contents and in particular average Zn/Fe ratios in gahnite alone may not be the best indicators of pegmatite evolution in some cases. Furthermore, although gahnite from the Nancy pegmatite plots below the gahnite from the Comechingones pegmatites due to its relatively low Fe content (and higher Mg and Mn), it has the highest average Zn/Fe ratio (6.995). Even though Mg and Mn are low, the substitutions within gahnite are significant, and this gahnite probably reflects a lower degree of evolution compared with that from the La Ona pegmatite, which has lower Zn/Fe ratios but similar Zn contents as well as (Fe+Mg)/Al and (Zn+Mn)/Al ratios (Figs. 5, 7, 8). Therefore, the Zn/Fe ratio in gahnite alone may not be the best indication of pegmatite evolution if other elements are present in the gahnite structure, and in this case it needs to be put in the context of all other chemical information. Therefore, another variant of the plot presented by Batchelor and Kinnaird (1984) was investigated.

A plot of molecular (Fe+Mg) *vs.* (Zn+Mn) was constructed to further investigate the substitutions within gahnite using only the elements common in the A site (Zn, Fe, Mn, and Mg) (Fig. 9). By combining Fe with Mg and Zn with Mn, the composition of gahnite from the Nancy pegmatite shifts up and to the right to join the gahnite from the Comechingones pegmatite district. The data now have an $R^2 = 0.99$ and slope = -1.03. This plot seems to better display the substitutions within the gahnite crystal structure in these crystals. To check that this is not only true for gahnite from Argentina, data of gahnite from pegmatites published in the literature were added (not shown) and they all together yielded an $R^2 = 0.92$ and slope = -1.01. Therefore, for all the gahnite compositions from granitic pegmatites Zn and Mn are inversely correlated with Fe and Mg.

Regarding pegmatite melt evolution, this new diagram illustrates that gahnite in the Nancy pegmatite probably reflects a slightly lower degree of evolution than that from the La Ona pegmatite, which is consistent with the information presented before but difficult to visualize using the classic binary diagram of Batchelor and Kinnaird (1984) only (Fig. 7). This diagram also displays a wider range of compositions in gahnite from the Magdalena pegmatite that reach higher Zn+Mn values than gahnite from the Sin Nombre pegmatite. Therefore, the Magdalena pegmatite is interpreted as being slightly more fractionated than the Sin Nombre pegmatite. Again, it is important to note that the pegmatites belong to different groups within the district and we are not implying that they are comagmatic and formed by differentiation from the same magma. Finally, this diagram shows the following overall order of evolution among the studied pegmatites: Sin Nombre → Magdalena → Juan Román → Blanca Dora → Nancy → La Ona. This order differs somewhat from the order obtained using only Zn contents and Zn/Fe ratios in gahnite. We consider that the parameters of Figure 9 better reflect the degree of evolution of

gahnite and its host pegmatites because it incorporates the major elements that are known to increase or decrease with fractional crystallization and eliminates other variables such as Al content that are not related to evolution.

1.6.3 Compositional zoning of gahnite

In granitic pegmatites, gahnite is commonly compositionally homogenous with respect to major elements (Batchelor and Kinnaird, 1984; Szuskiewicz and Łobos, 2004; Soares et al., 2007). In rare cases, gahnite was found to display complex and irregular zoning (Gomes et al., 1995; Merino et al., 2013; Neiva, 2013). Zoning in gahnite is more likely to occur in small crystals, < 400 μm, than in larger crystals (Heimann et al., in prep.). When zoning is present in gahnite from granitic pegmatites, it exhibits an enrichment of Zn in the rims and depletion of Fe and Mg in the cores (Dunlop, 2000; Neiva, 2013; Heimann et al., in prep.). This zoning is consistent with the enrichment of Zn in residual melts during magmatic differentiation (e.g., Tulloch, 1981; Batchelor and Kinnaird, 1984; Spry, 1987; Soares et al., 2007; Merino et al., 2010, 2013). However, two studies of pegmatites from Spain and Portugal found a reversed zoning with an enrichment of Zn and Mn and depletion of Fe and Mg in the core compared to the rim of gahnite (Gomes et al., 1995; Merino et al., 2013). These authors attributed the reversed zoning to an unidentified process (Gomes et al., 1995; Merino et al., 2013), but it is consistent with the reversed chemical zoning seen at the pluton scale in the Spain locality.

Gahnite from the Comechingones and Conlara pegmatite districts reaches up to several centimeters in size. It is expected that these large gahnite crystals would not record compositional zoning, and indeed the majority of the samples investigated here do not display compositional zoning from core to rim. Most of the large crystals of gahnite that were analyzed

with transects exhibit random variations of Zn, Fe, Mn, and Mg from core to rim. As Zn increases, Fe decreases with no apparent relationship with the zone of the gahnite crystals. This could be the result of the orientation of the analyzed crystals or the measurements not covering the entire crystal due to some samples being mineral separates and perhaps incomplete crystals. However, clear compositional zoning was identified in gahnite from the Blanca Dora and Sin Nombre pegmatites (Figs. 10, 11). Gahnite from the Blanca Dora pegmatite shows the most marked compositional zoning of all of the studied samples and is characterized by an increase in Zn and decrease in Fe from core to edge (Fig. 10). The variation is characterized by a change from 35.90 wt.% ZnO near the core to 38.62 wt.% ZnO at the edge and a variation in FeO from 9.04 wt.% in the core to 6.49 wt.% in the edge. The Zn content increases towards the edge of the crystal with an abrupt increase at the edge. The opposite is seen for the Fe content, which is characterized by a decrease towards the rim of the crystal. Decreases in Fe within the crystals were identified at points near fractures which likely is the result of a late process (Fig. 10). The Mn content exhibits a similar pattern as that of Fe with a very small change (< 0.1wt.% MnO) while the Mg content does not vary systematically from core to rim. The overall pattern of zoning in gahnite is consistent with magma evolution by fractional crystallization.

Gahnite from the Sin Nombre pegmatite shows compositional zoning representative of the complex nature of the zoning in other crystals of gahnite (Fig. 11). Within the crystals, the Zn content is not homogeneous as in the previous case but instead fluctuates from the core to the edge. However, there is a small but visible change in Zn and Fe, mostly seen at the edge of the crystal, characterized by a slight increase in Zn and decrease in Fe towards the edge. The many up and down fluctuations in Zn, Fe, Mn, and Mg seen within the crystals may be due to the high concentration of fractures, and many of the points analyzed lie near fractures.

The clear zoning pattern present in gahnite from the Comechingones pegmatite district is consistent with that identified in gahnite from a granitic pegmatite of the Belvís de Monroy pluton, Spain (Merino et al., 2013). With the progression of pegmatite melt crystallization, the Fe content in the melt continually decreases while the Zn content increases resulting in gahnite with higher Fe contents in the core than in the edge. This is also consistent with the information gained from the study of gahnite in granitic rocks that indicates that Zn is incompatible and stays in the melt until the crystallization of gahnite or other Zn-bearing minerals (Tulloch, 1981). Therefore, compositional zoning in gahnite from the Comechingones pegmatite district reflects the evolution of the magmatic melt via fractional crystallization during pegmatite crystallization and gahnite growth.

1.6.4 Comparison with gahnite in granitic pegmatites worldwide and rocks associated with MMSDs

Data obtained in this study, along with all other published data of gahnite from granitic pegmatites, were used to redefine the compositional field of zincian spinel in granitic pegmatites originally presented by Spry and Scott (1986a) (Fig. 12). Previously studied gahnite from granitic pegmatites and gahnite studied here fall in the upper, Zn end-member portion of the spinel ternary diagram characterized by low Mg contents and a wide range of Zn and Fe values, as defined by the following compositional ranges: $Ghn_{50-100}Hc_{0-50}Spl_{0-9}$. It is worth noting that in a recent study, Merino et al. (2013) redefined the compositional field of gahnite in granitic pegmatites from Spry and Scott (1986a) but they referred to gahnite in igneous rocks, not only in granitic pegmatites. Therefore, we have redefined the field here to include only the composition of gahnite in granitic pegmatites.

This gahnite compositional field partially overlaps that of gahnite from MMSDs in Fe-Al-rich metasedimentary and metavolcanic rocks, metabauxites, and unaltered and hydrothermally altered Fe-Al-rich metasedimentary and metavolcanic rocks defined by Heimann et al. (2005). Some gahnite from MMSDs have considerably higher Mg contents than gahnite from granitic pegmatites but comparable percentages of Zn and Fe. Gahnite in unaltered and hydrothermally altered Fe-Al-rich metasedimentary and metavolcanic rocks has similar Mg ranges as gahnite from granitic pegmatites but contains a more diverse range of Fe and Zn contents from nearly pure hercynite to pure gahnite. Unlike in these rocks, gahnite from metabauxites is constrained to the nearly pure zinc end member, ranging from 85 to 100 mol % gahnite with up to 7 mol % spinel.

1.7 CONCLUSIONS

Gahnite and sphalerite are the main Zn-bearing minerals in granitic pegmatites, but in the pegmatites of the Comechingones district and the Nancy pegmatite of the Conlara district of the Pampean Pegmatite Province of Argentina gahnite is the only one present, except for the reported occurrence of minor sphalerite in phosphate nodules in the Nancy pegmatite. The conditions required to form gahnite in granitic pegmatites are most often met by granitic pegmatites of the rare-element classes and LCT pegmatite family. However, several granitic pegmatites of the muscovite classes also meet these requirements and gahnite was also reported in one rare-element class, euxenite suptype granitic pegmatite of the NYF family. Gahnite is found in LCT family, rare-element class, beryl-columbite-phosphate subtype and LCT family, muscovite-rare element class, Li subtype granitic pegmatites of the Comechingones (Blanca

Dora, Juan Román, Magdalena, La Ona, and Sin Nombre pegmatites) and Conlara (Nancy pegmatite) pegmatite districts, Argentina.

Chemical compositions of gahnite, based on the molecular proportions of major element end-members (gahnite, hercynite, and spinel), from the Comechingones pegmatite district and the Nancy pegmatite yielded two clusters of data. Gahnite from the Nancy pegmatite has higher Mg and Mn contents than gahnite from the pegmatites of the Comechingones pegmatite district. Gahnite from the La Ona pegmatite has the highest Zn contents ($Ghn_{82.59-90.35}Hc_{9.07-16.74}Spl_{0.26-0.83}$) while gahnite from the Magdalena pegmatite exhibits the lowest Zn contents ($Ghn_{78.49-86.29}Hc_{13.15-20.52}Spl_{0.45-1.65}$). On the ternary diagram of spinel end members, gahnite from the granitic pegmatites studied plots within the previously defined field of granitic pegmatites.

A plot of molecular (Fe+Mg)/Al *vs.* (Zn+Mn)/Al in gahnite was used to understand the substitution mechanism involving Zn, Fe, Mn, and Mg and the degree of evolution of the pegmatites, but it was found that it does not adequately display the diadochy of gahnite from the Argentina pegmatites because the data do not define a good linear correlation. In this diagram gahnite from the Argentina pegmatites studied here plots near those from the Separation Rapids pegmatites. Based on a plot of molecular Fe *vs.* Zn and Zn/Fe ratios, used to display the diadochy and evaluate the degree of evolution of gahnite, the Magdalena, Sin Nombre, and Juan Román pegmatites are interpreted as the least evolved pegmatites of the districts by the lowest Zn/Fe ratios (3.505) of gahnite, which is consistent with mineralogical evidence. Gahnite in the La Ona pegmatite has among the highest Zn/Fe ratios and reflects the most evolved melts, also consistent with the mineralogy of the pegmatite. Gahnite from the Nancy pegmatite also has among the highest Zn/Fe ratios (6.995) but higher Mg and Mn contents than gahnite from the Comechingones pegmatites. A new diagram of molecular (Fe+Mg) *vs.* (Zn+Mn) better displays

the substitutions within the gahnite crystal structure showing that Zn and Mn are inversely correlated with Fe and Mg and the composition of gahnite defines a good linear correlation. In this plot, as well as in the original plot, gahnite from the Nancy pegmatite has a composition similar to that of the La Ona pegmatite but the relatively high Mn and Mg is consistent with a high, but slightly lower, degree of evolution of the former pegmatite compared with the latter one. Without implying a comagmatic origin of the pegmatites, based on the composition of gahnite and mineralogy, the relative degree of evolution of the pegmatites thus increases in the approximate order: Sin Nombre → Magdalena → Juan Román → Blanca Dora → Nancy → La Ona.

Compositional zoning in gahnite from granitic pegmatites is rarely observed. Gahnite from the Blanca Dora and Sin Nombre pegmatites exhibits compositional zoning characterized by decreasing Fe and increasing Zn contents from core to edge, and this compositional zoning is a direct reflection of the evolution of the melt during fractional crystallization. Gahnite from the Blanca Dora pegmatite displays the most marked compositional zoning of all the studied samples. Gahnite from the Sin Nombre pegmatite exhibits more complex zoning by fluctuating Zn and Fe from core to edge with an abrupt increase in Zn and decrease in Fe at the edge.

Based on the review of previously published compositions of gahnite from granitic pegmatites and the new data from Argentina, the re-defined compositional field of gahnite in this type of rock in the spinel ternary diagram has the following ranges: $Ghn_{50-100}Hc_{0-50}Spl_{0-9}$. This compositional field overlaps that of gahnite from MMSDs in Fe-Al rich metasedimentary and metavolcanic rocks, metabauxites, and unaltered and hydrothermally altered Fe-Al-rich metasedimentary and metavolcanic rocks. However, gahnite from MMSDs tends to reach higher Mg contents than gahnite from granitic pegmatites and the highest Zn contents are observed in

gahnite from the latter. Gahnite from granitic pegmatites also overlaps the composition of metabauxites, but these are limited to almost pure zincian spinel only. This study shows that the major element composition of gahnite in granitic pegmatites, in conjunction with mineralogy, can be used to determine the relative degree of evolution of the pegmatite melts. Detailed chemical studies combining major and trace elements in gahnite from granitic pegmatites may aid in further our understanding of pegmatite melt evolution.

ACKNOWLEDGEMENTS

Funding for this project was provided by the USGS Mineral Resources External Research Program (# G10AP00051) and East Carolina University Thomas Harriot College of Arts and Sciences and Research and Graduate Studies to AH, and Society of Economic Geologists Hugh E. McKinstry Fund and Grant-in-Aid of Research from Sigma Xi, The Scientific Research Society, to JY. We thank Nick Foster for help with the EMP analyses and Ton Fink for help with SEM-EDS analyses. We are grateful to C. Hub, who provided the gahnite samples from the Comechingones district sampled by him in the early 1990s and authorized their use in this study. The authors are also thankful for critical comments by Mike Wise and Terri Woods that helped improve the manuscript.

REFERENCES

Adams, C. J., Miller, H., Aceñolaza, F. G., Toselli, A. J., and Griffin, W. L., 2011. The Pacific Gondwana margin in the late Neoproterozoic-early Paleozoic: Detrital zircon U-Pb ages from metasediments in northwest Argentina reveal their maximum age, provenance and tectonic setting: Gondwana Research, v. 19, p. 71-83.

Alfonso, P., Corbella, M., and Melgarejo, J. C., 1995. Nb-Ta-minerals from the Cap de Creus pegmatite field, eastern Pyrenees: distribution and geochemical trends: Mineralogy and Petrology, v. 55, p. 53-69.

Alfonso, P., Melgarejo, J. C., Yusta, I., and Velasco, F., 2003. Geochemistry of feldspars and muscovite in granitic pegmatite from the Cap de Creus Field, Catalonia, Spain: Canadian Mineralogist, v. 41, p. 103-116.

Alfonso, P., and Melgarejo, J. C., 2008. Fluid evolution in the zoned rare-element pegmatite field at Cap de Creus, Catalonia, Spain: Canadian Mineralogist, v. 46, p. 597-617.

Batchelor, R., and Kinnaird, J., 1984. Gahnite compositions compared: Mineralogical Magazine, v. 48, p. 425-429.

Černý, P., and Hawthorne, F. C., 1982. Selected peraluminous minerals: MAC Short course handbook, p. 163-186.

Černý, P., and Ercit, T. S., 2005. The classification of granitic pegmatites revisited: Canadian Mineralogist, v. 43, p. 2005-2026.

Černý, P., London, D., and Novák, M., 2012. Granitic pegmatites as reflections of their sources: Elements, v. 8, p. 289-294.

Clarke, D. B., 1981. The mineralogy of peraluminous granites: a review: Canadian Mineralogist, v. 19, p. 3-17.

Demartis, M., Pinotti, L. P., D'Eramo, F. J., Coniglio, J. E., and Agulleiro, L. A., 2010. Emplazamiento de pegmatitas graníticas del sector sur del distrito pegmatítico Comechingones, Córdoba: Revista de la Asociación Geológica Argentina, v. 67, p. 536-544.

Demartis, M., Pinotti, L. P., Coniglio, J. E., D'Eramo, F. J., Tubía, J. M., Aragón, E., and Agulleiro, L. A., 2011. Ascent and emplacement of pegmatite melts in a major reverse shear zone (Sierras de Córdoba, Argentina): Journal of Structural Geology, v. 33, p. 1334-1346.

Domańska-Siuda, J., 2007. The granitoid Variscan Strzegom-Sobótka massif: Granitoids in Poland, AM Monograph No. 1, p. 179-191.

Drobe, M., López de Luchi, M., Steenken, A., Wemmer, A., Naumann, R., Frei, R., and Siegesmund, S., 2011. Geodynamic evolution of the Eastern Sierras Pampeanas (Central Argentina) based on geochemical, Sm-Nd, Pb-Pb and SHRIMP data: International Journal of Earth Science, v. 100, p. 631-657.

Druguet, E., and Hutton, D. H. W., 1998. Syntectonic anatexis and magmatism in a mid-crustal transpressional shear zone: an example from the Hercynian rocks of the eastern Pyrenees: Journal of Structural Geology, v. 20, p. 905-916.

Dunlop, S. D., 2000. Gahnite from metamorphosed massive sulphide deposits and rare-element pegmatites: Development of discriminators based on bedrock and overburden samples. M.Sc. thesis: Laurentian University, 169 p.

Eskola, P., 1914. An occurrence of gahnite in pegmatite near Träskböle in Perniö, Finland: Geologiska Föreningen i Stockholm Förhandlingar, v. 36, p. 25-30.

Fettes, D. J., and Mendum, J. R., 1987. The evolution of the Lewisian complex in the Outer Hebrides: Geological Society of London Special Publications, v. 27, p. 27-44.

Galliski, M. A., 1994. La Provincia Pegmatítica Pampeana. I: Tipología y distribución de sus distritos económicos: Revista de la Asociación Geológica Argentina, v. 49, p. 99-112.

Galliski, M. A., 1999a. Distrito pegmatítico Comechingones, Córdoba: Recursos Minerales de la República Argentina (Ed. E.O. Zappettini), Instituto de Geología y Recursos Minerales SEGEMAR, v. 35, p. 361-364.

Galliski, M. A., 1999b. Distrito pegmatítico Conlara, San Luis: Recursos Minerales de la República Argentina (Ed. E.O. Zappettini), Instituto de Geología y Recursos Minerales SEGEMAR, v. 35, p. 365-368.

Galliski, M. A., 2009. The Pampean Pegmatite Province, Argentina: a review: Estudos Geológicos, v. 19, p. 30-34.

Galliski, M. A., and Černý, P., 2006. Geochemistry and structural state of columbite-group minerals in granitic pegmatites of the Pampean Ranges, Argentina: The Canadian Mineralogist, v. 44, p. 645-666.

Galliski, M. A., and Sfragulla, J., 2014. Las pegmatitas graníticas de las sierras de Córdoba. 19th Congreso Geológico Argentino, Relatorio. p. 365-388.

Galliski, M. A., Márquez-Zavalía, M. F., Martínez, V., and Roquet, M. B., 2011. Granitic pegmatites of the San Luis Ranges: 5th International Symposium on Granitic Pegmatites, PEG2011 Argentina, Field Trip Guidebook: Ianigla-Conicet, 44 p.

Gomes, C. L., Castro, P., and Alves, C., 1995. Caracterização de espinelas zincíferas e do par ganite-nigerite no campo aplito-pegmatítico da Serra de Arga-Minho N de Portugal: Memórias Nº4, Publ. Museu Lab. Min. Geol., Univ. Porto, p. 629-633.

Gosen, W., and Prozzi, C., 1998. Structural evolution of the Sierra de San Luis (Eastern Sierras Pampeanas, Argentina): implications for the Proto-Andean Margin of Gondwana. In Pankhurst, R. J. and Rapela, C. W. (eds.) The Proto-Andean Margin of Gondwana. Geological Society of London Special Publications, v. 142, p. 235-258.

Hanson, S., Simmons, W. B., and Falster, A. U., 1998. Nb-Ta-Ti oxides in granitic pegmatites from the Topsham Pegmatite District, southern Maine: Canadian Mineralogist, v. 36, p. 601-608.

Heimann, A., Spry, P., and Teale, G., 2005. Zincian spinel associated with metamorphosed Proterozoic base-metal sulfide occurrences, Colorado: A re-evaluation of gahnite composition as a guide in exploration: Canadian Mineralogist, v. 43, p. 601-622.

Heimann, A., Yonts, J., and London, D., in preparation. The composition of gahnite in felsic dikes as reflection of pegmatite melt evolution: evidence from two new occurrences, Pala Chief and Elizabeth R layered dikes, California.

Hess, P. C., 1989. Origins of Igneous Rocks: Cambridge, Harvard University Press, 336 p.

Hub, C. 1994. Estudio geológico económico de pegmatitas del Distrito Comechingones. Informe Beca CONICOR (inédito), 156 p. Córdoba.

Hub, C. 1995. Estudio geológico económico de pegmatitas del Distrito Comechingones. Informe Beca CONICOR (inédito), 172 p. Córdoba.

Huhma, H., 1986. Sm-Nd, U-Pb, and Pb-Pb isotopic evidence for the origin of the Early Proterozoic Sveckarelian crust in Finland: Geological Survey of Finland, Bulletin 337, 52 p.

Jackson, B., 1982. Gem quality gahnite from Nigeria: The journal of Gemmology and proceedings of the Gemmological Association of Great Britain, v. 18, p. 265-276.

Janeczek, J., 2007. Intragranitic pegmatites of the Strzegom-Sobótka massif - an overview: Granitoids in Poland, AM Monograph No. 1, p. 193-201.

Johnson, R., G., 1998. Mineralogy and Geochemistry of the Lord Hill Pegmatite. MSci. Thesis, University of New Orleans, New Orleans, Louisiana, 127 p.

Martínez, V. A., Galliski, M. A., 2011. Geología, mineralogía y geoquímica de la pegmatite Las Cuevas, San Luis: Revista de la Asociación Geológica Argentina, v. 68, p. 526-541.

Merino, E., Villaseca, C., Orejana, D., Jeffries, T., 2013. Gahnite, chrysoberyl and beryl co-occurrence as accessory minerals in a highly evolved peraluminous pluton: The Belvís de Monroy leucogranite (Cáceras, Spain): Lithos, v. 179, p. 137-156.

Merino, E., Villaseca, C., Pérez-Soba, C., and Orejana, D., 2010. First occurrence of gahnite and chrysoberyl in an Iberian Hercynian Pluton: the Belvís de Monroy Granite (NE Cáceres, Spain): La Sociedad Española de Mineralogía, p. 159-160.

Morris, T. F., Breaks, F. W., Averill, S. A., Crabtree, D. C., and McDonald, A., 1997. Gahnite composition: Implications for base metal and rare-element exploration: Exploration and Mining Geology, v. 6, p. 253-260.

Morteani, G., Eichinger, F., Götze, J., Tarantola, A., and Müller, A., 2012. Evaluation of the potential of the pegmatite quartz veins of the Sierra de Comechingones (Argentina) as a source of high purity quartz by a combination of LA-ICP-MS, ICP, cathodoluminescence, gas chromatography, fluid inclusion analysis, Raman and FTIR spectroscopy in *Quartz: Deposits, Mineralogy and Analytics*, Götze, J., and Möckel, R. (eds): Berlin, Springer, p. 119-137.

Neiva, A. M. R., 2013. Micas, feldspars and columbite–tantalite minerals from the zoned granitic lepidolite-subtype pegmatite at Namivo, Alto Ligonha, Mozambique: European Journal of Mineralogy, v. 25, p. 967-985.

Neiva, A. M. R., and Champness, P. E., 1997. Nigerite and gahnite from the granitic pegmatite veins of Cabanas, Ponte do Lima, northern Portugal: Neues Jahrbuch Für Mineralogie - Monatshefte, p. 384-409.

Neiva, A. M. R., and Neiva, J. M. C., 2005. Beryl from the granitic pegmatite at Namivo, Alto Ligonha, Mozambique: Neues Jahrbuch Für Mineralogie- Abhandlungen, v. 181, p. 173-182.

Neiva, J. M. O., Rimsky, A., Sandréa, A., 1955. Sur une variété de gahnite stannifère de Cabanas (Portugal): Bulletin de la Société Française de minéralogie et de cristallographie, v. 78, p. 97-105.

Otamendi, J. E., Castellarini, P. A., Fagiano, M. R., Demichelis, A. H., and Tibaldi, A. M., 2004. Cambrian to Devonian geologic evolution of the Sierra de Comechingones, Eastern Sierra Pampeanas, Argentina: Evidence for the development and exhumation of continental crust on the Proto-Pacific margin of Gondwana: Gondwana Research, v. 7, p. 1143-1155.

Pehram, G., 1948. Gahnit von Rosendal auf Kimito, SW-Finland: Bulletin of the Geological Istitution of the University of Uppsala, v. 32, p. 329-336.

Rinaldi, C.A., 1969. Estudio de las pegmatitas uraniferas de las Sierras de Comechingones, Provincia de Córdoba: Revista de la Asociación Geológica Argentina, v. 23, p. 161-195.

Schwartz, J. J., Gromet, L. P., and Miró, R., 2008. Timing and duration of the calc-alkaline arc of the Pampean Orogeny: Implications for the Neoproterozoic to Cambrian evolution of western Gondwana: The Journal of Geology, v. 116, p. 39-61.

Siegesmund, S., Steenken, A., Mertino, R., Wemmer, K., López de Luchi, M., Frei, R., Presnyakov, S., and Guereschi, A., 2010. Time constraints on the tectonic evolution of the Eastern Sierras Pampeanas (Central Argentina): International Journal of Earth Sciences, v. 99, p. 1199-1226.

Sims, J. P., Ireland, T. R., Camacho, A., Lyons, P., Pieters, P. E., Skirrow, R. G., Stuart-Smith, P. G., and Miró, R., 1998. U-Pb, Th-Pb, and Ar-Ar geochronology from the southern Sierras Pampeanas, Argentina: implications for the Palaeozoic tectonic evolution of the western Gondwana margin: The Proto-Andean Margin of Gondwana. Geological Society of London Special Publications, v. 142, p. 259-281.

Soares, D.R., Beurlen, H., Ferreira, A.C.M., and Da-Silva, M.R.R., 2007. Chemical composition of gahnite and degree of pegmatite fractionation in the Borborema Pegmatite Province, northeastern Brazil: Anais da Academia Brasileira de Ciências, v. 79, p. 395-404.

Soares, D. R., Beurlen, H., de Brito Barreto, S., Silva, M. R. R., and Ferreira, A.C.M., 2008. Compositional variation of tourmaline-group minerals in the Borborema Pegmatite Province, northeastern Brazil: Canadian Mineralogist, v. 46, p. 1097-1116.

Spry, P. G., and Scott, S. D., 1986a. The stability of zincian spinels in sulfide systems and their potential as exploration guides for metamorphosed massive sulfide deposits: Economic Geology, v. 81, p. 1446-1463.

Spry, P.G., and Scott, S.D., 1986b. Zincian spinel and staurolite as guides to ore in the Appalachians and Scandinavian Caledonides: Canadian Mineralogist, v. 24, p. 147-163.

Spry, P.G., 1987. Compositional zoning in zincian spinel: Canadian Mineralogist, v. 25, p. 97-104.

Steenken, A., Siegesmund, S., López de Luchi, M., Frei, R., and Wemmer, K., 2006. Neoproterozoic to Early Palaeozoic events in the Sierra de San Luis: implications for the Famatinian geodynamics in the Eastern Sierras Pampeanas (Argentina): Journal of the Geological Society of London, v. 163, p. 965-982.

Steenken, A., Siegesmund, S., Wemmer, K., and López de Luchi, M., 2008. Time constraints on the Famatinian and Achalian structural evolution of the basement of the Sierra de San Luis (Eastern Sierras Pampeanas, Argentina): Journal of South American Earth Sciences, v. 28, p. 336-358.

Steenken, A., Wemmer, K., López de Luchi, M., Siegesmund, S., and Pawlig, S., 2004. Crustal provenance and cooling of the basement complexes of the Sierra de San Luis: An insight

into the tectonic history of the Proto-Andean margin of Gondwana: Gondwana Research, v. 7, p. 1171-1195.

Steenken, A., Wemmer, K., Martino R. D., López de Luchi, M., Guereschi, A., and Siegesmund, S., 2010. Post-Pampean cooling and the uplift of the Sierras Pampeanas in the west of Córdoba (Central Argentina): Neues Jahrbuch für Geologie und Paläontologie-Abhandlungen, v. 256, no. 2, p. 235-255.

Szuskiewicz, A., and Łobos, K., 2004. Gahnite from Siedlimowice, Strzegom-Sobótka granitic massif, SW Poland: Mineralogia Polonica, v. 35, p. 15-21.

Swanson, S. E., and Veal, W. B., 2010. Mineralogy and petrogenesis of pegmatites in the Spruce Pine District, North Carolina, USA: Journal of Geosciences, v. 55, p. 27-42.

Tait, K. T., Hawthorne, F. C., Černý, P., and Galliski, M. A., 2004. Bobfergusonite from the Nancy Pegmatite, San Luis Range, Argentina: Crystal-structure refinement and chemical composition: Canadian Mineralogist, v. 42, p. 705-716.

Tindle, A. G., and Breaks, F. W., 1998. Oxide minerals of the Separation Rapids rare-element granitic pegmatite group, northwestern Ontario: Canadian Mineralogist, v. 36, p. 609-635.

Tulloch, A. J., 1981. Gahnite and columbite in an alkali-feldspar granite from New Zealand: Mineralogical Magazine, v. 44, p. 275-278.

Turniak, K., Halas, S., and Wójtowicz, A., 2007. New K-Ar cooling ages of granitoids from the Strzegom-Sobótka Massif, SW Poland: Geochronometria, v. 27, p. 5-9.

von Knorring, O., and Dearnley, R., 1960. The Lewisian pegmatites of South Harris, Outer Hebrides: Mineralogical Magazine, v. 32, p. 366-378.

Whitney, D. L., and Evans, B. W., 2010. Abbreviations for names of rock-forming minerals: American Mineralogist, v. 95, p. 185-187.

Windley, B. F., Kröner, A., Guo, J., Qu, G., Li, Y., and Zhang, C., 2002. Neoproterozoic to Paleozoic Geology of the Altai Orogen, NW China: New Zircon Age Data and Tectonic Evolution: Journal of Geology, v. 110, p. 719-737.

Wise, M., and Francis, C., 1992. Distribution, classification and geological setting of granitic pegmatites in Maine: Northeastern Geology, v. 14, p. 82-93.

Yatsevitch, G. M., 1934. The crystallography of herderite from Topsham, Maine: Journal Mineralogical Society of America, p. 426-437.

Zhaolin, L., Wenlan, Z., Rongyong, Y., Wen, L., and Wei, Z., 1999a. Analysis of chemical composition of melt inclusion of beryl in pegmatite and discovery of zinc-spinel by electronic probe: Chinese Science Bulletin, v. 44, p. 2004-2010.

Zhaolin, L., Rongyong, Y., and Wen, L., 1999b. Pegmatite fluids of different origins and their implications for mineralization: Chinese Journal of Geochemistry, v. 18, p. 9-17.

Zhu, Y., Zeng, Y., and Gu, Y., 2006. Geochemistry of the rare-metal-bearing pegmatite No. 3 vein and related granites in the Keketuohai region, Altay Mountains, northwest China: Journal of Asian Earth Sciences, v. 27, p. 61-77.

Zimmerman, U., 2005. Terrane processes at the margins of Gondwana: Geological Society of London Special Publications, v. 246, p. 381-416.

Captions to Figures

Figure 1. General geologic map showing the location of the Comechingones and Conlara pegmatite districts in the Pampean Pegmatite Province, Argentina. Modified from Steenken et al. (2010), Gosen and Prozzi (1998), and Galliski and Sfragulla (2014). Numbers refer to pegmatites as follows: 1. Blanca Dora, 2. Sin Nombre, 3. Magdalena, 4. Juan Román, 5. La Ona, and 6. Nancy.

Figure 2. Plane-polarized transmitted-light photomicrographs of gahnite (Ghn) from granitic pegmatites of the Comechingones and Conlara pegmatite districts of Argentina. **A**. Bluish green gahnite crystal with muscovite (Ms), Juan Román pegmatite, sample GH007. **B**. Green gahnite crystal, La Ona pegmatite, sample GH243. **C**. Emerald green gahnite crystal with muscovite, Blanca Dora pegmatite, sample GH253. **D**. Dark green gahnite crystals with muscovite, microcline (Mc), and quartz (Qz), Magdalena pegmatite, sample GH272. **E**. Green gahnite crystal with muscovite, Sin Nombre pegmatite, sample GH274A. **F**. Green gahnite crystal with muscovite, Nancy pegmatite, sample NA001.

Figure 3. Scanned thick sections of gahnite (Ghn) from the Comechingones and Conlara pegmatite districts of central and northwestern Argentina. **A**. Green gahnite with muscovite (Ms), Nancy pegmatite, sample NA001. **B**. Dark green gahnite with muscovite, Blanca Dora pegmatite, sample GH253. **C**. Typical green gahnite, Juan Román pegmatite, sample GH013. **D**. Gahnite crystals with muscovite, Magdalena pegmatite, sample GH272.

Figure 4. Ternary diagrams of gahnite compositions in granitic pegmatites from the Pampean Pegmatite Province, Argentina, obtained in this study, in terms of: **A**. gahnite (Ghn, Zn), hercynite (Hc, Fe), and spinel (Spl, Mg) end members (in mol %). After Batchelor and Kinnaird (1984), and **B**. Ghn, Hc+Spl, and Glx (galaxite, Mn) end members (in mol %). Only the top 30 % of the diagram is shown (Ghn end member).

Figure 5. Binary diagram showing the composition of gahnite from granitic pegmatites of the Comechingones and Conlara pegmatite districts, Argentina, in terms of molecular (Fe+Mg)/Al *vs.* (Zn+Mn)/Al. After Batchelor and Kinnaird (1984).

Figure 6. Ternary diagram of spinel in terms of mol % gahnite (Ghn), hercynite (Hc), and spinel (Spl) end members and the compositional fields for: (1) marbles, (2) metamorphosed massive sulfide deposits and S-poor rocks in Mg-Ca-Al alteration zones, (3) metamorphosed massive sulfide deposits in Fe-Al-rich metasedimentary and metavolcanic rocks, (4) metabauxites, (5) granitic pegmatites, (6) unaltered and hydrothermally altered Fe-Al-rich metasedimentary and metavolcanic rocks, and (7) Al-rich granulites. The composition of gahnite from the studied pegmatites is superimposed. Fields from Spry and Scott (1986a) and Heimann et al. (2005). Modified from Merino et al. (2013).

Figure 7. Binary diagram showing the composition of gahnite in granitic pegmatites obtained in this and previous studies in terms of molecular (Fe^{2+}+Mg)/Al *vs.* (Zn+Mn)/Al. Red ellipse

outlines gahnite compositions from previous studies listed in Table 3. Black line represents the linear regression line for all the previously published compositions and the R^2 shown is for this line.

Figure 8. Binary diagram showing the composition of gahnite in granitic pegmatites from the Comechingones and Conlara pegmatite districts, Argentina, in terms of molecular Fe^{2+} *vs.* Zn. Based on 4 oxygen atoms per formula unit.

Figure 9. Binary diagram showing the composition of gahnite from the Comechingones and Conlara pegmatite districts, Argentina, in terms of molecular (Fe^{2+}+Mg) *vs.* (Zn+Mn). Based on 4 oxygen atoms per formula unit.

Figure 10. Compositional profile across gahnite of the Blanca Dora granitic pegmatite, Comechingones pegmatite district, Argentina. Sample GH253. Point analysis with low Fe content within the crystal is located in or close to a fracture.

Figure 11. Compositional profile across gahnite of the Sin Nombre granitic pegmatite, Comechingones pegmatite district, Argentina. Sample GH274A.

Figure 12. Compositions of gahnite from the Comechingones district and the Nancy pegmatite of the Conlara pegmatite district, Argentina, expressed in terms of gahnite, hercynite and spinel end members (mol %) superimposed on the redefined spinel compositional field for granitic pegmatites. Field numbers as in Figure 6. The inset shows the top 60% of the diagram presented (gahnite end member). Modified from Spry and Scott (1986a), Heimann et al. (2005), and Merino et al. (2013).

Table Headings

Table 1. Characteristics of the studied gahnite-bearing pegmatites from the Conlara and Comechingones pegmatite districts, Pampean Pegmatite Province, Argentina.

Table 2. Summary compositions of gahnite from granitic pegmatites of the Conlara and Comechingones pegmatite districts, Pampean Pegmatite Province, Argentina, obtained by EMP analysis.

Table 3. Summary information of granitic pegmatites with gahnite compositions reported in the literature.

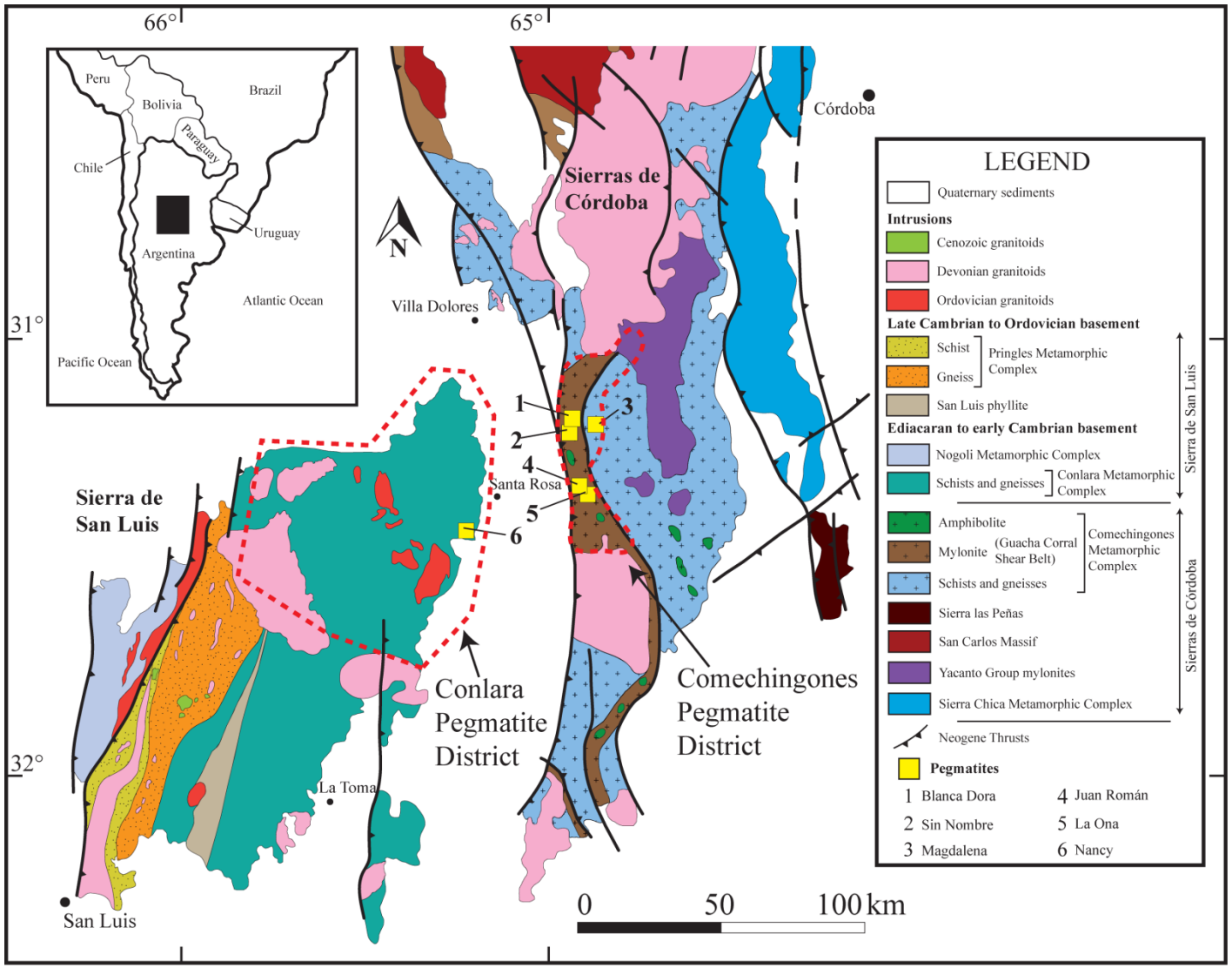
66°
65°
31°
32°
Peru
Bolivia
Brazil
Paraguay
Chile
Uruguay
Argentina
Atlantic Ocean
Pacific Ocean
N
Villa Dolores
Córdoba
Sierras de Córdoba
Sierra de San Luis
Santa Rosa
La Toma
San Luis
Conlara Pegmatite District
Comechingones Pegmatite District
1
2
3
4
5
6
0
50
100 km
LEGEND
Quaternary sediments
Intrusions
Cenozoic granitoids
Devonian granitoids
Ordovician granitoids
Late Cambrian to Ordovician basement
Schist
Gneiss
Pringles Metamorphic Complex
San Luis phyllite
Ediacaran to early Cambrian basement
Nogoli Metamorphic Complex
Schists and gneisses
Conlara Metamorphic Complex
Amphibolite
Mylonite
(Guacha Corral Shear Belt)
Schists and gneisses
Comechingones Metamorphic Complex
Sierra las Peñas
San Carlos Massif
Yacanto Group mylonites
Sierra Chica Metamorphic Complex
Sierra de San Luis
Sierras de Córdoba
Neogene Thrusts
Pegmatites
1 Blanca Dora
2 Sin Nombre
3 Magdalena
4 Juan Román
5 La Ona
6 Nancy

Figure 1

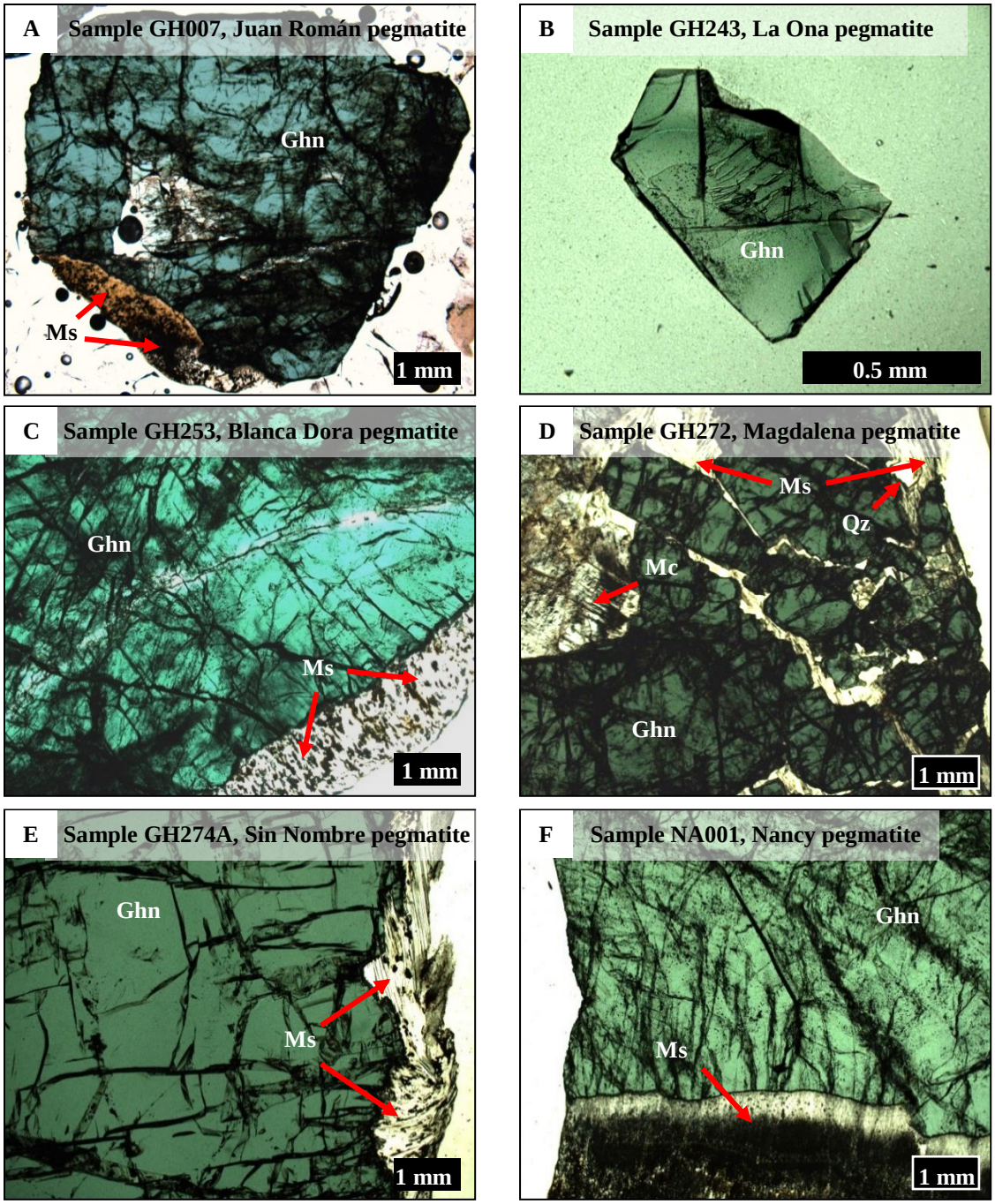
A
Sample GH007, Juan Román pegmatite
Ghn
Ms
1 mm
B
Sample GH243, La Ona pegmatite
Ghn
0.5 mm
C
Sample GH253, Blanca Dora pegmatite
Ghn
Ms
1 mm
D
Sample GH272, Magdalena pegmatite
Ms
Qz
Mc
Ghn
1 mm
E
Sample GH274A, Sin Nombre pegmatite
Ghn
Ms
1 mm
F
Sample NA001, Nancy pegmatite
Ghn
Ms
1 mm

Figure 2

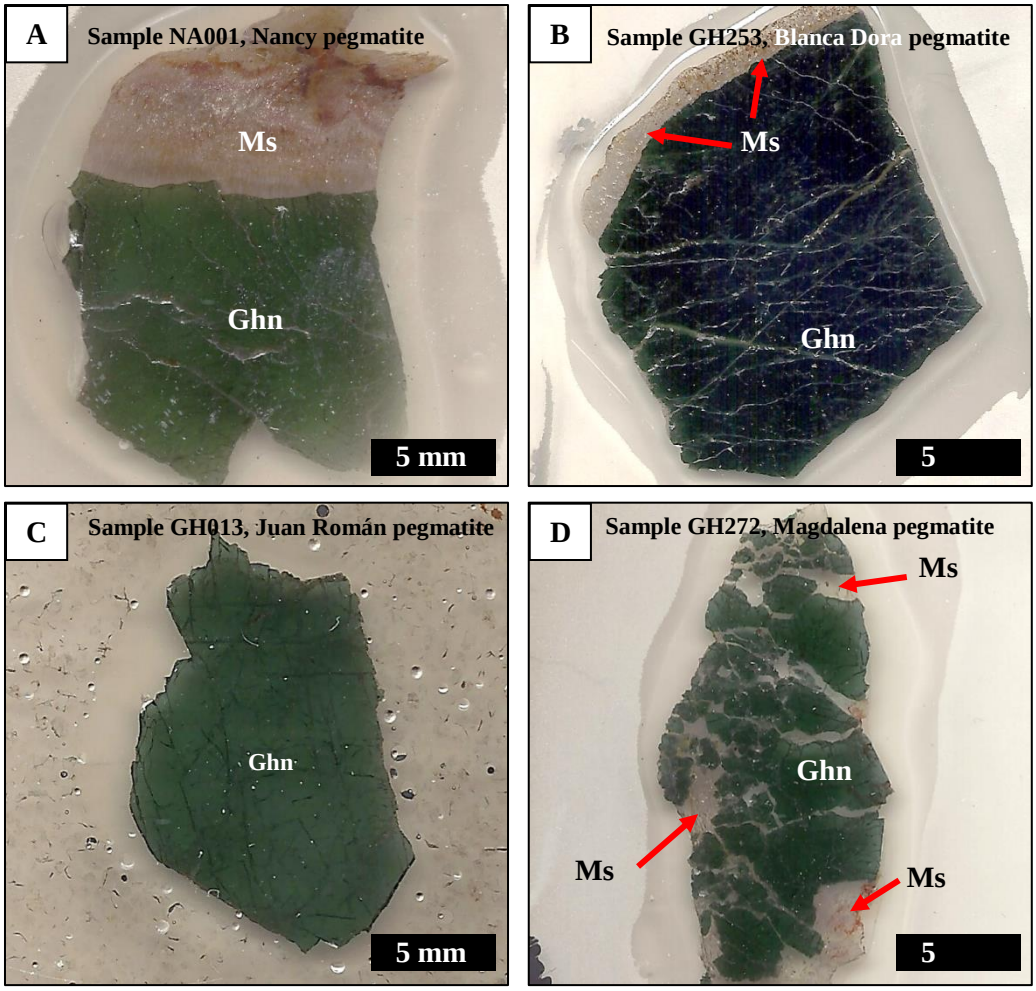
A
Sample NA001, Nancy pegmatite
Ms
Ghn
5 mm
B
Sample GH253, Blanca Dora pegmatite
Ms
Ghn
5
C
Sample GH013, Juan Román pegmatite
Ghn
5 mm
D
Sample GH272, Magdalena pegmatite
Ms
Ghn
Ms
Ms
5

Figure 3

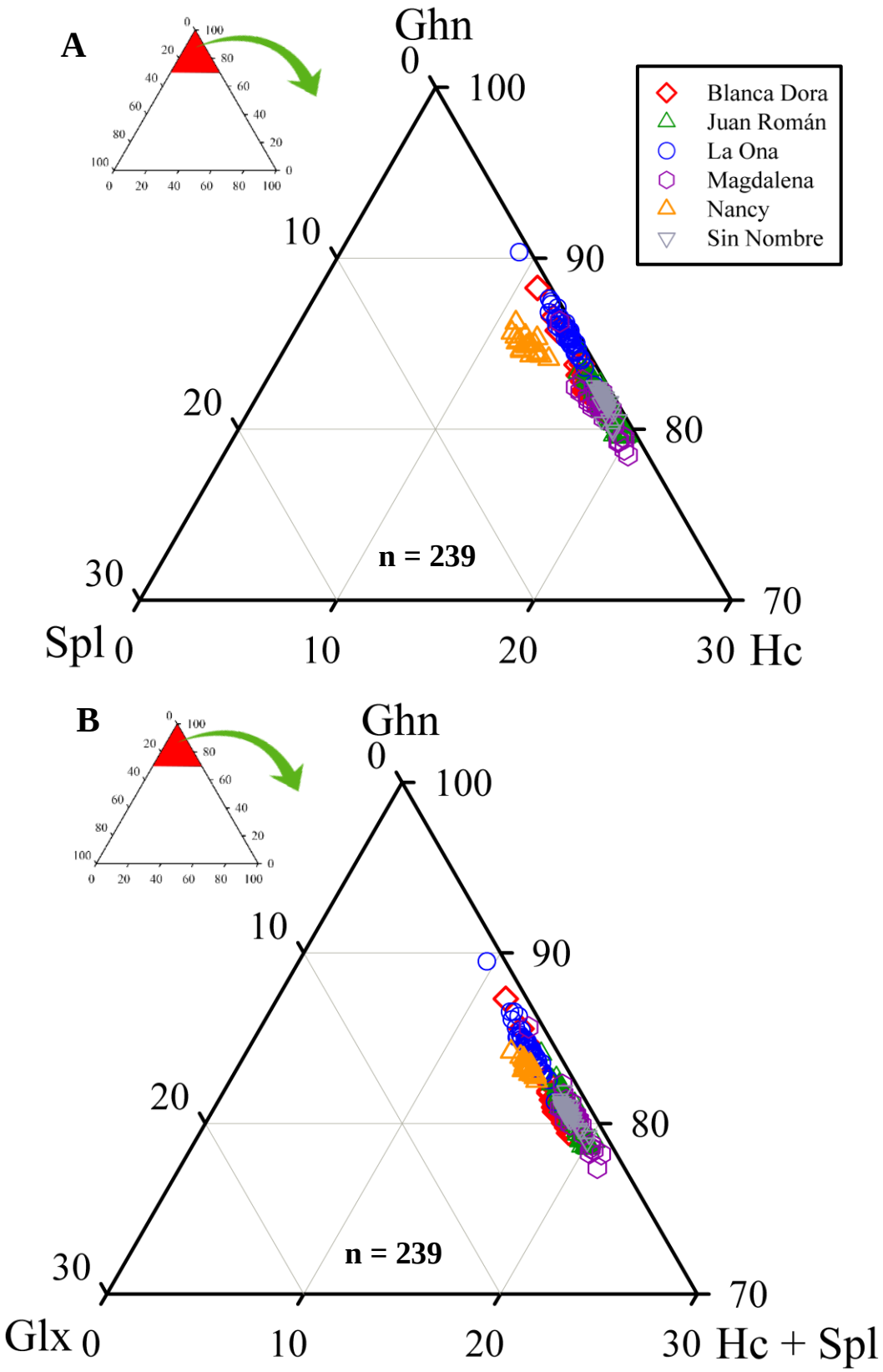
A
Ghn
0
100
10
90
20
80
30
70
Spl 0
10
20
30 Hc
n = 239
Blanca Dora
Juan Román
La Ona
Magdalena
Nancy
Sin Nombre
B
Ghn
0
100
10
90
20
80
30
70
Glx 0
10
20
30 Hc + Spl
n = 239

Figure 4

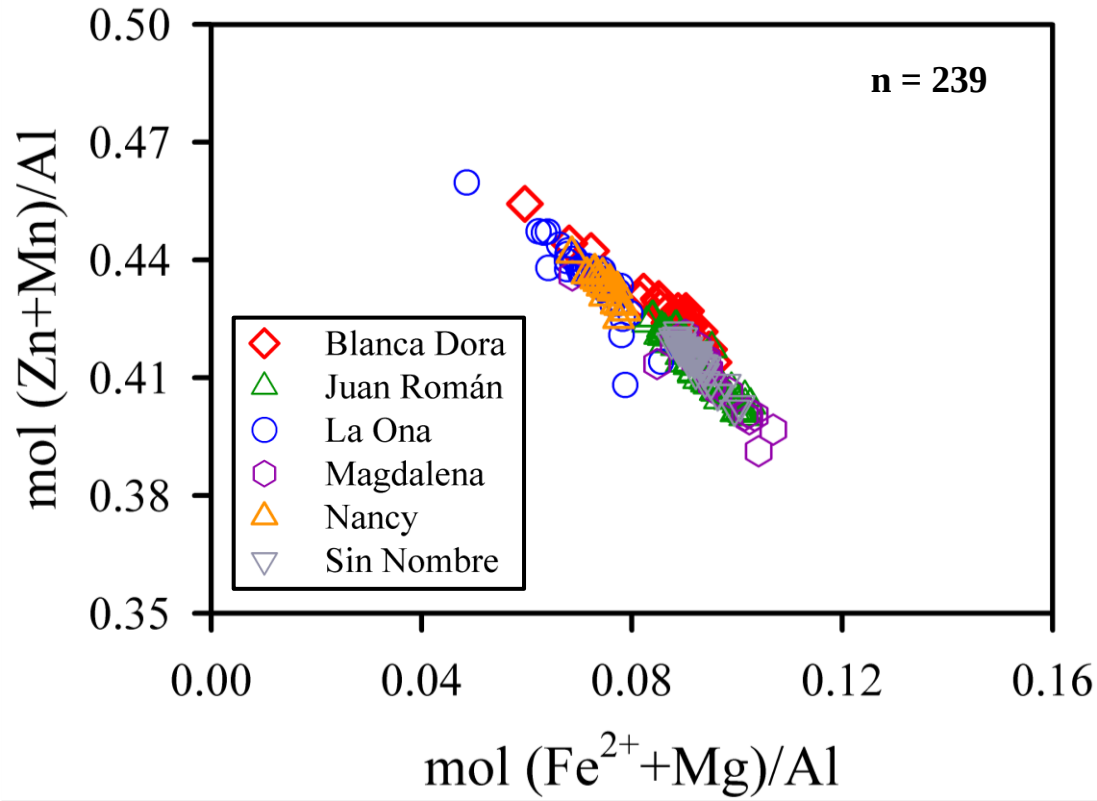
n = 239
Blanca Dora
Juan Román
La Ona
Magdalena
Nancy
Sin Nombre
mol (Zn+Mn)/Al
mol (Fe2+ +Mg)/Al
0.50
0.47
0.44
0.41
0.38
0.35
0.00
0.04
0.08
0.12
0.16

Figure 5

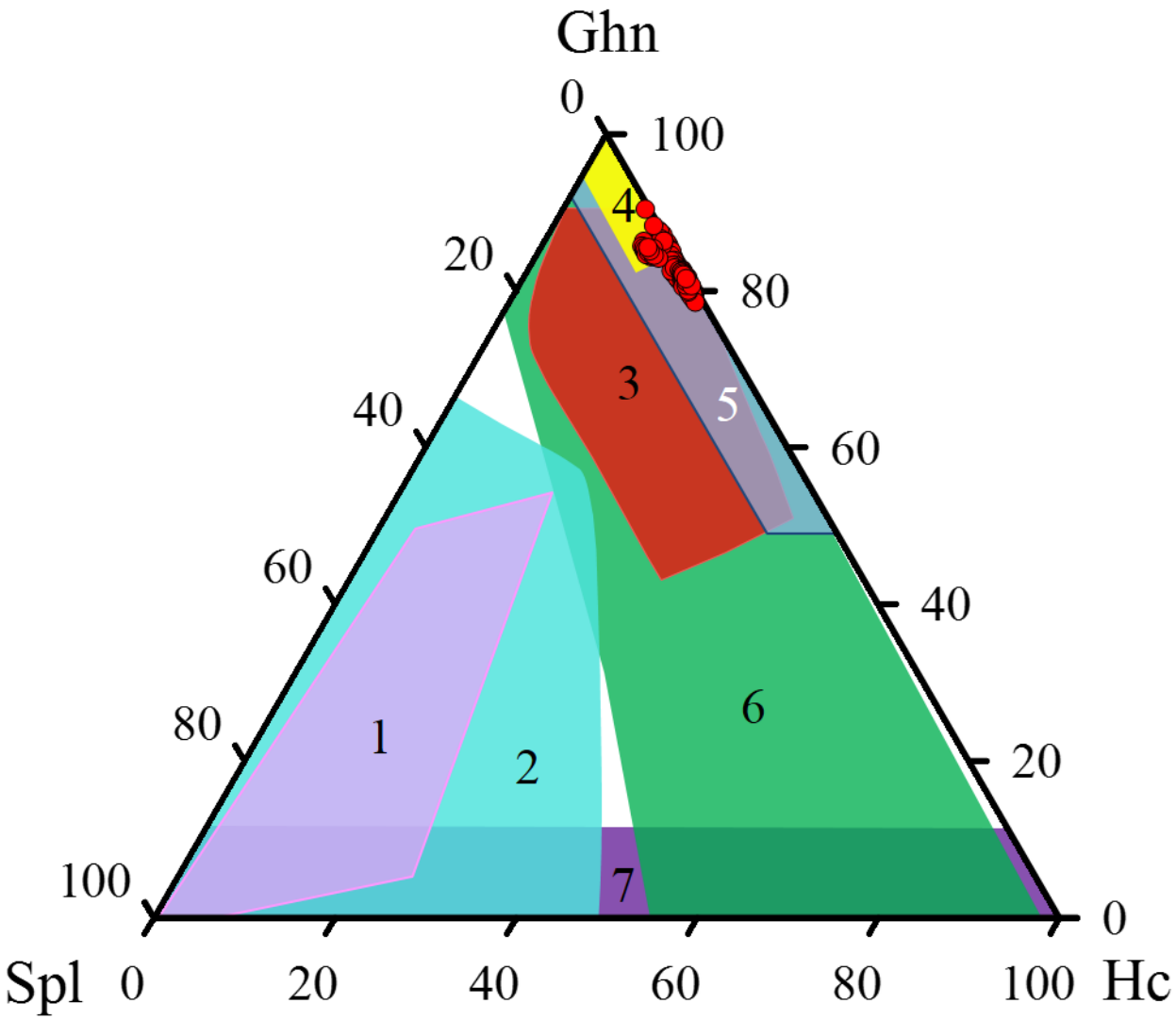
Ghn
0
100
20
80
40
60
60
40
80
20
100
0
Spl
0
20
40
60
80
100
Hc
1
2
3
4
5
6
7

Figure 6

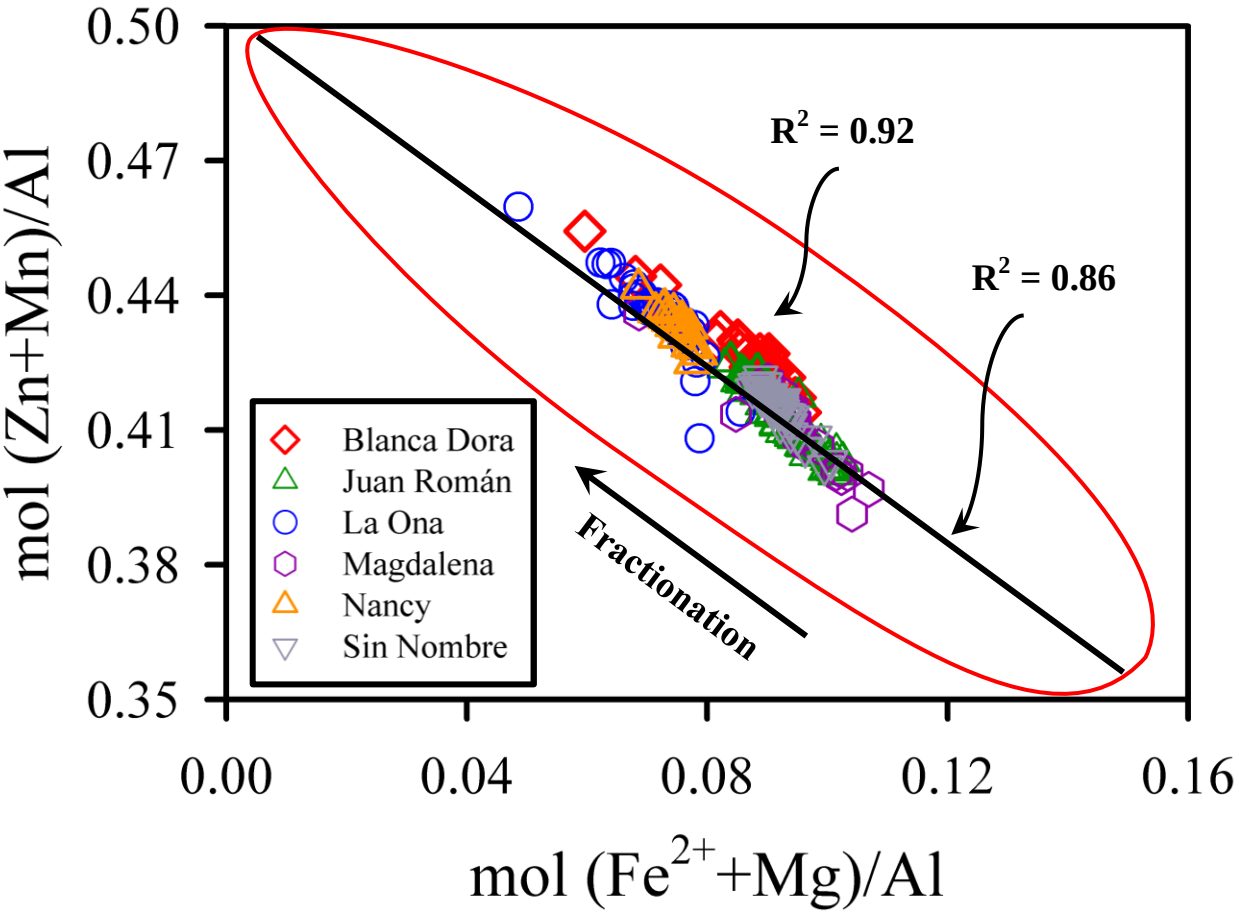
0.50
0.47
0.44
0.41
0.38
0.35
mol (Zn+Mn)/Al
0.00
0.04
0.08
0.12
0.16
mol (Fe2+ +Mg)/Al
R2 = 0.92
R2 = 0.86
Blanca Dora
Juan Román
La Ona
Magdalena
Nancy
Sin Nombre
Fractionation

Figure 7

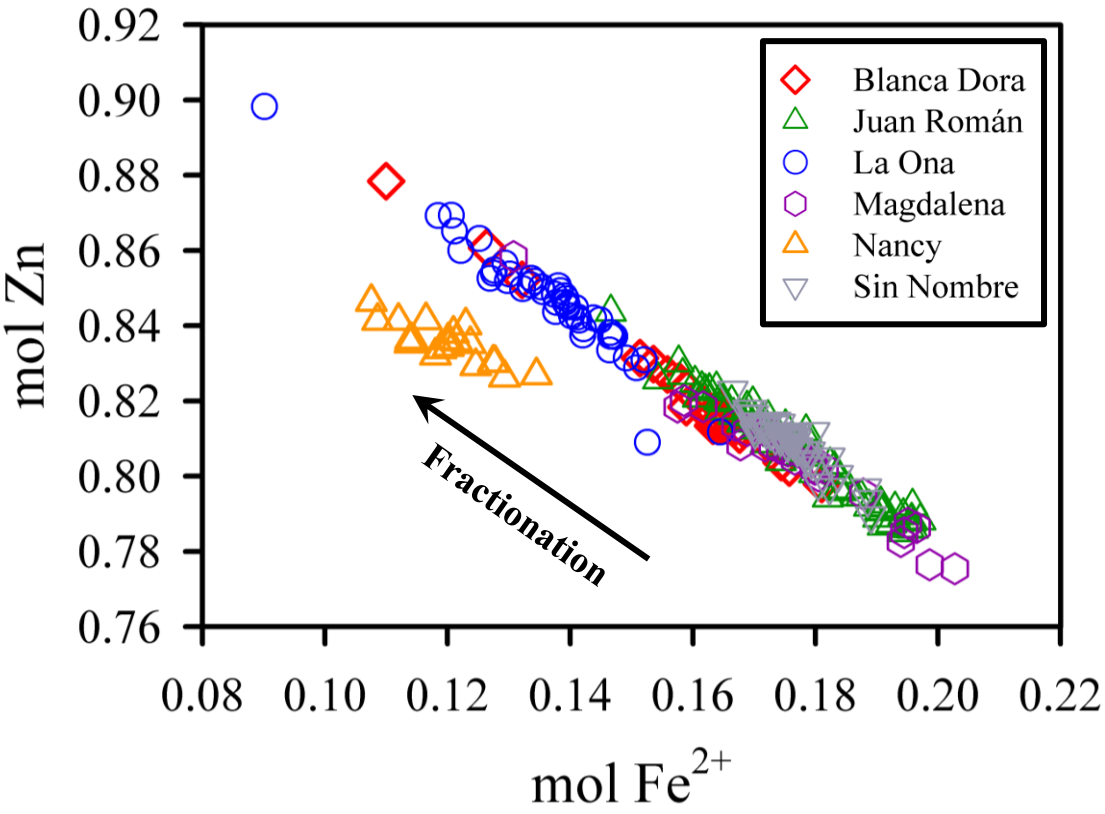
0.92
0.90
0.88
0.86
0.84
0.82
0.80
0.78
0.76
mol Zn
0.08
0.10
0.12
0.14
0.16
0.18
0.20
0.22
mol Fe2+
Blanca Dora
Juan Román
La Ona
Magdalena
Nancy
Sin Nombre
Fractionation

Figure 8

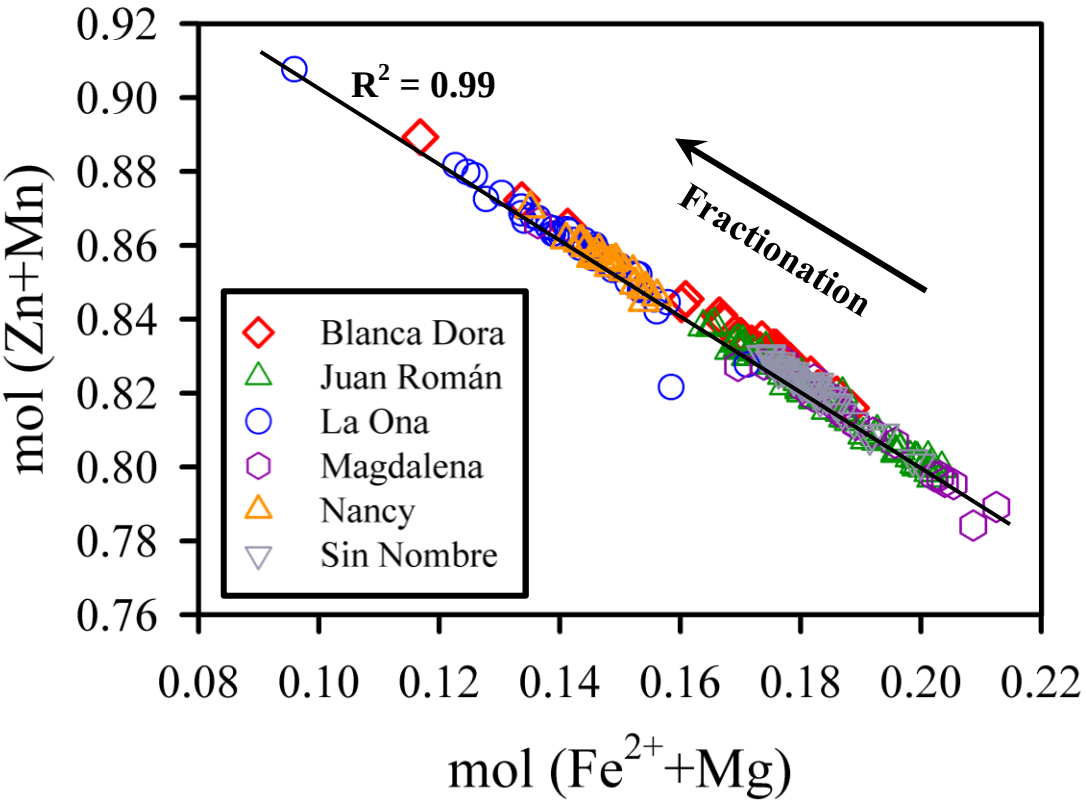
0.92
0.90
0.88
0.86
0.84
0.82
0.80
0.78
0.76
mol (Zn+Mn)
R2 = 0.99
Fractionation
Blanca Dora
Juan Román
La Ona
Magdalena
Nancy
Sin Nombre
0.08
0.10
0.12
0.14
0.16
0.18
0.20
0.22
mol (Fe2+ +Mg)

Figure 9

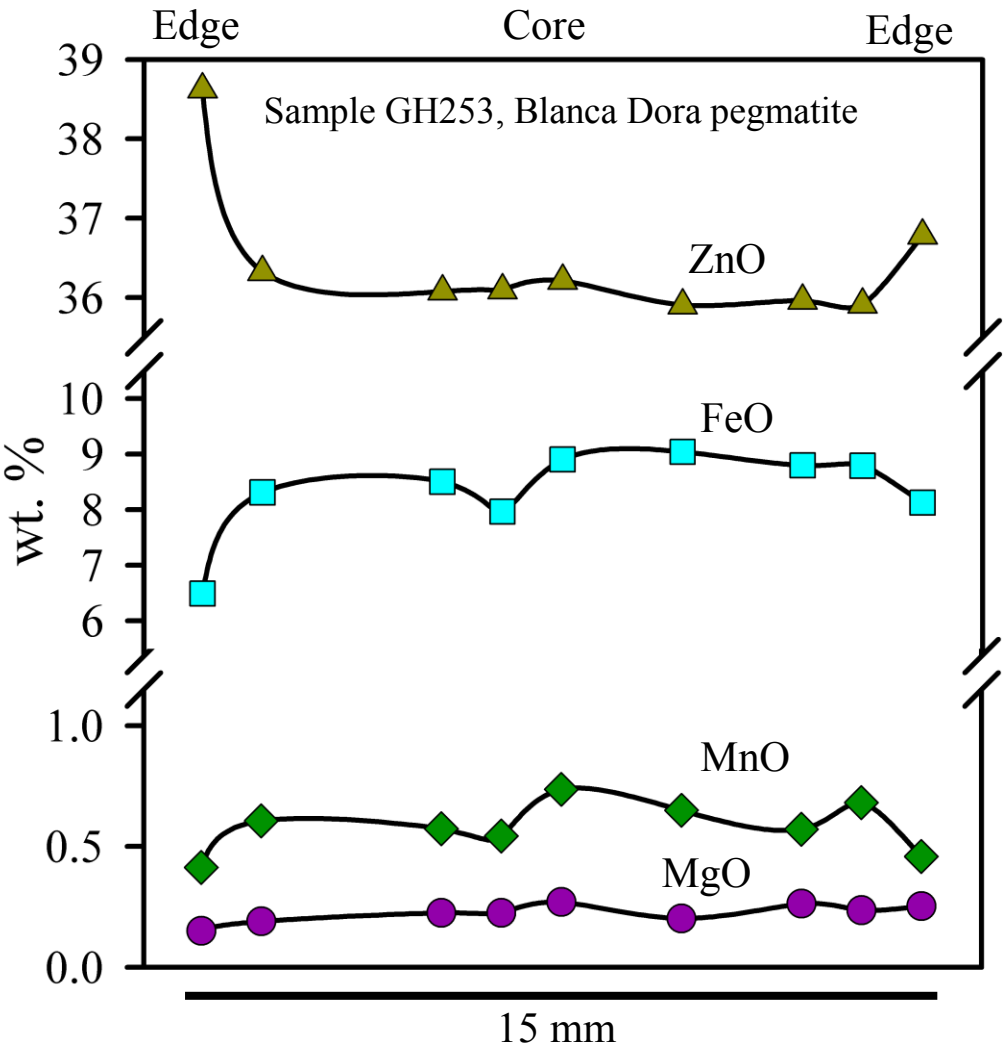
Edge
Core
Edge
Sample GH253, Blanca Dora pegmatite
ZnO
FeO
MnO
MgO
wt. %
39
38
37
36
10
9
8
7
6
1.0
0.5
0.0
15 mm

Figure 10

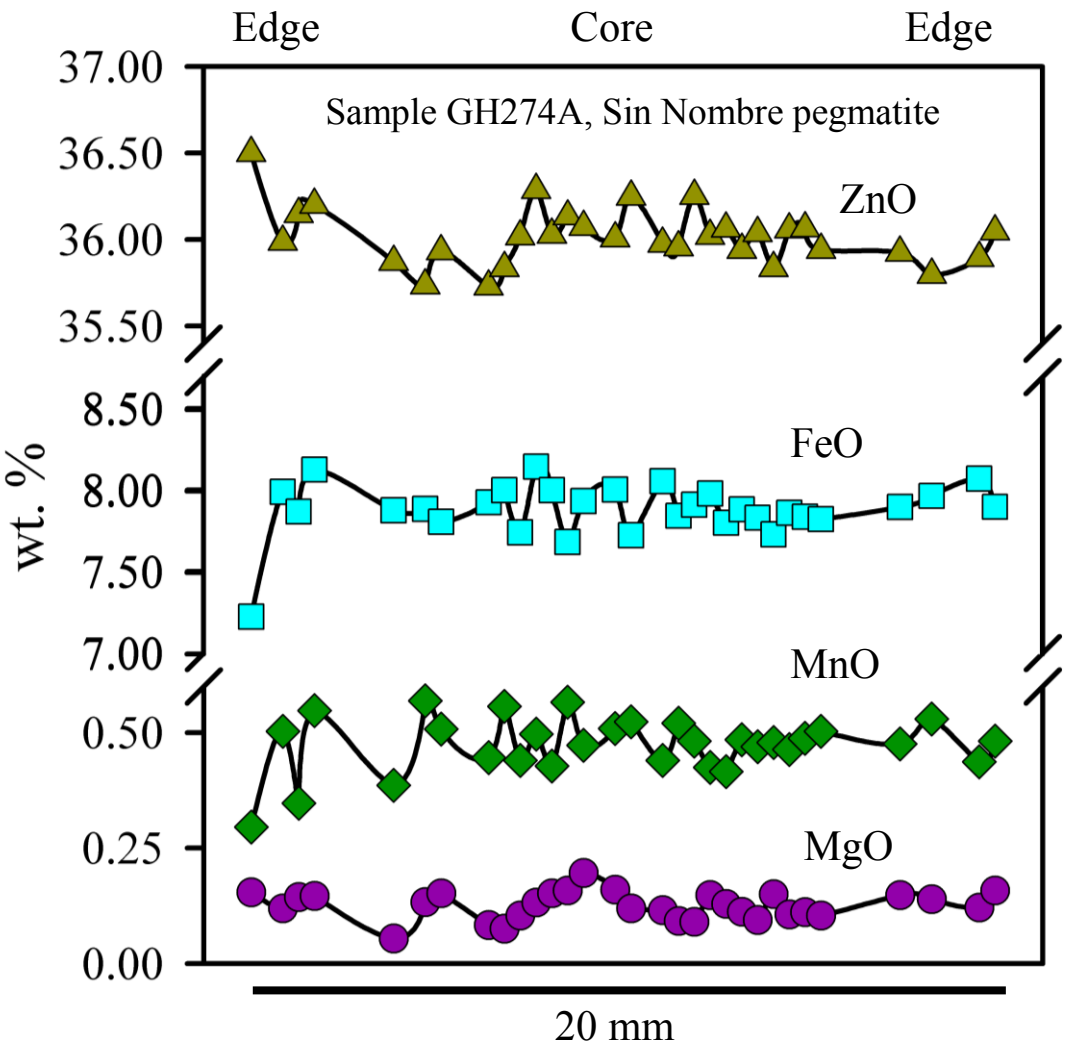
Edge
Core
Edge
Sample GH274A, Sin Nombre pegmatite
ZnO
FeO
MnO
MgO
wt. %
37.00
36.50
36.00
35.50
8.50
8.00
7.50
7.00
0.50
0.25
0.00
20 mm

Figure 11

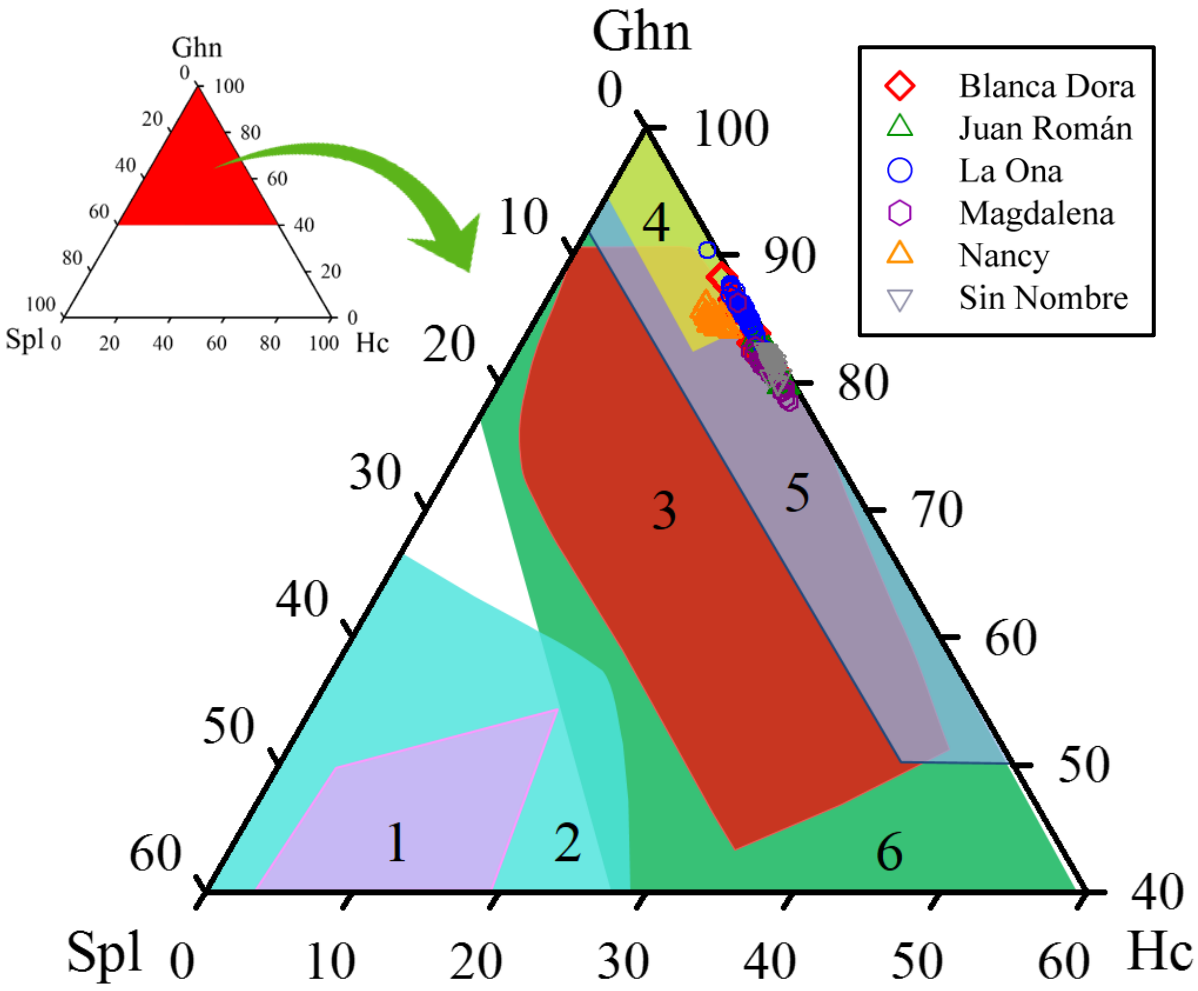
Ghn
Spl
Hc
Blanca Dora
Juan Román
La Ona
Magdalena
Nancy
Sin Nombre
1
2
3
4
5
6

Figure 12

Table 1. Characteristics of the studied gahnite-bearing pegmatites from the Conlara and Comechingones pegmatite districts, Pampean Pegmatite Province, Argentina.

Pegmatite	**Nancy**	**Blanca Dora**	**Juan Román**	**La Ona**	**Magdalena**	**Sin Nombre**
District	Conlara	Comechingones	Comechingones	Comechingones	Comechingones	Comechingones
Group	Villa Praga-Las Lagunas	Co. de Agustín	Co. Las Ovejas	Co. Las Ovejas	Co. Redondo	Co. de Agustín
Thickness (m)	4 – 28	5	20	-	5 – <40	30
Length (m)	> 140	300	240	1000	200	209
Shape	Tabular	Tabular	Tabular	Tabular	Tabular	Tabular
Orientation	Discordant	Concordant	Concordant	Concordant	Subhorizontal	Discordant
Host Rock	Medium-grade grey gneiss	Augen-gneiss	Augen-gneiss	Augen-gneiss	Cordierite migmatite	Augen-gneiss
Formation	Conlara Metamorphic Complex	Guacha Corral Shear Zone	Guacha Corral Shear Zone	Guacha Corral Shear Zone	Guacha Corral Shear Zone	Guacha Corral Shear Zone
Classification	REL-Li - beryl-columbite-phosphate subtype (LCT)	REL-Li - beryl-columbite-phosphate subtype (LCT)	REL-Li - beryl-columbite-phosphate subtype (LCT)	REL-Li - beryl-columbite-phosphate subtype (LCT)	REL-Li - beryl-columbite-phosphate subtype (LCT)	MS-REL – Li (LCT)
Mineralogy	Qz, Kfs, Ab, Ms, Grt, Brl, Ap, Ghn, Col-Ttl, Py, Sp, Bfg, Wyl, Hem[1], Lm[1]	Qz, Kfs, Ab, Ms, Grt, Brl, Ghn, Fap, Col	Qz, Kfs, Ab, Ms, Grt, Brl, Ghn, Fap, Col	Qz, Kfs, Ab, Ms, Grt, Brl, Ghn, Col, U minerals, Phos	Qz, Kfs, Ab, Ms, Grt, Brl, Ghn, Fap, Col, Trp	Qz, Kfs, Ab, Ms, Grt, Brl, Ghn, Tur, Aut, Ap, Hem[1]
Rare-metal mineralization	Be, Nb	Be, Nb	Be, Nb	Be, Nb, U	Be, Nb	Be
Age (Ma)	435 – 500	466 – 530	466 – 530	466 – 530	466 – 530	466 – 530
References	4, 5	2, 3, 7	2, 3, 7	2, 3, 7	2, 3, 6, 7	1, 2, 3, 7

Mineral abbreviations (* denotes those from Whitney and Evans, 2010): Ab* – Albite, Ap* – Apatite, Aut – Autunite, Brl* – Beryl, Bfg – Bobfergusonite, Col – Columbite, Fap – Fluorapatite, Ghn* – Gahnite, Grt* – Garnet, Hem*[1] – Hematite, Kfs* – K-feldspar, Lm* – Limonite, Ms* – Muscovite, Phos – Phosphates, Py* – Pyrite, Qz* – Quartz, Sp* – Sphalerite, Ttl – Tantalite, Trp – Triplite, Tur* – Tourmaline, Wyl – Wyllieite.. [1]Secondary. References as follows: 1 Rinaldi (1969), 2 Hub (1994), 3 Galliski (1999a), 4 Galliski (1999b), 5 Tait et al. (2004), 6 Galliski and Černý (2006), 7 Galliski and Sfragulla (2014). REL-Li refers to rare-element class, Li subclass pegmatites; MS-REL refers to muscovite-rare element class pegmatites.

Table 2. Summary compositions of gahnite from granitic pegmatites of the Conlara and Comechingones pegmatite districts, Pampean Pegmatite Province, Argentina, obtained by EMP analysis.

Pegmatite	**Nancy**		**Sin Nombre**		**Juan Román**		**Magdalena**		**La Ona**		**Blanca Dora**	
	Mean	**Ranges**	**Mean**	**Ranges**	**Mean**	**Ranges**	**Mean**	**Ranges**	**Mean**	**Ranges**	**Mean**	**Ranges**
n	20		50		70		27		45		27	
K_2O wt. %	0.02	0.00-0.04	0.01	0.00-0.04	0.02	0.00-0.06	0.02	0.00-0.04	0.02	0.00-0.04	0.02	0.00-0.03
SiO_2	0.02	0.00-0.07	0.02	0.00-0.09	0.01	0.00-0.09	0.02	0.00-0.10	0.01	0.00-0.09	0.01	0.00-0.05
CaO	0.01	0.00-0.03	0.01	0.00-0.03	0.01	0.00-0.03	0.00	0.00-0.02	0.01	0.00-0.04	0.01	0.00-0.02
TiO_2	0.01	0.00-0.03	0.01	0.00-0.05	0.01	0.00-0.06	0.01	0.00-0.04	0.01	0.00-0.06	0.01	0.00-0.05
MgO	0.63	0.48-0.74	0.13	0.054-0.30	0.15	0.072-0.24	0.22	0.10-0.36	0.12	0.06-0.18	0.21	0.15-0.29
Al_2O_3	55.45	54.65-55.97	55.07	54.59-56.16	55.14	54.05-55.77	55.27	54.58-56.75	54.90	53.99-56.71	54.46	53.89-55.33
MnO	0.78	0.68-0.92	0.47	0.30-0.57	0.45	0.26-0.59	0.42	0.28-0.63	0.52	0.36-0.64	0.60	0.41-0.74
FeO	5.98	5.62-6.16	7.87	7.23-8.15	7.91	6.69-8.74	7.86	5.66-8.36	6.64	4.81-7.50	8.30	6.49-9.04
ZnO	37.44	36.90-37.83	35.95	35.35-36.50	35.85	34.91-37.33	35.81	34.64-38.13	37.58	36.40-39.69	36.43	35.58-38.62
Cr_2O_3	0.01	0.00-0.04	0.01	0.00-0.04	0.01	0.00-0.08	0.01	0.00-0.07	0.01	0.00-0.05	0.01	0.00-0.04
Total	100.33		99.54		99.55		99.63		99.81		100.04	
***Apfu* based on 4 oxygen atoms**												
Si	0.001	0.000-0.002	0.001	0.000-0.003	0.000	0.000-0.003	0.001	0.000-0.003	0.000	0.000-0.003	0.000	0.000-0.001
Ti	0.000	0.000-0.001	0.000	0.000-0.001	0.000	0.000-0.001	0.000	0.000-0.001	0.000	0.000-0.001	0.000	0.000-0.001
Al	1.975	1.968-1.988	1.980	1.969-1.996	1.981	1.963-1.996	1.982	1.968-2.004	1.975	1.963-2.013	1.960	1.949-1.975
Cr	0.000	0.000-0.001	0.000	0.000-0.001	0.000	0.000-0.002	0.000	0.000-0.002	0.000	0.000-0.001	0.000	0.000-0.001
K	0.001	0.000-0.002	0.000	0.000-0.001	0.001	0.00-0.002	0.001	0.000-0.001	0.001	0.000-0.001	0.001	0.000-0.001
Fe^{3+}	0.031	0.018-0.042	0.025	0.000-0.039	0.025	0.005-0.050	0.023	0.000-0.038	0.033	0.000-0.050	0.052	0.033-0.066
Fe^{2+}	0.120	0.108-0.135	0.176	0.167-0.189	0.177	0.147-0.197	0.177	0.131-0.203	0.137	0.090-0.165	0.160	0.110-0.181
Mn	0.020	0.017-0.024	0.012	0.008-0.015	0.012	0.007-0.015	0.011	0.007-0.016	0.014	0.009-0.017	0.016	0.011-0.019
Mg	0.028	0.021-0.033	0.006	0.002-0.013	0.007	0.003-0.011	0.010	0.004-0.016	0.006	0.003-0.008	0.009	0.007-0.013
Ca	0.000	0.000-0.001	0.000	0.000-0.001	0.000	0.000-0.001	0.000	0.000-0.001	0.000	0.000-0.001	0.000	0.000-0.001
Zn	0.835	0.826-0.846	0.809	0.789-0.823	0.807	0.785-0.844	0.804	0.775-0858	0.847	0.809-0.898	0.821	0.798-0.878
Total	3.010		3.009		3.010		3.009		3.013		3.019	
Glx	0.020	0.017-0.024	0.012	0.008-0.015	0.012	0.007-0.015	0.011	0.007-0.016	0.014	0.009-0.017	0.016	0.011-0.019
Spl	0.028	0.021-0.033	0.006	0.002-0.013	0.007	0.003-0.011	0.010	0.004-0.016	0.006	0.003-0.008	0.009	0.007-0.013
Ghn	0.835	0.826-0.846	0.809	0.789-0.823	0.807	0.785-0.844	0.804	0.775-0858	0.847	0.809-0.898	0.821	0.798-0.878
Hc	0.120	0.108-0.135	0.176	0.167-0.189	0.177	0.147-0.197	0.177	0.131-0.203	0.137	0.090-0.165	0.160	0.110-0.181
(Zn+Mn)/Al	0.433	0.425-0.442	0.415	0.402-0.422	0.413	0.400-0.431	0.411	0.391-0.436	0.436	0.408-0.460	0.427	0.414-0.454
(Fe^{2+}+Mg)/Al	0.075	0.069-0.079	0.092	0.088-0.101	0.093	0.076-0.103	0.094	0.069-0.107	0.072	0.049-0.086	0.086	0.060-0.096
Zn/Fe^{2+}	6.995	6.147-7.868	4.609	4.176-4.941	4.584	3.990-5.753	4.592	3.824-6.563	6.245	4.935-9.964	5.213	4.407-7.989

n – number of analyses. *Apfu* – atoms per formula unit. Fe^{2+} and Fe^{3+} calculated from stoichiometry. Sample numbers: Nancy NA001, Sin Nombre GH274A and GH274B, Juan Román GH007, GH011, and GH013, Magdalena GH272 and GH273, La Ona GH243, Blanca Dora GH253. Detection limits, in parts per million are: 105 for SiO_2, 72 for K_2O, 85 for CaO, 167 for TiO_2, 122 for MgO, 153 for Al_2O_3, 176 for MnO, 162 for FeO, 120 for Cr_2O_3, and 190 for ZnO.

Table 3. Summary information of granitic pegmatites with gahnite compositions reported in the literature.

Location	Host Rock	Classification	Mineralogy	Rare-metal mineralization	Age (Ma)	References
Alto Ligonha, Mozambique (Namivo)	Migmatitic paragneiss	REL-Li lepidolite subtype (LCT)	Ab, Brl, Bt, Col, Cst, Ghn, Grt, Kfs, Lpd, Ms, Qz, Rt, Ttl, Tur, Znw	Be, Li, Nb, Sn, Ta, Ti		**20**, 22
Auburn, Maine	Metasedimentary rocks	REL-Li - beryl-columbite-phosphate subtype (LCT)	Ab, Ap, Brl, Bt, Cst, Ghn, Grt, Isk, Lpd, Mc, Mlt, Ms, Pl, Qz, Spd, Trp, Tur, Zrn	Be, Li, Sn	325 ± 3	**26**, 33
BPP, Brazil (Alto Mirador)	Quartzite	REL-Li - lepidolite subtype (LCT)	Ab, Ap, Brt, Brl, Bt, Cbl, Cld, Eul, Ghn, Grt, Lpd, Mlc, Ms, Qz, Ttl, Tur, Zrn	Be, Li, Ta	480 - 520	**24**, 25
BPP, Brazil (Capoeira 2)	Metaconglomerate	REL-Li (LCT)	Ab, Ap, Cld, Col, Drv, Elb, Ghn, Grt, Mc, Ms, Qz, Spd, Srl, Ixo, Umlt	Li, Nb, Sn, Ta, Ti, U	480 - 520	**24**, 25
BPP, Brazil (Quintos)	Quartzite	REL-Li (LCT)	Ab, Brt, Brl, Nbs, Elb, Ghn, Grt, Lpd, Ms, Qz, Spd, Ixo, Tur, Umlt	Be, Cs, Li, Ti, U	480 - 520	**24**, 25
Cabanas, Portugal	Mica schist	REL-Li (LCT)	Ab, Ap, Apy, Brl, Ccp, Col-Ttl, Cst, Ghn, Grt, Ilm, Mc, Mtb, Mnz, Ms, Or, Po, Py, Qz, Rt, Sil, Sp, Tpz, Tur, Znw, Zrn	Be, Nb, REEs, Sn, Ta		**21**
Cáceres, Spain	Metasedimentary rocks		Ap, Brl, Cbl, Kfs, Ms, Pl, Qz	Be	312 - 328	**17**
Cap de Creus, Spain	Andalusite-cordierite schist	REL-Li - beryl-columbite subtype (LCT)	And, Apy, Brl, Cbl, Col, Ghn, Ixo, Kfs, Ms, Qz, Sil, Srl, Urn, Wfm	Be, Ta, U, W	280 - 310	1, **2**, 3; 7
Jemaa, Nigeria	Hornblende-biotite gneiss		Ab, Cst, Ghn, Ms, Qz, Srl, Ttl	Sn, Ta	450 - 500	**4**, 14
Kimito, Finnland (Rosendal)	Hornblende gabbro		Ghn, Grt, Kfs, Ms, Pl, Qz, Sp			**23**
Pingjiang, China (Mufushan)	Monzogranite	REL-Li (LCT)	Ab, Brl, Bt, Col, Ghn, Mag, Mc, Mnz, Ms, Qz, Ttl	Be, Nb, Ta, REEs	96 - 136	**35**, 36

Location	Host Rock	Classification	Mineralogy	Rare-metal mineralization	Age (Ma)	References
Separation Rapids, Ontario	Mafic metavolcanic rock	REL-Li - petalite subtype (LCT)	Ab, Ald, Aln, Amp, Apy, Brl, Bt, Ccp, Col, Crd, Cst, Ep, Ftp, Fl, Fap, Ghn, Grt, Ilm, Kfs, Lo, Lpd, Mlt, Mnz, Ms, Ngt, Plc, Ptl, Prp, Py, Qz, Sch, Sp, Spd, Sbtf, Srv, Tpz, Ttl, Tur, Urn, Wdg, Xtm, Ypcl, Znw, Zrn	As, Be, Li, Nb, REEs, Sn, Ta	2,643 ± 2	**8**, **18**, 29
Serra de Arga, Portugal	Mica schist		Ab, Ap, Brl, Bt, Cbl, Chl, Col, Cst, Ghn, Ms, Ngt, Or, Qz, Rt, Spd, Tpz, Ttl, Znw, Zrn	Be, Li, Nb, Sn, Ta		**5**, **11**, 19
Siedlimowice, Poland	Two-mica granite	REL-Li - beryl-columbite subtype (LCT)	Ap, Brl, Bt, Chl, Col, Ghn, Grt, Kfs, Ms, Pl, Qz, Zrn	Be, Nb	300 - 310	6, 15, **28**, 30
South Harris, Scotland (Chiapaval)			Ab, Aln, Brl, Bt, Col, Ghn, Grt, Mag, Mc, Mnz, Ms, Py, Qz, Thr, Tur, Urn, Zrn	Nb, REEs, Th, U	1,700	10, **31**
Spruce Pine, NC (Burleson Mica Mine)	Amphibolite	MSREL	Brl, Bt, Col, Ghn, Grt, Ms, Pl, Qz, Tur	Be, Nb	377 - 404	**26**, 27
Stoneham, Maine (Lord Hill)	Diorite	REL-Li - beryl-columbite-phosphate subtype (LCT)	Ap, Brl, Bt, Cld, Col, Crl, Fl, Ghn, Ms, Pl, Py, Qz, Tpz, Tph, Trp, Zrn	Be, Nb	325 ± 3	**16**, **26**, 33
Topsham, Maine	Gneiss	REL-REE - euxenite subtype (NYF)	Ab, Ap, Brl, Bt, Col, Cst, Ghn, Grt, Kfs, Lpd, Mag, Mlt, Mnz, Ms, Pl, Qz, Smk, Tpz, Ttl, Tur, Urn, Zrn	Nb, REEs, Ta, Ti	367 ± 4	12, **26**, 33, 34
Träskböle, Finland	Gneiss		Ab, Bt, Ccp, Chl, Qz, Ghn,, Mc, Ms, Pl, Po, Py, Sp,		1,800	**9**, 13
Xinjian, China (Keketuohai)	Amphibolite	REL-Li (LCT)	Ab, Brl, Ghn, Mag, Mc, Ms, Plc, Qz, Rt, Spd, Tur	Be, Li, Nb, Ta, REEs	218.4 ± 5.8	32, **33**, 36, 37

Mineral abbreviations: Albite – Ab*, Allanite – Aln*, Alluaudite – Ald, Amphibole – Amp*, Andalusite – And*, Apatite – Ap*, Arsenopyrite – Apy, Bertrandite – Brt, Beryl – Brl*, Biotite – Bt*, Brannerite – Brt, Cassiterite – Cst*, Chalcopyrite – Ccp*, Chlorite – Chl*, Chrysoberyl – Cbl, Cleavelandite – Cld, Columbite – Col, Cordierite – Crd*, Cryolite – Crl*, Dravite – Drv*, Elbaite – Elb*, Epidote – Ep*, Euclase – Eul, Ferrotapiolite – Ftp, Fluorapatite – Fap, Fluorite – Fl*, Gahnite – Ghn*, Garnet – Grt*, Ilmenite – Ilm*, Ishikawaite – Isk, Ixiolite – Ixo, K-feldspar – Kfs*, Lepidolite – Lpd*, Löllingite – Lo*, Magnetite – Mag*, Malachite – Mlc*, Metatorbernite – Mtb, Microcline – Mc*, Microlite – Mlt, Monazite – Mnz*, Muscovite – Ms*, Natrobistantite – Nbs,

Nigerite – Ngt, Orthoclase – Or*, Petalite – Ptl*, Plagioclase – Pl*, Pollucite – Plc, Purpurite – Prp, Pyrite – Py*, Pyrrhotite – Po*, Quartz – Qz*, Rutile – Rt*, Samarskite – Smk, Scheelite – Sch*, Schorl – Srl*, Sillimanite – Sil*, Sphalerite – Sp*, Spodumene – Spd*, Stibiobetafile – Sbtf, Struverite – Srv, Tantalite – Ttl, Thorite – Thr*, Topaz – Tpz*, Triplite – Trp, Triphylite – Tph, Tourmaline – Tur*, Uraninite – Urn*, Uranomicrolite – Umlt, Wodginite – Wdg, Wolframite – Wfm, Xenotime – Xtm*, Yttropyrochlore – Ypcl, Zinnwaldite – Znw*, Zircon – Zrn*. *Abbreviations from Whitney and Evans (2010). Abbreviations for pegmatite nomenclature, based on the classification of Černý and Ercit (2005) and Černý et al. (2012): REL – rare-element class; MSREL – muscovite rare-element class; Li – Li subclass; REE – rare-earth element subclass; LCT – lithium, cesium, and tantalum pegmatite family; NYF – niobium, yttrium, and fluorine pegmatite family.

Location abbreviation: BPP – Borborema Pegmatite Province

References (bold numbers in table indicate those that present gahnite compositions): 1 Alfonso and Melgarejo (2008); **2** Alfonso et al. (1995); 3 Alfonso et al. (2003); **4** Batchelor and Kinnaird (1984); **5** Dias (2011); 6 Domańska-Siuda (2007); 7 Druguet and Hutton (1998); **8** Dunlop (2000); **9** Eskola (1914); 10 Fettes and Mendum (1987); **11** Gomes et al. (1995); 12 Hanson et al. (1998); 13 Huhma (1986); 14 Jackson (1982); 15 Janeczek, J., 2007; **16** Johnson (1998); **17** Merino et al. (2013); **18** Morris et al. (1997); 19 Neiva et al. (1955); **20** Neiva (2013); **21** Neiva and Champness (1997); 22 Neiva and Neiva (2005); **23** Pehram (1948); **24** Soares et al. (2007); 25 Soares et al. (2008); **26** Spry and Scott (1986b); 27 Swanson and Veal (2010); **28** Szuskiewicz and Łobos (2004); 29 Tindle and Breaks (1998); 30 Turniak et al. (2007); **31** von Knorring and Dearnley (1960); 32 Windley et al. (2002); 33 Wise and Francis (1992); 34 Yatsevitch (1934); **35** Zhaolin et al. (1999a); 36 Zhaolin et al. (1999b); 37 Zhu et al. (2006).

CHAPTER 2

MAJOR AND TRACE ELEMENT SIGNATURE OF GAHNITE IN GRANITIC PEGMATITES AND A METAMORPHOSED MASSIVE SULFIDE DEPOSIT: DIFFERENCES AND DISCRIMINATION GUIDELINES

Jason A. Yonts[1], Adriana Heimann[1], and Michael Wise[2]

To be submitted to the Journal of Geochemical Exploration

[1] Department of Geological Sciences, East Carolina University, 101 Graham Building, Greenville, NC 27858

[2] Department of Mineral Sciences, Smithsonian Institution, Washington, DC 20013

ABSTRACT

Rare-element granitic pegmatites are common hosts to economic deposits of rare-metals, including Li, Ta, and rare-earth elements, among others. Rare-metals are increasing in economic importance due to advancing technology. The major element composition of some minerals, in particular gahnite ($ZnAl_2O_4$), has been used as an exploration guide for metamorphosed massive sulfide deposits (MMSDs). Gahnite can also occur as an accessory mineral in rare-element granitic pegmatites, including those with rare metal mineralization, but detailed studies on the major element chemical composition of gahnite in pegmatites are scarce and there are only two trace element studies of gahnite in granitic pegmatites. Gahnite crystals from worldwide localities of granitic pegmatites and the Nine Mile MMSD, Australia, were analyzed for major and trace element chemistry. The compositions of gahnite from the pegmatites, expressed in terms of mol % gahnite (Ghn), hercynite (Hc), and spinel (Spl) end members, fall within the previously defined pegmatite field and are given by $Ghn_{70.63\text{-}98.48}Hc_{0.95\text{-}28.61}Spl_{0.00\text{-}4.52}$. Gahnite compositions from the Nine Mile deposit ($Ghn_{55.62\text{-}76.06}Hc_{17.47\text{-}37.34}Spl_{3.81\text{-}10.73}$) fall within the MMSD field characterized by reaching higher Mg and Fe and lower Zn contents compared to gahnite from granitic pegmatites. Analysis by LA-ICP-MS shows that the trace elements present in gahnite are first-series transition metals (e.g., Ti, V, Cr, Co, Ni, and Cu) that substitute for Fe and Zn in the gahnite structure. Other elements commonly present include Mn, Li, Ga, Cd, Sn, and Pb. Gahnite in the Nine Mile deposit contains higher Ti, V, Cr, Co, Ni, and Pb and lower Mn, Li, Ga, Sn, and Cu than gahnite from granitic pegmatites. There is no information from other MMSDs for Cu, Pb, Sn, or Li. Gahnite in some of the most evolved pegmatites has among the lowest Ga contents. Gahnite from highly evolved granitic pegmatites of the Borborema Pegmatite Province has the highest Cu (up to 68 ppm), Mn (up to 8,819 ppm), Li (up to 376

ppm), and Zn (up to 43 wt.% ZnO) contents, and these compositions may be good indicators of Li-rich pegmatites. With further studies, the composition of gahnite can be potentially used to discriminate granitic pegmatites with Li-mineralization from barren or Li-poor granitic pegmatites and MMSDs.

2.1 INTRODUCTION

Gahnite, or zincian spinel ($ZnAl_2O_4$), is found as an accessory mineral in a variety of rock types including aluminous metasedimentary rocks, metabauxites, skarns, marbles, metamorphosed massive sulfide deposits (MMSDs), quartz veins, granites, and granitic pegmatites (Spry and Scott, 1986; Morris et al., 1997; Heimann et al., 2005). The chemistry of gahnite has been investigated extensively in MMSDs and its major element composition is used as an indicator for Pb-Zn mineralization (e.g., Spry and Scott, 1986). Recent studies have begun to investigate the trace element composition of gahnite in MMSDs to further examine gahnite as an exploration guide in these rocks (O'Brien et al., 2013).

Gahnite also occurs as an accessory mineral in granitic pegmatites but detailed studies on the major element chemistry of gahnite in pegmatites are very scarce and only two trace element studies of this kind exist in the literature (Merino et al., 2013; Neiva, 2013). Because gahnite is a weathering-resistant mineral that occurs in surficial sediments, its chemical composition can potentially be used in the search for source granitic pegmatites with high concentrations of strategic rare-metals such as Li. Previous studies have indicated that the composition of gahnite can be potentially used to distinguish granitic pegmatites from MMSDs from surficial sediments (Dunlop, 2000; Morris et al., 1997). However, the relationship between the chemical

composition of gahnite and the presence of rare-metal, and in particular Li, mineralization in granitic pegmatites is unknown.

In this study, the major and trace element chemistry of gahnite from granitic pegmatites from the United States (California, Maine, Maryland, and North Carolina) and other countries (Argentina, Brazil, Mozambique, and Poland) and the small late Paleoproterozoic Nine Mile Pb-Zn MMSD, Curnamona Province, Australia, were investigated. Single- and multiple-spot analysis and transects across gahnite crystals were performed to determine the major and trace element content of gahnite in granitic pegmatites and identify compositional differences among various types of pegmatites and between these and the Nine Mile deposit, and determine the relative degree of evolution of the pegmatites. Trace element compositions of gahnite obtained in this study and the limited data available from previous studies were used to identify chemical differences between gahnite in Li-rich and Li-poor pegmatites and in pegmatites *vs.* MMSDs.

2.2 SAMPLING AND ANALYTICAL METHODS

Samples of gahnite from 22 granitic pegmatites were acquired by colleagues in the field and from the museum collections at the Smithsonian Institution in Washington, D.C, and the American Museum of Natural History in New York. Hand samples of gahnite were also acquired from a colleague from the late Paleoproterozoic Nine Mile Pb-Zn MMSD, Australia. Thirty-two polished thick sections (200 μm) from the granitic pegmatite samples and five polished-thick sections from the Nine Mile MMSD were commercially obtained from Vancouver Petrographics (Canada). These thick sections were used to conduct petrographic analysis, scanning electron microscope analysis with energy-dispersive X-ray spectroscopy (SEM-EDS), electron microprobe (EMP) analysis, and laser ablation-inductively coupled plasma-mass

spectrometry (LA-ICP-MS) analysis. Electron microprobe analysis was conducted at the Smithsonian Institution in Washington, D.C., using a JEOL 8900 Superprobe electron microprobe, and at Fayetteville State University (FSU) using a JEOL JXA 8530F Hyperprobe electron microprobe. Operating conditions for the first instrument were an accelerating voltage of 15 kV, a beam current of 20 nA, and a beam diameter of 1 micrometer. Standards used for these analyses included Kakanui hornblende (K, Mg), gahnite (Zn), ilmenite (Fe, Ti), fluorite (F), garnet (Si, Al), manganite (Mn), apatite (Ca, P), and chromite (Cr). Operating conditions for the instrument at FSU were an accelerating voltage of 20 kV, a beam current of 10 nA, and a beam diameter of 3 and 10 micrometers. Standards used for these analyses included Astimex almandine garnet (Si, Mg, Fe), bustamite (Ca, Mn), sanidine (K), synthetic chromium oxide (Cr), synthetic rutile (Ti), and Smithsonian gahnite (Al, Zn). Major element contents were used as internal standards for LA-ICP-MS analysis to acquire trace element abundances of 49 elements (including Li, rare earth elements (REEs), Cs, Sn, Nb, Ta, Cu, Co, Ni, Cr, As, Sb, Ba, Se, and Cd, among others). The LA-ICP-MS analysis was performed as transects across grains in the same spots or close to spots analyzed by EMP. The analysis was conducted at the US Geological Survey in Denver, Colorado, using a quadrupole ICP-MS system (Perkin Elmer ELAN DRC) coupled to a 193 nm ArF excimer LA system (Photon Machines Analyte G2 with 2 volume cell). Helium was used as a carrier gas and the ICP-MS was optimized for Th/ThO of < 0.2 %. A spot size of 110 and 160 micrometers, an energy density (fluence) of 8 J/cm^2, and a repetition rate of 12 Hz were used for all analyses. A background measurement of 30 seconds, prior to and after ablation, and an ablation time of 60 seconds was used for each analysis. The external calibration reference material was USGS synthetic basaltic glass GSD-1g (Jochum et al., 2005). Aluminum was used as the internal standard element for concentration calculations using an average Al

content of 29 wt.% Al derived from EMP analyses and using concentration calculation and detection limit equations of Longerich et al. (1996). All data were screened for inclusions using visual inspection of each analysis. All concentrations are reported in parts per million. A total of four analytical days were performed comprising two to three sample rotations per day. Each sample rotation included up to four thick-sections and two 1-inch round polished sections. External calibrations were performed at the beginning of each sample rotation.

2.3 GAHNITE CHEMISTRY

A total of 893 EMP analyses and 571 LA-ICP-MS analyses (Tables 1, 2, and Appendix Table A1) were obtained. The information gained from previous studies was used to aid in the understanding of the occurrence and compositions of gahnite from the granitic pegmatites. Trace element chemistry of gahnite was used to evaluate possible discriminators for Li-rich and Li-poor pegmatites, as well as differences between gahnite in pegmatites and the Nine Mile MMSD. These are described below.

2.3.1 Major Element Compositions of Gahnite in Granitic Pegmatites

The chemical composition of gahnite from all the granitic pegmatites investigated ranges from 31.60 to 43.00 wt.% ZnO, 0.69 to 11.79 wt.% FeO, 0.00 to 0.99 wt.% MgO, and 0.14 to 1.11 wt.% MnO. Gahnite compositions are expressed and plotted in terms of spinel end members (in mol %) of gahnite (Ghn), hercynite (Hc), and spinel (Spl) (Fig. 1). Gahnite analyzed in the present study from all the pegmatites has a composition defined by the ranges $Ghn_{70.63\text{-}98.48}Hc_{0.95\text{-}28.61}Spl_{0.00\text{-}4.52}$ (Fig. 1; Table 1). These compositions fall within the field of gahnite in pegmatites previously defined by Spry and Scott (1986). Gahnite from the pegmatites

of the Borborema Pegmatite Province (BPP), Brazil, has the highest Zn contents and an overall formula given by $Ghn_{89.39-98.48}Hc_{0.95-9.13}Spl_{0.00-4.52}$. Within the BPP, gahnite from the Quintos pegmatite reaches the highest Zn contents (< 43.00 wt.% ZnO) and has the lowest Fe contents (0.69 wt.% FeO). Gahnite compositions from an unknown pegmatite of the Spruce Pine district, the BPP, and the Tourmaline King Mine of the Pala District, California, all contain greater than 89.39 mol % gahnite end-member. Gahnite from the Pulsifer and Greenlaw pegmatites of Maine exhibits the lowest Zn and highest Fe content of the studied pegmatites and has a composition defined by $Ghn_{70.63-75.63}Hc_{23.76-28.61}Spl_{0.41-1.27}$. Gahnite from the granitic pegmatites of the Pampean Pegmatite Province, Argentina, has compositions that fall in the middle range of all the compositions obtained and plots with gahnite from the Keith Quarry pegmatite, Maine, and Mocuba pegmatite, Mozambique. The highest Mg values are exhibited by some gahnite crystals from the Alto Mirador pegmatite in the BPP, which is reflected by a shift towards the spinel corner in the spinel ternary diagram. These gahnite have a composition defined by $Ghn_{91.35-97.05}Hc_{0.95-4.34}Spl_{0.95-4.52}$.

In the diagram of molecular (Fe+Mg)/Al *vs.* (Zn+Mn)/Al used by Batchelor and Kinnaird (1984) to visualize the substitutions in gahnite and the compositional evolution of the pegmatite melt, all the gahnite analyzed here define a linear trend with some slight deviations seen in the Capoeira 2, Alto Mirador, and Siedlimowice pegmatites (Fig. 2). For gahnite from all the granitic pegmatites the ranges of molecular (Zn+Mn)/Al are from 0.356 to 0.497, whereas the (Fe+Mg)/Al vary from 0.007 to 0.146. Gahnite from the BPP exhibits the highest molecular (Zn+Mn)/Al ratios, ranging from 0.448 to 0.497, while gahnite from the Pulsifer and Greenlaw pegmatites has the highest molecular (Fe+Mg)/Al ratios, ranging from 0.122 to 0.146 (Fig. 2). Gahnite from the Siedlimowice pegmatite, Poland, has higher molecular (Zn+Mn)/Al ratios,

ranging from 0.374 to 0.396, and lower molecular (Fe+Mg)/Al ratios, ranging from 0.108 to 0.132, than gahnite from the Pulsifer and Greenlaw pegmatites. Gahnite from the Argentina pegmatites has intermediate values of (Fe+Mg)/Al, ranging from 0.049 to 0.107, and (Zn+Mn)/Al, ranging from 0.391 to 0.460. Gahnite from the Spruce Pine pegmatite, NC, with compositions defined by (Zn+Mn)/Al values from 0.465 to 0.487 and (Fe+Mg)/Al ranging from 0.027 to 0.042, and gahnite from the Tourmaline King Mine, CA, with (Zn+Mn)/Al ratios from 0.459 to 0.477 and (Fe+Mg)/Al values from 0.024 to 0.034, have similar ratios as some gahnite from the BPP.

2.3.2 Major Element Compositions of Gahnite in the Nine Mile MMSD

The chemical composition of gahnite from the Nine Mile Pb-Zn MMSD, Australia, ranges from 25.35 to 34.23 wt.% ZnO, 7.60 to 15.59 wt.% FeO, 0.85 to 2.42 wt.% MgO, and 0.07 to 0.42 wt.% MnO (Table 1). Gahnite compositions are defined by the following end member ranges: $Ghn_{55.62\text{-}76.05}Hc_{17.47\text{-}37.34}Spl_{3.81\text{-}10.73}$ (Fig. 1; Table 1). These compositions are more enriched in Mg and Fe and have lower Zn and Mn contents than gahnite from the granitic pegmatites investigated (Fig. 1). This is reflected in the binary plot (Fig. 2) in which gahnite from the Nine Mile deposit plots with the highest molecular (Fe+Mg)/Al ratios (0.12 - 0.22) and lowest molecular (Zn+Mn)/Al values (0.28 - 0.39) of all gahnite analyzed. Gahnite in this deposit falls within the metamorphic field of gahnite previously defined by Batchelor and Kinnaird (1984).

2.3.3 Trace Element Chemistry of Gahnite

Gahnite hosted in granitic pegmatites and the Nine Mile MMSD have similar trace elements present (Table 2 and Appendix Table A1). Many trace elements present are the first-series transition metals (e.g., Ti, V, Cr, Co, Ni, and Cu) that substitute for Fe and Zn in the gahnite structure. The other elements commonly present include Li, Ga, Cd, Sn, and Pb. Lithium contents in gahnite from granitic pegmatites range from 0 to 441.36 ppm while in gahnite from the Nine Mile MMSD they range from 0 to 66.65 ppm Li (Table 2). Copper contents in gahnite from granitic pegmatites range from 8.39 to 85.89 ppm, while in the Nine Mile deposit they vary from 11.05 to 60.36 ppm. Vanadium and Co contents are much higher in gahnite from the Nine Mile MMSD, reaching 262.55 ppm V and 216.42 ppm Co, while only reaching 31.03 ppm V and 50.80 ppm Co in gahnite from granitic pegmatites. Gallium contents in gahnite from granitic pegmatites range from 154.29 to 583.60 ppm while in the Nine Mile MMSD they vary from 64.20 to 290.40 ppm. Tin contents in gahnite from granitic pegmatites are higher than in that from the Nine Mile MMSD, reaching 14.36 ppm, while only reaching 4.21 ppm in the Nine Mile MMSD. Other trace elements are mostly absent in gahnite or were below detection limits under the current analytical conditions. The REEs are mostly below detection limits but reach up to 3.77 ppm in Gd. Niobium, Cs, and Ta are also commonly below detection limits (<0.0107 ppm Nb; <0.0837 ppm Cs; <0.0503 ppm Ta) but do occasionally record values slightly above the detection limits.

2.4 DISCUSSION

Gahnite from worldwide localities of granitic pegmatites were investigated for trace element compositions. Because gahnite is abundant in MMSDs, the trace element composition

of gahnite from the Nine Mile MMSD, Australia, was also studied and compared with those of gahnite from granitic pegmatites. However, we note that gahnite in the Nine Mile deposit does not represent the compositional ranges of all MMSDs. Trace element analyses of gahnite from any rock type are extremely scarce and derived mainly from one study of a granitic pegmatite and a pluton (Merino et al., 2013), and one extended abstract of a study of gahnite in massive sulfide deposits (O'Brien et al., 2013). Therefore, these data were compiled and also included in the investigation. Below we first present information about trace elements in gahnite available from previous studies. Then we evaluate the major element composition of gahnite, discuss the significance for the degree of fractionation of the hosting pegmatite, and identify major and trace element differences between poorly fractionated and the most highly fractionated pegmatites. Further, trace element compositions of gahnite are used to identify elemental differences between gahnite in granitic pegmatites and MMSDs, and between Li-rich and Li-poor pegmatites. Finally, we present compositional ranges of gahnite indicative of Li-rich pegmatites.

2.4.1 Previous Trace Element Studies of Gahnite

Several studies detected the presence of trace elements during electron microprobe analysis but only two studies have investigated the trace element chemical composition of gahnite *in situ* by LA-ICP-MS analysis. Trace elements that have been detected in gahnite include the first-series transition metals (Ti, V, Cr, Mn, Co, Ni, Cu), Li, Ba, Ga, W, Cd, and Sn (Eskola, 1914; Pehram, 1948; Neiva et al., 1955; von Knorring and Dearnley, 1960; Hicks et al., 1985; Spry and Scott, 1986; Tindle and Breaks, 1998; Soares et al., 2007; Merino et al., 2010, 2013; Neiva, 2013; O'Brien et al., 2013). These studies include compositions of gahnite in either MMSDs, granitic pegmatites, or granitoids.

The earliest recorded analysis of gahnite in granitic pegmatites is that from a pegmatite vein near Träskböle in Perniö, Finland, which detected Ni (0.02 wt.% NiO) and Ti (trace TiO_2) (Eskola, 1914) by wet chemical analysis. A later analysis of gahnite in granitic pegmatites by EMP detected trace amounts of Li (0.03 ± 0.01 wt.% Li_2O), Cd (0.001 wt.% of CdO), and Be (0.01 wt.% of BeO) in a pegmatite near Kimito, Finland (Pehram, 1948). Neiva et al. (1955) analyzed gahnite from granitic pegmatites of Cabanas, Portugal, by EMP and found Sn-rich gahnite (up to 13.5 wt.% SnO_2) with trace amounts of Mn, Nb, Be, Sc, Ga, and Ge, but did not detect B, P, Ti, Ni, Co, Cu, and Cr. Analysis of gahnite from the South Harris Lewisian pegmatites by qualitative spectrographic analysis showed trace amounts of K, Li, Na, Rb, Ca, Ba, Cu, Be, Ga, Ti, and Cr (von Knorring and Dearnley, 1960). Recent studies analyzed gahnite from a granitic pegmatite from the Belvís de Monroy pluton, Spain, and the Namivo pegmatite, Mozambique, by LA-ICP-MS analysis (Merino et al., 2013; Neiva, 2013). Gahnite from the pegmatite of the Belvís de Monroy pluton, Spain, contains Li (63.00-74.55 ppm), Be (27.75-33.40 ppm), V (3.41-4.31 ppm), Co (39.20-41.55 ppm), Ta (0.06-10.00 ppm), and Pb (0.17-0.33 ppm) (Merino et al., 2013). Gahnite from the Namivo pegmatite, Mozambique, contains Sn (0-9.98 wt.% SnO_2), Ti (0-1.05 wt.% TiO_2), Nb (0-0.29 wt.% Nb_2O_5), and Ta (0-0.33 wt.% Ta_2O_5) (Neiva, 2013).

The presence and major element chemistry of zincian spinel is commonly used as an exploration guide for MMSDs (e.g., Spry and Scott, 1986; Heimann et al., 2005). A review of previous studies suggests that gahnite from MMSDs contains similar trace elements as those detected in pegmatites. Green and blue gahnite from the Namaqualand Metamorphic Complex, South Africa, analyzed by electron microprobe showed trace amounts of Ti (<0.4 wt.% TiO_2) (Hicks et al., 1985). Lesser values for Ti (0-0.04 wt.% TiO_2) were found in metamorphosed ore

deposits of Australia and Colorado (Spry and Scott, 1986; Heimann et al., 2005). The most extensive study on the trace element chemistry of gahnite from any rock type is that of O'Brien et al. (2013). The authors analyzed gahnite from different types of metamorphosed ore deposits to determine if the trace element chemistry could be used as a discriminator for various kinds of mineralization. Trace amounts of Ti (1-161 ppm), V (0-706 ppm), Cr (0-741 ppm), Mn (318-12,276 ppm), Co (1-145 ppm), Ni (0-62 ppm), Ga (62-1,275 ppm), and Cd (1-16 ppm) were recorded in gahnite from sedimentary exhalative (Sedex) deposits, volcanogenic massive sulfide (VMS) deposits, and Broken Hill-type (BHT) deposits (O'Brien et al., 2013). Gahnite from BHT deposits contains higher values of Ti (1-161 ppm), V (10-706 ppm), Cr (0-741 ppm), Co (12-145 ppm), and Cd (1-16 ppm) than gahnite from Sedex and VMS deposits. Gahnite from Sedex deposits has the highest values of Mn (up to 12,276 ppm), while gahnite from VMS deposits contains the highest Ni contents (up to 62 ppm) (O'Brien et al., 2013).

2.4.2 Major Element Variations in Gahnite from Granitic Pegmatites and Relative Pegmatite Evolution

On a ternary diagram of spinel based on the molecular proportions of major elements expressed as end members of gahnite, hercynite, and spinel, the major element composition of gahnite from granitic pegmatites from California (Tourmaline King Mine), Maine (Keith Quarry, Greenlaw, Pulsifer, and Lord Hill pegmatites), Maryland (Ben Murphy Mica Mine), North Carolina (Spruce Pine and Burleson Mica Mine), Borborema Pegmatite Province (BPP), Brazil (Alto Mirador, Alto do Giz, Boqueirão, Capoeira 2, Carrascão, and Quintos pegmatites), Poland (Siedlimowice pegmatite), Argentina (Magdalena, Sin Nombre, Nancy, La Ona, Blanca Dora, and Juan Román pegmatites), and Mozambique (Mocuba pegmatite), plots close to the Zn end

member and within the field of gahnite in granitic pegmatites of Batchelor and Kinnaird (1984) and Spry and Scott (1986; Fig. 3; Table 1). The chemical composition of gahnite in these pegmatites is defined by the following end member ranges: $Ghn_{70.63\text{-}98.48}Hc_{0.95\text{-}28.61}Spl_{0.00\text{-}4.52}$. Gahnite from pegmatites of the BPP has the highest Zn contents among all the studied pegmatites, and its composition is defined by $Ghn_{89.39\text{-}98.48}Hc_{0.95\text{-}9.13}Spl_{0.00\text{-}4.52}$, while gahnite from the Pulsifer pegmatite exhibits the lowest Zn and highest Fe contents and has a composition given by $Ghn_{70.63\text{-}75.63}Hc_{23.76\text{-}28.61}Spl_{0.61\text{-}1.27}$. A population of gahnite crystals from the Alto Mirador pegmatite, BPP, exhibits the highest Mg values among gahnite from all the studied pegmatites, with contents reaching up to 4.52 mol % spinel (0.99 wt.% MgO).

A plot of molecular (Fe+Mg)/Al *vs.* (Zn+Mn)/Al in gahnite can be used to indicate the degree of evolution of the pegmatite by an increase in the (Zn+Mn)/Al ratio and decrease in the (Fe+Mg)/Al ratio with increasing fractionation (Fig. 4; Batchelor and Kinnaird, 1984; Soares et al., 2007). Gahnite from the BPP exhibits the highest degree of fractionation evidenced by the highest molecular (Zn+Mn)/Al ratio of all gahnite from worldwide granitic pegmatites analyzed in this study. This is consistent with the highest Zn contents and corresponding highest Zn/Fe ratios (Fig. 3) measured in these pegmatites, the information derived from the chemistry of associated minerals, and the fact that these pegmatites are highly evolved, LCT (lithium, cesium, tantalum) pegmatites that contain Li and Ta mineralization (Soares et al., 2007, 2009). Gahnite from the Pulsifer and Greenlaw pegmatites of Maine exhibits the lowest (Zn+Mn)/Al and highest (Fe+Mg)/Al ratios of all gahnite from granitic pegmatites, reflecting the lowest degree of evolution of all the analyzed pegmatites. Gahnite from Argentina pegmatites reflects moderate pegmatite fractionation with intermediate ranges of (Zn+Mn)/Al and (Fe+Mg)/Al ratios. This is consistent with pegmatites of moderate chemical evolution that contain Be and Nb

mineralization but lacking Li, Cs, or Ta mineralization as well as intermediate Zn contents and Zn/Fe ratios (Fig. 3; Galliski, 1999a, b; Galliski and Černý, 2006; Galliski and Sfragulla, 2014). Trace element compositions may help understand the degree of pegmatite evolution and this is discussed below.

2.4.3 Trace Element Variations of Gahnite in Granitic Pegmatites

Trace element compositions of gahnite were investigated in granitic pegmatites worldwide and trace contents of Li, Ti, V, Cr, Mn, Co, Ni, Cu, Ga, Cd, Sn, and Pb were detected (Tables 2 and A1). Elemental diagrams were used to investigate chemical differences of gahnite in different kinds of pegmatites, as well as gahnite in pegmatites and the Nine Mile MMSD. Granitic pegmatites were classified as Li-rich pegmatites, Li-poor pegmatites, and pegmatites of unknown Li content based on the presence or absence of Li mineralization within the pegmatite bodies (e.g., spodumene, lepidolite, petalite, elbaite, amblygonite) (Table 3). Samples from poorly studied or unknown locations were grouped separately as pegmatites of unknown Li content. Below we discuss the variations of several trace elements in gahnite and their significance.

2.4.3.1 Lithium

Lithium is an incompatible element that is concentrated in the most fractionated granitic pegmatites (Černý et al., 1985; Černý, 1991; Černý and Ercit, 2005). In highly fractionated pegmatite melts, Li is commonly incorporated into aluminosilicate minerals (e.g., spodumene, lepidolite, petalite, and elbaite) and phosphates (e.g., amblygonite, montebrasite, lithiophilite,

and triphylite) (e.g., London, 2008). Lithium can also exist in trace amounts in feldspars and micas (e.g., London, 2008).

Lithium concentrations in gahnite analyzed in this study from granitic pegmatites range from 0 to 243.5 ppm and average 53.9 ppm. Gahnite from the Belvís de Monroy and Namivo pegmatites has Li contents within these limits (Merino et al., 2013; Neiva, 2013). It would be expected that gahnite with the highest Zn/Fe ratios and highest Zn contents would reflect the high Li content of fractionated pegmatites. A binary plot of Zn *vs.* Li was used to compare gahnite compositions in Li-rich and Li-poor pegmatites (Fig. 5). Gahnite from the BPP pegmatites has the highest Zn/Fe ratios and Zn contents and these are the most fractionated pegmatites from which gahnite was analyzed. Gahnite from the Pulsifer and Greenlaw pegmatites has the lowest Zn/Fe ratios and would be expected to contain lower amounts of Li than gahnite from the BPP. Intermediate Zn/Fe ratios in gahnite are expected to produce moderate Li contents in gahnite. However, in contrast to what would be expected to result from fractional crystallization, gahnite from the most fractionated pegmatites does not have higher Li contents than gahnite from poorly fractionated pegmatites. The reason for this is not yet fully understood and more detailed trace element studies of gahnite in granitic pegmatites are needed. We note, however, that Li-rich minerals have Li concentrations orders of magnitude higher than gahnite. For example, spodumene can contain up to 8.03 wt.% Li_2O, lepidolite up to 7.70 wt.% Li_2O, and elbaite up to 4.07 wt.% Li_2O. Even garnet may incorporate higher levels of Li than gahnite in granitic pegmatites (up to ~300 ppm; Heimann unpublished data). Therefore, Li in gahnite is a very minor element incompatible in its structure, as expected. Because gahnite in Li-rich and -poor pegmatites contains similar levels of Li (based on the data currently available) this element is not likely to be a good indicator of rare-metal mineralization in granitic pegmatites.

2.4.3.2 Copper

In granitic pegmatites of the LCT pegmatite family, Cu is known to occur primarily in sulfides (e.g., chalcopyrite) and in trace amounts in tourmaline (Černý, 1991; Černý and Ercit, 2005; Soares et al., 2008). The concentration of Cu in gahnite does not vary systematically among pegmatite types, except for gahnite in granitic pegmatites of the BPP, which also has the highest Cu contents of all studied samples (Fig. 6). Gahnite from the evolved BPP pegmatites has Cu contents that vary from 16.9 to 68.2 ppm, averaging 41.6 ppm, while in gahnite from the other studied pegmatites they range from 8.4 to 37.7 ppm and average 20.2 ppm. There seems to be a slight positive correlation between Cu and Mn contents (Fig. 6) among all studied gahnite crystals, except for gahnite from the Capoeira 2 pegmatite that deviates from the general trend. Tourmaline from the BPP also has elevated Cu contents compared to tourmaline from other granitic pegmatites (Soares et al., 2008). Therefore, the elevated Cu content of gahnite from the BPP reflects the higher concentration of Cu of these pegmatite melts compared to that of other granitic pegmatites. Because the highest Cu contents in gahnite are found in the most evolved pegmatites from the BPP that contain Li and Ta mineralization and their gahnite also has the highest Zn and Mn contents, Cu in gahnite may be used as a good exploration guide to differentiate gahnite derived from Li-rich and Li-poor pegmatites. The difference in Cu contents between gahnite in granitic pegmatites and the Nine Mile deposit is discussed in Section 2.4.4 below.

2.4.3.3 Manganese

In granitic pegmatites, Mn is concentrated in the melt as fractional crystallization proceeds (e.g., Černý et al., 1985; Soares et al., 2007). Manganese is commonly found as an important component in garnet, micas, tourmaline, oxides (magnetite, columbite group minerals, wodginite), and phosphates (e.g., triplite, triphylite-lithiophilite, graftonite-beusite, alluaudite). Manganese is usually the most abundant of the trace elements present in gahnite from granitic pegmatites, reaching up to 9,000 ppm, and substituting for Zn in the gahnite structure (Tulloch, 1981; Batchelor and Kinnaird, 1984; Soares et al., 2007). It is expected that gahnite from the most highly fractionated pegmatites will have the highest Mn contents, while gahnite from poorly evolved granitic pegmatites will have the lowest Mn concentrations. Pegmatites of the BPP are the most fractionated of the studied pegmatites, while gahnite from the Pulsifer, Greenlaw, and Siedlimowice pegmatites are the least fractionated, as indicated by the Zn/Fe ratios and Zn contents in gahnite (Table 1) and the mineralogy of the pegmatites. This is in agreement with the Mn values of gahnite from these pegmatites (Fig. 6). Gahnite from pegmatites of the BPP has the highest Mn contents (4,245.0 - 8,818.7 ppm Mn), while gahnite from the Pulsifer, Greenlaw, and Siedlimowice pegmatites has the lowest Mn concentrations (1,898.4 - 3,650.6 ppm Mn). Gahnite from Keith Quarry (Maine) and the Mozambique pegmatite, has Mn and Cu contents that overlap those from the other two Maine pegmatites and Siedlimowice pegmatite. Therefore, these trace element concentrations indicate a low degree of evolution for these pegmatites in which gahnite has moderate to low Zn contents and Zn/Fe ratios. We note however, that the Keith Quarry pegmatite contains Li minerals (spodumene, elbaite, pollucite, Li-micas; Wise and Brown, 2010) but gahnite has a low Mn content. The Keith Quarry is part of the complex Oxford pegmatite field from Maine that also includes the

Lord Hill, Greenlaw, and Pulsifer pegmatites (Wise et al., 2012). These pegmatites have a complex and unusual character that needs more detailed studies to clarify their true chemical nature. Gahnite in pegmatites from Argentina reflects moderate degrees of fractionation as noted by their Zn/Fe ratios and this is consistent with their intermediate Mn contents (2,381.2 - 5,415.4 ppm Mn). We note that Mn contents in gahnite from the unknown Spruce Pine pegmatite are medium to low, and the Cu contents are low and lower than in gahnite from the Burleson Mica Mine pegmatite (NC), which is consistent with the Spruce Pine pegmatite being interpreted as a muscovite-rare element pegmatite of low degree of evolution (Swanson and Veal, 2010). However, the Zn content is high in gahnite from both pegmatites, indicating that the Spruce Pine pegmatite is a complex pegmatite and that further detail studies of gahnite from North Carolina pegmatites will help elucidate the type of pegmatites and their relative degree of evolution. Manganese concentrations in gahnite from granitic pegmatites thus reflect the degree of evolution of the host pegmatite, and the highest Mn contents are characteristic of highly evolved pegmatites that contain rare-metal (Li, Ta) mineralization.

2.4.3.4 Gallium

Gallium is typically a minor element in granitic pegmatites of the LCT family (Černý et al., 1985; Černý, 1991; Černý and Ercit, 2005) and a common trace element in pegmatite minerals that contain Al^{3+} (e.g., feldspars, micas, beryl, tourmaline, garnet, petalite, eucryptite) (Černý et al., 1985). Previous studies suggest that Ga gradually increases with fractional crystallization replacing Al^{3+}, and its increase is paralleled by decreasing Al/Ga ratios (Černý et al., 1985; Černý, 1991; Černý and Ercit, 2005). However, the present understanding of the variations in Al/Ga ratios in various minerals and their relationship with pegmatite evolution is

very limited (Černý et al., 1985). Therefore, because gahnite is an aluminous mineral, this was investigated to determine if the Al/Ga ratio and Ga contents in this mineral may serve as an indication of evolution of the host pegmatites.

Gallium concentrations in gahnite from granitic pegmatites range from 154.3 to 570.3 ppm and average ~346.4 ppm, while Al/Ga ratios range from 516 to 1,872 (Table 2; Fig. 7). There is a negative correlation between Al/Ga ratios and the Ga content in gahnite, consistent with information for other pegmatite minerals (Černý et al., 1985) (Fig. 7). The Al/Ga ratio is lowest (down to 516) and Ga contents are highest (up to 514.60 ppm) in gahnite from granitic pegmatites of Maine (Pulsifer and Greenlaw) and Mozambique. Gahnite from the Ben Murphy Mica Mine, MD, Spruce Pine, NC, and the Nancy pegmatite, Argentina, has the highest Al/Ga ratios (>895 and up to 1,872) and lowest Ga contents (down to 154.29 ppm) of all the studied samples. The information gained from the Ga contents and Al/Ga ratios in gahnite shows that they do not reflect the degree of fractional crystallization of the pegmatite. Pegmatites of the BPP are the most fractionated of the studied pegmatites and are expected to have the highest Ga and lowest Al/Ga ratios. However, gahnite from these pegmatites has intermediate Ga contents and Al/Ga ratios. The same is true for gahnite from the least evolved pegmatites of Maine and Siedlimowice, which has some of the highest Ga contents and lowest Al/Ga ratios of the analyzed gahnite. This apparent random distribution of Ga contents and Al/Ga ratios in gahnite from pegmatites of varying degrees of fractionation may be related to large-scale metasomatic processes (albitization or muscovitization). Gahnite commonly succumbs to muscovitization in granitic pegmatites and this process may remove Ga that was initially present in its structure (Černý and Hawthorne, 1982). Alternatively, because other aluminous minerals that crystallize before or together with gahnite will incorporate Ga, their crystallization will change the amounts

available to enter gahnite and this may result in concentrations in gahnite that also reflect the partitioning among various phases and not only fractional crystallization. Studies of the partitioning of Ga among coexisting phases will help understand the significance of Al/Ga ratios and Ga contents for magmatic fluid evolution.

2.4.3.5 Transition Metals (Ti, V, Cr, Co, Ni, and Cd)

The majority of the trace elements present in gahnite from granitic pegmatites are the transition metals (Ti, V, Cr, Co, Ni, and Cd) (Table 2). These transition elements can be incorporated into the spinel structure based on stoichiometry. Gahnite has a spinel-type structure with the general formula AB_2O_4 where A represents the major divalent cations Zn^{2+}, Fe^{2+}, and Mg^{2+}, or a minor divalent cation such as Co^{2+}, Ni^{2+}, and Cd^{2+}, and B represents the major trivalent cation Al^{3+} or minor cations such as Fe^{3+}, Ti^{3+}, V^{3+}, and Cr^{3+} (Černý and Hawthorne, 1982; London, 2008; Nadoll et al., 2012). Many of these transition metals occur in variable concentrations in gahnite from granitic pegmatites. For example, Co contents range from 0 to 50.80 ppm, with the highest values being from gahnite in the Ben Murphy Mica Mine (32.29 - 39.88 ppm Co), a poorly evolved pegmatite (Bernstein, 1976). Cadmium is as widely varied as Co in gahnite from granitic pegmatites, ranging from 0 to 42.09 ppm. Gahnite from the Quintos pegmatite in the BPP records the highest Cd values (up to 42.09 ppm) and mean (20.47 ppm) of all the studied samples. All of the analyses of gahnite from Quintos record values greater than 11.14 ppm Cd, except for two points which recorded 0 and 3.68 ppm. This is not surprising since Cd is known to substitute for Zn in the structure of sphalerite and the same is expected in gahnite (e.g., Ross, 1937; Tindle and Breaks, 1998). Nickel is not as variable as Co or Cd in gahnite from granitic pegmatites in which it reaches up to 16.47 ppm. The highest average Ni

values are in gahnite from the La Ona pegmatite (0 - 14.26 ppm, mean = 4.74 ppm), whereas the lowest are from the Lord Hill pegmatite, in which all the analyses record values below detection limits, except for one point which recorded 5.97 ppm. Titanium is the most variable transition metal present in gahnite from granitic pegmatites. In most analyses, Ti was not detected or was below detection limits but when present it ranges from 6.14 to 63.22 ppm. Gahnite from the Siedlimowice pegmatite records the second highest Ti value (62.38 ppm) and the highest Ti mean (14.13 ppm). All of the analyses of gahnite from Alto Mirador record values less than detection limits for Ti, except for two points which recorded 8.83 and 7.80 ppm. Similarly, gahnite from the Tourmaline King, recorded values below detection limits except for two points which have 9.93 and 16.11 ppm. Chromium is consistently low in gahnite from granitic pegmatites with values reaching up to 10.02 ppm in the Burleson Mica Mine pegmatite and averaging 2.25 ppm. Vanadium is low in gahnite from granitic pegmatites, with values reaching up to 28.05 ppm in the unknown Spruce Pine pegmatite and the majority being lower than 10 ppm. Gahnite from the unknown Spruce Pine pegmatite exhibits the highest V values near an intergrowth with muscovite (16.14 - 28.05 ppm V). Due to the transition metals occurring in variable and low to absent concentrations in gahnite from granitic pegmatites, these elements are not likely to be good indicators of rare-metal mineralization in granitic pegmatites.

2.4.4 Comparison with Gahnite in Metamorphosed Massive Sulfide Deposits

Compositions of gahnite from the small late Paleoproterozoic Broken Hill-type Pb-Zn Nine Mile MMSD were compared with those of gahnite from granitic pegmatites. Elements analyzed previously in gahnite from MMSDs (O'Brien et al., 2013) were included in the comparison, but not all elements were available. The Zn *vs.* Li binary plot was used to compare

the compositions of gahnite in Li-rich and Li-poor pegmatites as well as gahnite in pegmatites with those from the Nine Mile MMSD (Fig. 8). Lithium is present in both rock types but is expected to be higher in gahnite from granitic pegmatites. Fractional crystallization would allow for crystallizing gahnite to incorporate the available Li after removal by major Li carriers. This gahnite is expected to incorporate more Li than that in MMSDs, in which gahnite is expected to have low Li contents because the mechanism that concentrates Li in granitic pegmatites is absent during the genesis of these deposits. Indeed, gahnite from granitic pegmatites contains more Li (6.24 to 243.45 ppm) than gahnite from the Nine Mile MMSD (0.00 to 59.30 ppm Li) (Fig. 8). However, Li contents are not available for gahnite from other MMSDs and these data are needed to accurately describe compositional differences.

Gahnite from granitic pegmatites and the Nine Mile MMSD has a similar minimum Cu content (~18 ppm; Figs. 6, 9, 10). However, gahnite from Li-rich pegmatites and gahnite in one sample of the Nine Mile MMSD generally displays higher Cu values than gahnite in Li-poor pegmatites. The highest Cu contents in gahnite reach 68.22 ppm in Li-rich pegmatites, 60.36 ppm in the Nine Mile MMSD, and 37.71 ppm in Li-poor pegmatites. We note that Cu contents in gahnite from other MMSDs are not available, and more data are needed to identify any significant compositional differences in gahnite from both rock types.

In the majority of Li-rich pegmatites gahnite has higher Zn and Mn contents than in Li-poor pegmatites and the Nine Mile MMSD (Figs. 5, 6, 8-10). Exceptions are the Pulsifer and Greenlaw Li-rich pegmatites of Maine in which gahnite has lower Zn and Mn contents than in the other Li-rich pegmatites. A combination of high Zn (> 315,000 ppm) and Cu (40 ppm) contents is typical of gahnite in Li-rich pegmatites, and a combination of high Zn (> 275,000 ppm) and Li (> 60 ppm) contents is characteristic of gahnite from granitic pegmatites and not of

MMSDs (Figs. 8, 9). We note that gahnite in other MMSDs also reaches high Zn contents, and this element alone is not an indication of Li-rich granitic pegmatites. However, if the relationships among Li and Zn, and Zn and Cu in gahnite shown here are valid after more data from MMSDs become available, these can potentially become good indicators for the presence of Li mineralization in granitic pegmatites.

Gallium is higher in gahnite from granitic pegmatites than in the Nine Mile MMSD (Fig. 10). However, previously studied gahnite from various types of MMSDs contains higher Ga than gahnite from granitic pegmatites (Fig. 12; O'Brien et al., 2013). Therefore, it seems that Ga cannot be used to distinguish gahnite in granitic pegmatites from that in MMSDs.

Gahnite from the Nine Mile MMSD has higher values of Ti, V, Co, Ni, and Pb than gahnite from granitic pegmatites. These elements are typically present in trace amounts in granitic pegmatites, whereas in the Nine Mile and other MMSDs these elements reach higher concentrations. Many of these elements record similar ranges in various types of MMSDs (O'Brien et al., 2013). Due to the mineralogy of the Nine Mile MMSD rocks, consisting mostly of quartz and gahnite, many of these elements are not incorporated into quartz but in gahnite, and probably into minor phases such as ilmenite. These elements also reflect the composition of the hydrothermal fluids that formed these deposits, which leached these elements from underlying rocks. In contrast, these elements are compatible elements in magmas and are expected to be low in the evolved melts that form granitic pegmatites.

2.4.5 Chemistry of Gahnite in Li-Rich and Li-Poor Pegmatites

Even though we classified granitic pegmatites as Li-rich and Li-poor, the division is subjective due to various degrees of Li mineralization present in different pegmatites. On the

other hand, major and trace element contents in gahnite may help determine the nature of some pegmatites that are of doubtful or unknown classification. Numerous plots were created to identify combinations of elements that can be used as discriminators towards Li mineralization in granitic pegmatites.

Several trace elements, including Ti, V, Cr, Co, Ni, Cd, and Pb, do not vary between Li-rich and Li-poor pegmatites. These elements could possibly be useful in the future as more work is performed on gahnite from other granitic pegmatites but at the time of this study are not valuable discriminatory elements. Gahnite in the majority of the Li-rich pegmatites has similar Li values (7.25 to 191.46 ppm) as that in Li-poor pegmatites (0.00 to 243.45 ppm) (Figs. 5, 8). Lithium may be useful with additional data and revision of the Li classification for some pegmatites for which not enough information is available, including the Argentina pegmatites, the Poland pegmatite, the Pulsifer, Greenlaw, and Lord Hill pegmatites from Maine, and the unknown pegmatite from Spruce Pine, and this is discussed below. The elements that may be useful, including Zn, Fe, Mn, Mg, Ga, and Al were used in the construction of discriminant diagrams.

A ternary diagram of molecular % of Ga x100 - Zn/10 - Fe separates gahnite in Li-rich pegmatites from those in Li-poor pegmatites with minimal overlap (Fig. 11). The Li-rich pegmatite field is defined by lower Fe and slightly higher Ga ranges compared with the Li-poor pegmatite field, which is characterized by higher Fe and lower Ga than in the Li-rich pegmatite field. Gahnite analyses from Li-poor pegmatites that overlap the Li-rich pegmatite field are from the Siedlimowice and Lord Hill pegmatites. Based on the composition of gahnite, this pegmatite seems to have a chemical affinity with Li-rich pegmatites, and this merits further investigation. The Siedlimowice pegmatite is classified as an LCT family pegmatite (Szuskiewicz and Łobos,

2004; Janeczek, 2007) and the Lord Hill pegmatite is considered a mixed NYF-LCT (niobium, yttrium, fluorine; classification of Černý, 1991) family pegmatite (Wise and Brown, 2010). On the other hand, gahnite from the Li-rich pegmatite field that contains the highest Fe and lowest Zn belongs to the Greenlaw and Pulsifer pegmatites of Maine. Gahnite from these pegmatites has compositions that overlap with those of gahnite from the Li-poor pegmatites of Siedlimowice and Lord Hill. The Lord Hill, Greenlaw, and Pulsifer pegmatites are part of the Oxford pegmatite field (Wise et al., 2012). Therefore, the composition of gahnite in these pegmatites from Maine also reflects their complex nature and both a Li-rich and -poor signature within the field, and detailed studies of each pegmatite will help clarify their true chemical character.

A binary plot of Ga (ppm) *vs.* Zn (ppm) shows that gahnite from Li-rich pegmatites has higher Ga contents for a given Zn value than that from Li-poor pegmatites (Fig. 12). Therefore, the Li-rich pegmatite field is located towards higher Ga values compared with the Li-poor pegmatite field. An overall negative correlation exists between Ga and Zn contents in gahnite, and Li-rich and -poor pegmatites define two parallel fields with some overlap. Gahnite from Li-rich pegmatites plots in three small clusters that correspond to pegmatites from the BPP, Greenlaw and Pulsifer pegmatites, and the Keith Quarry pegmatite. Gahnite from the BPP pegmatites has the lowest Ga and highest Zn contents of all gahnite from Li-rich pegmatites. Gahnite from the Greenlaw and Pulsifer pegmatites has intermediate Ga and Zn contents, while gahnite from the Keith Quarry pegmatite displays the highest Ga and lowest Zn contents of the Li-rich pegmatites (Fig. 12). Therefore, again, gahnite in the Pulsifer and Greenlaw pegmatites seems to reflect a low degree of evolution. Gahnite from the unknown pegmatite and the Burleson Mica Mine, both from the Spruce Pine district, has the highest Zn contents of the Li-poor pegmatites and they overlap the field defined for Li-rich pegmatites. Gahnite from the

Burleson Mica Mine displays slightly higher Ga and lower Zn contents than gahnite from the unknown pegmatite of the Spruce Pine district. The observation that gahnite in some of the most evolved pegmatites has some of the lowest Ga contents seems to contradict the idea that Ga contents increase with magmatic differentiation. Alternatively, this may reflect overprint of Al-rich fluids at the end of the crystallization process. Detailed studies of gahnite, as well as of other pegmatite minerals are needed to understand the behavior of Ga and Al in pegmatite melts.

2.5. CONCLUSIONS

The major element compositions of gahnite from granitic pegmatites investigated here, expressed as end members of gahnite, hercynite, and spinel, are defined by $Ghn_{70.63\text{-}98.48}Hc_{0.95\text{-}28.61}Spl_{0.00\text{-}4.52}$. Major element compositions show that gahnite from the granitic pegmatites of the BPP exhibits the highest degree of evolution. Within the BPP, gahnite from the Quintos pegmatite has the highest Zn contents and a population of gahnite from the Alto Mirador pegmatite has the highest Mg contents. Gahnite from the Pulsifer and Greenlaw pegmatites of Maine reflects the lowest degree of evolution, as indicated by the highest Fe contents and (Fe+Mg)/Al ratios. Gahnite from the remaining pegmatites plot with intermediate values and indicate intermediate degree of melt evolution between that of the BPP and the Pulsifer and Greenlaw pegmatites. Gahnite in Li-rich and -poor pegmatites defines the following compositional ranges: $Ghn_{70.63\text{-}98.48}Hc_{0.95\text{-}28.61}Spl_{0.00\text{-}4.52}$ and $Ghn_{73.66\text{-}95.12}Hc_{4.64\text{-}25.87}Spl_{0.00\text{-}3.37}$, respectively.

Major and trace element chemical compositions of gahnite in granitic pegmatites were evaluated to understand relative pegmatite fractionation, identify elements that can be used as indicators of Li mineralization, and distinguish gahnite in MMSDs and granitic pegmatites.

Many trace elements in gahnite do not vary systematically from Li-rich to Li-poor pegmatites but Zn, Fe, Mn, Mg, Ga, and Al, and possibly Cu and Li, do vary as expected between these types. Lithium concentrations in gahnite from granitic pegmatites range from 0 to 243.5 ppm (average 53.9 ppm) and do not vary systematically among various types of pegmatites or do not clearly reflect pegmatite evolution. However, because Li concentrations are higher in granitic pegmatites than in MMSDs, this is reflected in the composition of gahnite. In granitic pegmatites it contains more Li (0.0 - 243.5 ppm) than in the Nine Mile MMSD (0.0 - 59.3 ppm Li). Because no Li contents are available from other MMSDs further studies of gahnite in these rocks are needed to provide exploration guides in the search for MMSDs and granitic pegmatites that may host rare-metal mineralization.

Copper concentrations are also similar in various granitic pegmatites except for gahnite from the BPP which has the highest Cu contents (68.2 ppm). Gahnite from these pegmatites reflects the generally high Cu content of the pegmatites as also evidenced by the elevated Cu concentrations in tourmaline. Gahnite with concentrations of Cu higher than 30 ppm and Mn higher than 4,200 ppm may be good indicators of the presence of Li-rich pegmatites in covered areas. However, we note that Cu contents in gahnite from MMSDs are not available, and in Cu-rich deposits, Cu contents in gahnite can be expected to be as high as in granitic pegmatites. Therefore, even though Cu contents in gahnite crystals will likely help distinguish highly evolved, Li-rich pegmatites from Li-poor pegmatites, exploration guidelines to differentiate gahnite from granitic pegmatites and MMSDs cannot be defined at this point and until further investigations of gahnite in MMSDs are available.

Gahnite from the most highly fractionated pegmatites of the BPP reflects the increase in Mn with the progress of fractional crystallization by containing the highest values of Mn (up to

8,818.7 ppm). The same is shown by gahnite in the least fractionated pegmatites, the Pulsifer, Greenlaw, and Siedlimowice pegmatites, which have the lowest Mn contents (1,898.4 - 3,650.6 ppm Mn). Manganese concentrations in gahnite thus reflect the degree of fractionation of the host pegmatite. Therefore, Mn contents in gahnite higher than ~4,200 ppm may be used as an indication of the presence of evolved, Li-bearing pegmatites in covered areas. However, Mn does not help discriminate gahnite from pegmatites and MMSDs.

Gallium in gahnite from granitic pegmatites ranges from 154.3 ppm to 570.3 ppm, while Al/Ga ratios range from 516 to 1,872. Gahnite from the Ben Murphy Mica Mine, Spruce Pine, and the Nancy pegmatites has the highest Al/Ga ratios and lowest Ga contents. Pegmatites of the BPP are considered the most highly fractionated of the studied pegmatites and are expected to have the highest Ga and lowest Al/Ga ratios in gahnite. Instead, their gahnite has intermediate values and there is an overall random abundance of these elements in gahnite in all the pegmatites. Therefore, either these elements in gahnite do not reflect the degree of fractionation of the granitic pegmatites because their behavior is still unknown, or their distribution may be related to late metasomatic processes such as albitization or muscovitization.

A ternary diagram of Ga x100 - Zn/10 - Fe in gahnite revealed a compositional separation between Li-rich and Li-poor pegmatites with a slight overlap. The overlap includes gahnite from the mixed (LCT-NYF) Lord Hill pegmatite, the LCT Siedlimowice pegmatite, and the Greenlaw and Pulsifer pegmatites. The Greenlaw and Pulsifer pegmatites are spatially related to the mixed type (LCT-NYF) Lord Hill pegmatite and may also include an NYF component, and this likely explains the observations. A diagram of Ga (ppm) *vs.* Zn (ppm) shows a negative correlation between the two elements and separates gahnite in Li-rich pegmatites and -poor pegmatites. Gahnite from pegmatites of the Li-poor Spruce Pine district plots with the highest Zn and lowest

Ga contents and overlaps the Li-rich pegmatite field. However, due to the lack of exact information of the origin of this sample this needs to be taken with caution as the sample may be derived from a Li-rich pegmatite. Gallium contents are higher in gahnite from granitic pegmatites than in that from MMSDs but previous studies have found similar values of Ga in the latter. Therefore, Ga alone does not help discriminate between gahnite in the two geologic settings.

The trace elements present in gahnite in granitic pegmatites include Li, the transition metals Ti, V, Cr, Co, Ni, and Cd, as well as Mn, Cu, Ga, and Pb. Gahnite from granitic pegmatites has variable Ti, Co, and Cd contents. Cadmium has variable concentration in gahnite from granitic pegmatites (0 - 42.09 ppm) but it is highest in gahnite from the Quintos pegmatite in the BPP (up to 42.09 ppm). Gahnite from the Siedlimowice pegmatite records the highest Ti values, and Co is highest in the Ben Murphy Mica Mine. Nickel is less variable and is highest in the La Ona pegmatite (0 - 14.26 ppm). Chromium is low in gahnite from granitic pegmatites, reaching concentrations up to 28.05 ppm with the majority containing less than 10 ppm. Vanadium is low to absent from the majority of the samples except for several analyses at the edge of gahnite in contact with muscovite. Gahnite from the Nine Mile MMSD has higher concentrations of Ti, V, Co, Ni, and Pb than gahnite from granitic pegmatites. However, this is not the case in gahnite from other MMSDs. This is due to the composition of the hydrothermal fluids that formed the deposits and the fact that they are mostly compatible elements in magmas and reach very low levels at the pegmatite stage. These elements do not seem to serve as indicators of Li content of the pegmatite and do not discriminate gahnite in granitic pegmatites from MMSDs.

This study shows that trace element contents in gahnite in granitic pegmatites may be used to understand relative pegmatite evolution and may even help elucidate the chemical nature of pegmatites of unknown, complex, or mixed type. Some elements are also useful indicators to distinguish gahnite in granitic pegmatites that contain Li-mineralization from barren pegmatites. Further studies of gahnite in MMSDs are needed to identify chemical differences in gahnite in these two different geologic settings. As expected, the major and trace chemistry of gahnite reflects that of the host rock, as well as the partitioning of elements among coexisting phases.

ACKNOWLEDGEMENTS

Funding for this project was provided by the USGS Mineral Resources External Research Program (# G10AP00051) and East Carolina University Thomas Harriot College of Arts and Sciences and Research and Graduate Studies to AH, and Society of Economic Geologists Hugh E. McKinstry Fund and Grant-in-Aid of Research from Sigma Xi, The Scientific Research Society, to JY. We thank Nick Foster for help with the EMP analyses, Tom Fink for help with SEM analysis, and Alan Koenig for help with LA-ICP-MS analyses. We thank David London for fruitful discussions. Some EMP analyses were performed by Josh Bitner. Comments from Terri Woods helped improve the manuscript.

REFERENCES

Batchelor, R., and Kinnaird, J., 1984. Gahnite compositions compared: Mineralogical Magazine, v. 48, p. 425-429.

Bernstein, L. R., 1976. Minerals of Washington, D.C. and vicinity: U. S. Geological Survey Open File Report 76-849, 205 p.

Černý, P., Meintzer, R. E., and Anderson, A. J., 1985. Extreme fractionation in rare-element granitic pegmatites: selected examples of data and mechanisms: Canadian Mineralogist, v. 23, p. 381-421.

Černý, P., 1991. Rare element granitic pegmatites: Part 1: Anatomy and internal evolution of pegmatite deposits: Geoscience Canada, v. 18, p. 49-67.

Černý, P., and Hawthorne, F. C., 1982. Selected peraluminous minerals: MAC Short course handbook, p. 163-186.

Černý, P., and Ercit, T. S., 2005. The classification of granitic pegmatites revisited: Canadian Mineralogist, v. 43, p. 2005-2026.

Dunlop, S. D., 2000. Gahnite from metamorphosed massive sulphide deposits and rare-element pegmatites: Development of discriminators based on bedrock and overburden samples. M.Sc. thesis: Laurentian University, 169 p.

Eskola, P., 1914. An occurrence of gahnite in pegmatite near Träskböle in Perniö, Finland: Geologiska Föreningen i Stockholm Förhandlingar, v. 36, p. 25-30.

Galliski, M. A., and Černý, P., 2006. Geochemistry and structural state of columbite-group minerals in granitic pegmatites of the Pampean Ranges, Argentina: The Canadian Mineralogist, v. 44, p. 645-666.

Galliski, M. A., and Sfragulla, J., 2014. Las pegmatitas graníticas de las sierras de Córdoba. 19th Congreso Geológico Argentino, Relatorio. p. 365-388.

Galliski, M. A., 1999a. Distrito pegmatítico Comechingones, Córdoba: Recursos Minerales de la República Argentina (Ed. E.O. Zappettini), Instituto de Geología y Recursos Minerales SEGEMAR, v. 35, p. 361-364.

Galliski, M. A., 1999b. Distrito pegmatítico Conlara, San Luis: Recursos Minerales de la República Argentina (Ed. E.O. Zappettini), Instituto de Geología y Recursos Minerales SEGEMAR, v. 35, p. 365-368.

Heimann, A., Spry, P., and Teale, G., 2005. Zincian spinel associated with metamorphosed Proterozoic base-metal sulfide occurrences, Colorado: A re-evaluation of gahnite composition as a guide in exploration: Canadian Mineralogist, v. 43, p. 601-622.

Heimann, A., Yonts, J., and London, D., in preparation. The composition of gahnite in felsic dikes as reflection of pegmatitic melt evolution: evidence from two new occurrences, Pala Chief and Elizabeth R layered dikes, California.

Hicks, J. A., Moore, J. M., and Reid, A. M., 1985. The co-occurrence of green and blue gahnite in the Namaqualand Metamorphic Complex, South Africa: Canadian Mineralogist, v. 23, p. 535-542.

Janeczek, J., 2007. Intragrantiic pegmatites of the Strzegom-Sobótka massif – an overview: Granitoids in Poland, AM Monograph No. 1, p. 193-201.

Jochum, K. P., Willbold, M., Raczek, I., Stoll, B. and Herwig, K., 2005. Chemical Characterisation of the USGS reference glasses GSA-1G, GSC-1G, GSD-1G, GSE-1G, BCR-2G, BHVO-2G and BIR-1G using EPMA, ID-TIMS, ID-ICP-MS and LA-ICP-MS: Geostandards and Geoanalytical Research, v. 29, p. 285–302.

London, D., 2008. Pegmatites: Canadian Mineralogist Special Publication 10, 347 p.

Longerich, H. P., Jackson, S. E., and Günther D., 1996. Laser ablation inductively coupled plasma mass spectrometric transient signal data acquisition and analyte concentration calculation: Journal of Analytical Atomic Spectrometry, v. 11, p. 899-904.

Merino, E., Villaseca, C., Pérez-Soba, C., and Orejana, D., 2010. First occurrence of gahnite and chrysoberyl in an Iberian Hercynian pluton: the Belvís de Monroy Granite (NE Cáceres, Spain): Revista de la Sociedad Española de Mineralogía, p. 159-160.

Merino, E., Villaseca, C., Orejana, D., Jeffries, T., 2013. Gahnite, chrysoberyl and beryl co-occurrence as accessory minerals in a highly evolved peraluminous pluton: The Belvís de Monroy leucogranite (Cáceras, Spain): Lithos, v. 179, p. 137-156.

Morris, T. F., Breaks, F. W., Averill, S. A., Crabtree, D. C., and McDonald, A., 1997. Gahnite composition: Implications for base metal and rare-element exploration: Exploration and Mining Geology, v. 6, p. 253-260.

Nadoll, P., Mauk, J. L., Hayes, T. S., Koenig, A. E., and Box, S. E., 2012. Geochemistry of magnetite from hydrothermal ore deposits and host rocks of the Mesoproterozoic Belt Supergroup, United States: Economic Geology, v. 107, p. 1275-1292.

Neiva, J. M. O., Rimsky, A., Sandréa, A., 1955. Sur une variété de gahnite stannifère de Cabanas (Portugal): Bulletin de la Société Française de minéralogie et de cristallographie, v. 78, p. 97-105.

Neiva, A. M. R., 2013. Micas, feldspars and columbite–tantalite minerals from the zoned granitic lepidolite-subtype pegmatite at Namivo, Alto Ligonha, Mozambique: European Journal of Mineralogy, v. 25, p. 967-985.

O'Brien, J., Spry, P., Teale, G., Jackson, S., and Rogers, D., 2013. Major and trace element chemistry of gahnite in metamorphosed massive sulphide deposits: discrimination diagrams to determine provenance: 26th International Applied Geochemistry Symposium Application of Indicator Mineral Methods to Mineral Exploration, Short Course SC07, p. 29-34.

Pehram, G., 1948. Gahnit von Rosendal auf Kimito, SW-Finland: Bulletin of the Geological Istitution of the University of Uppsala, v. 32, p. 329-336.

Ross, C., 1937. Sphalerite from a pegmatite near Spruce Pine, North Carolina: American Mineralogist, v. 22, p. 643-650.

Soares, D. R., Beurlen, H., Ferreira, A. C. M., and Da-silva, M. R. R., 2007. Chemical composition of gahnite and degree of pegmatitic fractionation in the Borborema Pegmatitic Province, northeastern Brazil, Anais da Academia Brasileira de Ciências, v. 79, p. 395-404.

Soares, D. R., Beurlen, H., de Brito Barreto, S., Silva, M. R. R., and Ferreira, A.C.M., 2008. Compositional variation of tourmaline-group minerals in the Borborema Pegmatite Province, northeastern Brazil: Canadian Mineralogist, v. 46, p. 1097-1116.

Soares, D. R., Beurlen, H., Ferreira, A.C.M., Gomes, M. M. C., Barreto, S. B., and Anastácio, E. M., 2009. Elevated zinc contents in elbaites from pegmatites of the Borborema Pegmatite Province, NE Brazil: Estudos Geológicos, v. 19, p. 348-351.

Spry, P. G., and Scott, S. D., 1986. The stability of zincian spinels in sulfide systems and their potential as exploration guides for metamorphosed massive sulfide deposits: Economic Geology, v. 81, p. 1446-1463.

Swanson, S. E., and Veal, W. B., 2010. Mineralogy and petrogenesis of pegmatites in the Spruce Pine District, North Carolina, USA: Journal of Geosciences, p. 27-42.

Szuskiewicz, A., and Łobos, K., 2004, Gahnite from Siedlimowice, Strzegom-Sobótka granitic massif, SW Poland: Mineralogia Polonica, v. 35, p. 15-21.

Tindle, A. G., and Breaks, F. W., 1998. Oxide minerals of the Separation Rapids rare-element granitic pegmatite group, northwestern Ontario: Canadian Mineralogist, v. 36, p. 609-635.

Tulloch, A. J., 1981. Gahnite and columbite in an alkali-feldspar granite from New Zealand: Mineralogical Magazine, v. 44, p. 275-278.

von Knorring, O. and Dearnley, R., 1960. The Lewisian pegmatites of South Harris, Outer Hebrides: Mineralogical Magazine, v. 32, p. 366-378.

Wise, M. and Brown, C., 2010. Mineral chemistry, petrology and geochemistry of the Sebago granite-pegmatite system, southern Maine, USA: Journal of Geosciences, v. 55, p. 3-26.

Wise, M., Francis, C. A., and Černý, P., 2012. Compositional and structural variations in columbite-group minerals from granitic pegmatites of the Brunswick and Oxford fields, Maine: differential trends in F-poor and F-rich environments: Canadian Mineralogist, v. 50, p. 1515-1530.

Captions to Figures

Figure 1. Ternary diagram of spinel in terms of gahnite (Ghn, Zn), hercynite (Hc, Fe), and spinel (Spl, Mg) end members (mol %) showing the composition of gahnite in granitic pegmatites and the Nine Mile MMSD, Australia, obtained in this study. After Batchelor and Kinnaird (1984). Only the top 50 % of the diagram is shown (gahnite end member). Squares denote Li-rich pegmatites, circles Li-poor pegmatites, rhombs pegmatites with an unknown Li content, and triangles the Nine Mile MMSD.

Figure 2. Binary diagram in terms of molecular $(Fe^{2+}+Mg)/Al$ *vs.* (Zn+Mn)/Al showing the composition of gahnite in granitic pegmatites and the Nine Mile MMSD, Australia. After Batchelor and Kinnaird (1984). Symbols as in Fig. 1.

Figure 3. Compositions of gahnite from worldwide granitic pegmatites analyzed in the present study expressed in terms of mol % gahnite (Ghn), hercynite (Hc), and spinel (Spl) end members. Only the top 30 % of the diagram is shown (gahnite end member). Symbols as in Fig. 1.

Figure 4. Binary diagram showing the composition of gahnite from worldwide granitic pegmatites analyzed in the present study in terms of molecular (Fe+Mg)/Al *vs.* (Zn+Mn)/Al. After Batchelor and Kinnaird (1984). Symbols as in Fig. 1.

Figure 5. Binary diagram of gahnite from worldwide granitic pegmatites in terms of Zn *vs.* Li in parts per million (ppm). Symbols as in Fig. 1.

Figure 6. Binary diagram of gahnite compositions from worldwide granitic pegmatites in terms of Mn *vs.* Cu (ppm). Symbols as in Fig. 1.

Figure 7. Binary diagram of Ga (ppm) *vs.* Al/Ga (calculated from ppm) in gahnite from worldwide granitic pegmatites and the Nine Mile deposit. Symbols as in Fig. 1.

Figure 8. Binary diagram of Zn *vs.* Li (ppm) for gahnite in granitic pegmatites and the Nine Mile MMSD. [1]Zinc range from Heimann et al. (2005). Squares denote Li-rich pegmatites, circles Li-poor pegmatites, rhombs pegmatites with an unknown Li content, and triangles the Nine Mile MMSD.

Figure 9. Binary diagram of Zn *vs.* Cu (ppm) for gahnite in granitic pegmatites (Li-rich, -poor, and of unknown content) and the Nine Mile MMSD. [1]Zinc range from Heimann et al. (2005). Symbols as in Fig. 8.

Figure 10. Binary diagram of Mn *vs.* Cu (ppm) for gahnite in granitic pegmatites and the Nine Mile MMSD. [2]Manganese range from O'Brien et al. (2013). Symbols as in Fig. 8.

Figure 11. Ternary diagram of gahnite compositions in granitic pegmatites and the Nine Mile MMSD obtained in this study in terms of Ga x100, Zn/10, and Fe. Symbols as in Fig. 8.

Figure 12. Binary diagram of gahnite compositions from worldwide granitic pegmatites in terms of Ga *vs.* Zn (ppm). [1]Zn range from Heimann et al. (2005) and [2]Ga from O'Brien et al. (2013). Symbols as in Fig. 8.

Table Headings

Table 1. Summary mean compositions of gahnite from worldwide granitic pegmatites and the Nine Mile metamorphosed massive sulfide deposit (MMSD), Australia, obtained by EMP.

Table 2. Summary compositions of gahnite from worldwide granitic pegmatites and the Nine Mile MMSD, Australia, obtained by LA-ICP-MS and EMP.

Table 3. Characteristics of pegmatites from around the world whose gahnite was analyzed in this study.

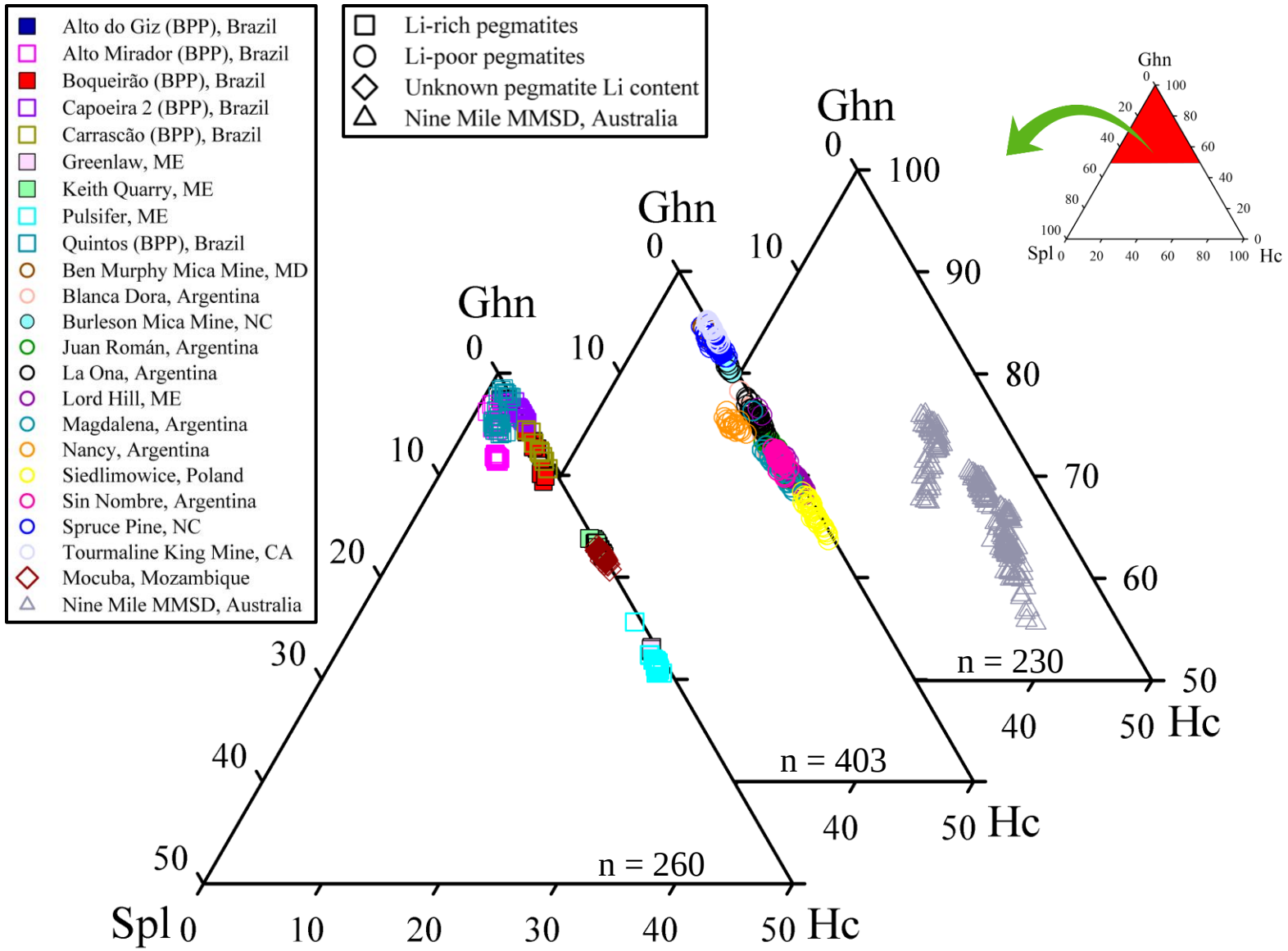
Alto do Giz (BPP), Brazil
Alto Mirador (BPP), Brazil
Boqueirão (BPP), Brazil
Capoeira 2 (BPP), Brazil
Carrascão (BPP), Brazil
Greenlaw, ME
Keith Quarry, ME
Pulsifer, ME
Quintos (BPP), Brazil
Ben Murphy Mica Mine, MD
Blanca Dora, Argentina
Burleson Mica Mine, NC
Juan Román, Argentina
La Ona, Argentina
Lord Hill, ME
Magdalena, Argentina
Nancy, Argentina
Siedlimowice, Poland
Sin Nombre, Argentina
Spruce Pine, NC
Tourmaline King Mine, CA
Mocuba, Mozambique
Nine Mile MMSD, Australia
Li-rich pegmatites
Li-poor pegmatites
Unknown pegmatite Li content
Nine Mile MMSD, Australia
Ghn
Spl
Hc
n = 260
n = 403
n = 230

Figure 1

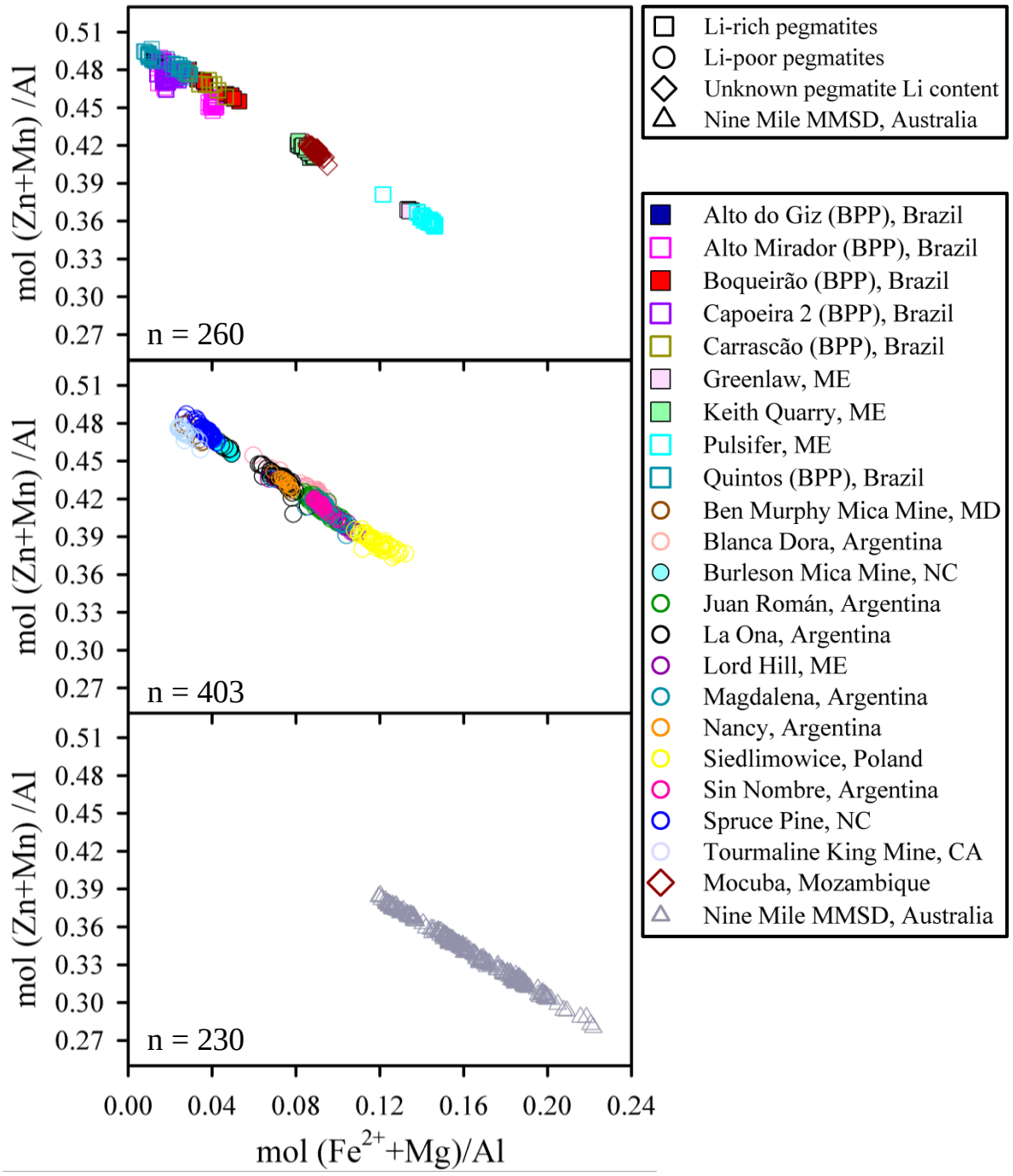
mol (Zn+Mn) /Al
0.51
0.48
0.45
0.42
0.39
0.36
0.33
0.30
0.27
n = 260
n = 403
n = 230
0.00
0.04
0.08
0.12
0.16
0.20
0.24
mol (Fe2+ +Mg)/Al
Li-rich pegmatites
Li-poor pegmatites
Unknown pegmatite Li content
Nine Mile MMSD, Australia
Alto do Giz (BPP), Brazil
Alto Mirador (BPP), Brazil
Boqueirão (BPP), Brazil
Capoeira 2 (BPP), Brazil
Carrascão (BPP), Brazil
Greenlaw, ME
Keith Quarry, ME
Pulsifer, ME
Quintos (BPP), Brazil
Ben Murphy Mica Mine, MD
Blanca Dora, Argentina
Burleson Mica Mine, NC
Juan Román, Argentina
La Ona, Argentina
Lord Hill, ME
Magdalena, Argentina
Nancy, Argentina
Siedlimowice, Poland
Sin Nombre, Argentina
Spruce Pine, NC
Tourmaline King Mine, CA
Mocuba, Mozambique
Nine Mile MMSD, Australia

Figure 2

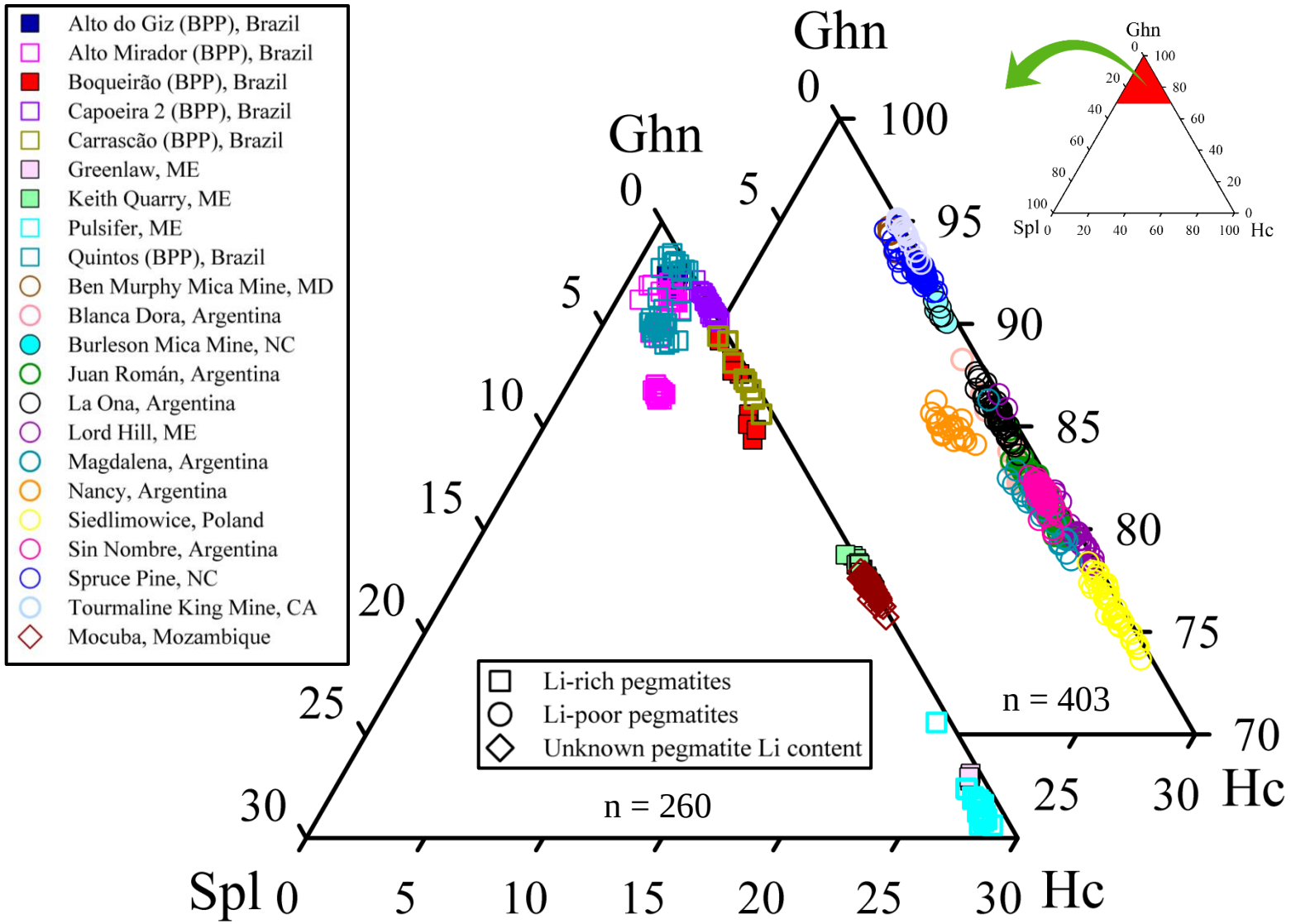
Alto do Giz (BPP), Brazil
Alto Mirador (BPP), Brazil
Boqueirão (BPP), Brazil
Capoeira 2 (BPP), Brazil
Carrascão (BPP), Brazil
Greenlaw, ME
Keith Quarry, ME
Pulsifer, ME
Quintos (BPP), Brazil
Ben Murphy Mica Mine, MD
Blanca Dora, Argentina
Burleson Mica Mine, NC
Juan Román, Argentina
La Ona, Argentina
Lord Hill, ME
Magdalena, Argentina
Nancy, Argentina
Siedlimowice, Poland
Sin Nombre, Argentina
Spruce Pine, NC
Tourmaline King Mine, CA
Mocuba, Mozambique
Ghn
Spl
Hc
Li-rich pegmatites
Li-poor pegmatites
Unknown pegmatite Li content
n = 260
n = 403

Figure 3

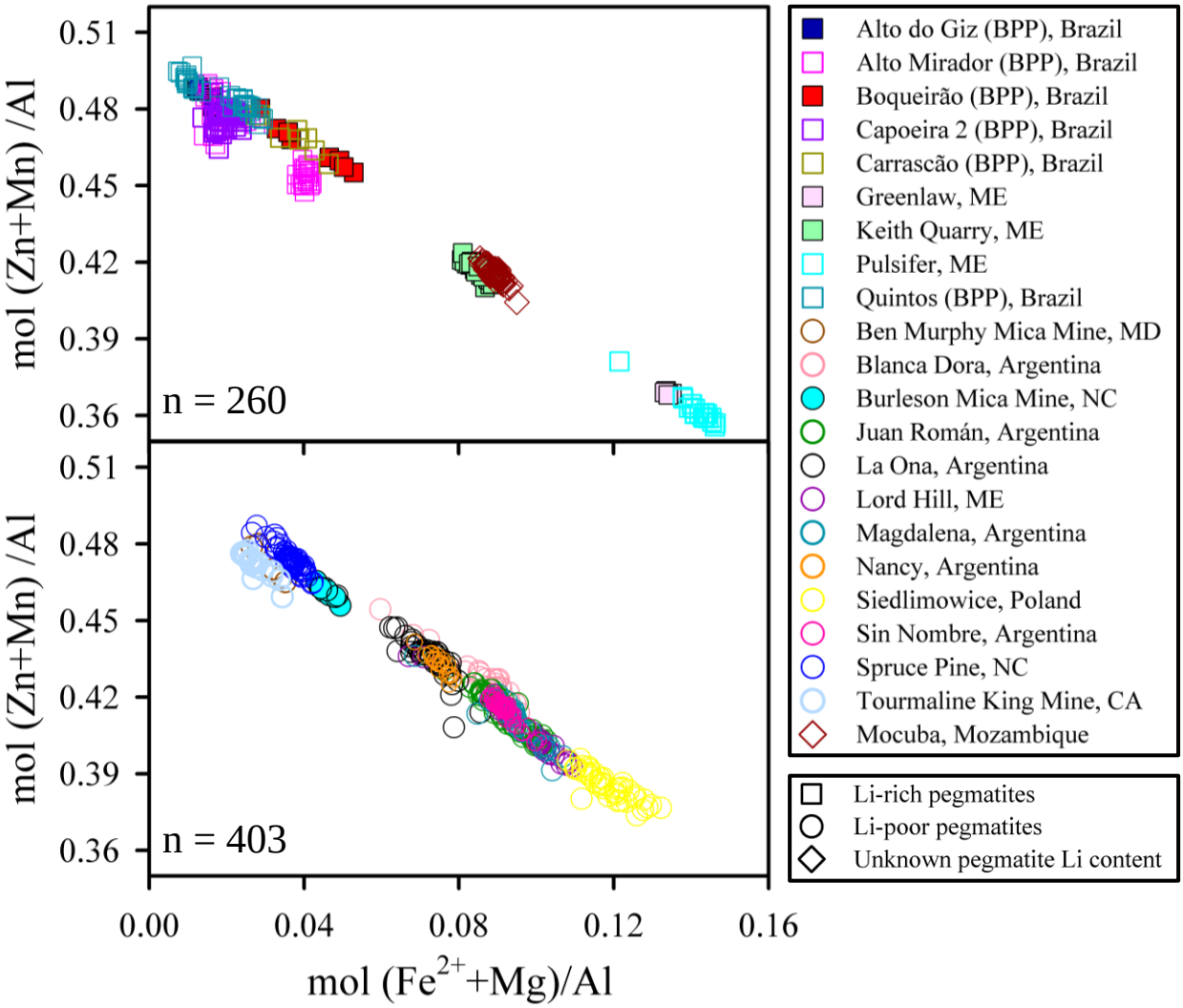
0.51
0.48
0.45
0.42
0.39
0.36
mol (Zn+Mn) /Al
n = 260
n = 403
0.00
0.04
0.08
0.12
0.16
mol (Fe2+ +Mg)/Al
Alto do Giz (BPP), Brazil
Alto Mirador (BPP), Brazil
Boqueirão (BPP), Brazil
Capoeira 2 (BPP), Brazil
Carrascão (BPP), Brazil
Greenlaw, ME
Keith Quarry, ME
Pulsifer, ME
Quintos (BPP), Brazil
Ben Murphy Mica Mine, MD
Blanca Dora, Argentina
Burleson Mica Mine, NC
Juan Román, Argentina
La Ona, Argentina
Lord Hill, ME
Magdalena, Argentina
Nancy, Argentina
Siedlimowice, Poland
Sin Nombre, Argentina
Spruce Pine, NC
Tourmaline King Mine, CA
Mocuba, Mozambique
Li-rich pegmatites
Li-poor pegmatites
Unknown pegmatite Li content

Figure 4

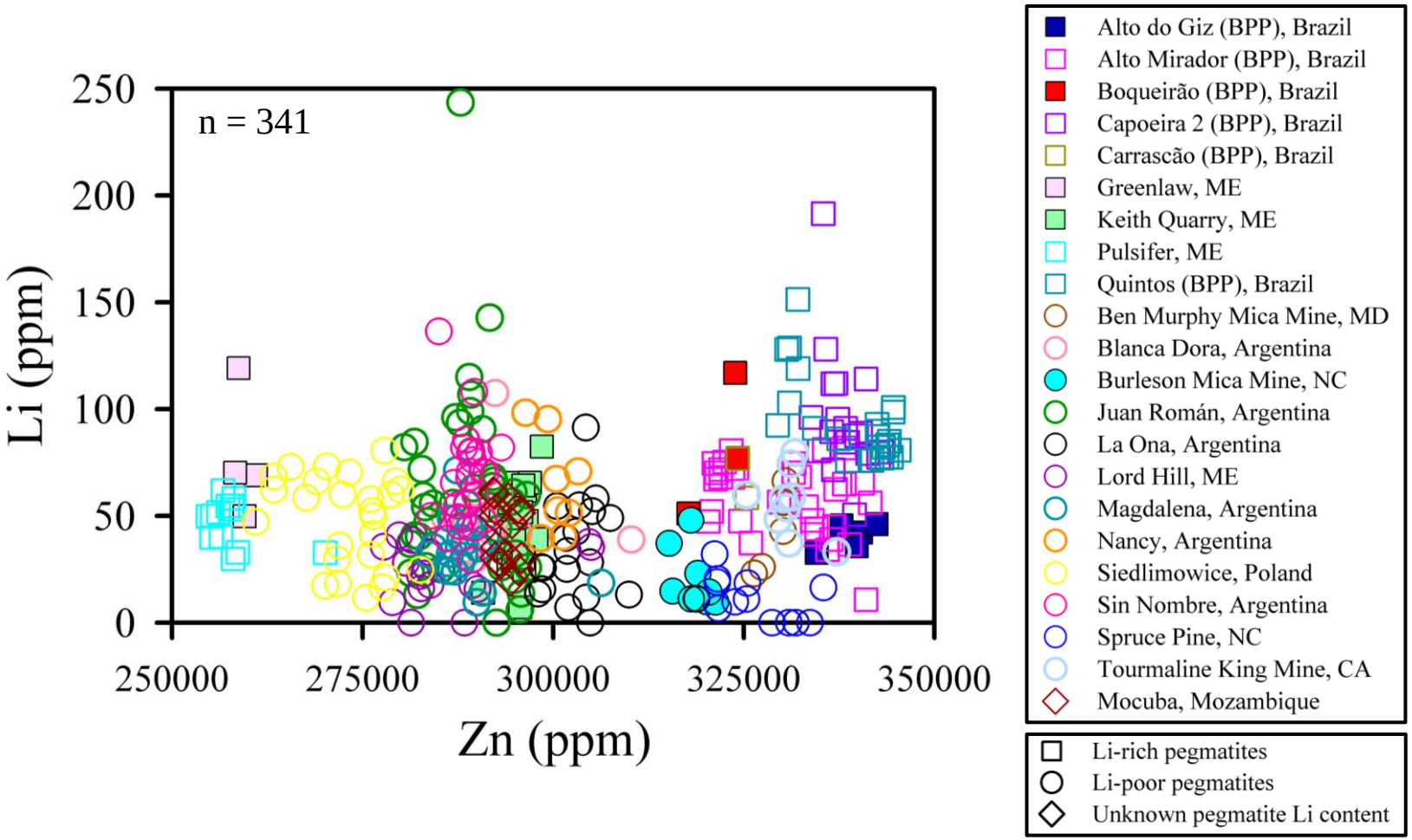
n = 341
Li (ppm)
Zn (ppm)
250
200
150
100
50
0
250000
275000
300000
325000
350000
Alto do Giz (BPP), Brazil
Alto Mirador (BPP), Brazil
Boqueirão (BPP), Brazil
Capoeira 2 (BPP), Brazil
Carrascão (BPP), Brazil
Greenlaw, ME
Keith Quarry, ME
Pulsifer, ME
Quintos (BPP), Brazil
Ben Murphy Mica Mine, MD
Blanca Dora, Argentina
Burleson Mica Mine, NC
Juan Román, Argentina
La Ona, Argentina
Lord Hill, ME
Magdalena, Argentina
Nancy, Argentina
Siedlimowice, Poland
Sin Nombre, Argentina
Spruce Pine, NC
Tourmaline King Mine, CA
Mocuba, Mozambique
Li-rich pegmatites
Li-poor pegmatites
Unknown pegmatite Li content

Figure 5

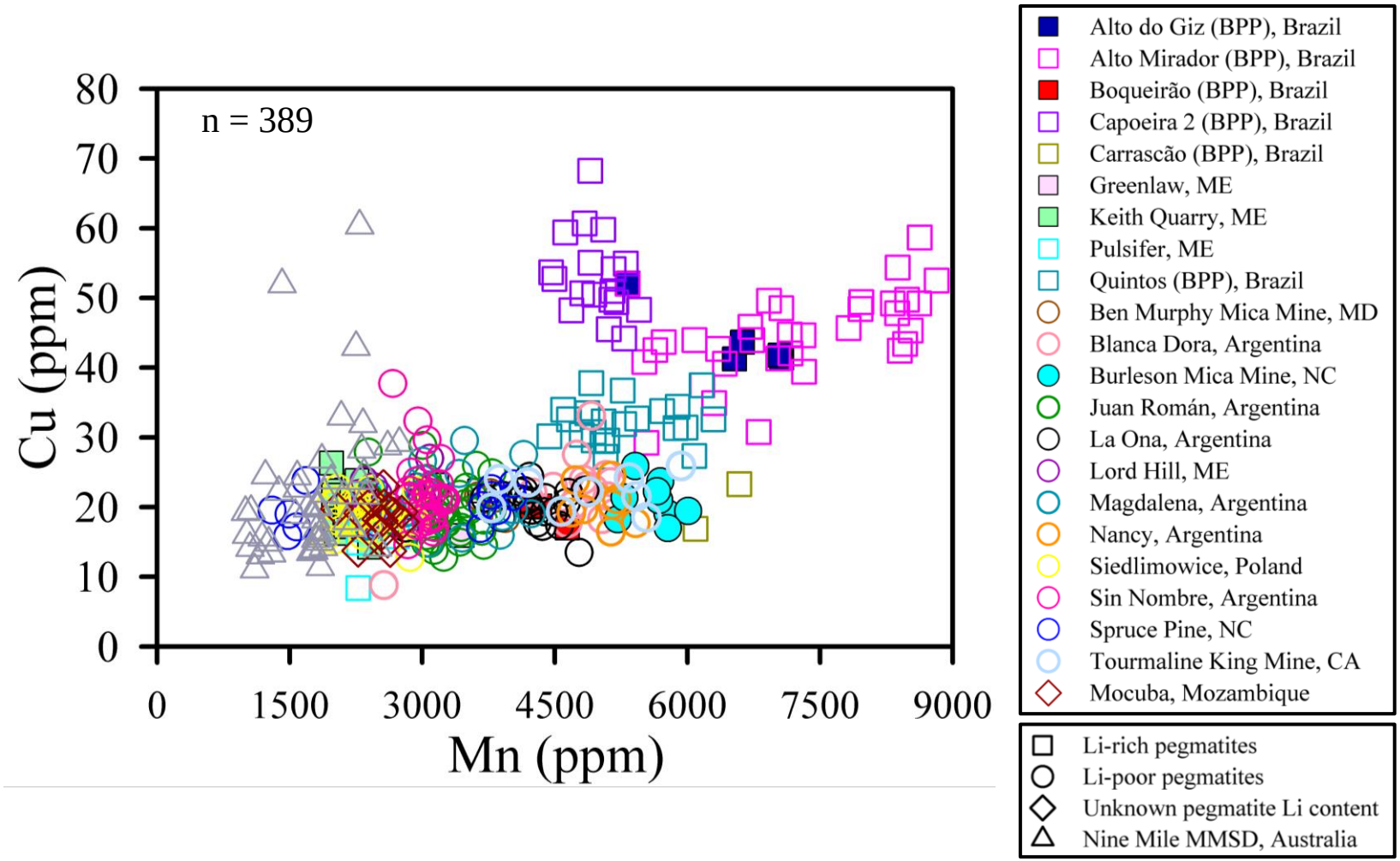
n = 389
Cu (ppm)
Mn (ppm)
0
10
20
30
40
50
60
70
80
0
1500
3000
4500
6000
7500
9000
Alto do Giz (BPP), Brazil
Alto Mirador (BPP), Brazil
Boqueirão (BPP), Brazil
Capoeira 2 (BPP), Brazil
Carrascão (BPP), Brazil
Greenlaw, ME
Keith Quarry, ME
Pulsifer, ME
Quintos (BPP), Brazil
Ben Murphy Mica Mine, MD
Blanca Dora, Argentina
Burleson Mica Mine, NC
Juan Román, Argentina
La Ona, Argentina
Lord Hill, ME
Magdalena, Argentina
Nancy, Argentina
Siedlimowice, Poland
Sin Nombre, Argentina
Spruce Pine, NC
Tourmaline King Mine, CA
Mocuba, Mozambique
Li-rich pegmatites
Li-poor pegmatites
Unknown pegmatite Li content
Nine Mile MMSD, Australia

Figure 6

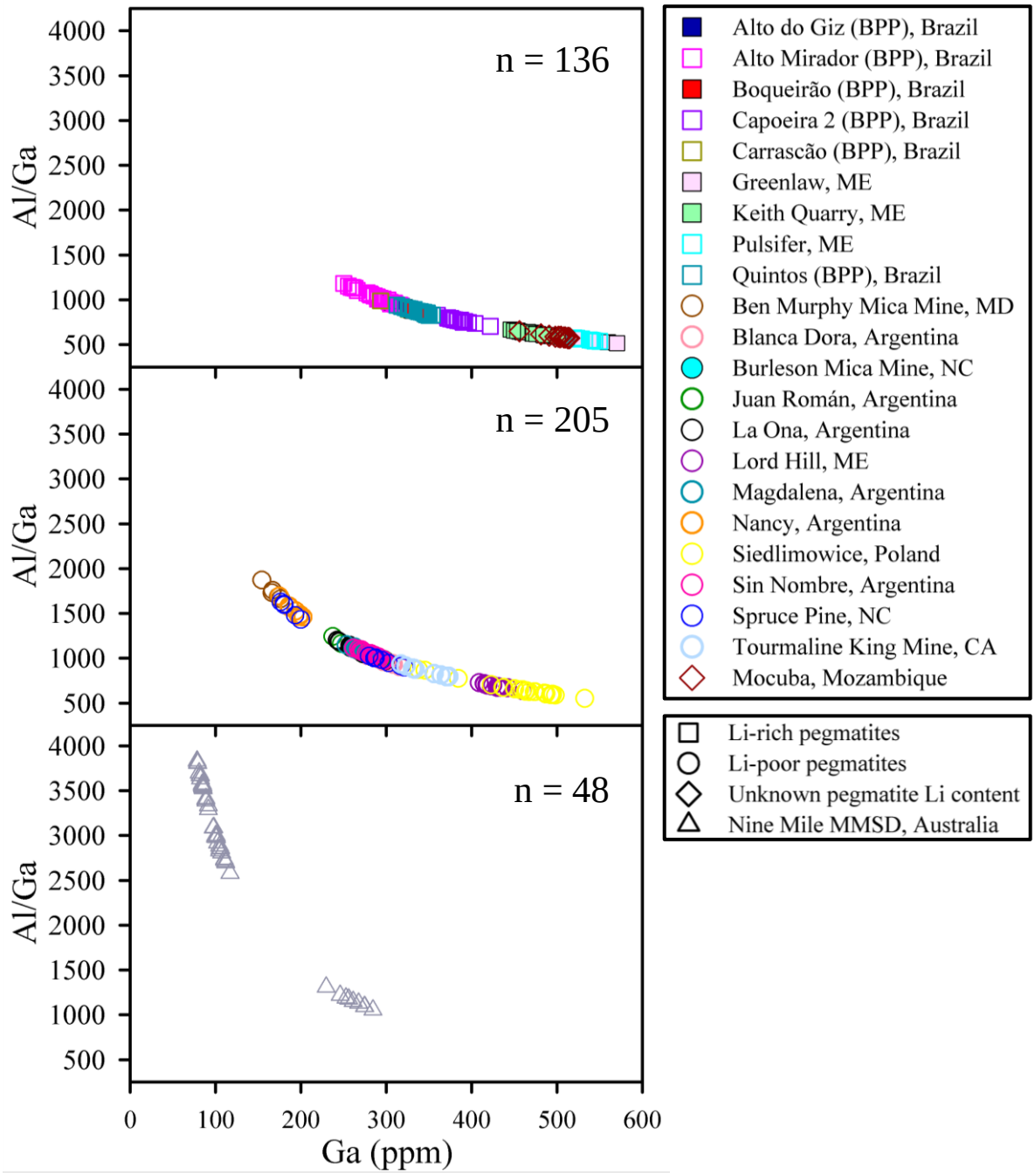
n = 136
n = 205
n = 48
Al/Ga
Ga (ppm)
0
100
200
300
400
500
600
500
1000
1500
2000
2500
3000
3500
4000
Alto do Giz (BPP), Brazil
Alto Mirador (BPP), Brazil
Boqueirão (BPP), Brazil
Capoeira 2 (BPP), Brazil
Carrascão (BPP), Brazil
Greenlaw, ME
Keith Quarry, ME
Pulsifer, ME
Quintos (BPP), Brazil
Ben Murphy Mica Mine, MD
Blanca Dora, Argentina
Burleson Mica Mine, NC
Juan Román, Argentina
La Ona, Argentina
Lord Hill, ME
Magdalena, Argentina
Nancy, Argentina
Siedlimowice, Poland
Sin Nombre, Argentina
Spruce Pine, NC
Tourmaline King Mine, CA
Mocuba, Mozambique
Li-rich pegmatites
Li-poor pegmatites
Unknown pegmatite Li content
Nine Mile MMSD, Australia

Figure 7

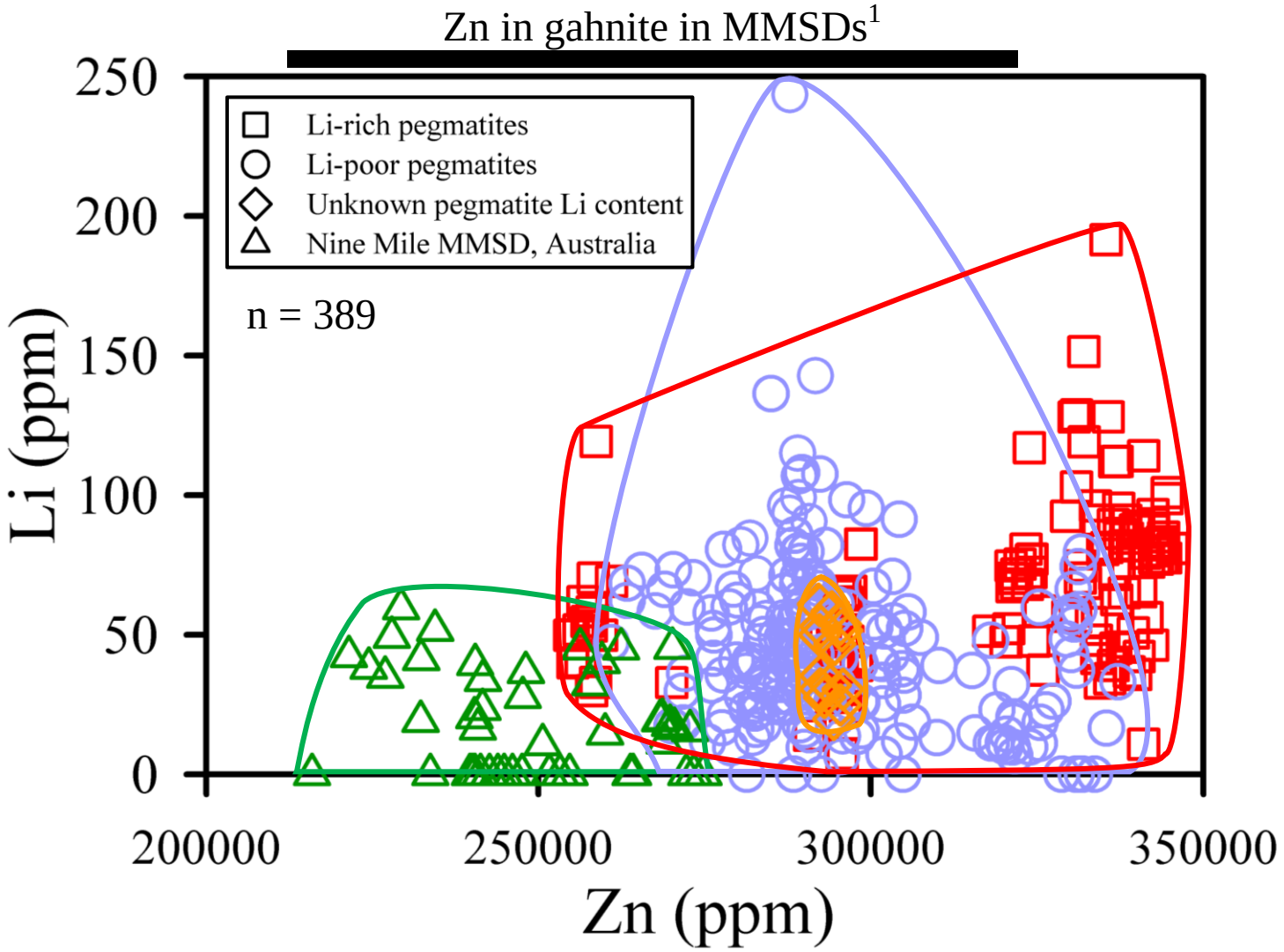
Zn in gahnite in MMSDs[1]
Li-rich pegmatites
Li-poor pegmatites
Unknown pegmatite Li content
Nine Mile MMSD, Australia
n = 389
Li (ppm)
250
200
150
100
50
0
200000
250000
300000
350000
Zn (ppm)

Figure 8

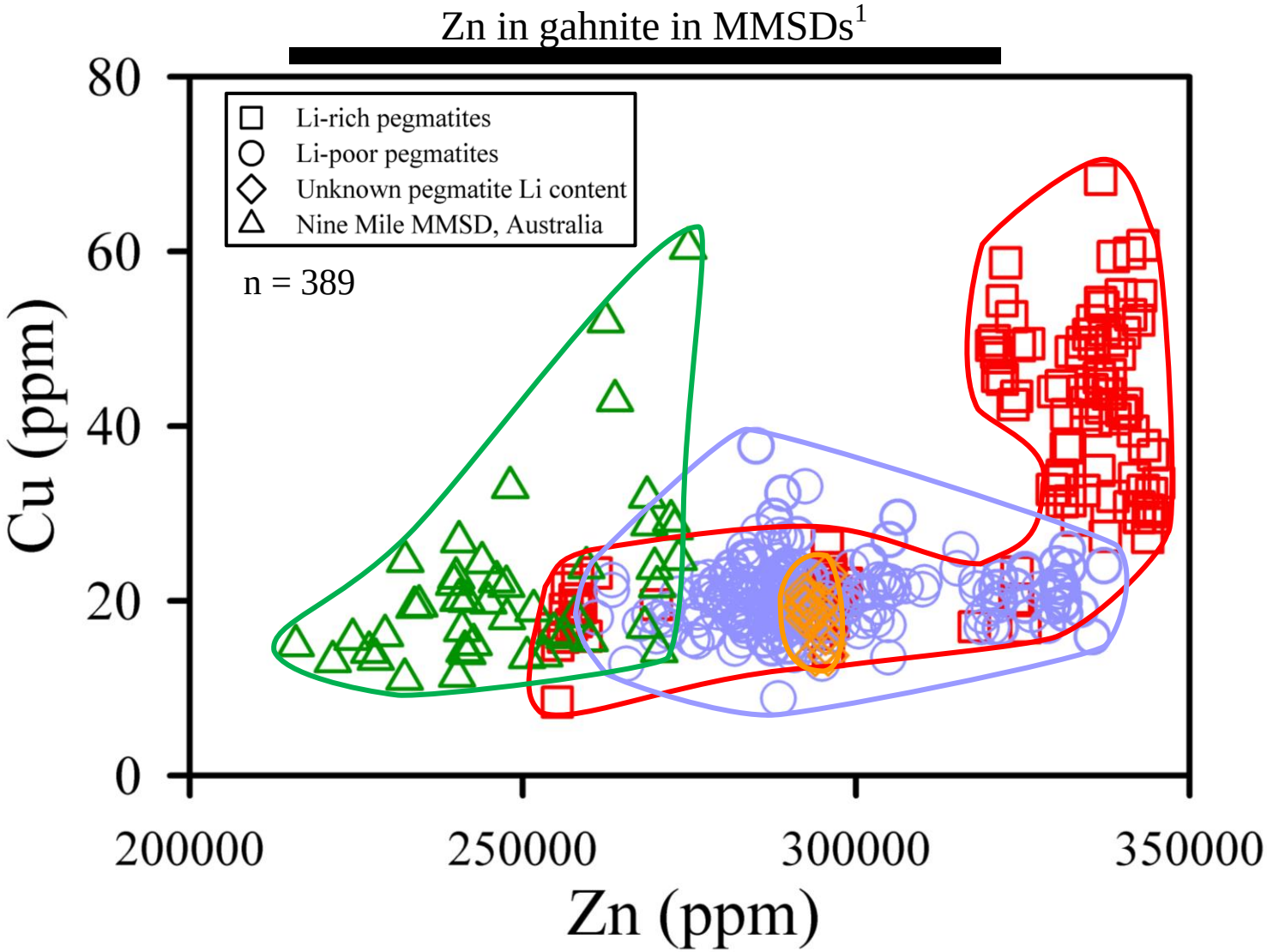
Zn in gahnite in MMSDs[1]
Li-rich pegmatites
Li-poor pegmatites
Unknown pegmatite Li content
Nine Mile MMSD, Australia
n = 389
Cu (ppm)
Zn (ppm)
0
20
40
60
80
200000
250000
300000
350000

Figure 9

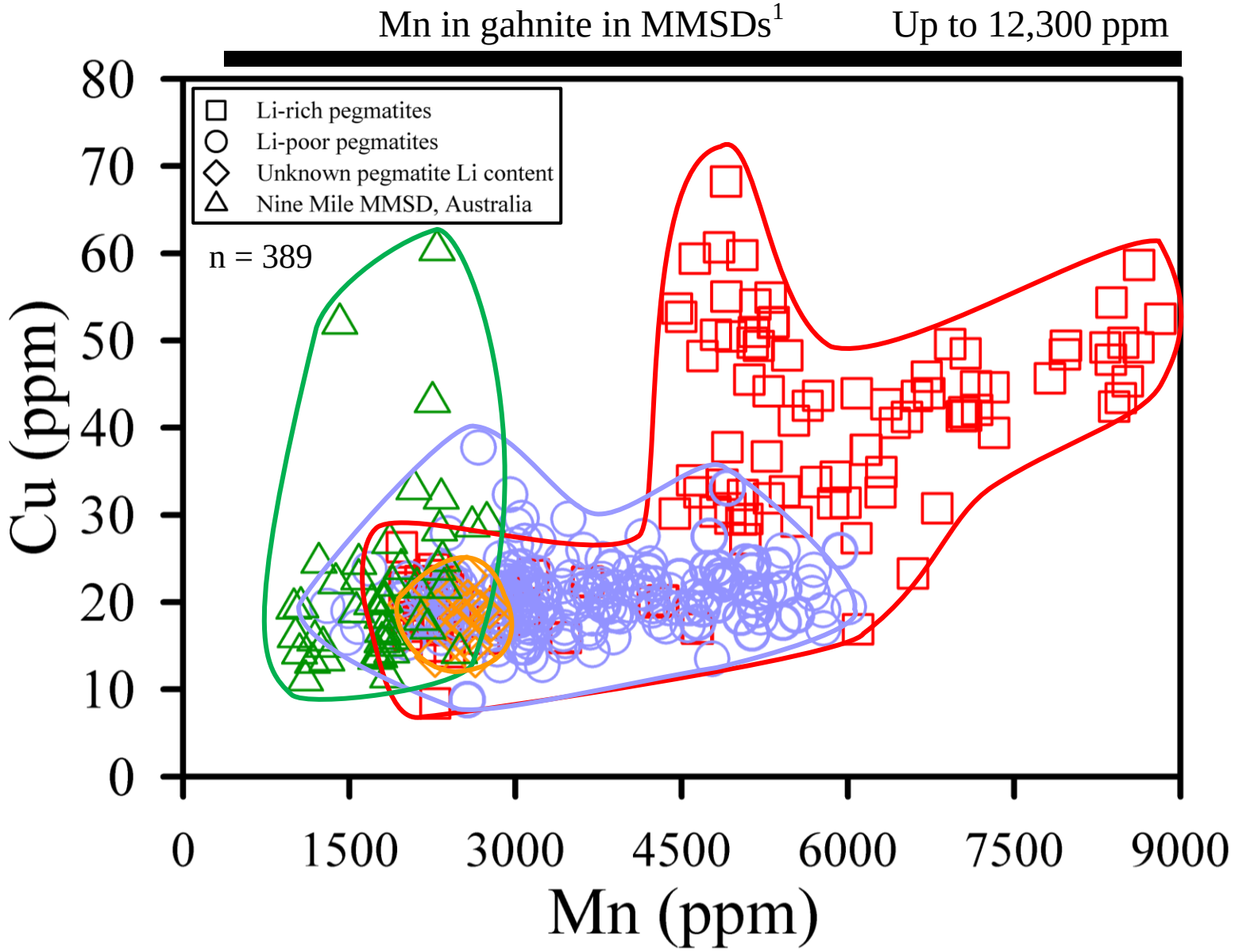
Mn in gahnite in MMSDs[1]
Up to 12,300 ppm
Li-rich pegmatites
Li-poor pegmatites
Unknown pegmatite Li content
Nine Mile MMSD, Australia
n = 389
Cu (ppm)
Mn (ppm)
0
10
20
30
40
50
60
70
80
0
1500
3000
4500
6000
7500
9000

Figure 10

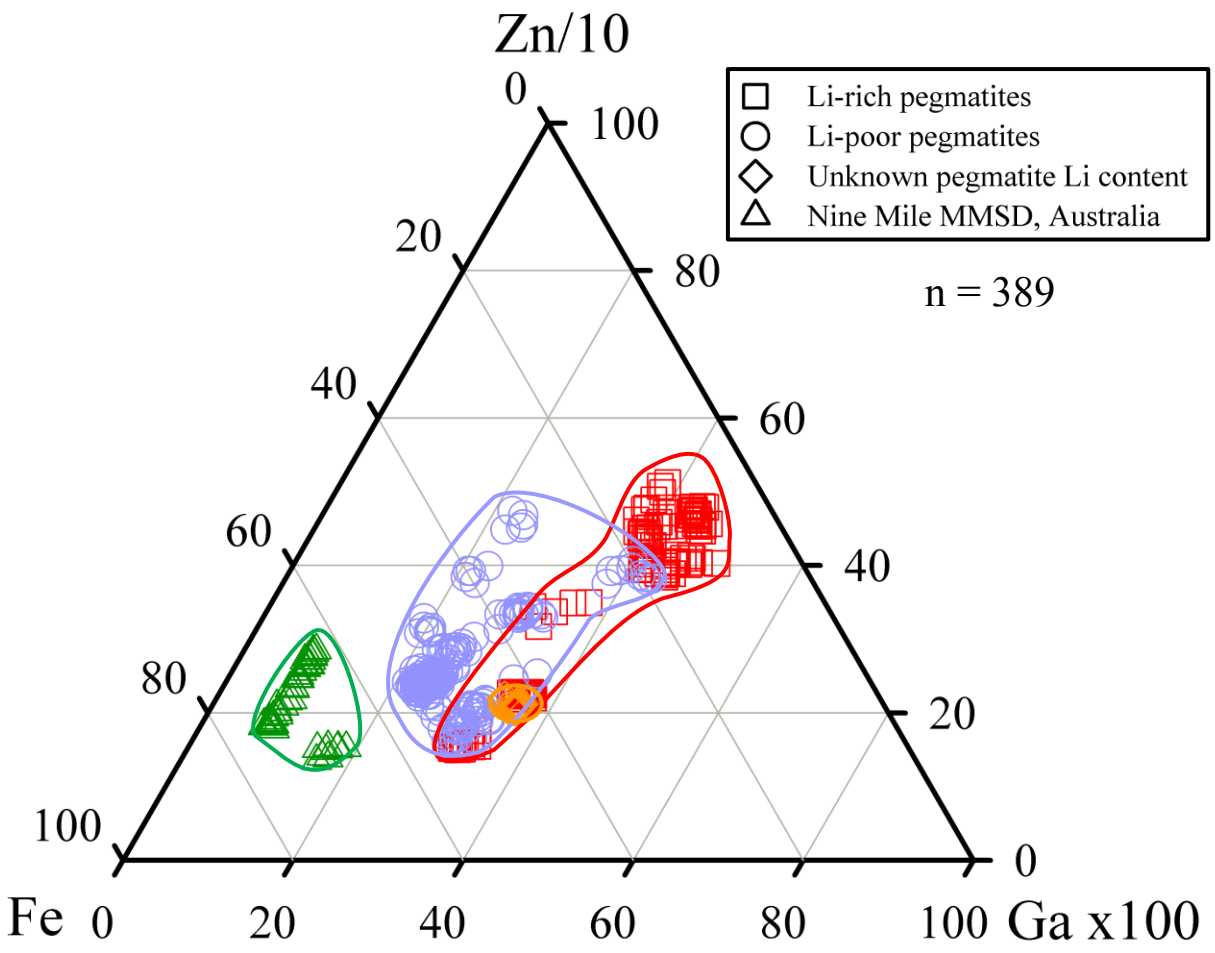
Zn/10
0
100
20
80
40
60
60
40
80
20
100
0
Fe
0
20
40
60
80
100
Ga x100
Li-rich pegmatites
Li-poor pegmatites
Unknown pegmatite Li content
Nine Mile MMSD, Australia
n = 389

Figure 11

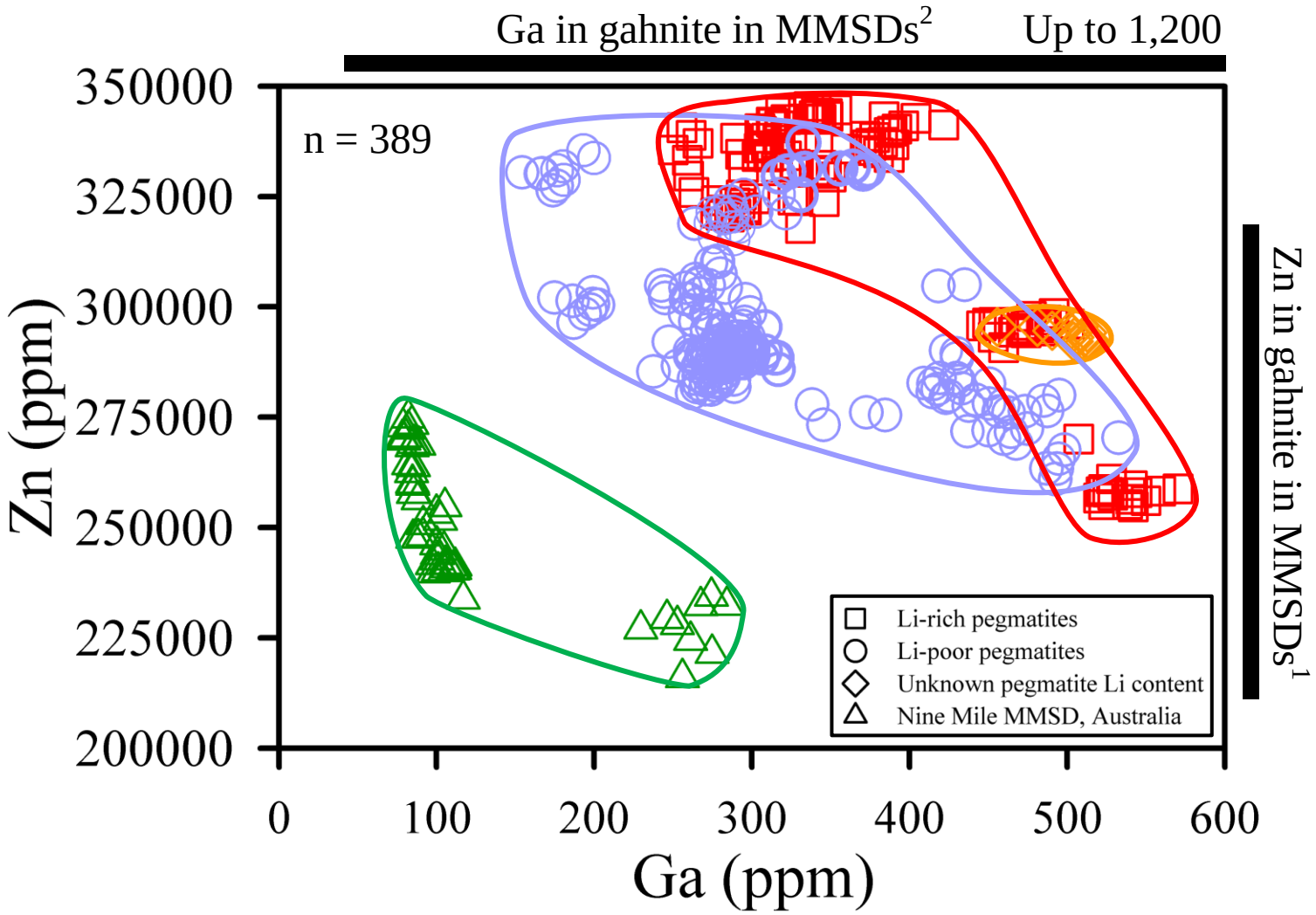
Ga in gahnite in MMSDs[2]
Up to 1,200
n = 389
Zn (ppm)
350000
325000
300000
275000
250000
225000
200000
0
100
200
300
400
500
600
Ga (ppm)
Zn in gahnite in MMSDs[1]
Li-rich pegmatites
Li-poor pegmatites
Unknown pegmatite Li content
Nine Mile MMSD, Australia

Figure 12

Table 1. Summary mean compositions of gahnite from worldwide granitic pegmatites and the Nine Mile metamorphosed massive sulfide deposit (MMSD), Australia, obtained by EMP analysis.

Sample	Alto do Giz[1]	Alto Mirador[1]	Boqueirão[1]	Capoeira 2[1]	Carrascão[1]	Quintos[1]	Blanca Dora[2]	Juan Román[2]	La Ona[2]	Magdalena[2]	Nancy[2]	Sin Nombre[2]
n	5	48	8	37	8	36	26	70	46	27	20	50
K_2O (wt. %)	0.01	0.02	0.02	0.02	0.02	0.01	0.02	0.02	0.02	0.02	0.02	0.01
SiO_2	0.00	0.01	0.02	0.00	0.03	0.02	0.01	0.01	0.01	0.02	0.02	0.02
CaO	0.00	0.00	0.01	0.00	0.01	0.01	0.00	0.00	0.01	0.00	0.01	0.00
TiO_2	0.01	0.02	0.00	0.01	0.00	0.00	0.01	0.01	0.01	0.01	0.00	0.00
MgO	0.21	0.62	0.18	0.01	0.08	0.38	0.21	0.15	0.12	0.22	0.63	0.13
Al_2O_3	55.81	56.06	54.82	55.91	54.89	55.45	54.46	55.14	54.89	55.26	55.45	55.07
MnO	0.96	0.65	0.72	0.33	0.68	0.81	0.60	0.45	0.52	0.42	0.78	0.47
FeO	0.86	1.26	4.03	1.63	3.75	1.50	8.30	7.91	6.64	7.86	5.98	7.87
ZnO	42.21	41.02	39.93	42.11	40.36	42.01	36.43	35.85	37.58	35.81	37.44	35.95
Cr_2O_3	0.02	0.02	0.01	0.03	0.02	0.01	0.01	0.01	0.01	0.01	0.01	0.01
Total	100.10	99.67	99.74	100.05	99.83	100.20	100.04	99.55	99.81	99.63	100.33	99.54
***Apfu* based on 4 oxygen atoms**												
Si	0.000	0.000	0.001	0.000	0.001	0.001	0.000	0.000	0.000	0.001	0.001	0.001
Ti	0.000	0.000	0.000	0.000	0.000	0.000	0.000	0.000	0.000	0.000	0.000	0.000
Al	1.998	2.002	1.977	2.002	1.979	1.986	1.960	1.981	1.975	1.982	1.975	1.980
Cr	0.001	0.000	0.000	0.001	0.000	0.000	0.000	0.000	0.000	0.000	0.000	0.000
K	0.001	0.001	0.001	0.001	0.001	0.001	0.001	0.001	0.001	0.001	0.001	0.000
Fe^{3+}	0.003	0.003	0.029	0.002	0.026	0.017	0.052	0.025	0.033	0.023	0.031	0.025
Fe^{2+}	0.019	0.029	0.074	0.040	0.070	0.021	0.160	0.177	0.137	0.177	0.120	0.176
Mn	0.025	0.017	0.019	0.008	0.018	0.021	0.016	0.012	0.014	0.011	0.020	0.012
Mg	0.009	0.028	0.008	0.000	0.004	0.017	0.009	0.007	0.006	0.010	0.028	0.006
Ca	0.000	0.000	0.000	0.000	0.000	0.000	0.000	0.000	0.000	0.000	0.000	0.000
Zn	0.946	0.918	0.902	0.944	0.911	0.942	0.821	0.807	0.847	0.804	0.835	0.809
Total	3.001	2.998	3.011	2.999	3.010	3.006	3.020	3.009	3.012	3.009	3.012	3.009
Spl	0.965	2.873	0.846	0.034	0.357	1.744	0.951	0.682	0.561	0.987	2.867	0.6143
Ghn	97.103	94.113	91.622	95.948	92.530	96.090	82.921	81.447	85.593	81.161	84.946	81.652
Hc	1.931	3.013	7.532	4.018	7.112	2.165	16.128	17.872	13.845	17.851	12.187	17.734
(Zn+Mn)/Al	0.486	0.467	0.466	0.476	0.469	0.485	0.427	0.413	0.436	0.411	0.433	0.415
(Fe^{2+}+Mg)/Al	0.014	0.029	0.042	0.020	0.037	0.019	0.086	0.093	0.072	0.094	0.075	0.092
Zn/Fe	51.215	36.848	12.627	24.279	13.450	48.525	5.213	4.584	6.245	4.592	6.995	4.609

Table 1. Continued

Sample	Ben Murphy Mica Mine[3]	Burleson Mica Mine[4]	Greenlaw[5]	Keith Quarry[5]	Lord Hill[5]	Mocuba[6]	Pulsifer[5]	Siedlimowice[7]	Spruce Pine[4]	Tourmaline King Mine[8]	Nine Mile MMSD[9]
n	5	10	4	26	27	67	21	40	63	19	230
K_2O (wt. %)	0.02	0.02	0.02	0.01	0.02	0.02	0.01	0.02	0.02	0.02	0.02
SiO_2	0.00	0.01	0.00	0.00	0.00	0.00	0.01	0.01	0.00	0.00	0.01
CaO	0.00	0.00	0.00	0.00	0.00	0.01	0.00	0.00	0.00	0.01	0.00
TiO_2	0.00	0.02	0.01	0.00	0.01	0.01	0.00	0.01	0.01	0.00	0.01
MgO	0.13	0.09	0.11	0.01	0.03	0.02	0.19	0.09	0.08	0.01	1.33
Al_2O_3	55.02	55.00	55.80	55.84	55.58	55.63	56.12	55.82	54.52	55.76	56.91
MnO	0.46	0.68	0.50	0.32	0.34	0.34	0.36	0.33	0.51	0.73	0.26
FeO	2.83	4.54	10.92	7.03	8.35	7.78	11.42	9.87	4.32	2.31	11.28
ZnO	40.95	39.69	32.29	36.79	35.41	36.51	32.02	33.93	40.65	41.17	30.53
Cr_2O_3	0.01	0.01	0.00	0.01	0.00	0.01	0.01	0.01	0.01	0.01	0.01
Total	99.43	100.06	99.65	100.03	99.74	100.33	100.15	100.08	100.13	100.03	100.34
***Apfu* based on 4 oxygen atoms**											
Si	0.000	0.000	0.000	0.000	0.000	0.000	0.000	0.000	0.000	0.000	0.000
Ti	0.000	0.000	0.000	0.000	0.000	0.000	0.000	0.000	0.000	0.000	0.000
Al	1.988	1.978	1.989	1.993	1.989	1.984	1.989	1.987	1.968	1.998	1.990
Cr	0.000	0.000	0.000	0.000	0.000	0.000	0.000	0.000	0.000	0.000	0.000
K	0.001	0.001	0.001	0.001	0.001	0.001	0.001	0.001	0.001	0.001	0.001
Fe^{3+}	0.016	0.029	0.015	0.009	0.015	0.021	0.015	0.017	0.042	0.004	0.013
Fe^{2+}	0.056	0.087	0.262	0.169	0.197	0.176	0.273	0.232	0.068	0.055	0.267
Mn	0.012	0.018	0.013	0.008	0.009	0.009	0.009	0.009	0.013	0.019	0.007
Mg	0.006	0.004	0.005	0.000	0.001	0.001	0.009	0.004	0.004	0.000	0.059
Ca	0.000	0.000	0.000	0.000	0.000	0.000	0.000	0.000	0.000	0.000	0.000
Zn	0.927	0.894	0.721	0.822	0.794	0.815	0.711	0.756	0.919	0.924	0.669
Total	3.006	3.011	3.005	3.003	3.006	3.008	3.006	3.006	3.016	3.001	3.005
Spl	0.591	0.431	0.501	0.050	0.121	0.108	0.859	0.394	0.379	0.025	5.905
Ghn	93.711	90.736	73.003	82.930	79.996	82.148	71.655	76.202	92.713	94.390	67.252
Hc	5.698	8.834	26.496	17.021	19.883	17.743	27.486	23.405	6.907	5.585	26.843
(Zn+Mn)/Al	0.472	0.461	0.369	0.417	0.403	0.415	0.362	0.385	0.474	0.472	0.339
(Fe^{2+}+Mg)/Al	0.031	0.046	0.134	0.085	0.100	0.089	0.141	0.119	0.037	0.055	0.164
Zn/Fe	16.788	10.292	2.755	4.878	4.087	4.633	2.612	3.266	13.594	17.108	2.635

n – number of analyses. *Apfu* – atoms per formula unit. Fe^{2+} and Fe^{3+} calculated from stoichiometry. 1 Borborema Pegmatite Province, Brazil, 2 Argentina, 3 Maryland, 4 North Carolina, 5 Maine, 6 Mozambique, 7 Poland, 8 California, and 9 Australia.

Sample numbers: Alto do Giz 165054*, Alto Mirador AM PEG1A, PEG1A-A, PEG1BB, and PEG1BB1, Boqueirão BOQ PEG2AB, Capoeira 2 CAP2PEG2A and CAP2PEG2B, Carrascão CARRPEG, Quintos QUINTOS 2B and QUINTOS 3, Blanca Dora GH253, Juan Román GH007, GH011, and GH013, La Ona GH243, Magdalena GH272 and GH273, Nancy NA001, Sin Nombre GH274A and GH274B, Ben Murphy Mica Mine 113021*, Burleson Mica Mine R1957*, Greenlaw GREENLAW-17*, Keith Quarry KEITH-9*, Lord Hill 16109* and 128537*, Mocuba 25605**, Pulsifer HOLE-21* and HOLE-5*, Siedlimowice SIED 1, SIED 2, and SIED 3, Spruce Pine 18270**, Tourmaline King Mine 126115*, Nine Mile GH1B, GH2AB, GH3AB, GH5B, and GH7B. *Denotes samples borrowed from the Smithsonian Institution, Washington, D.C., and **from the American Museum of Natural History, New York.

Table 2. Summary compositions of gahnite from worldwide granitic pegmatites and the Nine Mile MMSD, Australia, obtained by LA-ICP-MS and EMP.

Sample	ppm	Al*	Fe*	Zn*	Mg	Li	Ti	V	Cr	Mn	Co	Ni	Cu	Ga	Cd	Pb	Al/Ga
Alto do Giz	Min	295015	6413	334563	1233	32.7	0.0	1.5	2.3	5330	8.0	0.0	41.2	305.0	0.0	0.0	919
(BPP), Brazil	Max	295893	7649	342435	1495	46.2	26.9	4.1	5.0	7068	50.8	7.8	52.1	321.6	21.1	0.0	970
n = 5	Mean	295380	6719	339010	1362	40.5	11.3	3.1	3.4	6520	23.1	1.6	44.0	311.2	9.0	0.0	950
Alto Mirador	Min	290135	5379	320354	1573	10.8	0.0	0.0	0.0	5324	4.6	0.0	29.2	250.2	0.0	0.0	901
(BPP), Brazil	Max	301689	12818	341599	5765	81.8	37.9	12.6	7.7	8819	15.4	16.5	58.7	327.8	36.8	1.6	1183
n = 33	Mean	296299	9499	330449	3638	58.3	5.9	5.2	1.9	7213	9.5	2.8	44.7	290.5	16.6	0.3	1025
Boqueirão (BPP),	Min	289463	25690	317759	993	51.2	0.0	0.0	0.0	4245	5.0	0.0	17.0	329.2	0.0	0.0	837
Brazil	Max	290802	35313	324233	1812	116.9	19.3	4.7	2.7	4642	8.1	0.0	20.1	345.9	30.0	0.7	883
n = 3	Mean	290341	29512	321952	1278	81.7	6.4	2.7	1.7	4406	7.0	0.0	19.1	335.3	18.6	0.3	866
Capoeira 2	Min	292247	8504	333808	0	50.6	0.0	0.0	0.0	4459	0.0	0.0	44.2	359.7	0.0	0.0	705
(BPP), Brazil	Max	299545	15321	343069	231	191.5	63.2	7.6	5.7	5454	1.7	10.0	68.2	421.8	36.8	9.6	827
n = 18	Mean	296183	12515	338266	68	96.1	10.1	1.3	2.3	4972	0.6	2.4	53.1	384.4	16.4	1.0	771
Carrascão (BPP),	Min	290161	31162	324169	259	58.5	0.0	0.0	0.0	6091	0.0	10.4	16.9	293.3	0.0	0.0	894
Brazil	Max	291405	32693	325390	391	76.8	30.1	0.0	4.9	6587	3.4	11.6	23.3	326.1	35.4	0.9	989
n = 2	Mean	290783	31928	324780	325	67.6	15.1	0.0	2.4	6339	1.7	11.0	20.1	309.7	17.7	0.4	941
Quintos (BPP),	Min	288521	6203	329422	525	75.9	0.0	0.0	0.0	4437	2.7	0.0	27.2	312.4	0.0	0.0	824
Brazil	Max	296497	16191	345391	4018	151.4	50.9	11.9	6.8	6293	22.3	11.5	37.8	353.8	42.1	2.4	941
n = 22	Mean	293749	10305	339219	1898	94.7	11.2	4.6	2.4	5289	10.2	2.2	32.1	337.2	20.5	0.4	872
Blanca Dora	Min	285218	50447	285767	1131	30.1	0.0	0.0	0.0	2567	0.0	0.0	8.8	277.5	0.0	0.0	905
(PPP), Argentina	Max	292834	70276	310233	1669	107.5	30.4	8.2	6.9	5168	4.0	14.0	33.1	316.8	18.9	9.5	1055
n = 16	Mean	288722	65090	291439	1355	50.3	7.2	3.6	2.8	4707	1.6	1.9	21.9	299.6	6.8	1.4	965
Juan Román	Min	287547	58080	280441	563	6.2	0.0	0.0	0.0	2389	0.0	0.0	12.8	237.6	0.0	0.0	985
(PPP), Argentina	Max	294909	65892	296691	1398	243.4	31.7	9.5	9.9	3791	3.8	12.1	28.8	298.0	22.6	3.8	1241
n = 39	Mean	291903	61749	288548	911	62.9	5.6	1.5	2.7	3233	1.7	1.3	19.5	278.5	10.3	0.5	1050
La Ona (PPP),	Min	285737	37357	297984	381	7.0	0.0	0.0	0.0	2811	8.9	0.0	13.5	242.5	0.0	0.0	968
Argentina	Max	294739	54963	318812	974	91.3	38.4	13.9	7.5	4842	22.9	14.3	24.4	298.9	32.1	1.0	1201
n = 20	Mean	289931	49692	303653	772	34.4	4.5	6.1	2.4	4236	15.3	4.7	20.0	267.2	8.3	0.4	1088
Magdalena	Min	288854	44019	283710	927	9.5	0.0	0.0	0.0	2381	0.0	0.0	14.8	253.1	0.0	0.0	993
(PPP), Argentina	Max	296285	65014	306281	1955	71.3	37.2	4.7	5.4	4235	18.8	10.8	29.5	291.6	23.6	3.8	1149
n = 19	Mean	290963	61286	288762	1364	34.1	7.3	1.3	2.3	3207	5.1	1.6	20.7	272.0	9.2	0.5	1072
Nancy (PPP),	Min	289256	44384	296377	3552	39.5	0.0	4.8	0.0	4688	1.3	0.0	16.5	174.8	0.0	0.0	1460
Argentina	Max	296206	47898	303261	4289	98.2	31.3	25.8	7.6	5415	7.8	15.3	24.5	202.5	9.6	1.1	1693
n = 8	Mean	294386	46433	300214	3923	64.4	11.1	15.4	2.5	5036	5.4	3.2	20.4	192.5	3.2	0.5	1532
Sin Nombre	Min	289669	56191	283943	463	29.3	0.0	0.0	0.0	2851	0.0	0.0	16.4	261.7	0.0	0.0	975
(PPP), Argentina	Max	297216	63234	293180	1125	108.1	45.2	3.9	5.4	3266	4.1	8.7	27.0	298.2	18.6	3.4	1113
n = 26	Mean	292198	60938	288745	824	69.5	9.4	1.2	1.6	3109	2.1	1.6	20.3	284.7	9.0	0.5	1032

Table 2. Continued

Sample	ppm	Al*	Fe*	Zn*	Mg	Li	Ti	V	Cr	Mn	Co	Ni	Cu	Ga	Cd	Pb	Al/Ga
Spruce Pine, NC	Min	285562	31217	321165	534	9.7	0.0	7.9	1.5	5212	5.6	0.0	17.0	273.8	0.0	0.0	895
n = 12	Max	289738	35344	335431	809	48.0	36.8	14.2	10.0	6007	9.6	10.7	25.9	291.7	20.0	0.9	1628
	Mean	287605	33594	326759	718	19.9	9.1	11.1	3.7	5611	7.0	3.2	20.9	283.1	9.2	0.3	1208
Tourmaline King	Min	292543	16106	325334	0	33.1	0.0	0.0	0.0	3780	0.0	0.0	18.5	317.2	0.0	0.0	794
Mine, CA	Max	296550	21166	337190	128	79.6	16.1	7.7	6.4	5926	1.9	9.4	25.9	373.4	24.7	5.0	933
n = 9	Mean	294512	17681	330883	39	55.9	2.9	3.6	1.7	4836	0.5	2.8	22.1	344.6	8.7	1.0	858
Greenlaw, ME	Min	294057	84198	258264	594	49.8	0.0	0.0	0.0	3087	0.5	0.0	15.9	528.1	0.0	0.0	516
n = 4	Max	297359	85985	261019	619	119.2	34.6	1.6	3.7	3651	1.7	6.9	23.2	570.3	11.6	0.4	563
	Mean	295332	84888	259378	605	77.1	8.7	0.4	1.8	3338	0.9	3.4	20.1	549.8	5.7	0.2	538
Lord Hill, ME	Min	289854	46553	277774	0	0.0	0.0	0.0	0.0	2286	0.0	0.0	16.4	409.0	0.0	0.0	639
n =16	Max	296867	69413	304980	383	40.9	16.5	3.4	8.3	3085	3.7	6.0	27.0	459.6	15.9	1.0	726
	Mean	293833	63582	285840	144	23.2	4.7	0.7	2.4	2593	2.3	1.7	20.8	427.1	3.7	0.3	689
Pulsifer, ME	Min	294126	75997	254714	918	29.9	0.0	0.0	0.0	2276	0.0	0.0	8.4	507.3	0.0	0.0	536
n = 13	Max	298974	90595	270063	1511	61.8	35.8	3.3	6.7	2908	4.6	9.2	21.5	550.0	25.0	1.0	583
	Mean	296581	88115	257866	1230	46.9	11.7	0.6	1.4	2513	2.4	1.8	17.6	531.1	6.1	0.2	559
Keith Quarry,	Min	292898	52810	290811	0	7.3	0.0	0.0	0.0	1973	0.0	0.0	14.3	445.6	0.0	0.0	589
ME	Max	298603	56837	298514	237	82.5	30.0	3.9	4.4	2408	2.2	15.3	26.3	501.3	28.9	0.8	668
n = 21	Mean	295261	54849	295457	69	43.8	6.1	0.7	1.9	2182	0.4	3.7	20.4	473.0	10.7	0.4	625
Ben Murphy	Min	287600	20832	326354	718	23.1	0.0	0.0	0.0	3636	32.3	0.0	18.4	154.3	0.0	0.0	1663
Mica Mine, MD	Max	293369	24019	330450	1164	66.3	28.5	4.3	4.5	3942	39.9	5.0	22.0	176.2	24.6	0.0	1872
n = 5	Mean	291209	21998	328908	957	42.9	14.5	0.9	1.4	3774	37.0	1.7	20.9	167.5	12.0	0.0	1742
Burleson Mica	Min	289749	33906	315213	534	9.7	0.0	7.9	1.5	5212	5.6	0.0	17.0	273.8	0.0	0.0	997
Mine, NC	Max	292252	36347	321318	809	48.0	36.8	14.2	10.0	6007	9.6	10.7	25.9	291.7	20.0	0.9	1060
n = 9	Mean	291020	35210	318655	718	19.9	9.1	11.1	3.7	5611	7.0	3.2	20.9	283.1	9.2	0.3	1029
Mocuba,	Min	292585	59246	292152	0	19.8	0.0	0.0	0.0	2036	0.8	0.0	13.7	455.8	0.0	0.0	571
Mozambique	Max	296830	63125	295847	489	60.9	33.5	2.1	6.8	2782	6.1	15.5	23.0	514.6	19.0	0.9	649
n = 15	Mean	294551	60843	293773	244	42.3	10.7	0.1	1.7	2524	3.6	4.9	18.2	501.6	5.9	0.2	588
Siedlimowice,	Min	291283	67610	260979	296	11.6	0.0	0.0	0.0	1898	0.0	0.0	12.8	338.3	0.0	0.0	551
Poland	Max	299482	88387	282570	878	80.5	62.4	3.0	7.9	2934	6.3	8.0	22.7	532.6	33.3	2.7	873
n = 26	Mean	295161	77012	273143	569	48.3	14.1	0.5	2.5	2370	3.7	1.5	18.7	454.4	11.0	0.4	658
Nine Mile MMSD,	Min	296830	60793	215958	12921	0.0	30.1	1.8	0.0	1795	139.1	16.8	18.0	84.9	0.0	0.3	1056
Australia	Max	304637	112694	274810	15094	40.0	67.2	7.9	0.0	2148	148.5	26.8	23.8	88.6	9.7	6.6	3831
n = 48	Mean	300911	83869	248956	14126	24.9	47.3	4.2	0.0	2006	145.2	21.5	20.4	86.0	3.8	1.9	2856
D.L.					26.9	4.78	5.7	1.4	1.0	11	0.4	1.7	0.7	0.5	2.9	0.2	

n – number of analyses. *Obtained by EMP and converted to ppm. D.L. = Detection limits for LA-ICP-MS. BPP = Borborema Pegmatite Province. PPP = Pampean Pegmatite Province.

Table 3: Characteristics of pegmatites from around the world whose gahnite was analyzed in this study.

Pegmatite	Location	Pegmatite Group	Pegmatite Type	Pegmatite Subtype	Family	Lithium Content
Blanca Dora	Córdoba, Argentina	Comechingones Pegmatite District	REL-Li	Beryl-columbite-phosphate	LCT	Poor
Juan Román	" "	" "	REL-Li	Beryl-columbite-phosphate	LCT	Poor
La Ona	" "	" "	REL-Li	Beryl-columbite-phosphate	LCT	Poor
Magdalena	" "	" "	REL-Li	Beryl-columbite-phosphate	LCT	Poor
Sin Nombre	" "	" "	MSREL-Li	-	LCT	Poor
Nancy	San Luis, Argentina	Conlara Pegmatite District	REL-Li	Beryl-columbite-phosphate	LCT	Poor
Alto do Giz	Río Grande do Norte, Brazil	Borborema Pegmatite Province	REL-Li	Spodumene	LCT	Rich
Alto Mirador	" "	" "	REL-Li	Lepidolite	LCT	Rich
Boqueirão	" "	" "	REL-Li	Spodumene	LCT	Rich
Capoeira 2	" "	" "	REL-Li	Spodumene	LCT	Rich
Carrascão	" "	" "	REL-Li	Lepidolite	LCT	Rich
Quintos	" "	" "	REL-Li	Spodumene	LCT	Rich
-	Mocuba, Mozambique	Alto Ligonha District	-	-	-	-
Siedlimowice	Świdnica, Poland	Strzegom-Sobótka	REL-Li	Beryl-columbite	LCT	Poor
Tourmaline King Mine	California, USA	Pala District	MI-Li	Lepidolite	LCT	Rich
Greenlaw	Maine, USA	Oxford Pegmatite Field	REL-Li	Beryl-columbite	LCT	Rich
Keith	" "	" "	REL-Li	Beryl-columbite-phosphate	LCT	Rich
Pulsifer	" "	" "	REL-Li	Beryl-columbite-phosphate	LCT	Rich
Lord Hill	" "	Paris-Rumford District	REL-Li	Beryl-columbite-phosphate	Mixed	Poor
Ben Murphy Mica Mine	Maryland, USA	Wissahickon Group	MSREL	-	-	Poor
-	North Carolina, USA	Spruce Pine District	-	-	-	Poor
Burleson Mica Mine	" "	" "	MSREL	-	-	Poor

Abbreviations of pegmatite classes and subclasses as follows: MI-Li – Miarolitic class, Li subclass; MSREL – Muscovite rare-element class, Li subclass; REL-Li – Rare-element class, Li subclass.

APPENDIX. Table A1. Trace element chemical composition of gahnite from granitic pegmatites and the Nine Mile MMSD obtained by LA-ICP-MS (in ppm).

Location	Analysis	Spot#	Li	Na	Mg	P	Ca
Alto do Giz (BPP), Brazil	**58 165054 25 160m**	**58**	45.56		1397	60.72	
	59 165054 27 160m	**59**	32.69	0.91	1384		792.15
	60 165054 28 160m	**60**	46.16		1303		
	61 165054 P2 160m	**61**	35.76		1495		
	62 165054 P1 160m	**62**	42.16		1233	210.40	
	63 165054 160m	**63**	45.66		1252		1159.14
	64 165054 160m	**64**	76.61		1329		401.08
	65 165054 160m	**65**	46.70	1.10	1434		
	66 165054 160m	**66**	50.63		1726		885.42
	67 165054 160m	**67**	55.08	0.79	1397		
	68 165054 160m	**68**	56.87		1533		
Alto Mirador (BPP), Brazil	**69 PEG 1B-B C6 160m**	**69**	36.65		2244	74.60	
	70 PEG 1B-B C6 160m	**70**	44.04	1.55	2715		
	71 PEG 1B-B C6 160m	**71**	34.15	2.34	2733	112.57	
	72 PEG 1B-B C6 160m	**72**	65.29		2003	68.96	
	73 PEG 1B-B C6 160m	**73**	81.15	2.17	2541	62.09	345.74
	74 PEG 1B-B C6 160m	**74**	70.27		3631		
	93 PEG 1A-A 1 160m	**93**	38.94	1.30	1573	133.14	605.56
	94 PEG 1A-A 3 160m	**94**	10.78		1717		
	95 PEG 1A-A 5 160m	**95**	64.98		1849		
	96 PEG 1A-A 9 160m	**96**	56.09	1.76	2010		
	97 PEG 1A-A 12 160m	**97**	74.51		1938	265.86	776.63
	98 PEG 1A-A 15 160m	**98**	68.30		2018	176.34	
	99 PEG 1A-A 18 160m	**99**	47.98		2134		
	100 PEG 1A-A 22 160m	**100**	56.32	0.92	2116		
	101 PEG 1A-A 26 160m	**101**	45.11	3.43	2144		
	102 PEG 1A-A 160m	**102**	41.36	2.40	2160		
	120 AM PEG 1A 160m	**120**	67.16		5355		662.03
	121 AM PEG 1A 160m	**121**	37.30		5473		
	122 AM PEG 1A 160m	**122**	74.61	1.40	5242		
	123 AM PEG 1A 160m	**123**	70.17		5366		959.01
	124 AM PEG 1A 160m	**124**	71.72		5765	91.76	
	125 AM PEG 1A 160m	**125**	68.05	1.49	5448		1022.21
	126 AM PEG 1A 160m	**126**	80.60	1.25	5556	62.20	
	127 AM PEG 1A 160m	**127**	52.12	0.64	5277	144.36	575.24
	128 AM PEG 1A 160m	**128**	47.43	1.39	5282		
	129 AM PEG 1A 160m	**129**	47.64	1.81	5534		
	130 AM PEG 1A 160m	**130**	72.27	6.01	5520		
	131 AM PEG 1A 160m	**131**	68.07		5644		
	132 AM PEG 1A 160m	**132**	75.28	0.83	5271		
	165 PEG1B-B1 C2 160m	**165**	54.32	1.58	3020		
	166 PEG1B-B1 C2 160m	**166**	62.44	0.98	4143		
	167 PEG1B-B1 C2 160m	**167**	56.54	1.24	3400	221.12	
	168 PEG1B-B1 C2 160m	**168**	81.81		3229	68.12	
	169 PEG1B-B1 C2 160m	**169**	18.68		4161		
	170 PEG1B-B1 C2 160m	**170**	69.16	1.22	3713		488.86
	171 PEG1B-B1 C2 160m	**171**	51.33		2877		
	172 PEG1B-B1 C2 160	**172**	39.34	0.97	3616	73.66	
Ben Murphy Mica Mine, MD	**146 113021 160m**	**146**	56.30	0.73	841	216.13	
	147 113021 3 160m	**147**	26.09		1020		339.79
	148 113021 4 160m	**148**	23.06		718		
	149 113021 P2 160m	**149**	66.28		1041	210.14	
	150 113021 P3 160m	**150**	42.83		1164	274.70	
	151 113021 160m	**151**		1.28	862		
	152 113021 160m	**152**	58.29	2.19	1051		354.43
Blanca Dora, Argentina	**164 GH253 T1 1 160m**	**164**	64.19	1.37	1288		1005.94
	165 GH253 T1 2 160m	**165**	57.95	2.06	1538		291.28
	166 GH253 T1 3 160m	**166**	107.50		1406		423.77
	167 GH253 T1 4 160m	**167**	60.21		1172	258.70	

Table A1 continued.

Spot#	Sc	Ti	V	Cr	Mn	Co	Ni	Cu	Ga	Ge	As	Rb	Sr
58		8.22	4.08	5.01	6624	37.85		43.66	316.3			0.52	0.16
59			3.64	2.30	6533	9.10	7.83	41.24	306.6		1.76		0.31
60		26.93	1.91	3.66	5330	50.80		52.11	321.6	2.81	5.73	0.20	
61		21.52	4.13	2.79	7047	9.77		41.77	306.2	1.20			
62			1.53	3.01	7068	8.03		41.41	305.0			0.62	0.80
63			2.98	4.71	6855	11.14		46.62	319.3				
64	2.91	18.20	3.88	4.36	6393	18.87	2.94	50.40	304.7			0.21	
65		21.43	4.28	2.88	6898	10.58		41.84	320.5		6.65		0.25
66				10.67	7156	11.66		44.87	318.4		4.48	0.51	0.16
67	2.60	23.97	6.96	2.50	6917	8.48		44.49	317.2		1.41		
68			4.47	3.28	6661	8.02		43.49	306.7	1.04			
69	2.17		3.96		5512	9.59		40.82	261.5				0.41
70	2.10		4.08	3.94	6346	10.05		42.68	292.9		1.35		0.19
71	1.20		12.62	4.37	6424	10.35	9.37	40.57	304.7		4.99		
72	2.31		7.74		5637	14.22		42.53	255.7	2.77			0.51
73	1.66		12.59		5324	10.44	2.06	52.03	250.2			0.35	
74			4.65	3.14	6165	14.19	16.47	37.48	294.7				0.38
93			2.12	1.05	6301	10.35	1.87	34.92	309.3			0.48	0.69
94	1.71	31.56		1.47	6806	10.34	6.13	30.77	317.7	1.81	1.41	0.67	
95		17.33	8.61		6712	10.63	9.20	45.87	309.3			0.18	
96			8.43		7320	8.35		39.42	313.2		10.61	0.74	
97	3.11	9.54	4.32		7026	9.50	7.68	41.30	315.6			0.67	0.80
98		17.17	9.21	3.18	7062	9.03		48.51	327.8				0.61
99			5.68	1.19	6924	10.14		49.59	310.7	1.75			0.28
100	2.02		1.53	4.30	7314	10.17	5.10	44.64	316.3				0.18
101			8.47	1.38	7166	10.23		42.04	317.8	2.36	7.46	0.74	
102	1.42				6735	10.33		43.96	303.3	1.02		0.64	0.16
120			5.12		7822	6.31	4.84	45.69	277.2	1.31		0.26	
121	2.09		4.06		7967	5.66	5.99	49.40	263.4	1.10		0.22	0.55
122					7956	5.21	4.07	48.41	289.8			0.35	0.11
123			6.67	5.42	8371	6.37	2.07	47.81	280.5	1.24		1.50	
124		37.91	2.82	4.21	8378	10.54	4.44	54.35	296.4	0.88		0.81	0.40
125	1.06		2.64	3.43	8401	4.69	3.15	42.43	289.2			1.17	0.71
126		11.58	5.96	1.76	8819	4.58	3.23	52.50	292.5	3.51	6.14	0.36	
127		20.53		1.75	8484	8.03	2.60	49.75	280.5			0.38	
128			3.72		8623	7.33		49.23	285.8		4.59		
129		14.00	3.01	7.73	8322	6.93		49.20	301.9	1.11			0.22
130			4.59		8460	5.17		43.38	277.4			1.38	
131			3.99	2.85	8525	9.38		45.35	281.7	2.03			
132		19.63	8.54	7.10	8627	8.01		58.65	295.7			2.10	0.82
165		7.80	10.31		5537	15.40		29.22	259.0	0.68			
166			9.44		7156	12.02	2.27	44.75	265.9		3.82		
167	4.01			3.84	6079	14.76		43.93	259.9		1.50		0.77
168		8.83	7.81		5732	14.57	3.51	43.67	289.6		4.24		0.16
169			5.10		6662	14.59		47.56	268.4			0.21	0.12
170			7.11	1.01	6409	14.69		50.50	264.0	0.71	4.89	0.29	0.22
171	3.41	24.75	7.74		5419	28.84	3.58	40.09	268.0			0.38	
172			8.53	4.47	6544	14.09		38.93	265.0				
146	0.89		4.29	2.30	3636	32.29	4.99	21.57	167.0	0.80	5.37	0.59	
147	2.85				3841	37.47		21.30	176.2		5.47	0.66	0.17
148	1.15	27.18		4.49	3942	39.88		18.37	173.8				0.63
149		16.90			3680	38.23	3.75	21.04	154.3				
150		28.50			3771	37.37		22.04	166.1		6.23		
151	0.92		1.51	6.53	3795	38.92		18.25	161.7	0.61			
152	4.10				3687	39.70	8.15	20.03	175.9		10.18	0.30	
164	2.22		4.18		4480	1.56	2.69	22.91	277.5			0.90	
165	4.11	21.52	4.12	2.18	4825	1.01	4.77	23.90	300.7	1.50	1.55	20.55	0.52
166	4.16	8.56	5.98	1.43	4912			33.08	296.3			1.87	
167	1.09		2.72	2.44	4645	1.99	5.61	17.65	289.6	1.03		2.28	

Table A1 continued.

Spot#	Y	Zr	Nb	Mo	Cd	In	Sn	Sb	Cs	Ba	La	Ce	Pr	Nd	Sm	Eu
58		0.64	0.45		5.63			1.51	0.12		0.19		0.17			
59	0.27			0.43	11.35								0.39			
60				0.51	6.91		0.97		0.20		0.08			0.70		
61	0.24	0.27				0.28	1.06	0.87	0.27		0.24	0.09				0.14
62	0.42			1.57	21.14	0.24			0.30		0.25	0.33	0.12			
63			0.63	2.36							0.22	0.23		0.61		
64		0.37		0.52	16.38		0.95	1.06	0.17		0.14					
65	0.14		0.38		6.52					1.16					0.36	0.29
66	0.15		0.74		8.47	0.47							0.27			
67	0.33				4.38		0.40		0.13		0.11	0.07				
68	0.12	0.69	0.37		16.56	0.29		0.73		2.76		0.09	0.20	0.70		
69	0.20	0.84	0.49		23.16				0.25	1.35		0.33	0.18			
70	0.28	0.64	0.34		9.86						0.31	0.40			1.68	
71		0.72	0.37		19.93		1.41			1.40					0.70	
72			0.12				0.60				0.15		0.10			
73					31.73	0.12	0.76					0.09		0.63	0.41	
74	0.28	0.36	0.23		32.06				0.15		0.52	0.20		1.88	1.51	
93					5.47							0.22				
94	0.26				16.84							0.34			0.60	
95		0.42			23.73	0.50	2.54	0.81			0.42		0.31		0.40	
96	0.57			0.64	13.93				0.24		0.07	0.43	0.08			
97			0.11		21.22		1.25		0.18				0.25			0.34
98	0.25	1.03			24.20		1.75		0.50					1.81	0.92	
99	0.11		0.28		14.40		1.37			0.89		0.13				
100			0.51	0.39	32.18		0.56	1.55	0.31	3.44			0.12		0.47	
101				2.93	16.09	0.24		1.17	0.42	0.88		0.21			0.51	0.20
102			0.15	0.47		0.33		1.18				0.17		0.79	0.48	0.16
120			0.34		2.93	0.42		0.56	0.40	0.57			0.14	0.58	0.81	0.49
121				0.85	9.06	0.30		0.66	0.50					1.46		
122	0.13		0.58		16.91	0.22				0.72	0.12	0.19		0.48	0.81	
123		0.27	0.40		13.12	0.29			1.17	0.94	0.34		0.16		0.84	0.26
124			0.25	1.17	17.56				0.36				0.15		0.63	
125					16.90	0.30	0.33		0.94						0.69	
126		1.07	0.29		8.80		0.80			1.69	0.12	0.35	0.17			
127							0.80		0.41							
128				1.05	19.45	0.17			0.70	0.57		0.16				
129			0.30	1.61	16.93		0.95						0.06	0.66		0.32
130	0.20		0.32	0.46	12.75	0.14	0.84	0.91	2.48	1.21	0.20	0.08				
131	0.55				26.60					1.16		0.09			1.04	0.41
132			0.18	1.24	3.54	0.25		1.05	1.18	1.92	0.64	0.91	0.13			
165	0.36		0.45		25.75		0.65				0.15		0.15		0.51	0.17
166			0.22		22.61			0.96		1.14		0.18		0.34		0.40
167		0.57		0.93	14.24	0.27	1.36	1.27			0.22	0.37			1.04	
168	0.21				36.84			0.65	0.25		0.18	0.22				
169			0.11		11.46		1.48		0.28	2.23			0.16		1.13	
170			0.39		20.17		1.14		0.22	2.28	0.13	0.19	0.09		1.13	0.22
171	0.29				29.49				0.10	0.92	0.39	0.14		1.91		
172			0.42	0.93	17.63	0.15		0.36	0.28			0.13		0.41		
146				0.71	10.69							0.07				
147	0.31	0.52		2.58	3.25		0.65	0.68		0.89	0.07		0.17	0.31		0.14
148	0.53					0.25	0.49				0.07				0.84	0.50
149	0.54	1.52			24.64				0.21			0.60		1.17	1.84	
150	0.49		0.17	0.72	21.46			1.63				0.17	0.06		1.67	0.31
151			0.27	0.50	9.26				0.09		0.51		0.33			0.42
152	0.13			1.50	6.70		1.79				0.09	0.17				
164						0.53					0.48		0.23		1.42	
165	0.10	0.74			13.98	0.11	2.22		0.75	2.53		0.09	0.17	0.59	0.82	
166		2.80		0.92	9.23		2.42	1.11			0.30		0.07	1.08	1.37	
167							0.45			2.21		0.20				

Table A1 continued.

Spot#	Gd	Tb	Dy	Ho	Er	Tm	Yb	Lu	Hf	Ta	W	Tl	Pb	Th	U
58	1.45	0.26	0.30		0.68						0.78	0.34			
59		0.10	0.39		0.55		0.71				1.25	0.53		0.13	0.23
60			0.30	0.05	0.79			0.06	0.32					0.23	0.26
61					0.50				0.22		0.95	0.17			
62		0.12			0.37		1.15			0.17		0.20		0.20	0.20
63	0.39					0.12	0.52		0.16			0.27		0.24	
64		0.21	0.40				1.18	0.07	0.40		0.64	0.57	0.54		
65				0.12	0.26	0.20						0.39			
66				0.07	0.49			0.17		0.40		0.17	0.52	0.12	0.23
67	0.55		0.33			0.16		0.16			0.31		0.41		
68			1.15			0.12	0.51								
69		0.15	0.46		0.46				0.18		1.38	0.54			
70								0.17	0.28	0.22			1.59	0.36	
71					0.44	0.19				0.09			0.33		0.10
72					0.18	0.18	0.72	0.06	0.13		0.66	0.56			
73							1.41						0.71		0.59
74			0.65	0.12		0.13			0.18	0.26	0.40				0.09
93											0.76	0.37	0.54		0.30
94	0.65		0.50			0.05	0.52	0.13					0.20		
95		0.06	1.54		0.51	0.16		0.26		0.11			0.59	0.10	0.11
96		0.06			0.38		0.86		0.26						
97				0.31			0.99	0.14							
98		0.25	0.55	0.06				0.22		0.26	1.10	0.35	0.56	0.16	
99		0.12	0.85	0.13								0.17	0.51		0.31
100				0.16			0.57	0.14		0.18	0.86				0.34
101	0.52	0.13			0.79			0.20		0.14		0.14			
102		0.26						0.19				0.30		0.23	0.28
120															
121				0.09		0.05	0.39		0.31	0.23		0.48		0.23	
122				0.13		0.14			0.28	0.07	0.78			0.10	
123				0.09					0.39		0.98				
124						0.16	0.69	0.09		0.14				0.18	0.17
125		0.08	0.58			0.26	1.39				0.94		0.83		0.07
126		0.14							0.20			0.16	0.96		
127		0.17			0.40	0.19				0.17					
128	0.73		0.91	0.16		0.07							0.89		0.17
129	0.78	0.07		0.26			0.34		0.30	0.08				0.44	0.35
130						0.08	0.73			0.15		0.71	0.23		
131	1.25						0.39		0.22	0.20	0.45	0.16	0.38		0.15
132					0.66	0.18	1.16		0.47	0.06	0.39		0.27		0.10
165		0.11		0.28	0.86	0.13	0.82			0.26		0.29	0.46		
166		0.05	1.08								0.60				0.15
167			0.85		0.95				0.44		0.29		0.35		
168	1.21	0.15					1.65	0.06					1.61		
169						0.28		0.10	0.28	0.14			0.40		
170			0.57	0.09					0.22				2.15	0.33	
171		0.23			0.27							0.24	0.33		0.07
172					0.59		0.53		0.19			0.47			0.13
146				0.17		0.16			0.38			0.22			0.10
147		0.06	1.15	0.07	0.78							0.37			
148		0.11							0.24		1.46				0.30
149				0.31	0.76		1.21	0.16			0.93				0.21
150	2.40		1.11	0.21	0.75				0.46		1.03	0.18			
151							0.71		0.26				0.41		0.65
152	1.53			0.08							0.38		0.53	0.22	
164			0.33				1.54	0.09			1.08				
165			0.66		0.40					0.17			1.48		
166			0.42					0.15							0.43
167		0.05					0.48	0.06		0.10				0.12	

Table A1 continued.

Location	Analysis	Spot#	Li	Na	Mg	P	Ca
Blanca Dora, Argentina	**168 GH253 T1 5 160m**	**168**	39.37	100.94	1502	309.86	
	169 GH253 T1 6 160m	**169**	48.80		1270		455.36
	170 GH253 T1 7 160m	**170**	49.41		1481		588.13
	171 GH253 T1 160m	**171**	43.52	1.00	1379	354.85	
	172 GH253 T1 160m	**172**	7.52	2.97	1233		
	173 GH253 L2 1 160m	**173**	38.90	1.15	1131	131.50	
	174 GH253 L2 2 160m	**174**	42.94	2.95	1156	111.94	
	175 GH253 L2 160m	**175**	13.37		1139		474.51
	176 GH253 L2 160m	**176**	32.40	0.77	1509		
	177 GH253 L2 5 160m	**177**	30.12		1401		309.40
	178 GH253 L2 6 160m	**178**	60.93	0.86	1669		
	179 GH253 L2 7 160m	**179**	49.44		1520		
	180 GH253 L2 160m	**180**	22.92		1340		769.67
	181 GH253 L2 9 160m	**181**	34.46	0.93	1358		
	182 GH253 L2 160m	**182**	32.69	1.69	1422		
	183 GH253 L2 11 160m	**183**	33.28		1323	130.27	
	184 GH253 L2 12 160m	**184**	45.96		1288	194.25	
	185 GH253 L2 13 160m	**185**	42.03		1185		470.32
	186 GH253 L2 160m	**186**	11.87		1047		
Boqueirão (BPP), Brazil	**29 BOQ AB C1 110m**	**29**	77.13	5.84	1028		
	30 BOQ AB C1 110m	**30**	84.27		1557		927.88
	31 BOQ AB C1 110m	**31**	51.17		1812	247.95	644.21
	32 BOQ AB C1 110m	**32**	116.94		993		
Burleson Mica Mine, NC	**87 R1957 Cr1 P16 160m**	**87**	23.02	1.42	720	256.54	
	88 R1957 Cr1 160m	**88**	29.31		599		
	89 R1957 Cr1 P15 160m	**89**	9.86	2.51	796		
	90 R1957 Cr1 P14 160m	**90**	11.33	1.91	626	107.63	
	91 R1957 Cr1 160m	**91**	45.50	1.46	773		420.03
	92 R1957 Cr1 P13 160m	**92**	14.77	3.15	716	60.17	
	93 R1957 Cr2 P1 160m	**93**	9.65	3.66	784		
	94 R1957 Cr2 P2 160m	**94**	14.33		809		783.12
	95 R1957 Cr2 160m	**95**	22.08		674	89.87	308.60
	96 R1957 Cr2 P3 160m	**96**	11.14	1.45	534		370.56
	97 R1957 Cr2 160m	**97**	32.14	2.28	674	322.93	519.45
	98 R1957 Cr2 P18 160m	**98**	37.12		696		729.45
	99 R1957 Cr2 160m	**99**	9.07	0.92	701		598.48
	100 R1957 Cr2 P19 160m	**100**	47.97		779	236.85	
Capoeira 2 (BPP), Brazil	**117 CAP 2B 160m**	**117**	128.07				399.61
	118 CAP 2B 160m	**118**	191.46	2.80	38	84.09	
	119 CAP 2B 160m	**119**	94.69			62.86	
	120 CAP 2B 160m	**120**	173.42	1.57	201		
	121 CAP 2B 160m	**121**	96.11				296.01
	122 CAP 2B 160m	**122**	95.34		105		
	123 CAP 2B 160m	**123**	89.48	0.95	30		
	124 CAP 2B 160m	**124**	84.22		114		
	125 CAP 2B 160m	**125**	69.59	1.11			
	126 CAP 2B 160m	**126**	88.83		145		
	127 CAP 2B 160m	**127**	46.81	2.01	194		768.07
	128 CAP 2B 160m	**128**	77.36				410.89
	129 CAP 2B 160m	**129**	119.05			131.31	
	130 CAP 2B 160m	**130**	92.87	0.74		86.94	434.16
	131 CAP 2B 160m	**131**	62.56		66	131.29	1223.92
	132 CAP 2B 160m	**132**	79.16			94.42	
	186 CAP2A 160m	**186**	375.64	7.13			
	187 CAP2A 1 160m	**187**	111.86	3.41	175	78.99	
	188 CAP2A 3 160m	**188**	112.02	2.17			
	189 CAP2A 5 160m	**189**	84.54		221		
	190 CAP2A 8 160m	**190**	79.93	1.38	108	224.94	417.47
	191 CAP2A 10 160m	**191**	114.12	3.38	231	195.50	464.06

Table A1 continued.

Spot#	Sc	Ti	V	Cr	Mn	Co	Ni	Cu	Ga	Ge	As	Rb	Sr
168				6.91	2567	3.33		8.82	314.7	5.33		1426.48	0.32
169				1.93	5034	0.99		18.23	294.3	3.39			0.20
170	1.90		1.46	5.17	5168	2.85	3.83	19.12	316.8		6.97		
171			3.14		4937	0.49	11.88	20.56	312.5	1.54			
172					4282	1.78		21.49	289.5		1.95	2.76	0.60
173		30.35	4.90	5.19	4250	1.66	13.98	22.08	278.4	1.89		0.15	
174	1.44		4.87	5.48	4868	4.05		22.07	296.5		3.06	0.63	0.34
175			5.12		4148	2.46		20.25	307.0	1.33	4.69	0.59	0.38
176			1.55	2.07	4809	0.82	6.44	22.73	287.3		2.43		
177	1.63	13.05	8.18	2.06	4859	2.33		23.03	298.0	0.96		3.67	
178			3.65		5133			23.55	308.4			2.86	0.25
179	1.13		5.08	4.00	5097	0.44		21.53	291.7		2.68	1.36	
180		26.31		0.98	4862	1.04	2.76	20.09	287.3		5.19	0.44	
181	0.85	25.95	5.49		5081	0.50		24.60	306.6		8.85	0.92	
182	0.95		4.73	1.49	5450	2.78		19.58	312.3	1.10	5.88	0.67	
183				3.24	4935	2.62		22.60	300.6	1.30	3.48	0.15	0.60
184	1.83		3.74	1.74	4748	1.59		27.50	315.9	1.42		2.35	
185	0.84	16.04	3.12	2.53	4704	1.27		20.27	308.2	1.76			
186				2.31	3832	0.85		23.50	272.8	2.25			0.73
29	4.16		4.73	2.70	4331	8.07		20.14	329.2	2.72		1.08	
30	1.73				4691	5.84	3.71	16.75	348.7			0.45	0.76
31	4.75	19.27	3.42	2.39	4642	5.00		17.01	330.8	1.00		0.32	0.54
32					4245	7.84		20.00	346.0	4.53		0.79	
87			13.22	10.02	5212	7.65		18.23	273.8	3.41		0.43	0.95
88	3.73		13.08	3.95	5572	6.51	7.68	23.66	286.5	1.01	6.95		0.21
89	1.12	14.69	12.26	1.85	5680	9.59	2.45	21.00	284.3	3.45			
90	3.83	36.77	14.17	2.88	5775	7.08	1.97	19.08	282.5				
91	1.13	7.10	9.07	3.68	5604	7.00		16.07	284.3		5.56		0.46
92		9.88	9.97	6.22	5410	6.55	6.25	25.88	276.3			0.40	0.32
93		11.48	12.12	4.78	6007	5.59	7.29	19.44	275.0	0.58	6.90		
94			9.21	2.20	5779	7.62		16.96	288.1	1.64	8.21	0.62	
95	4.02	15.88	5.50	1.98	5474	6.94		23.55	299.6	1.22	1.51	0.25	
96	1.80		10.21	1.45	5287	6.00		21.36	287.7				
97	2.72		9.85		5770	7.29	9.05	22.18	280.4	1.78	7.86		
98		9.07	7.87	2.08	5692	7.03	10.66	23.68	288.4	0.96		0.28	0.27
99		9.64	9.41	3.67	5853	8.89		20.26	268.2				0.70
100	2.68		11.30	1.96	5655	5.56		22.25	291.7	2.00			
117		23.29			5195	0.63	4.82	49.39	359.7	1.09	3.70	6.71	
118				3.07	5284	1.64		44.16	372.1			3.31	1.26
119	1.66	13.32			5719			51.76	408.4			1.50	0.21
120	2.84	16.69		5.59	5176	1.09	5.34	46.61	390.8			17.55	1.07
121	2.58			2.84	5454	1.59		48.32	387.1	1.81		0.49	0.22
122		50.36		2.35	5152	0.99		50.98	383.0			0.66	
123	2.78		5.21		5110			45.51	375.5		3.43		
124					5085		6.20	47.53	392.4				
125	2.79	24.38		3.57	4671			49.24	401.1	0.95	4.84		0.45
126	2.98		7.56	4.01	4809			50.67	391.9	1.07		0.16	
127	2.87				5057		4.29	55.49	388.0	1.36	2.82	0.29	0.43
128	2.12	16.07		5.25	5302	1.75		54.92	404.1	2.42	1.94	0.26	
129	1.26			1.61	5019		5.18	55.47	414.2			1.06	
130	1.38			4.26	4928			57.73	405.8			2.65	0.13
131	2.57			2.18	4643	0.69		61.19	418.8			0.21	
132	4.08			4.29	4495	0.44		52.71	421.8	2.62			
186			9.36		4804	2.30	6.04	67.99	369.3	6.42	2.79	8.82	0.82
187		9.71			4900		7.74	68.22	373.3	2.55		0.24	
188				4.63	4459		2.97	53.66	375.4				
189			2.57		4617	1.24		59.40	371.8				
190	1.93	9.83		5.67	4838	1.58		60.69	383.8				
191		9.68	1.88	4.25	5048		1.80	59.79	396.3	0.96			0.21

Table A1 continued.

Spot#	Y	Zr	Nb	Mo	Cd	In	Sn	Sb	Cs	Ba	La	Ce	Pr	Nd	Sm	Eu
168			8.15		11.73	0.35	3.60		18.54	15.86			0.10			
169					12.05	0.28	1.67	1.64			0.08	0.14	0.16			0.32
170	0.16		0.12	1.88		0.17				2.06				0.68		
171		0.64			16.54		1.05		0.18			0.08	0.08		0.93	0.11
172		0.33			7.05	0.11	1.15	1.11	0.51	10.49		0.14		0.72		
173						0.30	0.39		0.43			0.09				
174	0.70	0.25		1.51	6.27	0.13					0.09					0.37
175		0.38			6.33				0.14				0.07	0.81		
176	0.23				9.92	0.11	0.67	0.51						1.12		0.25
177	0.35	0.36			11.42				0.15	2.75			0.16	0.30		
178	0.25	1.19	0.45	0.51	18.91		1.23	2.19							1.54	
179		0.25	0.21	1.32	8.02							0.07		0.72	0.41	0.13
180			0.23		8.47	0.21	0.86		0.21	2.01	0.09		0.12			0.47
181	0.45		0.35		13.73			1.31			0.10	0.08			0.89	
182			0.21		5.06	0.35	1.91	0.39	0.25			0.21		0.55	1.27	
183		0.68	0.16					0.83						1.00	0.61	
184					3.61	0.22	1.58		0.21	1.71	0.63					
185			0.23			0.43	2.00			1.68					0.75	
186		1.04	0.22		9.07				0.23	1.74		0.07	0.08	0.79	1.09	
29	0.60		1.06		30.04	0.35	0.67		0.76						1.17	0.84
30	0.62	12.71	1.38		12.23			3.68	0.58	3.93			0.25	2.13		
31	0.44	0.84					1.07				0.24	0.49		1.78		
32					25.75		0.66					0.17		1.74		0.45
87				1.53			0.57			0.62				1.87		
88	0.20				6.56				0.30		0.29	0.13			1.41	0.50
89						0.14	2.27	0.86						0.99		
90	0.52		0.26	0.62	8.00			0.55		1.12				1.49		0.20
91			0.54	0.53	13.99	0.23	0.50		0.22		0.09		0.09		0.48	
92		0.23			12.21		1.04	0.45		1.65	0.21	0.12		1.05	0.45	0.38
93	0.11			1.05	15.11		0.79	0.59	0.23	0.87	0.07	0.32		0.44		
94					13.71	0.29			0.16	2.34	0.18					
95		0.71	0.16	1.06	10.26		1.54									
96					9.45	0.41	1.90			1.29			0.08	1.63		
97	0.17		0.26		14.96		1.49	0.69	0.17	1.96		0.12	0.11	0.33		
98			0.19	0.71	19.97		1.14	0.33		1.52	0.28	0.35		0.70	0.63	0.16
99				1.23				0.56	0.47			0.13				0.11
100		0.44			4.35	0.42		1.68	0.89	0.86		0.24	0.29			
117	0.29	0.26			8.03			1.06	0.51	3.37		0.14	0.08	1.73		
118		0.61		1.74			3.22		0.64	1.72	0.07			0.58		
119				1.06	14.43		1.05	1.01				0.09		0.47	0.67	0.17
120		0.53	0.59		21.98		0.57		1.35	9.04	0.23			0.58	0.41	
121	0.31		0.38	1.24	7.51			1.48		2.99		0.33				
122	0.48	0.34	0.39		15.25						0.18					
123			0.17		17.38										1.20	
124		0.52			17.02	0.18		0.77	0.22			0.10	0.32		1.29	
125	0.25	0.44		1.13	3.65	0.73	0.71	1.81		1.91		0.11		1.29	1.17	
126	0.23	0.55	0.14	0.68	13.25	0.11	0.38	1.85					0.13	0.41		
127			0.65		20.96	0.10	0.74		0.49		0.09	0.12				
128	0.14			0.77	26.82		1.57		0.26			0.14			0.57	
129	0.24		0.19		21.64	0.25	2.07	1.42		3.01	0.20					0.13
130		0.77		1.53	5.57			0.88	0.09			0.20	0.34			
131		0.82		1.98	11.97	0.23		1.19		0.59			0.10	0.77		
132		0.48	0.17		28.64	0.12	0.82		0.44	1.22	0.66	0.12		0.94	0.76	
186			1.02	1.24	22.84	0.12		0.87		7.88	0.75	0.41	0.12		1.41	0.32
187	0.21				8.84		0.43	0.96								
188	0.49			0.51	36.79	0.31	1.59	0.44	0.29	0.63	0.32	0.19				
189				2.14	21.19	0.56			0.32	0.65		0.12	0.33	0.40	1.18	0.28
190			0.21		21.35	0.69	1.24	0.70		3.88		0.27	0.09	3.02	0.38	
191				0.66	3.23			0.77	0.28		0.20	0.12	0.08	1.29		

Table A1 continued.

Spot#	Gd	Tb	Dy	Ho	Er	Tm	Yb	Lu	Hf	Ta	W	Tl	Pb	Th	U
168			0.53	0.13	0.83	0.11				1.60	8.72	7.67	9.46		
169									0.37		0.61				
170	1.29		0.31	0.18	0.32	0.18					0.32		8.10		
171	0.62	0.31	0.38			0.25						0.18		0.34	
172	1.08									0.07	0.99	0.17	0.94	0.20	0.47
173			0.56			0.06							0.47	0.31	0.53
174	1.50							0.08	0.44			0.25			
175		0.14	0.34			0.26	0.51	0.17							
176						0.07		0.10			0.42			0.11	0.30
177	0.72				0.66			0.11	0.64	0.08	0.51				0.15
178		0.13		0.06	0.61			0.13			0.49				
179	1.15	0.07		0.18				0.14		0.32			0.67	0.19	
180		0.21	1.08	0.10	0.32			0.13	0.27	0.11	0.61		0.23		0.19
181			1.76	0.06					0.16			0.27			0.17
182					0.79						0.62			0.10	
183	0.40			0.06	0.90					0.19	0.59	0.24	0.83		
184		0.10	1.07				0.79				0.98		0.79		0.13
185			0.78	0.19		0.20	0.78	0.09	0.16	0.05	1.04	0.20			
186		0.09				0.12	0.81		0.46	0.19					0.25
29	0.66	0.37	2.67	0.15	0.86		2.01		1.53			1.09	0.34		
30	2.27			0.13			2.72		0.55	0.12	0.55	0.37	0.30		10.73
31		0.14	0.88					0.13		0.34			0.66		
32		0.37	2.00		0.64							0.60			0.39
87	1.03	0.26	0.33			0.15	0.98						0.31		
88	4.23	0.12	0.83		0.29										
89	0.62	0.13		0.19		0.11		0.23			0.78	0.17	0.19		
90	0.47					0.17	0.59	0.20				0.24	0.64	0.15	0.12
91	0.68		0.86	0.18			1.52						0.77	0.39	0.11
92	0.49		1.67	0.20		0.09			0.27			0.55	0.87	0.17	
93						0.07	1.28	0.16		0.32	0.77				0.39
94	1.28	0.24							0.27	0.24					
95		0.08	1.23	0.15	0.32		0.90					0.46	0.58		0.13
96	0.38								0.84		1.11	0.21			0.14
97											0.30	0.31	0.48	0.18	
98													0.34		
99				0.08	0.33		0.28			0.10			0.96	0.13	
100			1.69			0.12	1.14	0.07		0.26	0.72	0.37		0.11	
117						0.25						0.76	0.36		0.25
118						0.30						0.22			
119			1.78		0.31	0.37		0.07	0.32					0.28	0.16
120		0.37						0.08		0.11	0.34	0.54		0.20	0.21
121						0.24	0.63	0.11		0.08	0.63	0.88			
122	0.78	0.08	0.64	0.28			1.58		0.17						
123		0.11	0.30	0.07	0.36	0.10		0.12	0.37					0.35	
124				0.06				0.10	0.33		0.42				0.19
125				0.21		0.05			0.33						0.82
126			1.59	0.20						0.07			0.45		
127		0.12					1.19		0.26		0.62		0.42		
128				0.06		0.13							0.83	0.10	
129	0.77			0.18		0.11	1.15		0.20			0.18		0.54	0.27
130	1.83							0.28							
131		0.08			0.19			0.05			1.44	0.29	0.30	0.19	
132		0.07		0.25		0.17		0.11	0.45	0.31	0.75		0.62	0.20	0.53
186	0.83				0.72		0.68						1.23		0.54
187					0.27					0.08	0.54		0.28		
188			1.59	0.18					0.20				1.40		
189		0.11		0.14		0.22			0.53				0.24		
190	1.32			0.09	0.52										0.31
191		0.28	0.74		0.38		3.06		0.31	0.13		0.22		0.45	

Table A1 continued.

Location	Analysis	Spot#	Li	Na	Mg	P	Ca
Capoeira 2 (BPP), Brazil	**192 CAP2A 13 160m**	**192**	50.58			68.89	
	193 CAP2A 160m	**193**	65.90	1.06	174		1559.04
	194 CAP2A 18 160m	**194**	71.59				
	195 CAP2A 21 160m	**195**	80.43	1.89	101	310.33	771.92
	196 CAP2A 24 160m	**196**	87.51			66.61	
	197 CAP2A 27 160m	**197**	91.06		79	242.66	
	198 CAP2A 160m	**198**	79.70	2.77	175	134.70	
	199 CAP2A 160m	**199**	63.10	0.87	370		617.23
	187 CARR PEG 110m	**187**	76.79		259		
	188 CARR PEG 110m	**188**	58.49		391	259.57	
Greenlaw, ME	**19 Greenlaw17 160m**	**19**	83.15	0.84	666		794.66
	20 Greenlaw17 P2 160m	**20**	69.03		594		304.81
	21 Greenlaw17 160m	**21**	63.35	0.72	748		295.13
	22 Greenlaw17 160m	**22**	202.12	2.58	635	59.22	505.13
	23 Greenlaw17 160m	**23**	49.80		600		
	24 Greenlaw17 160m	**24**	70.25		606	57.40	
	25 Greenlaw17 160m	**25**	45.04	3.62	795		495.71
	26 Greenlaw17 160m	**26**	48.64		618		
	27 Greenlaw17 160m	**27**	441.36	1.36	700		
	28 Greenlaw17 160m	**28**	119.19		619		
Juan Román, Argentina	**19 GH007 Cr1 T1 1 160m**	**19**	82.13	2.60	832		
	20 GH007 Cr1 T1 2 160m	**20**	59.39	1.08	816	183.24	
	21 GH007 Cr1 T1 4 160m	**21**	71.84	2.36	563		771.83
	22 GH007 Cr1 T1 5 160m	**22**	84.54		745		474.28
	23 GH007 Cr1 L1 3 160m	**23**	90.50	0.78	777		
	24 GH007 Cr1 L1 4 160m	**24**	66.39	1.91	683	191.26	
	25 GH007 Cr1 L1 5 160m	**25**	68.23		687		
	26 GH007 Cr1 L2 1 160m	**26**	25.88		1033		327.76
	27 GH007 Cr1 L2 4 160m	**27**	106.84		978	310.64	826.07
	28 GH007 Cr1 L2 5 160m	**28**	96.12	0.98	640	181.53	
	29 GH007 Cr1 160m	**29**	101.80		620		555.97
	30 GH007 Cr1 160m	**30**	85.96	6.72	705		
	31 GH007 Cr1 160m	**31**	69.33		741		594.06
	32 GH007 Cr1 160m	**32**	42.18		947		
	33 GH007 Cr2 L3 1 160m	**33**	114.97		837	111.81	
	34 GH007 Cr2 L3 2 160m	**34**	99.03		809		
	35 GH007 Cr2 L3 160m	**35**	100.85	0.84	774		
	36 GH007 Cr2 L3 4 160m	**36**	93.43		813		
	37 GH007 Cr2 L3 5 160m	**37**	142.72		905	63.79	414.68
	38 GH007 Cr2 L3 6 160m	**38**	243.45	0.72	959		392.11
	38 GH011 L2 1 160m	**38**	63.76	1.60	987		
	39 GH007 Cr2 L3 160m	**39**	80.53	1.18	816		825.34
	39 GH011 L2 2 160m	**39**	80.19		1197	90.34	
	40 GH007 Cr2 L3 160m	**40**	96.80	1.17	825	160.06	
	40 GH011 L2 160m	**40**	68.90	2.28	1236	69.31	736.58
	41 GH011 L2 160m	**41**	49.89	1.23	1173	165.66	545.18
	42 GH011 L2 6 160m	**42**	55.67	1.93	1398	158.89	370.65
	43 GH011 L2 160m	**43**	47.88	0.96	1141		846.00
	44 GH011 L2 160m	**44**	55.98		866	182.63	
	45 GH011 L2 160m	**45**	56.74	2.28	1000		
	46 GH011 L3 160m	**46**	15.16	2.34	986		
	47 GH011 L3 1 160m	**47**	54.10	1.29	898		
	48 GH011 L3 2 160m	**48**	47.48		1093	60.50	949.54
	49 GH011 L3 3 160m	**49**	13.04	0.72	787		
	49 GH013 L1 160m	**49**	66.25	1.18	806		
	50 GH011 L3 4 160m	**50**	36.96		892		
	50 GH013 L1 160m	**50**	27.15		637		370.66
	51 GH011 L3 5 160m	**51**	40.29	2.53	891		
	51 GH013 L1 160m	**51**	60.96		905	104.59	

Table A1 continued.

Spot#	Sc	Ti	V	Cr	Mn	Co	Ni	Cu	Ga	Ge	As	Rb	Sr
192					4687		5.50	48.22	387.0	1.51		3.63	0.40
193		35.45	2.18		4888		11.67	53.21	380.8	3.00	3.18		0.93
194			2.88	3.23	5163			54.14	390.0	5.08			0.28
195	1.91				4945		7.52	50.47	380.3			0.39	
196	0.87	63.22		2.28	4903		9.96	55.04	389.0				
197			2.79		5140	0.65	2.64	49.75	378.0	3.15	9.21		
198		28.87		4.55	4831		7.09	45.58	371.5			0.55	
199	1.30		6.13	3.23	4763		8.16	47.33	393.1	3.99		0.72	
187		30.12		4.88	6587		11.62	23.29	326.10		17.81	0.31	
188					6091	3.37	10.39	16.90	293.30		3.17		0.21
19		8.06		3.29	3325	1.13		14.09	509.5				0.21
20				3.72	3164	0.99	3.66	23.16	528.1	0.70			
21		11.99			3221	2.38	2.32	16.96	533.0				
22	1.47				3517	1.47	10.04	16.99	564.7	2.36		4.91	0.25
23	2.97		1.60		3450	0.54	6.95	15.92	541.4	1.77		0.29	
24				1.82	3651	1.70	2.95	22.31	559.4			0.51	
25	1.44			3.42	3558		3.95	21.58	546.8			0.18	
26			2.33	3.48	3805	0.83		15.66	564.7				
27	1.72		1.52	8.84	3498			20.56	583.6			66.93	0.66
28	1.19	34.62		1.86	3087	0.56		19.18	570.3	1.62	1.92		
19		18.91		3.70	2937	0.49		20.81	262.2	1.39			
20	3.47		9.49	1.36	3265	2.58		17.72	276.7			0.54	
21					3119	1.10		15.44	279.9	1.47	1.63	0.21	0.22
22				5.40	3424	1.62		21.82	288.7	1.97		1.01	1.50
23		6.74	4.44	9.12	3134	2.99	1.82	13.77	275.0		6.54		0.21
24					3135	0.43	7.12	18.53	287.3	1.34		0.92	0.51
25	4.17		4.98		3062	3.77		22.21	287.8	1.09		0.27	
26	1.62	12.39		9.91	2404	2.95		21.29	264.2			0.20	
27			2.04	2.66	3090	0.59		14.79	284.2	1.09			
28				3.53	2973	1.73		21.76	285.4			0.67	0.23
29	1.04		1.51	1.25	3281	1.44		18.00	291.1	2.26		0.62	0.22
30	2.29	17.23		4.30	3214	0.75		17.43	287.7		4.28	0.53	0.38
31		23.98		4.37	3163	2.81		16.51	282.0		7.73	0.59	
32			2.48		3098	2.65	5.16	21.06	296.7		2.78	0.97	0.41
33			2.97	7.52	3254	2.99	2.10	19.79	282.5		6.05	0.96	
34	4.39	8.87	2.20	2.29	3432			16.33	291.6	2.09		0.44	0.56
35			1.48	1.27	3322	3.66	8.45	22.53	289.5	1.39		1.20	
36			3.01	3.71	3100	3.83		22.77	286.8		10.69	0.49	0.79
37	2.28			1.94	3278	2.41		17.65	289.6	2.11		0.79	
38	0.82				3006	2.53	9.55	28.82	286.1			0.68	
38				3.61	2648	1.21	12.09	18.13	247.4	0.97		0.15	0.23
39	2.89			3.54	3201			22.65	281.7	2.75	7.92	0.46	
39		25.09		1.29	3035	2.29		21.98	268.1			0.27	
40		12.24			3204	3.05		21.60	296.6	2.54			
40				1.06	3372	3.32		21.26	246.6			1.06	
41		27.67	2.17		3361	0.46		24.02	265.6	2.43		1.70	
42	3.86			5.20	3484	2.74		20.46	272.6	2.09	2.52		
43		7.99		3.02	3381	2.01		21.32	259.2	2.46		0.83	
44	1.13			2.02	3791	0.82		19.57	284.7			1.23	0.21
45				1.78	3905	0.69	7.24	21.28	281.0			3.29	
46			2.32		2702	3.22	8.07	43.45	275.0	1.29		5.91	3.07
47		8.06		2.65	3614	2.38		25.96	277.8		2.57	0.38	0.63
48		12.42			3674	0.68		16.53	288.7	1.31		0.23	0.31
49		6.59	1.65	2.09	3532	1.50		19.56	276.7	2.01		0.53	
49	2.59	9.19	4.85	6.99	2890	4.51		18.53	263.6				
50				2.19	3592	2.68		21.24	274.2	1.90	4.50		
50			3.35	3.79	3195	1.16	5.48	21.88	276.7	2.41		0.57	0.20
51		6.14		4.96	3503	3.17		22.86	266.7		6.87		
51	1.70		6.13	4.47	3039	0.77	7.21	14.83	271.5	2.15			0.26

Table A1 continued.

Spot#	Y	Zr	Nb	Mo	Cd	In	Sn	Sb	Cs	Ba	La	Ce	Pr	Nd	Sm	Eu
192	0.18	0.23		3.91	20.65		1.06	1.74	2.97			0.11				
193		0.50	0.44		20.20	0.32		1.66		1.07		0.16				
194					10.04	0.39								1.08		0.26
195	0.17		0.18	2.08	7.49						0.45	0.11				
196		1.22			29.60				0.48	0.78		0.11	0.25			
197				2.33	18.49	0.52						0.13			0.34	
198				1.73	22.07		2.15	0.41					0.27			
199			0.40		14.35					2.19						0.30
187					35.41	0.42										
188	0.61			1.20		0.64	0.82	0.54		2.82			0.23		2.87	
19		0.21	0.38													
20					6.37		1.38				0.15	0.18				
21	0.15			1.56		0.11	1.44		0.38			0.14				
22		1.02	0.33		14.53		3.75		2.94	1.42					2.07	0.24
23	0.13					0.11	1.22	0.91		1.16						0.20
24		0.31			11.57			0.57	0.12			0.22	0.07	1.49		
25	0.21	0.28	0.11	0.61		0.19	1.21	1.07			0.17	0.19	0.32			
26		0.43				0.41								0.99		
27		1.20	0.67	1.61	14.25		14.36	1.05	56.23							0.38
28				1.11	4.70		1.34		0.33			0.29			0.63	
19	0.52	0.84	0.23	0.80	10.87		0.63	1.43	0.27					0.81		
20					12.12			2.90	0.45			0.41	0.26	0.54		
21		1.11	0.28	0.85	18.08		2.11				0.19		0.07			
22					9.00	0.38	1.16	2.67	0.15	0.91	0.34	0.19			1.76	0.42
23		1.43		0.60	5.94				0.10	1.44	0.21	0.20	0.07	0.93		0.35
24		0.41	0.75		9.55		3.35			1.21					3.62	
25					11.68			1.53	0.38		0.07		0.08	0.75		0.52
26					13.27		0.85		0.19			0.43	0.20	0.32	1.15	0.58
27			0.31	1.28	19.84				0.31	2.21			0.44	0.60	1.91	
28	0.31			0.51	16.15		0.54	1.83	0.29		0.16	0.43	0.11	0.87		
29		0.40	0.14		21.05		1.08	1.56			0.11					
30	0.33			0.65	38.44		1.94						0.24	2.27	1.19	0.10
31	0.98	0.82		1.78	18.64		1.13	1.24			0.20					0.12
32	0.18	0.47				0.26		1.20	0.69		0.09	0.07				
33	0.31		0.24	0.66	22.63	0.59	1.38	0.45			0.08	0.45			1.62	
34	0.42	0.76	0.17		10.33	0.41		0.36	0.09	1.32	0.44					
35			0.15	2.78	11.95		1.27	0.35				0.12	0.15			
36					17.74		0.85	2.05	0.47	1.92		0.18	0.07		1.83	
37	0.88	2.89	0.68		21.91	0.79	1.37	0.70	0.39		0.11				2.19	
38	0.25		0.36		5.84		1.07	1.96				0.29	0.08			0.22
38			0.33		7.05		1.49	1.49	0.53					0.90		
39	0.16	1.12		1.14	32.80	0.19	0.53			1.40				1.63		0.25
39		0.69			4.97	0.42	0.92		0.52						1.53	0.45
40		2.03	0.95		33.65	0.14	1.43		0.25		0.24	0.33		0.52	1.65	
40								0.53		0.64				0.84		
41							0.94	1.57			0.15	0.20	0.09		0.55	
42	1.18				7.17				0.13			0.11				0.10
43		1.11	0.20		18.27				0.17	1.06		0.07		1.98		0.36
44			0.32	1.63	9.62	0.37	0.80		0.12	0.62	0.10	0.25				
45	0.22		0.45		11.37	0.18		0.42	0.54	1.15			0.15		0.44	0.18
46		1.62	0.32		26.79		1.50	1.36	0.91	43.72		0.09			0.73	
47	0.34						0.80	0.64	0.29	1.12	0.09		0.15		1.65	
48		0.44			4.61		1.43		0.10		0.08					
49		0.30		0.69	3.74	0.48	0.82			1.16		0.11	0.26		1.59	0.22
49	0.24	0.33				0.12	0.68						0.22	0.39	1.50	0.38
50				0.46	13.66		0.70	1.00			0.11	0.22	0.67	0.96		
50				0.44	9.19	0.18	2.63		0.10	2.04	0.26			1.13		
51	0.61	0.91			6.63		1.98	0.49	0.32	2.17	0.31	0.23	0.10	0.89	1.55	
51			0.40	0.81	13.50										2.47	0.30

Table A1 continued.

Spot#	Gd	Tb	Dy	Ho	Er	Tm	Yb	Lu	Hf	Ta	W	Tl	Pb	Th	U
192	0.99	0.33		0.29			0.34	0.25	0.68	0.31		0.19	1.18		0.10
193		0.22	0.82		0.48	0.23							0.41	0.14	
194				0.29			0.99	0.21	0.43		0.27		1.11	0.29	0.07
195			0.33	0.09	0.28			0.08		2.07			0.83	0.26	0.33
196		0.22				0.06		0.19				0.68	9.60		0.24
197	1.03									0.29		0.25	0.37		
198	1.96			0.12	0.43		1.41	0.19	0.70	0.12		0.15		0.27	
199	0.51		1.35			0.13	1.41	0.09	0.39	0.12	0.58				0.19
187	0.89							0.15	0.83	0.48			0.88	0.22	
188				0.12	1.02			0.16	0.23	0.34	2.28				0.17
19					0.65	0.18		0.10	0.17	0.11			0.53		
20	1.27	0.15			0.36	0.07	0.29	0.08	0.71	0.11			0.25	0.17	
21		0.09	1.82	0.11		0.06		0.11					0.31		
22	0.79	0.06	0.53				0.32								
23			0.81		0.43	0.09	0.85	0.07		0.14			0.38		0.10
24	0.36	0.12		0.13		0.05		0.18	0.45	0.13	0.56				
25			1.09			0.11				0.25	0.55	0.21	0.79	0.30	0.20
26			1.19		0.32						0.80		0.38	0.13	0.08
27	2.27					0.12		0.45	0.37	0.29	1.67	0.94	1.68	0.20	0.51
28			0.74		0.39		0.54			0.10	0.45		0.24		
19					0.78		0.81	0.17	0.51	0.06				0.25	0.15
20		0.15	0.44		0.87		1.92		0.49		0.86		0.23	0.10	0.48
21		0.19	0.73				0.37	0.15	0.20	0.08	1.31	0.77	0.88	0.56	
22		0.08								0.12	0.52			0.12	0.20
23		0.05				0.10	0.86			0.27	0.42			0.18	0.19
24		0.27		0.45		0.07	0.80				0.89	0.48			
25	0.77		2.18	0.26		0.11		0.23				0.25			
26					0.23		0.34	0.10		0.15	0.37		0.50		0.22
27	1.16	0.24	0.54		1.14	0.17		0.07		0.17	1.35	0.39			
28					0.85						0.74				0.18
29	0.79		2.24			0.09						0.79	0.26		0.08
30	2.36			0.20	0.30	0.19			0.18	0.51		0.78	0.25	0.40	
31		0.05		0.47				0.33		0.24	0.50				0.20
32	0.71		0.80						0.51			0.64	0.69		
33		0.18		0.08				0.06	0.32	0.21	0.32		0.68		
34		0.35	0.90			0.10	0.45	0.29	0.41			0.19			0.29
35	1.33	0.06	0.67		0.64			0.19	0.16					0.14	0.29
36		0.10	1.31		0.24	0.11				0.09	0.36	0.47	0.33	0.26	
37	1.57		1.26	0.13		0.26		0.30		0.17		0.67			
38		0.29			0.90			0.06	0.42	0.18					
38					0.61	0.26	0.92				0.59	0.57		0.12	
39	1.82						0.46	0.18	0.28		0.73	0.67			0.24
39			1.00			0.15		0.15		0.10			0.34		
40									0.39			0.93		0.12	
40			0.32	0.13	0.66	0.17							0.42		0.09
41	1.93	0.08					0.76	0.05	0.67	0.19	0.39		0.30		
42			1.71	0.05		0.07		0.35			0.86				0.55
43			0.48	0.06		0.05			0.23	0.30			0.28	0.21	0.54
44	1.59	0.07	0.49	0.18		0.23							0.64	0.53	
45	1.86		1.03	0.05				0.31	0.13			0.60	0.69	0.35	
46	0.71	0.13			0.36	0.19	0.51	0.18		0.13			5.54		0.15
47		0.11	0.59	0.24							0.68		0.41	0.23	
48			0.43				0.38		0.28		1.12			0.67	
49			1.27		0.49				0.33		0.88				
49		0.06	1.22			0.13	0.62	0.16		0.31	1.35	0.29	0.49	0.49	
50						0.13							0.42		
50		0.10			0.19				0.65		0.90		0.23		0.15
51		0.14					0.95		0.48					0.32	
51		0.07	0.71	0.06			0.73						0.45		0.19

Table A1 continued.

Location	Analysis	Spot#	Li	Na	Mg	P	Ca
Juan Román, Argentina	**52 GH011 L3 6 160m**	**52**	26.32		1036		
	52 GH013 L1 160m	**52**	56.68	1.31	1131		
	53 GH011 L3 160m	**53**	45.40		892	52.47	690.90
	53 GH013 L1 160m	**53**	59.69		874		327.16
	54 GH011 L3 8 160m	**54**	40.79		1157		
	54 GH013 L1 160m	**54**	43.89	2.76	916		417.30
	55 GH011 L3 9 160m	**55**	23.27		1191		
	55 GH013 L1 160m	**55**	6.24		775		
	56 GH011 L3 160m	**56**	26.81	2.61	1083		
	56 GH013 L1 160m	**56**	20.02		937	75.15	592.88
	57 GH011 L3 160m	**57**	25.07		951		1174.76
	57 GH013 L1 160m	**57**	32.34		800		1588.18
	58 GH013 L1 160m	**58**	13.59		937		442.24
	59 GH013 L1 160m	**59**	67.68	4.60	846	174.39	
	60 GH013 L2 160m	**60**	63.05		915	187.99	
	61 GH013 L2 160m	**61**	67.06		907	80.63	
	62 GH013 L2 160m	**62**	25.99		906	167.16	476.08
	63 GH013 L2 160m	**63**			1016	311.67	
	64 GH013 L2 160m	**64**	22.38		941	220.93	
Keith Quarry, ME	**52 Keith9 C1 CrE 160m**	**52**	47.62	0.66	48		691.96
	53 Keith9 C1 CrE 160m	**53**	40.17		123		
	54 Keith9 C1 CrE 160m	**54**	27.65		59	112.44	
	55 Keith9 C1 CrE 160m	**55**	45.38			103.37	
	56 Keith9 C1 CrE 160m	**56**	52.53	4.06	142		
	57 Keith9 C1 CrC 160m	**57**	25.39	0.69	152	228.67	373.15
	58 Keith9 C1 CrC 160m	**58**	22.75				
	59 Keith9 C1 CrC 160m	**59**	47.76	0.86	74	246.47	623.28
	60 Keith9 C1 CrC 160m	**60**	34.81		109		
	61 Keith9 C1 CrC 160m	**61**	33.27		133	136.20	
	62 Keith9 C1 CrC 160m	**62**	14.05		89	140.63	
	63 Keith9 C2 160m	**63**	56.83	3.32	82	275.89	578.01
	64 Keith9 C2 T1 160m	**64**	61.65		136	221.38	
	65 Keith9 C2 T1 160m	**65**	24.21	0.86			578.33
	66 Keith9 C2 T1 160m	**66**	14.05		42		
	67 Keith9 C2 T1 160m	**67**	52.62				
	68 Keith9 C2 160m	**68**	11.10	2.87		141.70	
	69 Keith9 C2 T1 160m	**69**	56.08		37		
	70 Keith9 C3 T1 160m	**70**	29.06				
	71 Keith9 C3 T1 160m	**71**	32.14	0.64			498.94
	72 Keith9 C3 T1 160m	**72**	42.29			151.17	
	73 Keith9 C3 T1 160m	**73**	38.50		48		
	74 Keith9 C3 T1 160m	**74**	7.25				
	109 Keith9 C3 T1 160m	**109**	39.13	3.58	55		
	110 Keith9 C3 T1 160m	**110**	65.50	0.96	123		
	111 Keith9 C3 T1 160m	**111**	82.47		143		
	112 Keith9 C3 T1 160m	**112**	65.49		37		
	113 Keith9 C3 T2 160m	**113**	87.78				
	114 Keith9 C3 T2 160m	**114**	51.74		148	188.54	
	115 Keith9 C3 T2 160m	**115**	94.51	1.00	215		
	116 Keith9 C3 T2 160m	**116**	64.22		146		503.37
	117 Keith9 C3 T2 160m	**117**	30.53		237	327.39	
La Ona, Argentina	**65 GH243 A1 110m**	**65**	54.90	9.66	624.18	115.45	
	66 GH243 A1 110m	**66**			617.80		
	67 GH243 A1 110m	**67**	55.80	15.45	731.60	375.53	
	68 GH243 A1 110m	**68**	58.09		838.68		
	69 GH243 A1 110m	**69**	15.59		968.49		
	70 GH243 A2 CrA 160m	**70**	28.25		854	145.66	
	71 GH243 A2 CrA 160m	**71**	7.04		859	154.17	
	72 GH243 A2 CrA 160m	**72**	52.20		908		

Table A1 continued.

Spot#	Sc	Ti	V	Cr	Mn	Co	Ni	Cu	Ga	Ge	As	Rb	Sr
52				7.36	3788	0.66		24.90	270.9	1.09			0.32
52				2.52	3204	2.60		18.50	282.1		6.47	0.68	0.18
53				2.45	3786			22.18	280.4	1.93			0.78
53	3.38		2.46		3103	0.42		17.18	295.3	0.99	7.92		0.17
54	1.00			3.76	3694	2.18		14.51	265.3	2.18	4.29		0.23
54		6.62	1.66	1.88	3426			14.97	282.4	1.42	3.95		
55				1.83	3695	1.65		18.13	270.4	3.05			
55			4.71	6.04	3131		3.80	19.53	294.3	1.48	5.32	0.66	
56	4.27	11.16			3056	0.91	9.87	23.68	284.4	3.35			0.21
56			2.47		3242	0.70	4.36	12.79	290.9		5.11	0.29	
57					2389	2.52		27.88	237.6			5.26	
57		25.58	2.16	2.29	3442	2.58		17.07	281.2			3.92	
58		12.61			3044	0.76		15.91	274.5	0.61		1.01	
59					2953	3.05	2.82	23.57	271.1	4.19		1.33	
60		31.73			3058	1.83	2.32	24.09	279.5		4.91		0.60
61			1.70	4.89	3174	2.76		22.92	283.5				0.31
62		10.45	3.35		3067			22.71	298.0			0.64	0.75
63		25.12	6.67		3280	2.12		18.52	281.9	1.78		0.78	0.61
64				1.80	3128	1.76	6.12	23.26	278.0			1.05	
52				4.36	2298			17.40	453.6		2.82		
53	1.13				1996	0.74	2.84	22.31	445.6	1.37	5.78	0.35	0.17
54	1.36		1.50	2.24	2027			16.24	473.9				0.13
55	1.44	36.70			2026	0.86		18.26	464.0	0.98	4.25		
56					2229	1.30	1.95	20.85	474.7	2.08	2.80	3.09	
57				3.00	2053			26.92	475.8				
58	0.94			1.04	1965			19.38	459.8		3.17		
59					2143	0.60	3.32	22.42	471.2	1.70		0.15	
60				1.60	2291	2.46		23.55	487.4		5.70		
61			2.25		2262			21.58	499.9	2.53	3.73		
62		10.30		2.24	2188			21.34	459.0	1.81			
63				1.12	1949		9.12	28.20	437.8	0.89	9.64		
64			2.26	1.47	2023			18.30	449.6	4.61			0.20
65		17.09		2.57	2221			23.12	456.0	1.81			0.37
66	1.43	6.81			2220		7.86	20.99	459.8				
67		15.69		4.14	2128		5.14	17.94	453.2	1.78			0.40
68	2.60			1.29	2209			19.42	467.2	2.10			
69		29.98		3.23	2203		3.45	18.61	465.8		3.54		
70					1999	0.42		21.70	471.3	0.86	2.68	0.21	
71	1.75				2244	1.71		20.96	490.9	1.74		0.37	0.25
72	0.99			4.06	2136			17.18	483.6	2.37	4.92		
73		16.24		2.77	2370		5.16	22.33	472.0	2.18	2.67	0.31	
74					1973		8.88	26.31	484.2	0.90			
109		7.62	2.34	1.64	2163	1.00	5.92	20.08	477.4				0.44
110	2.29		3.91	4.34	2205		10.54	21.06	486.8		8.03		
111			2.76		2319	2.16	5.01	21.97	491.8	3.89			
112	2.81			2.68	2139	1.66	15.26	20.13	484.8			0.66	
113				5.87	2398	0.71		19.41	473.5	3.43		0.44	1.08
114	0.85				2408			14.25	475.5			0.44	
115			5.78		2305	1.24		24.93	480.3	1.06			
116		16.05	1.56	1.56	2337			21.21	484.1	2.25			1.07
117		19.02		3.82	2262	0.92	3.56	23.78	501.3	1.81		0.18	0.34
65			6.27		4842	17.63		22.42	244.5	2.97	4.16	0.38	0.61
66	3.05			7.47	4774	15.14	11.17	13.49	242.5	2.15		0.97	0.84
67	3.80		12.34		4264	15.68	13.98	22.82	264.9		10.30		
68			9.81		4387	15.28	7.73	21.35	267.0	1.46			
69			12.59		4490	19.09		19.27	257.5	2.06		1.06	0.29
70	2.64		6.63	4.79	4359	16.25	13.44	17.23	272.6			0.27	
71				3.46	4119	18.35		21.12	245.2			1.01	
72			5.53		4098	16.40	2.37	22.16	266.6		5.77		

Table A1 continued.

Spot#	Y	Zr	Nb	Mo	Cd	In	Sn	Sb	Cs	Ba	La	Ce	Pr	Nd	Sm	Eu
52	0.23	1.21		0.68	9.59		0.60		0.37	2.13	0.16		0.26	0.32		0.17
52			0.63	1.06				0.52		1.01	0.23	0.10		1.38		
53	0.29	1.43		0.40	20.21	1.22	0.88	1.37	0.37	4.56		0.14		1.38		0.62
53		0.31	0.22	1.02	9.18	0.32	0.35			1.22				1.39	0.65	
54		0.37			12.41		0.35		0.20			0.28		0.69		
54					7.50		1.79	0.45			0.22	0.19				
55				0.95	16.61				0.45	1.83	0.09	0.07				
55		0.92	0.52	1.66	2.98		0.34		0.09	1.83			0.13		0.96	
56					25.30			0.48	0.33			0.13	0.09	0.39	1.71	
56	0.12	0.43			12.60		0.98	0.75	0.28		0.18		0.09	0.49	0.80	
57	0.11		0.34		20.13				0.52	8.03	0.10		0.06			
57					7.10	0.23	2.40	9.67		1.91	0.15		0.13	1.53		
58	0.22	0.75						1.36					0.16			
59	0.56	1.32	0.31	0.81		0.75				3.40	0.11				2.52	
60	0.12		0.19		3.23		0.58		0.11				0.16	0.96		0.21
61	0.12						1.43	0.33		3.38		0.15				0.31
62	0.60		0.27		9.71		2.01			0.99					0.57	0.41
63				1.41	13.72		1.32			2.34	0.39	0.15		0.53		
64			0.41		6.02				1.18	1.33	0.37					0.17
52		1.02	0.25				1.19		0.27	1.08		0.07				
53		1.04	0.36	0.67	13.78	0.39		1.09		1.00	0.09				0.55	
54			0.13		12.44		2.05			1.68	0.17					
55				0.53	17.64	0.13	0.44									
56			0.36		23.63		1.01		211.35	0.72			0.30			0.30
57			0.22			0.14	1.39		0.19		0.08					
58		1.49	0.24			0.11	0.88	1.38		1.21	0.14	0.11	0.10			0.14
59		0.74	0.74			0.10	0.43	1.73	0.09	1.85	0.12			0.42	2.68	0.18
60	0.50					0.47	0.64			2.06				1.63		
61		0.35	0.52	0.70	6.50	0.10										0.42
62		0.51	0.41		14.18	0.42	1.42	0.53		2.15				0.75		
63			0.41		13.96			0.83		1.94					1.01	0.26
64	0.24		0.59		12.43			0.94			0.20	0.19	0.10			0.78
65			0.24	1.01	7.33		0.86	1.40		1.26					1.14	
66	0.41		0.29				0.50	0.92		0.87		0.33				
67							0.65					0.12				
68							2.61	1.21		0.56		0.19	0.25			0.55
69		0.27			28.89	0.56						0.16	0.06	0.92	1.24	
70		0.53			19.59			1.21	0.11	0.64					0.42	
71	0.63		0.24	0.72	3.42	0.11	0.90			1.34					1.11	
72		0.22										0.13		1.29		
73	0.42					0.16				1.88			0.33			
74				1.59	12.84	0.34	1.49		0.09							0.34
109	0.77	0.70	0.28	1.27	26.14	0.57			0.34			0.28		1.82		0.24
110		0.30			4.43	0.35				2.05	0.15			0.66		
111	0.44	0.53	0.59	1.15		0.53			0.51		0.24	0.14			1.45	0.29
112				0.99	24.06				0.52	1.65				0.68		
113				2.78	10.37	0.15	2.11		0.50						0.61	0.13
114		0.32			23.47		0.82				0.37	0.13		1.08		0.32
115	0.26	0.26			5.80	0.14				1.42		0.13	0.10		0.80	0.28
116	0.43				9.86					1.46	0.37	0.94			1.53	
117	0.49	0.51	0.44	0.78	25.06	0.45		1.28			0.37			0.61	0.79	0.20
65		1.03	0.84		32.13		1.36				0.22	0.29			1.21	
66				3.25			1.86					0.42	0.26			0.70
67		0.88			21.95											0.67
68		0.56			12.81							0.27	0.19			0.29
69		0.66					2.97	2.06		2.04		0.27	0.10			
70	0.15		0.39	0.47	17.26		0.37								0.41	
71	0.20	0.60	0.28	1.20	8.08			0.69	0.09		0.22	0.09				0.29
72	0.35	0.68		2.02	14.47		1.33	0.35	0.23		0.08			0.45	0.35	

Table A1 continued.

Spot#	Gd	Tb	Dy	Ho	Er	Tm	Yb	Lu	Hf	Ta	W	Tl	Pb	Th	U
52		0.15				0.10						0.44	3.77	0.09	
52			1.31				1.84	0.09						0.15	
53	0.45	0.12			0.60		0.95	0.31	0.28				0.18		
53		0.13					0.80		0.32				1.02		
54						0.18	0.49			0.07	0.82		0.81		
54				0.15	0.26	0.08	0.72				1.10			0.17	
55	0.37					0.14		0.17			0.58	0.40	3.52		
55		0.12		0.25	0.35		0.31		0.45	0.19			0.25	0.20	
56			0.39			0.29			0.38		0.41	0.55			
56			1.00			0.11	1.43							0.13	
57		0.19					0.99	0.20	0.35	0.08	0.27		0.23		0.16
57	1.34	0.30				0.18		0.34	0.25						
58	0.53			0.19						0.21			3.64		0.30
59		0.19		0.07			0.62						0.64	0.35	
60	1.16	0.12	0.76		0.38	0.07					0.69	0.40	0.34	0.23	
61							0.37						0.92	0.16	
62	2.38				0.49			0.06	0.38		2.19	0.22	1.28		0.32
63	0.75	0.27			0.34		1.01	0.24	0.66				0.78		
64	2.07									0.07			0.27	0.61	
52					0.43						0.37		0.51	0.14	
53	0.70			0.08		0.06		0.17	0.51						
54	0.61				0.59	0.19		0.16			0.64	0.59	0.25		0.21
55						0.19		0.21	0.13	0.09				0.14	
56		0.20						0.06				0.35	0.25		0.43
57	1.88			0.09		0.20	0.34			0.21		0.15	0.43	0.12	0.18
58	1.60		0.70	0.12					0.29				1.01	0.24	
59	0.43	0.17	1.28				0.35	0.10	0.24						
60				0.07						0.10	0.34	0.20	2.78		
61					0.72		0.42			0.10		0.41	0.31		
62	1.92		0.42			0.20				0.12			1.04		0.36
63	1.05	0.10										0.32			0.13
64		0.12					0.52	0.08				0.40	0.46		0.27
65		0.27		0.09	0.46	0.09		0.05				0.23	0.73		
66						0.08		0.09	0.27						0.09
67		0.16		0.07	0.33	0.30	0.69		0.54						
68		0.15					0.69							0.34	
69					0.39			0.16	0.31			0.44	0.55		
70	0.46				0.54		1.30			0.07		0.47	0.78	0.21	
71	1.35		1.11	0.11			1.71						0.47		
72			0.65	0.15	0.67		0.77							0.13	0.10
73			0.31		0.19		0.75		0.53		0.65			0.46	
74								0.20		0.13			0.67	0.12	
109				0.10				0.24	0.16						0.31
110		0.21	0.49	0.20				0.16	0.21	0.20					
111		0.26			1.06		1.35						0.61		0.15
112	1.43			0.28						0.27	1.64		0.75	0.31	0.23
113	1.11		1.03		1.48	0.19	1.97	0.32			0.44	0.58			0.11
114	1.13			0.34	0.62		0.57		0.34		1.30		0.40		0.36
115		0.16	1.36								0.56			0.25	0.41
116	0.96		0.31			0.25	0.36	0.05		0.51			0.74		0.30
117		0.19	0.89		0.68		1.17			0.27			0.74		
65		0.11			0.79							0.90	0.69		
66			0.64			0.10	0.76			0.25	0.66	0.44			
67		0.24	0.54	0.42		0.32	1.79	0.42			1.72	0.65		0.46	
68			1.13						0.58				1.01	0.43	0.31
69		0.38	1.34	0.47		0.23	1.57				1.37		0.64	0.32	
70		0.05				0.06	1.52	0.09	0.76		0.40		0.75		0.93
71				0.08						0.18				0.38	
72	1.16			0.12	0.49			0.17			0.90		0.63		

Table A1 continued.

Location	Analysis	Spot#	Li	Na	Mg	P	Ca
La Ona, Argentina	**73 GH243 A2 CrA 160m**	**73**	14.42		728	76.58	397.02
	74 GH243 B1 160m	**74**	25.17		724		
	75 GH243 B1 160m	**75**	33.55		974		
	76 GH243 B1 160m	**76**	11.75	0.66	848		
	77 GH243 B1 160m	**77**	42.70	1.22	723	217.58	
	78 GH243 B2 CrA 160m	**78**	13.53	2.32	826	170.38	322.82
	79 GH243 B2 CrA 160m	**79**	25.69		816	58.33	
	80 GH243 B2 CrA 160m	**80**	26.06		695		427.48
	81 GH243 C1 CrA 110m	**81**	54.53		967		703.19
	82 GH243 C1 CrA 110m	**82**	91.32		866	148.34	
	83 GH243 C3 160m	**83**	39.59		381		483.02
	84 GH243 C3 160m	**84**	49.00		865	74.43	
	85 GH243 C3 160m	**85**	13.14	2.15	668	166.03	542.47
	86 GH243 C3 160m	**86**	11.17		411	66.82	
Lord Hill, ME	**85 16109 C1 T1 160m**	**85**	16.04	1.20	145	177.90	
	86 16109 C1 T1 160m	**86**	28.03		79		417.36
	87 16109 C1 T1 160m	**87**	21.83		383		
	88 16109 C1 T1 160m	**88**	38.68	1.97	80	279.69	
	89 16109 C1 T1 160m	**89**	22.94		66		
	90 16109 C1 T1 160m	**90**	32.90		281	237.62	
	91 16109 C1 160m	**91**	28.82	2.30	320		
	92 16109 C2 T1 160m	**92**	40.88	1.30	274		638.56
	93 16109 C2 T1 160m	**93**	35.52		53	95.68	
	94 16109 C2 T1 160m	**94**	9.52		286	94.69	
	95 16109 C2 T1 160m	**95**	17.59		232		
	96 16109 C2 T1 160m	**96**			177		319.95
	1128537 T1 1 160m	**101**	37.75				
	1128537 T1 2 160m	**102**		1.14	34	128.60	
	103 128537 160m	**103**	24.22			109.87	297.60
	104 128537 160m	**104**	14.76	2.59	105		
	105 128537 160m	**105**	27.27	2.82	44	259.85	
	106 128537 B P5 160m	**106**	17.66				
	107 128537 160m	**107**	9.19			148.07	
	108 128537 B P7 160m	**108**	15.74	2.07	74	140.58	
	109 128537 160m	**109**	8.59	0.71	183	172.65	
	110 128537 B P8 160m	**110**	35.39	4.90	138	65.49	542.87
Magdalena, Argentina	**33 GH273 T1 160m**	**33**	48.56	1.64	989		
	34 GH273 T1 160m	**34**	16.88		1117	255.71	
	35 GH273 T1 160m	**35**	23.93	1.34	1674		
	36 GH273 T1 160m	**36**	35.25		1220	257.95	
	37 GH273 T1 160m	**37**	32.14		1283		
	38 GH273 L2 160m	**38**	18.59	0.95	1014		
	39 GH273 L2 160m	**39**	56.42		1034		
	40 GH273 L2 160m	**40**	40.87		935	171.96	
	41 GH273 L2 160m	**41**	31.75	1.16	988	241.78	
	42 GH273 L2 160m	**42**	27.98		1570		852.31
	133 GH272 L1 3 160m	**133**	37.65		1650	169.24	
	134 GH272 L1 4 160m	**134**	9.51	3.54	1522		
	135 GH272 L1 5 160m	**135**	31.14		927	123.73	
	136 GH272 L1 6 160m	**136**	44.58	1.09	1914		
	137 GH272 L1 7 160m	**137**	39.41	3.53	1101		
	138 GH272 L1 8 160m	**138**	27.83	1.03	1521	203.07	
	139 GH272 L1 9 160m	**139**	27.44	2.12	1038		545.28
	140 GH272 L1 10 160m	**140**	39.52		1856	200.89	
	141 GH272 L1 12 160m	**141**	55.44	6.43	1038		
	142 GH272 L2 3 160m	**142**	24.20		1230	215.83	
	143 GH272 L2 6 160m	**143**	34.81		1489		460.05
	144 GH272 L2 7 160m	**144**	71.31		1505	174.88	516.63
	145 GH272 L2 9 160m	**145**	14.11		1955		1112.48

Table A1 continued.

Spot#	Sc	Ti	V	Cr	Mn	Co	Ni	Cu	Ga	Ge	As	Rb	Sr
73				1.35	3983	15.78	5.95	22.14	264.9	0.67			0.29
74			4.22	4.85	4186	16.19	6.03	20.95	258.2		3.17	0.44	
75		17.30	4.74	2.46	3893	16.30	7.44	18.48	259.6			0.18	
76			5.24	1.39	4153	19.51	14.26	22.35	283.3	2.06			
77			4.16		4302	17.17	2.75	17.73	266.8			0.84	0.51
78	0.91		6.86	3.45	4554	10.31		17.37	272.6	2.22	1.44		
79			7.74	5.34	4243	16.14		19.54	298.9	3.64		0.19	0.37
80			3.42	3.48	4384	15.13		19.33	271.2		5.24		
81			4.62		4633	22.93	12.50	20.67	265.7	5.05			0.38
82			13.89		4656	10.67		22.10	258.0	3.20			0.24
83	3.10	6.55	8.58		4215	11.56	9.28	24.39	295.9				0.14
84		38.41	3.91	4.96	3917	11.42	2.15	21.65	280.1			0.36	
85	1.43	6.18	8.20	3.67	3708	12.59		21.28	274.1		4.38		
86		22.37	4.91	2.17	2811	8.88	5.75	16.97	263.6	0.76	7.10	0.26	
85				7.22	2351	2.53	2.05	20.70	409.0				0.79
86	1.70	7.10		3.40	2451	2.83	2.88	22.92	414.8				
87	1.12	16.50		1.98	2490		2.74	17.71	415.1	2.44		0.30	0.82
88			2.84		2421	2.29		18.73	433.0		3.46	0.23	
89				3.99	2413	2.20		17.22	431.5	1.43	3.21		
90		15.22	2.65	1.46	2361	1.64	2.17	18.90	429.9	1.97	4.28	0.53	0.36
91	2.47		1.56	1.22	2250	1.00	6.35	16.51	434.1	2.77	4.62	9.06	0.56
92	0.86		2.33	8.31	2416	3.33		20.24	424.7	2.45	7.24		0.20
93	1.42			1.98	2818	2.90	4.94	16.36	459.6		5.96		
94	1.22	7.11		3.89	2499	3.56	2.23	21.94	442.0		5.26		0.31
95	0.89	8.70		3.38	2286	3.69		21.93	419.1		6.43	0.62	0.51
96					2344	1.73	4.14	23.82	417.8	0.71			
101		12.81			3000	0.88		21.11	418.3	0.61	7.00	1.48	
102					2936	3.13	5.97	22.86	430.1				
103	1.28			1.17	2789	2.30		23.50	442.9			2.46	0.72
104	3.30		3.22	2.95	2702	4.35		15.86	443.3				0.25
105	3.07		1.77		2593	4.07		18.31	423.8		1.83	0.33	
106					2994	3.59		21.34	430.0				
107		30.67	1.92		2764	5.07		24.41	431.7	0.71		0.38	0.22
108		7.23		1.34	2628	1.63		20.04	423.2	2.01			
109				1.73	3118	4.31		27.32	422.8	0.84	7.96	0.33	0.23
110			3.41	1.45	3085	1.10		26.99	435.0			0.35	0.11
33	3.44		3.18	5.36	2824	1.84		18.54	253.1		4.85	2.19	
34	2.20		2.84		2196	9.65		21.61	258.2	1.98		3.02	
35				5.24	2427	5.51	3.80	22.40	267.5			0.83	0.35
36		33.00			2997	3.22	10.81	24.03	266.5			1.95	
37	1.02				2381	5.40		17.28	265.8		3.82	1.45	0.15
38	1.25	17.61		1.36	3478			29.54	264.4	1.96		0.74	
39				3.27	3357	2.24		18.54	273.2		5.70	4.30	
40	1.08			2.30	3555		5.48	20.22	269.8	3.13	1.37	10.69	0.36
41		7.45		5.41	3417	2.51		24.81	263.4			0.31	
42		26.03	5.11		2526	6.50		35.73	274.6	3.30	4.64	19.59	0.26
133					2854	4.96		19.26	262.6	1.09		0.76	
134			4.74	4.16	3068	5.68		14.82	260.9			0.71	
135				1.87	4032	2.23	4.00	19.63	291.6	0.56		0.87	
136		37.24	4.65		2682	13.48	5.60	19.14	275.1	2.53		14.00	0.16
137			1.78	5.39	4148	4.10		27.54	283.5	2.92	2.80	4.50	0.48
138			4.29	1.40	3451	3.69		15.53	272.3				0.43
139		9.98			3883			15.95	284.3			0.24	
140					2786	9.54		19.09	274.3	1.43			
141				3.21	3905	2.22	2.46	18.62	260.9	0.61	2.48	3.43	
142	1.84		2.13		4235	2.15		19.03	280.2	0.83		1.53	0.32
143	2.80		2.50	5.14	2966	4.88		21.62	271.9		2.16	0.87	
144		32.67	1.50		3003	6.06		26.57	291.5			6.16	0.57
145				4.66	2404	18.77	2.78	19.11	277.4	1.84	3.46	3.06	

Table A1 continued.

Spot#	Y	Zr	Nb	Mo	Cd	In	Sn	Sb	Cs	Ba	La	Ce	Pr	Nd	Sm	Eu
73	0.26						1.43	1.25	0.14			0.26		0.69		
74	0.19		0.35	0.80	2.91				0.54	2.39		1.75	0.12			0.48
75			0.49		9.26	0.68			0.27						0.77	
76	0.23				17.72					0.80		0.12	0.09	1.37	0.54	0.23
77	0.19	1.12				0.51	1.54				0.13			0.92		0.41
78			0.14	1.36							0.23		0.21			
79	0.24	0.88	0.14	1.02			1.47		0.40					0.42	0.68	
80	0.53				10.20	0.17	1.39						0.17	0.84	1.35	
81				0.86				1.88		1.68			0.37			
82		2.73		1.36							0.32					
83	0.13	1.15			8.78					1.36				1.82		0.29
84	0.24		0.52	0.46	11.41		2.20					0.15	0.05			
85		0.89		1.76	7.29				0.37		0.07		0.05		1.36	0.24
86	0.10	0.58	0.36		13.19		0.42		0.20		0.16		0.20		1.10	
85			0.36	1.42	7.15					1.37	0.20		0.21		0.48	
86							0.70	1.01					0.18			
87		0.21									0.17		0.08	0.31	0.56	0.24
88	0.47	0.26	0.16	2.15		0.32	1.25	0.86			0.13					
89	0.15		0.26	0.72			0.46		0.30					0.75		0.26
90	0.12								0.23	1.05					0.54	
91		0.93	0.67				0.57		0.71	2.28	0.08		0.13			0.35
92		0.23				0.23	0.49						0.17		0.77	0.29
93	0.33				6.25		0.69			0.85						
94	0.19				15.87				0.38	0.83	0.27		0.09			
95	0.17	0.88		0.99			1.53		1.79					0.70		
96			0.19		7.77	0.38	0.37		0.12			0.07			1.90	
101	0.18		0.25	1.28				1.00	0.17							
102			0.26	1.93		0.22	1.57							0.73	0.93	
103	0.31	0.22						1.86	0.36			0.10				
104				1.67	4.69						0.20					
105			0.26	1.50			0.43		0.41			0.30	0.06		1.29	
106				1.87	6.99		1.10	1.50	0.21	3.65				0.34	0.48	
107					19.20			0.91		1.35	0.09				0.58	
108					7.05		0.83									
109							0.91				0.15	0.10				0.22
110	0.26	1.26			7.70		1.04			1.40	0.08					
33		0.61		0.95	3.27			1.71				0.14		0.47	0.92	
34		0.54					1.43	0.76	0.70	1.51		0.08	0.30	1.73	0.48	
35		0.53	0.48		5.88		0.39	1.49				0.27	0.10			
36		0.51	0.47		23.58			0.89		0.77				0.58		0.42
37					6.58			0.81			0.47	0.07				0.38
38				0.60	4.50		0.50		0.13			0.19			1.37	
39		1.17	0.25	1.53	16.15		2.18		0.13		0.10	0.28				
40					9.45			0.35			0.25	0.24				
41							1.01	1.45	0.33	1.01					1.32	
42		3.32	0.45		5.52	0.21			1.16			0.18	0.27		0.82	0.18
133		0.59	0.18	0.91		0.29			0.37		0.14					0.69
134				0.55	6.94		1.96	0.64	0.36	0.82			0.06			
135	0.32							1.01	0.26			0.07				
136		0.55	0.73	1.18	6.64	0.27			0.85	2.66		0.09				
137	0.13	0.67	0.21	0.65	3.61						0.28		0.31	0.30	0.88	0.62
138	0.52		0.28	0.52	17.64		0.99		0.21	2.12		0.13	0.17		0.92	0.11
139	0.22	0.22		0.68	9.86	0.34	2.51	0.96	0.31		0.15					
140					19.03				0.23	0.52	0.07	0.31	0.31			0.23
141		0.69		0.64	23.50	0.71			2.92	2.43	0.07		0.13			0.29
142					10.82		1.34	0.73	0.70			0.24	0.15		0.34	0.46
143		0.53			12.07	0.13							0.16	0.62	2.42	0.37
144		0.31	0.43				0.75			1.31	0.40	0.22				
145					20.24	0.23			0.12	0.56	0.21					

Table A1 continued.

Spot#	Gd	Tb	Dy	Ho	Er	Tm	Yb	Lu	Hf	Ta	W	Tl	Pb	Th	U
73								0.10	0.27	0.13		0.74		0.27	
74	0.92	0.10	0.29	0.13		0.14		0.16	0.18		0.76				
75					0.54	0.05			0.18				1.01		
76	0.47			0.20			0.67			0.14	0.82			0.13	
77			1.70	0.20	0.44			0.48	0.33	0.15		0.61	0.77		
78						0.05	0.95		0.18	0.05			0.59	0.25	
79				0.07				0.18		0.18					
80			0.65		0.17	0.09			0.29		1.07				
81	0.78							0.08	0.32				0.45	0.56	0.62
82		0.58	2.47							0.56					
83								0.07	0.34	0.12	1.00		0.97		
84		0.10	0.52			0.22									0.08
85		0.17		0.14		0.18				0.16					
86	1.33		1.03			0.19							0.23		0.20
85	0.50		0.33		0.77	0.14					2.26	0.16	0.37		
86		0.07		0.06	0.23	0.19	0.34	0.09	0.21				0.41	0.30	
87					0.26							0.36	0.45		0.10
88		0.14		0.09		0.14		0.05	0.42	0.27			0.95	0.32	0.22
89	0.82			0.13				0.12			0.34	0.36		0.18	0.20
90		0.22	0.74	0.15	0.21										0.12
91				0.10	0.41		0.68	0.10							0.11
92		0.16				0.27	1.10	0.10							
93	0.90			0.33	0.17	0.05			0.37		0.45	0.29			
94	0.57						0.86				2.19	0.24	0.50	0.30	
95					0.85				0.20		0.68				
96	1.01	0.16	1.68	0.15			1.64		0.42			0.27		0.30	0.25
101	0.73	0.18	0.63				0.28			0.05	0.79		0.64	0.16	0.70
102	0.47	0.37			0.54										
103	2.33	0.10	0.57							0.16		0.22			0.41
104						0.05	0.41			0.20	0.97				0.11
105	0.87				0.17			0.19		0.15	0.69		0.50		
106	1.55				0.53	0.11					0.37				
107	0.96							0.06	0.78	0.11		0.38			
108			0.90	0.13	0.64	0.27						0.47	0.39		
109		0.22				0.16			0.30	0.26		0.28	0.19	0.45	0.20
110	3.77		1.98	0.10					0.13	0.58	0.94		0.60	0.22	1.38
33			0.93							0.27	1.10		0.44		0.20
34				0.14		0.06	1.76		0.16		1.22			0.39	
35				0.49	0.98		0.93	0.10	0.80		0.89	0.40	0.39	0.27	
36			0.51			0.16		0.12		0.07		0.51			
37		0.28		0.19		0.16			0.24						
38			1.87	0.09			0.84			0.17			0.35		
39		0.16	1.23		0.37	0.07								0.21	
40				0.20	0.38	0.08					0.50	0.82	0.62		0.07
41			0.47				1.90	0.27					0.26	0.29	0.14
42				0.11				0.35	0.27			0.24	2.44		0.24
133	0.40									0.11			0.30		
134		0.09			0.63		1.09			0.06					
135		0.17		0.26		0.26		0.23		0.43					
136						0.07	0.43			0.30	0.55				
137				0.20				0.10				0.43	0.99	0.53	
138		0.05		0.08		0.12		0.06		0.21			0.54		0.14
139					0.55			0.05					0.50	0.60	0.44
140		0.13								0.13		0.24	0.52		
141		0.09		0.15			1.57	0.09		0.14			0.85		
142				0.07	0.52	0.21				0.11				0.21	0.16
143		0.09		0.05				0.13	0.69	0.05	0.65		0.70		0.13
144	1.03						0.89	0.21			0.48		0.44	0.20	
145		0.14		0.07			1.03	0.30		0.09	0.51	0.33	3.76	0.10	

Table A1 continued.

Location	Analysis	Spot#	Li	Na	Mg	P	Ca
Mocuba, Mozambique	**31 25605 Cr1 T1 160m**	**31**	60.94	116.39	207		
	32 25605 Cr1 T1 160m	**32**	51.46	2.23	176		
	33 25605 Cr1 T1 160m	**33**	52.97	0.82	197		412.81
	34 25605 Cr1 T1 160m	**34**	58.18		159		
	35 25605 Cr1 T1 160m	**35**	19.77		365		
	36 25605 Cr1 T1 160m	**36**	60.36			77.45	
	37 25605 Cr1 T1 160m	**37**	50.00	2.08	301	114.69	437.52
	38 25605 Cr1 T1 160m	**38**	35.34	2.43	397	114.21	774.35
	39 25605 Cr1 T1 160m	**39**	53.73	0.79	294	61.86	1487.11
	40 25605 Cr1 T1 160m	**40**	46.66		226		
	41 25605 Cr2 T1 160m	**41**	19.41		106	465.81	
	42 25605 Cr2 T1 160m	**42**	24.83		84	192.77	963.70
	43 25605 Cr2 T1 160m	**43**	27.52		250		
	44 25605 Cr2 T1 160m	**44**	32.03		394	181.31	524.74
	45 25605 Cr2 T1 160m	**45**	30.57	3.92	226		1714.23
	46 25605 Cr2 T1 160m	**46**	30.36		287	137.72	
	47 25605 Cr2 T1 160m	**47**	20.92	1.37	66		
	48 25605 Cr2 T1 160m	**48**	31.85	3.94	489		
Nancy, Argentina	**104 NA001 T1 160m**	**104**	95.23	0.82	3674		580.98
	105 NA001 T1 160m	**105**	23.94		3688	284.90	
	106 NA001 T1 160m	**106**	40.23	0.87	4289		
	107 NA001 T1 160m	**107**	46.60	1.00	3730		
	108 NA001 T1 160m	**108**	52.57	0.99	3869		575.06
	109 NA001 T1 160m	**109**	31.56		3572	73.31	736.94
	110 NA001 T1 160m	**110**	98.22	1.11	3914		
	111 NA001 T1 160m	**111**	60.76	0.78	3984		
	112 NA001 T1 160m	**112**	67.27	1.46	3753		
	113 NA001 T1 160m	**113**	80.29	2.34	3999		
	114 NA001 T1 160m	**114**	70.82		4248	233.74	
	115 NA001 T1 160m	**115**	40.29		4026	183.17	
	116 NA001 T1 160m	**116**	39.54	3.00	4086		
	117 NA001 T1 160m	**117**	79.57	2.98	4093		
	118 NA001 T1 160m	**118**	51.29	1.94	3552	75.87	
	119 NA001 T1 160m	**119**	30.98		3661	115.07	947.75
Nine Mile MMSD, Australia	**19 GH5 B T1 160m**	**19**		1.99	8926	89.57	
	20 GH5 B T1 160m	**20**			6735		
	21 GH5 B T1 160m	**21**	7.55		6632		
	22 GH5 B T1 160m	**22**			7567		
	23 GH5 B T1 160m	**23**			6924		
	24 GH5 B T1 160m	**24**		0.84	7020		
	25 GH5 B T1 160m	**25**			6939		
	26 GH5 B T1 160m	**26**			7735	281.79	
	27 GH5 B T1 160m	**27**	10.67		7088	58.49	395.45
	28 GH5 B T1 160m	**28**			7091		827.36
	29 GH5 B T1 160m	**29**		1.97	7465	140.49	
	60 GH2AB C1 T1 160m	**60**	51.73		9952	96.28	
	61 GH2AB C1 T1 160m	**61**	15.94	0.99	12001		
	62 GH2AB C1 T1 160m	**62**	51.36	0.66	11132	142.67	
	63 GH2AB C1 T1 160m	**63**	37.29	1.48	11187	240.46	
	64 GH2AB C1 T1 160m	**64**	29.44	2.29	9709	251.99	820.76
	65 GH2AB C1 T1 160m	**65**	28.90		9855		
	66 GH2AB C2 T1 160m	**66**	53.02		10235	670.24	
	67 GH2AB C2 T1 160m	**67**	25.12	12.83	9966		3011.04
	68 GH2AB C2 T1 160m	**68**	22.04	2.68	10521		680.94
	69 GH2AB C2 T1 160m	**69**	20.89	2.00	11487	66.42	
	70 GH2AB C2 T1 160m	**70**			10874		
	71 GH2AB C2 T1 160m	**71**	25.82	1.35	11715	133.34	
	72 GH2AB C2 T1 160m	**72**	19.69		10738		
	73 GH2AB C3 T1 160m	**73**	15.61		10530		627.46

Table A1 continued.

Spot#	Sc	Ti	V	Cr	Mn	Co	Ni	Cu	Ga	Ge	As	Rb	Sr
31		17.61			2769	6.12	12.59	19.31	504.2			0.15	
32				2.82	2560	1.84		23.04	507.9	2.93			0.15
33	1.54	17.16			2569	4.28		20.23	509.6			1.15	
34		11.91		1.65	2678	1.18		19.03	512.8		8.22		
35				1.58	2782	5.16		17.87	501.5		1.91		0.13
36					2609	5.37		19.49	513.1				
37	2.06				2439	5.03		20.80	514.6			0.34	
38		33.47		6.82	2545	4.19	7.34	18.04	512.4	4.20	3.59		0.46
39	4.23	22.04			2539	3.10	12.46	16.11	481.3	2.61	3.20	0.25	0.40
40	1.44	25.26	2.08	5.10	2036	3.66	3.88	19.79	490.7	2.54	7.06		0.41
41				7.86	2230	3.06		15.92	496.2		5.94	0.90	
42	1.50				2609	0.79	4.38	15.08	455.8	2.32	16.42		0.25
43	5.34	22.77			2505	2.39	8.23	18.26	504.6				
44				1.86	2541	0.63		21.77	504.3	2.02			
45	3.60			2.31	2298	0.90	9.40	19.14	514.3	1.00	10.05		
46				3.53	2277	5.82		13.76	497.9			0.14	0.42
47	7.10		4.91		2481	3.75	3.02	14.18	491.8		3.49		
48		9.63		0.99	2640	4.51	15.45	13.69	503.2	3.01			
104		7.06	23.17	7.57	4734	7.78		23.83	197.7		4.72	11.67	
105		40.23	11.61	7.24	4973	6.55		11.09	177.1	2.76		0.80	0.58
106	1.82	15.52	14.32	1.65	5415	7.25	2.40	17.68	186.2			0.49	0.68
107			14.34	3.37	5164	6.25	3.41	18.95	195.9	1.99	2.90		0.66
108		31.34	11.85		5201	4.46		21.14	199.1	1.13			0.25
109	2.70	10.22	13.17	1.88	4505	4.34		19.92	195.6	1.92	2.17	0.30	
110	2.40		25.82		4824	4.81		19.67	186.9			4.49	0.26
111			13.41	1.53	4904	5.20	9.22	23.69	196.1	0.79		0.99	
112	4.26	9.63	4.81	3.79	5135	6.42	15.31	16.47	202.5	0.82		0.85	0.62
113	2.66	33.84	9.58	3.23	4822	5.52		16.56	186.8	1.90	2.18	1.12	0.33
114	0.97	16.55	24.81		4688	6.67	4.24	19.21	199.2	2.55		5.62	1.06
115		28.58	15.34		5442	4.98		19.14	196.1		2.76		0.35
116		8.86	10.46	3.74	5150	1.31	3.35	20.31	194.0			1.79	
117			6.16	5.16	5053	2.97		19.20	180.0				0.33
118			8.32	2.91	5142	4.54		24.50	174.8		4.83		
119		11.41	10.29	2.38	5320	6.49		15.56	180.9				
19		5.89	144.92	7.45	1000	169.78	26.34	19.29	116.9		14.14	5.67	1.80
20	2.55	8.15	122.59	5.76	1380	179.21	31.41	22.19	100.2		13.72		
21		32.82	181.51	3.41	1309	186.20	33.36	18.24	105.4			1.55	0.80
22		21.48	176.56		1564	180.72	42.66	18.86	102.4			1.05	0.21
23	3.02		178.67	1.19	1773	186.38	26.31	13.71	100.0				0.58
24	0.89		183.32	5.06	1724	180.69	38.35	13.77	108.7	3.28			0.58
25		46.06	196.89		1855	173.94	36.59	16.30	105.3		1.66		0.65
26			176.57	4.26	1959	186.81	35.13	19.68	112.9			0.51	
27		16.47	169.70		1738	172.17	34.04	13.53	91.5			0.30	0.42
28		27.38	211.16		1701	179.64	35.94	19.76	104.8		10.96	4.05	0.67
29		20.67	214.00	3.98	1584	168.42	48.40	24.39	100.5		9.17	2.93	0.53
60		10.68	141.97	107.04	1932	186.30	35.59	34.18	94.1	1.51	4.00	0.68	0.15
61	2.14	31.84	157.01	30.59	2160	187.82	31.42	23.63	93.1			0.17	3.24
62	1.33	15.09	161.55	97.16	2112	191.92	37.77	17.55	90.0	1.30		1.22	
63		57.28	166.21	91.98	2228	192.31	35.38	29.61	113.2		1.78	0.86	0.83
64		44.95	143.17	72.91	2144	193.11	21.79	48.77	91.8		171.40	1.13	6.58
65		40.53	131.84	131.40	1842	179.07	22.59	37.63	93.0			2.76	0.53
66	4.02	37.36	132.69	115.76	2066	190.92	27.88	21.93	88.9	0.76	2.13	0.49	
67	1.51	41.89	155.41	5.84	1916	177.39	19.73	21.58	78.6	0.92			7.77
68	3.43	31.50	174.08	37.23	1919	178.57	27.83	23.43	89.2	1.71	71.59	0.33	0.63
69		28.48	181.92	103.13	2128	187.86	16.67	17.74	98.6	0.61	3.33		
70	2.14	24.11	181.60	244.56	2059	189.33	32.19	29.65	88.2		16.43	0.49	0.32
71		65.54	190.13	118.85	2040	190.46	26.78	17.90	93.9	1.22		0.20	
72	0.90	8.53	136.03	92.62	2190	179.75	26.32	36.09	85.1		4.13	0.38	1.45
73	3.44	39.02	121.97	97.42	1665	216.42	44.78	15.12	91.3			0.39	

Table A1 continued.

Spot#	Y	Zr	Nb	Mo	Cd	In	Sn	Sb	Cs	Ba	La	Ce	Pr	Nd	Sm	Eu
31			1.75	1.22	9.13	6.81		0.94	1.30	3.80	0.13			1.33	1.19	1.64
32	0.25			1.72				0.33	0.14	3.69			0.07			
33	0.65		0.64	1.62	9.94	0.11	1.36		0.43			0.22			0.71	
34		1.03			7.80		0.80	0.80				0.22				0.24
35		1.04								2.23	0.07			1.11		
36	0.46				4.90	0.14	1.95		0.99		0.36	0.33		0.46		
37	0.18				4.10	0.33					0.16	0.07			1.55	
38		0.89		1.70		0.22			0.10		0.16		0.28			
39			0.57				1.68						0.15			
40	0.54	1.13		1.77	13.81			0.98			0.07	0.32	0.26	0.44	0.39	0.74
41	0.43	1.01	0.73			0.37			0.28	3.07	0.20	0.10				
42		0.70				0.77	1.26		0.20							0.38
43			1.06		17.07		1.64					0.12				1.06
44			0.33			0.83	0.60						0.43		2.09	0.43
45	0.41				18.97			1.07			0.10			1.18	2.25	0.38
46	0.47			1.46		0.50				2.43	0.33		0.13	1.17		
47			0.25		4.89		2.23		0.15	4.18		0.16		0.73		0.91
48					3.40	0.50	0.53	1.87	0.21		0.67	0.25	0.30			
104	0.18			3.12	7.19				3.55	1.12						
105				2.11		0.50	0.60	0.44						1.12	1.79	
106			0.31		3.43				0.20		0.09	0.10	0.10		0.53	
107			0.14		4.43			0.66	0.40			0.17		0.51	0.34	0.12
108							0.78		0.23		0.28				0.64	0.18
109		0.28	0.15	0.62	11.61		0.87	0.36	0.44	1.32	0.09	0.08	0.28			0.29
110		0.93	0.18	1.27		0.28	0.56		1.41		0.11		0.27			
111		0.37		0.50			2.53	0.68	1.16	1.69	0.09			1.18		
112			0.33		9.57		2.30		0.36			0.13	0.10	0.41	0.86	0.46
113		0.45					0.66		0.37	1.81		0.12	0.09	0.64		0.15
114				2.26			0.57		2.07	6.35		0.19				
115			0.83								0.25	0.12		2.49	0.69	
116			0.27	1.74	5.35		0.42	1.18	4.30		0.26					0.27
117	0.26	0.48	0.68			0.21	1.28	0.71			0.22	0.11				
118				1.67							0.16		0.14	0.66		
119	0.39	0.29			7.75		1.28				0.36			0.34		0.61
19	0.38	0.43					0.99			5.61	0.42	0.17	0.12		1.28	
20	0.15			0.84	5.51		0.34				0.21	0.11				
21			0.14		7.58				0.49	1.30	0.13	0.22	0.31	0.70		0.32
22			0.56	1.55			0.94			3.35	0.27	0.18				0.14
23		0.60		0.72	9.94		1.38	0.76	0.36	2.26	0.17	0.17		0.76		
24				2.46			1.85	1.23	0.29	2.25		0.21			0.48	
25		0.88	0.40	0.76		0.25					0.07	0.25	0.21		0.40	
26						0.18			0.24							
27		0.51	0.46					1.45	0.34		0.30		0.08	1.55	0.72	0.30
28	0.34		0.63	2.75	2.93	0.85			0.26	2.01	0.54	0.56			0.48	0.17
29	0.19	0.69	0.31			0.17		2.24	0.19		0.08				2.13	
60	0.34	0.40	0.74	0.42	14.61	0.16	1.76		0.35			0.43	0.10	0.90		
61	0.24		0.69	1.03	10.39	0.17	0.53				0.50	1.09	0.08			
62		0.45	0.14		8.71	0.52	1.08	0.76			0.43	0.27			0.79	
63	0.49	1.46	0.26	1.30			1.25	1.03				0.77	0.05		0.79	0.26
64	0.70	0.82			17.38	0.35				46.40	0.88	1.82	0.50	1.57		0.58
65		1.24	0.11	1.04		0.15	1.47	1.22		7.68	0.23	1.11	0.21			
66	0.33		0.34	0.68	22.57					1.42		0.08		0.57		
67	0.38	0.42	0.55		12.62	0.37	0.62		0.56	0.99	0.24	0.23	0.07		0.65	0.75
68	0.39	0.39	0.30	0.86	7.65				0.12	0.85	0.27	0.53	0.11			
69	0.33				16.63			0.69	0.52		0.25		0.22		0.90	
70	0.37	1.35			6.94	0.10	0.95	0.76	0.31		0.07		0.07			
71			0.44		27.81	0.16	0.81		0.14	3.08		0.31	0.23			0.22
72	0.34						2.04	1.22	0.21	30.36		0.22	0.20	0.38	0.48	0.10
73	0.84	1.07		2.19		0.79	0.53	2.16	1.17	1.16				0.88	3.58	0.67

Table A1 continued.

Spot#	Gd	Tb	Dy	Ho	Er	Tm	Yb	Lu	Hf	Ta	W	Tl	Pb	Th	U
31		0.22	0.85		0.53			0.12		0.15		0.13		1.06	0.94
32	0.77	0.22		0.11	0.69			0.43						0.17	
33											0.51		0.39	0.24	0.15
34	1.37		1.02		0.32	0.12		0.16			0.44		0.88		0.15
35			2.24	0.09			0.36	0.31	0.14	0.06			0.55		
36	0.87	0.11	0.34			0.06			0.53			0.16			
37		0.08								0.14	0.72				
38						0.24	1.41							0.77	
39															
40	2.48		1.40	0.16		0.14	1.73			0.75			0.68		
41	1.93	0.19	0.83				0.45	0.22	0.49	0.44	0.60				
42	1.33		2.60		0.87		0.98		0.87	0.32			0.21	0.72	0.21
43				0.21		0.08		0.23		0.12	1.83			0.59	0.55
44	0.84			0.38	0.42			0.15	0.51	0.08					
45	0.37		0.44				0.50	0.26	0.44	0.52	0.87	0.54			
46		0.07			0.38		1.43	0.19	0.58					0.84	
47						0.14		0.06					0.94		0.16
48	1.56		0.34		0.45			0.31			1.06		0.45		
104	0.97							0.20		0.26	0.67	0.59	0.48		0.27
105		0.15	0.97	0.10			0.45	0.28	0.79	0.07			1.29		0.40
106		0.14		0.12	0.81		0.43			0.14				0.11	
107	0.40	0.06								0.18	0.75	0.22			0.22
108		0.15			0.48			0.19		0.10	0.69				
109	0.77	0.12		0.27	0.37	0.08			0.30	0.16	0.47		0.45		
110	0.41				0.25				0.47				0.76		0.12
111	0.91	0.06				0.14				0.09				0.22	0.14
112			0.34	0.09	0.57		1.02		0.19	0.11		0.19	0.72		
113		0.28		0.11	0.32	0.07		0.10			1.01		0.22		0.42
114					0.25	0.18		0.08		0.30		0.26	0.43		0.17
115	0.83		1.23				1.48		0.18	0.19					
116	0.40		0.85				1.17	0.13	0.38				1.14		0.47
117	1.84		0.71	0.21		0.24				0.14		0.55			
118				0.15		0.23					0.74		0.57		
119					0.78		0.99	0.09	0.66		0.62				
19		0.15	2.14	0.08			0.89	0.25					4.06	0.29	
20	1.45			0.09	0.16	0.08					0.92		1.14		0.20
21	1.27	0.09									1.61	0.29	6.54	0.47	
22				0.18	0.20		0.68	0.05		0.18			4.84	0.24	
23		0.12							0.28		0.41	0.23	8.67	0.27	0.15
24			0.76				0.68				0.38	0.45	20.86	0.20	
25	1.11	0.07		0.17		0.14	0.59						2.98		
26			0.87	0.18				0.33					1.98	0.20	
27	0.64	0.16										0.21	2.56	0.55	
28			0.28						0.85	0.17	1.75	0.27	2.56	0.20	
29		0.07		0.14					0.15		1.12	0.22	16.99	0.24	0.32
60	1.88	0.08						0.09	0.67	0.14	0.42		20.07	0.20	
61			0.66		0.33					0.14	0.73		13.31	0.16	0.11
62		0.25			0.78							0.96			
63	0.91						0.73				2.87	0.86	16.41	0.59	0.28
64		0.34	0.74	0.21	0.63			0.23						0.15	0.54
65	0.43	0.08	1.09		0.45					0.26	0.28		25.40	0.10	0.09
66	1.11		0.33	0.06					0.33			0.47	1.46	0.51	0.21
67						0.05		0.13				0.41	34.21	0.12	
68	1.33	0.16				0.10								0.09	0.26
69	0.75		0.59						0.39	0.15		0.16	1.59		
70			0.42	0.13		0.12								0.40	0.17
71						0.13		0.19		0.13					
72	1.43	0.23		0.19	0.78				0.28			0.22	22.33		
73	0.97		4.47	0.08		0.39			0.41				90.76		

Table A1 continued.

Location	Analysis	Spot#	Li	Na	Mg	P	Ca
Nine Mile MMSD, Australia	**74 GH2AB C3 T1 160m**	**74**			11692	221.45	
	75 GH2AB C3 T1 160m	**75**	26.56		10702		
	76 GH2AB C3 T1 160m	**76**	18.03	2.68	10143		
	77 GH2AB C3 T1 160m	**77**		2.01	10046		
	78 GH1B C1 T1 160m	**78**	59.30	2.58	7740		
	79 GH1B C1 T1 160m	**79**	34.90	1.20	9198		
	80 GH1B C1 T1 160m	**80**	42.25		8742	160.05	392.16
	81 GH1B C1 T1 160m	**81**		5.26	7365		
	82 GH1B C1 T1 160m	**82**	51.68	4.25	7404		
	83 GH1B C1 T1 160m	**83**	41.21		7771	193.95	863.13
	84 GH1B C1 T1 160m	**84**	18.98	2.31	8366	316.15	
	85 GH1B C1 T1 160m	**85**			7197	226.46	295.29
	86 GH1B C2 T1 160m	**86**	38.02		7370	186.47	1852.86
	87 GH1B C2 T1 160m	**87**	26.17	9.34	7520		538.24
	88 GH1B C2 T1 160m	**88**	21.48		8785	105.49	
	89 GH1B C2 T1 160m	**89**		1.87	8107		
	90 GH1B C2 T1 160m	**90**	49.11		8382	155.55	
	93 GH1B C3 T1 160m	**93**	14.51	2.70	12210	238.74	
	94 GH1B C3 T1 160m	**94**	36.46		14637	149.63	
	95 GH1B C3 T1 160m	**95**	44.93	1.53	10693		396.43
	96 GH1B C3 T1 160m	**96**	44.93	1.02	12068	264.10	
	97 GH1B C3 T1 160m	**97**	21.39	1.91	13670		
	98 GH1B C4 T1 160m	**98**	25.13		12263	176.50	
	99 GH1B C4 T1 160m	**99**		0.76	14539		293.07
	100 GH1B C4 T1 160m	**100**	27.54	1.80	15094		331.59
	101 GH1B C4 T1 160m	**101**	32.14		13950		
	102 GH1B C4 T1 160m	**102**	40.05	3.56	12921	130.90	
	118 GH3AB C1 T1 160m	**118**	40.20	1.58	9202	97.07	978.42
	119 GH3AB C1 T1 160m	**119**	13.84	3.29	9248		893.69
	120 GH3AB C1 T1 160m	**120**		1.13	9828		
	121 GH3AB C1 T1 160m	**121**		3.55	10224		
	122 GH3AB C1 T1 160m	**122**		1.34	9761	65.94	
	124 GH3AB C3 T1 160m	**124**			9311		
	125 GH3AB C3 T1 160m	**125**			8830	57.52	388.89
	126 GH3AB C3 T1 160m	**126**	15.71	4.06	8600		545.04
	127 GH3AB C3 T1 160m	**127**		1.62	9562	149.72	
	128 GH3AB C3 T1 160m	**128**	16.53		9265		
	129 GH3AB C4 T1 160m	**129**	45.26	2.90	8856	119.89	
	130 GH3AB C4 T1 160m	**130**	17.59		9223		
	131 GH3AB C4 T1 160m	**131**	19.24		8996	95.23	
	132 GH3AB C4 T1 160m	**132**	11.33	1.88	8874		
	133 GH3AB C4 T1 160m	**133**	19.66	2.17	8903		948.72
	134 GH7B C1 T1 160m	**134**			5763	139.28	
	135 GH7B C1 T1 160m	**135**		2.14	5326	184.28	
	136 GH7B C1 T1 160m	**136**	20.31	2.17	5867		
	137 GH7B C1 T1 160m	**137**	23.22		5678	224.22	
	138 GH7B C1 T1 160m	**138**	16.30		5355		
	139 GH7B C1 T1 160m	**139**	39.44	1.99	5992		474.62
	140 GH7B C1 T1 160m	**140**			5785		
	141 GH7B C2 T1 160m	**141**		0.92	6599		
	142 GH7B C2 T1 160m	**142**			6436	173.79	
	143 GH7B C2 T1 160m	**143**	35.46	2.93	5610		446.87
	144 GH7B C2 T1 160m	**144**	5.89		5398	318.02	
	145 GH7B C2 T1 160m	**145**	66.65	4.40	5664	255.42	
	146 GH7B C2 T1 160m	**146**			6013		
	147 GH7B C2 T1 160m	**147**	39.39	3.31	5936		971.64
	148 GH7B C3 CrA T1 160m	**148**			5904		398.75
	149 GH7B C3 CrA T1 160m	**149**	21.13		5687	268.36	
	150 GH7B C3 CrA T1 160m	**150**			5569		1017.96

Table A1 continued.

Spot#	Sc	Ti	V	Cr	Mn	Co	Ni	Cu	Ga	Ge	As	Rb	Sr
74	1.68	18.06	166.68	15.56	2326	182.91	29.20	23.16	99.0	2.66	425.32	0.68	0.85
75		14.24	166.56	68.34	1993	176.10	23.89	14.62	96.6		3.95		0.45
76		16.75	146.75	8.64	2129	180.37	19.70	16.43	90.4		6.63	2.62	
77	1.52		133.09	141.71	1797	182.65	29.62	17.53	90.1			1.03	0.46
78	2.15	104.68	253.40	10.30	1015	193.45	27.20	16.00	246.1	1.83	7.23	0.35	
79		52.08	214.28	8.14	1052	190.19	33.59	14.12	229.5	0.95	14.78		
80			245.68	7.13	1169	195.12	31.41	13.06	274.7		11.73	0.18	0.44
81	4.70	48.82	228.77	3.15	1055	189.30	35.35	28.17	290.4			6.05	1.97
82	3.36	18.39	224.58		1063	196.19	32.57	19.42	274.3			3.67	0.67
83			224.50	2.61	1227	195.17	36.31	24.52	284.2			4.68	1.11
84		50.67	235.62	7.13	1105	184.47	28.50	11.05	267.7			0.77	0.39
85		53.25	262.55	9.06	1187	186.74	28.82	21.22	280.2		2.32	0.22	
86		84.46	237.62	23.04	1190	181.47	26.26	15.62	261.2	3.24			
87		55.96	196.80	3.03	1415	184.33	33.71	28.53	274.7			14.85	3.63
88		51.35	169.00	9.46	1385	196.22	45.04	17.65	287.7		2.72		
89	3.80	76.51	214.62	10.49	1264	192.13	21.94	14.89	256.1	3.78		0.40	0.23
90		48.83	217.71	10.15	1296	184.23	33.99	13.35	252.7		3.68		
93		56.86		6.82	1796	136.31	5.90	15.43	84.8		4.77	0.15	
94	1.70	21.86	3.89		2083	142.28	23.09	32.97	91.4	2.36		0.60	
95		37.04	2.34	4.06	1414	144.74	19.36	51.94	84.1		2.63	3.14	2.90
96	0.80	70.62	2.27		1876	150.34	17.33	15.80	88.2		7.98		
97		73.72	2.51	5.22	1768	151.19	23.84	14.57	88.4				0.20
98		43.22	5.77	1.24	1879	132.58	13.43	12.77	78.9				0.25
99		30.09	1.83		2113	146.20	18.03	21.66	85.0				
100		33.82	7.92		2148	139.14	26.83	17.99	88.6			0.18	
101	1.33	67.17	3.65		1795	148.49	24.34	18.22	85.4			0.30	
102		58.26	3.23		1968	146.99	16.81	23.80	84.9		5.71	1.11	0.67
118		27.25	116.58	9.98	2382	138.88	16.00	43.36	64.2			0.21	
119		57.53	134.24	7.49	2480	158.67	36.79	32.60	97.8		9.21	0.22	0.55
120		35.67	127.87	4.51	2251	170.74	29.37	42.94	85.3	0.88	3.07	0.16	0.16
121		52.03	120.88	1.68	2414	185.09	42.30	106.66	82.4		2.73	3.41	1.85
122	2.50	26.39	127.75	5.94	2468	165.40	24.54	13.01	89.5				
124	1.92	16.95	140.92	0.96	2742	153.30	24.00	29.17	82.1			2.31	
125			124.33		2292	168.35	32.83	60.36	82.0	1.46		3.53	0.79
126	1.11	9.13	134.86	24.74	2316	163.28	33.84	28.24	78.8				0.39
127		58.29	128.64	40.53	2341	170.87	27.65	24.75	84.3			1.28	0.64
128		21.67	130.35	3.66	2494	172.90	19.90	14.19	80.5	5.15	5.95		
129	1.59	41.30	133.48	9.33	2357	188.56	35.88	21.64	78.3	2.78			0.43
130	2.94	35.81	126.03	6.61	2299	169.22	18.64	23.74	79.2		4.30		
131	3.61		172.85	90.13	2210	145.93	17.45	17.00	84.5	2.11	2.05		0.14
132		7.04	157.94	134.70	2609	118.38	15.68	28.70	85.5	2.37		6.87	0.29
133		8.26	136.17	11.61	2331	172.16	19.70	31.87	88.8	2.01		0.63	0.24
134			83.93	1.45	1586	102.57	23.78	22.62	104.7			1.12	
135		38.00	94.31	1.47	1796	106.46	9.07	12.82	109.0		3.40	0.47	0.13
136	2.18	21.40	124.13	1.57	1827	102.48	12.76	20.09	110.2		6.68	5.88	0.54
137	1.29	26.36	128.30	3.12	1806	102.89	2.17	19.95	97.3	0.82		1.64	0.44
138		52.99	105.39	4.71	1802	104.19	14.11	16.60	107.1	0.63			
139		39.94	96.76		1620	117.11	18.17	42.15	109.7	1.60	2.89	9.76	0.23
140	4.84	72.97	109.10		1733	95.85	19.87	16.92	102.7	2.62		1.91	0.87
141	3.85	19.43	84.75		1866	97.03	13.42	26.77	110.2		7.53	0.81	
142	2.40		109.34	4.02	1881	106.69	22.85	14.23	111.7			0.85	0.18
143		14.16	109.80	2.51	1837	116.98		13.96	117.7		4.56	5.88	0.61
144		10.47	106.91	5.26	1981	98.52	15.49	18.37	109.6	1.63			0.40
145	3.12	20.71	132.92	3.65	1892	108.60	2.87	17.36	102.0	2.82			
146		15.78	136.39		1842	102.00		15.00	100.5			1.07	
147		19.79	116.86		1801	114.37	13.19	20.15	111.6		5.43		
148		26.47	105.18		1848	98.38	19.29	11.40	101.1	4.13	5.53	2.64	0.14
149	1.19	29.28	138.92	1.13	1913	104.69	29.12	990.01	104.7	2.98		0.32	
150	4.38	29.82	134.22		1774	103.24	11.80	19.47	104.5	1.68	3.92	0.35	0.93

Table A1 continued.

Spot#	Y	Zr	Nb	Mo	Cd	In	Sn	Sb	Cs	Ba	La	Ce	Pr	Nd	Sm	Eu
74		0.24			22.76		1.75	0.99			0.25	2.52	0.18	2.26		0.13
75	0.59	0.84	0.25	0.56							0.26	0.16	0.08	1.26		0.18
76		0.60		1.04	23.32		0.70			6.82			0.18			0.35
77		0.52				0.22	1.10			2.25			0.13	1.73	1.18	
78		1.06			11.56	0.61			0.09	1.04	0.23	0.07	0.10			
79				0.90						1.00		0.23				
80				0.47	5.11		0.33	2.65		4.85		0.10	0.16			
81		0.47	0.23	1.32		0.25	2.94	0.34	0.17	15.46			0.25	0.97		
82				1.37	11.93	0.75	2.96	0.52		17.50			0.15	2.54		0.29
83					26.89		0.34		0.34	13.87	0.21	0.52	0.09		1.42	
84		0.49		0.77	15.92					1.94			0.11	1.13	1.36	0.18
85		1.62	0.36	2.25	20.71	0.10		1.20				0.10			0.34	
86	0.48	0.75		0.94	8.57		0.73	2.19		0.66	0.50	0.31	0.29	0.30		1.08
87	0.78	0.24	0.49	1.78	8.20	0.82	4.21	0.88	0.90	41.40					2.63	
88	0.29	0.54	0.93		4.30		1.03	1.61	0.24				0.37	1.13		
89	0.42	0.76	0.19				0.34	0.53					0.17			
90	0.41		0.28	0.76		0.19		2.49		1.50	0.27					0.19
93	0.30				3.06	0.10	2.26	0.78					0.11			
94		0.24	0.14	0.74	16.64	0.37	2.16					0.16			0.79	
95	0.33	5.21	0.14	1.95	24.97				0.76	9.16	0.52		0.42	1.42		
96		0.39	0.21	1.36	18.26								0.09		0.39	
97				1.46				0.94		2.45		0.56	0.24	0.78		0.29
98				1.53		0.31	0.35		0.08		0.25	0.12				
99			0.26				1.28		0.29					0.75		
100		1.02			5.50				0.35							
101	0.14	0.69	0.44					0.93				0.20		0.33		
102		0.36	0.29		9.73		2.37			1.92		0.22		0.52		0.16
118	0.10	1.33		7.03								0.43			2.59	1.15
119	0.51	0.30		1.36	21.73	0.17	0.39	1.43			0.24	1.91	0.26			
120	0.34	0.45			22.42		1.07				0.20			0.95	0.71	
121		2.30	0.25	1.96			0.71		0.81		0.29	0.40				
122			0.36	4.47	20.02		0.54	0.92			0.09					0.27
124		2.35	0.45		48.66	0.53			0.24			0.25	0.39			
125	0.29	0.84			11.80	0.14	2.88	1.78	0.10	2.03		0.15			0.80	0.16
126	0.20	0.95	0.57		16.15		0.36		0.19	3.15				0.38	0.76	
127		0.89			17.10		0.48	0.52		0.73	0.27		0.11		0.58	
128					10.02					1.21						
129	0.40				14.91	0.53	0.73			2.30	0.22	0.19	0.08			
130		0.28					1.55		0.37		0.14				1.49	
131				1.87	5.82	0.33	0.48			1.43	0.40				0.96	0.53
132	0.14	1.02		2.13	9.38	0.35	3.19	1.59	0.12	6.63		0.10	0.16			
133	0.41		0.30	0.91			0.64	1.06	0.55		0.50	0.22	0.22			
134		0.70	0.20	1.68	21.70		1.84		0.42		0.20	0.52	0.33	0.64	0.87	0.27
135	0.40		0.48	0.45	16.52	0.13		1.06		1.76	0.19	0.17	0.41	1.18		
136	0.41	0.79	0.49	1.07	9.69	0.20	0.79		0.23	7.81	0.07			1.71	0.97	
137				2.95		0.28	0.66	0.87		4.52				0.69	1.59	
138	0.16	0.57			13.35		2.14		0.21	0.74	0.13					
139	0.17	0.32	0.46						0.66	6.61			0.08		0.42	
140	0.51		0.52	1.16	14.23	0.41	1.46			2.41			0.15		0.65	
141						0.44			0.41			0.50		1.88	1.13	
142	0.43		0.43	0.60	3.28				0.09	1.18						0.13
143	0.15	0.73		1.85	11.26	0.53	2.44			1.53		0.40				
144	0.13					0.20		0.96	0.56		0.46	0.09	0.05	2.55		
145		0.77	0.33		15.25	0.19	0.94	1.03		1.09		0.17		0.52	0.99	
146	0.23		0.14	3.55	6.17	0.48				4.71	0.07					0.16
147	0.94		0.31		14.41		0.64			1.54				0.42	0.79	
148		1.30		3.60	16.43			0.88		14.51	0.31		0.18	1.44	1.66	
149				1.09					0.09				0.18	2.64		
150	0.47	0.65	0.16		13.84	0.74			1.36	1.82		0.62				0.90

Table A1 continued.

Spot#	Gd	Tb	Dy	Ho	Er	Tm	Yb	Lu	Hf	Ta	W	Tl	Pb	Th	U
74		0.24			0.72	0.15	0.63	0.11						0.22	1.37
75				0.15		0.29		0.09		0.22			0.57	0.10	
76	0.77			0.25					0.95	0.13		0.14	22.66	0.45	0.09
77	0.50						0.70	0.10				0.44	22.26		0.21
78	0.76	0.06		0.28		0.06	1.07	0.18			0.58		0.37		
79		0.15		0.06	0.57			0.15	0.54		0.45				0.21
80			1.18									0.71			
81				0.15				0.29				1.21	12.05	0.20	
82				0.13					1.97			0.47	3.46		
83		0.48	3.10	0.15	0.34						1.71	0.67	3.84	0.40	
84	1.46		1.23			0.18	1.50	0.18			0.34	0.20		0.14	
85		0.29	0.95	0.23		0.14	0.40		0.40			0.28			0.45
86	1.04	0.09			0.21	0.24				0.07		0.35			0.34
87	1.73	0.17	1.06	0.27			0.87	0.40	0.48		1.81		11.52	0.36	0.29
88		0.08	0.87	0.07			1.94	0.09						0.39	
89		0.40		0.11		0.11				0.36			1.71	0.39	
90	0.54		1.60		0.29				0.87	0.23	1.26	0.21			0.17
93		0.17				0.11	0.67	0.23		0.06	0.61				
94	0.58	0.10						0.06	0.57	0.26		0.79	0.47		0.19
95		0.29	0.68	0.11				0.28			1.37	0.61		0.36	0.88
96	0.61		1.40		0.91	0.33									
97		0.29	0.57		0.20		0.34	0.07		0.05		1.36			
98	1.20				0.67		0.90	0.21					0.56		
99							0.69		0.33	0.34	0.58		0.46	0.15	
100			0.65	0.19			0.29	0.13			0.42		0.29		
101								0.25					0.27		
102		0.27		0.30			2.04						6.57	0.26	0.24
118	3.39				0.96	0.06	0.57	0.30	1.08				89.29		0.25
119		0.42				0.20	1.51	0.06				0.33	20.04	0.34	
120					0.60	0.22	1.06	0.13			0.43		60.66	0.16	0.35
121		0.16				0.19						0.24	12.72	0.33	0.10
122	1.89	0.14	0.90				1.93	0.35					14.73	0.26	0.13
124		0.14	0.48			0.40		0.14			0.62		10.94		
125	0.94		0.55	0.29				0.10	0.55	0.11		0.35	21.74		0.13
126	1.61			0.19				0.23	0.45	0.21			65.26		
127				0.14	0.37		0.39			0.27	1.97		25.97		
128		0.30	0.97		0.59	0.13		0.08			0.50	0.50	2.80		0.19
129	0.85								0.35				14.22	0.21	
130	2.80	0.13			0.32	0.08						0.92	0.52		0.08
131	1.41						1.09				1.73	1.10	1.15	0.42	0.32
132		0.22	1.79	0.21		0.05			0.23	0.11		0.66	20.16		
133		0.44							0.77		0.39		3.71		
134	0.92			0.38	0.29	0.16	0.47		0.78		0.58		4.99	0.14	0.17
135								0.11		0.17			0.98		0.34
136	0.77			0.25		0.08	1.94	0.45					14.50		
137	1.42		1.01	0.16	0.92	0.08							0.44	0.14	0.10
138	0.51	0.14	2.07			0.28		0.30		0.18		1.01	3.10		
139	0.39	0.24		0.25		0.22				0.30			2.19	0.41	
140				0.14				0.43				0.36	4.66		
141					0.33	0.07	1.49		0.24	0.16		1.47	5.02		
142	0.45			0.10	0.26			0.25	0.31			1.09	0.63	0.24	0.64
143		0.35			0.61			0.36	0.35				1.17		
144										0.09	0.73	0.58	0.20	0.09	
145		0.27			0.64	0.06	0.87	0.17					0.97	0.09	
146		0.26		0.36		0.17	0.75	0.17			0.68	0.62	0.33		
147			0.49	0.24			0.34		0.39				0.96		
148				0.11	0.58	0.11					0.31		2.60	0.37	0.22
149		0.11											7.75		0.47
150		0.10		0.09	0.75	0.09	1.91				0.45		11.62		

Table A1 continued.

Location	Analysis	Spot#	Li	Na	Mg	P	Ca
Nine Mile MMSD, Australia	**151 GH7B C3 CrA T1 160m**	**151**			5954	55.77	
	152 GH7B C3 CrA T1 160m	**152**	33.60		6108		
Pulsifer, ME	**43 Hole5 T2 160m**	**43**	61.79		1234	154.84	
	44 Hole5 160m	**44**	49.91	2.23	1141		
	45 Hole5 T2 160m	**45**	39.92		1016	70.07	
	46 Hole5 T2 160m	**46**	32.88		1253		
	47 Hole5 T2 160m	**47**	49.80		1332		
	48 Hole5 T2 160m	**48**	40.34		1219		
	49 Hole5 T2 160m	**49**	53.13	0.72	1163		
	50 Hole5 T2 160m	**50**	54.71	1.50	1277	95.63	
	51 Hole5 T2 160m	**51**	49.98		1197	63.01	871.22
	153 Hole21 P21 160m	**153**	32.82	2.35	918	123.43	
	154 Hole21 P22 160m	**154**	58.23	2.19	1395		
	155 Hole21 P23 160m	**155**	29.88		1449		
	156 Hole21 P24 160m	**156**	54.72		1022		442.99
	157 Hole21 P1 160m	**157**	51.69		1511		340.48
	158 Hole21 160m	**158**	51.76		1290		324.94
	159 Hole21 160m	**159**	40.97	1.22	1190		
	160 Hole21 160m	**160**	34.56		696		441.58
	161 Hole21 160m	**161**	63.13	0.88	1468	293.25	544.26
	162 Hole21 160m	**162**	31.70		1369		608.21
	163 Hole21 160m	**163**	23.68		1206	167.00	403.57
Quintos (BPP), Brazil	**75 Quintos 3 C2 160m**	**75**	92.36		3022		
	76 Quintos 3 C2 160m	**76**	102.90	0.75	3649	55.64	
	77 Quintos 3 C2 160m	**77**	127.97	3.57	4018		621.09
	78 Quintos 3 C2 160m	**78**	113.15		2876		
	79 Quintos 3 C2 160m	**79**	166.18		3354	75.84	635.34
	80 Quintos 3 C2 160m	**80**	77.63		2534		
	81 Quintos 3 C1L1 160m	**81**	128.69	1.21	3151	279.82	
	82 Quintos 3 C1L1 160m	**82**	119.02	0.86	3991		
	83 Quintos 3 C1L1 160m	**83**	151.37	4.49	3856		803.03
	84 Quintos 3 C1L2 160m	**84**	91.05	1.37	3493		
	85 Quintos 3 C1L1 160m	**85**	86.17	0.96	3141		296.21
	86 Quintos 3 C1L1 160m	**86**	75.86	0.70	2979	156.75	324.70
	173 Quintos2B P4 160m	**173**	75.95	0.92	966	189.64	
	174 Quintos2B P5 160m	**174**	87.22		580		
	175 Quintos2B P6 160m	**175**	83.26		622	141.35	
	176 Quintos2B P7 160m	**176**	93.00		707		
	177 Quintos2B P8 160m	**177**	77.56		712		
	178 Quintos2B P9 160m	**178**	77.04		838		
	179 Quintos2B P10 160m	**179**	89.71	2.99	1214		
	180 Quintos2B P11 160m	**180**	98.67	1.12	972		
	181 Quintos2B P13 160m	**181**	80.80		722		
	182 Quintos2B P15 160m	**182**	100.80		1068	287.92	896.04
	183 Quintos2B P16 160m	**183**	77.47		925	53.04	770.43
	184 Quintos2B 2 160m	**184**	84.96		525		957.41
	185 Quintos2B 3 160m	**185**	82.16		612	150.27	
Sin Nombre, Argentina	**122 GH274B Area1 7 160m**	**122**	136.31		812	143.88	375.52
	123 GH274B Area1 8 160m	**123**	50.00	0.82	958		
	124 GH274B Area1 10 160m	**124**	70.61	1.50	631	181.06	298.63
	125 GH274B Area1 11 160m	**125**	45.26	4.26	698	62.68	
	126 GH274B Area1 12 160m	**126**	47.84		714	495.51	
	127 GH274B Area1 160m	**127**	73.69	0.79	861	146.03	
	128 GH274B Area1 160m	**128**	59.57	3.70	1019		
	129 GH274B Area1 160m	**129**	44.73		2608		
	130 GH274B Area1 160m	**130**	122.98	3.50	897		
	131 GH274B Area2 3 160m	**131**	54.82		2564		1086.21
	132 GH274B Area2 6 160m	**132**	39.42	1.00	1483	123.68	
	133 GH274B Area2 160m	**133**	70.81	2.20	1037		

Table A1 continued.

Spot#	Sc	Ti	V	Cr	Mn	Co	Ni	Cu	Ga	Ge	As	Rb	Sr
151		24.89	119.63	3.95	1892	116.16	17.05	21.90	97.8	3.06			
152	2.13	27.24	94.68	5.20	1766	114.63	32.21	13.96	105.8	0.79			
43				1.21	2392	1.00		21.47	519.9		5.08		0.25
44	1.20		4.35		2438	2.54		16.06	533.3				0.40
45				2.01	2276	3.09		8.39	523.2	2.20	5.35		0.29
46		31.94		3.20	2426	2.89		19.46	523.0	0.59	4.66		
47		12.69		1.14	2295	3.06	3.96	16.82	541.8				
48	1.10	9.46			2392	3.08		19.01	540.5	1.01	2.88		
49	1.02				2337	1.82		20.19	540.0	1.79		0.43	0.51
50					2457	3.03		17.27	528.9	0.87	1.44		
51		8.47	2.23		2284	1.31		14.89	538.4			0.65	0.27
153		32.22	3.31		2635	2.57	9.17	19.53	507.3				0.35
154		35.82			2642		2.23	17.77	521.4		3.61	0.54	
155		7.35	2.18	6.72	2903	2.19	3.97	17.58	525.8	0.75			0.44
156				3.98	2908	4.55		20.14	544.3	1.26			0.45
157		13.53			2716	3.25	3.81	15.83	550.0	1.24	9.15		
158	3.38		3.84	1.55	2920	2.96		18.44	537.6		3.76	0.15	
159					2892	1.22	18.70	20.20	533.6				0.87
160		26.20			2433	2.18		19.97	504.9		6.55	0.22	0.46
161		13.52	1.40	1.67	2774	3.90		15.52	524.9	0.61			
162				3.15	2649	6.35		19.98	511.3			0.66	
163				7.72	3072	3.85	9.12	25.97	546.5	0.57		0.32	0.11
75	2.65		7.50		5430	15.85		32.73	350.2			0.22	
76		12.35	9.29	3.23	5888	22.29		34.39	347.3			0.43	0.25
77		50.95	9.88	5.78	5713	20.10	10.07	33.78	345.4	1.32		1.36	0.16
78		34.93	12.84	4.80	4954	17.85		35.07	335.7			0.75	0.20
79			10.02	1.90	5887	16.34		26.37	343.8			0.36	
80	1.80		15.00	2.37	5262	18.41		32.85	321.2				0.29
81	1.12		2.46	5.93	5867	16.92	4.12	31.33	339.6	1.54		0.29	
82	1.10		8.41	3.72	5978	17.72		31.41	343.8				
83			6.92	1.33	6159	18.63		37.48	327.3	1.50	7.77	4.65	0.72
84	2.93		11.85	2.52	6293	18.07		32.60	321.9				
85			11.26	2.12	6078	14.49	9.86	27.36	331.9		2.63		0.34
86		9.76	6.43		5285	15.27		31.93	325.2	3.16			0.44
173	0.81		2.42		4594	5.85		33.98	312.4	1.99			0.24
174	1.12	18.80	4.89	3.30	4939	4.78	2.45	29.56	332.6			0.32	0.36
175	1.43	35.88			4806	5.01		30.38	342.6	4.91	5.22	0.43	0.14
176				2.33	4938	4.31		30.75	343.9	1.71			0.11
177			2.28	6.79	5074	4.42	8.33	27.23	347.8		1.75	0.58	0.61
178				1.77	4662	7.04		32.59	348.3	2.06			
179		16.77		4.36	5040	3.60		29.48	337.9		10.04		
180	1.58	21.76	2.46		5268	5.42		36.70	340.9	0.72			
181	3.59	13.44	3.32	3.80	4866	5.98	11.50	33.48	336.2	0.59			
182			6.11		5091	6.41		29.54	353.8	1.27	6.29	0.38	
183		15.65	3.52		5051	2.71		32.27	332.6	4.37		0.47	
184		27.86	1.85	3.35	4437	5.50	2.33	30.16	318.2			0.32	0.28
185	0.78	23.14		2.89	4911	4.33		37.77	339.5	1.10	5.91		0.46
122		17.52	6.52	1.01	2667	3.63	2.83	37.71	282.3	4.00		6.02	
123	1.89	6.87	3.39	1.18	2871	2.68	8.61	25.01	282.1	1.09			0.14
124	3.56	31.14		1.00	2951	1.46		32.31	291.2	0.81	1.48	2.41	
125		15.47	1.97	1.49	3056	1.40		29.64	271.4	2.98		1.94	0.63
126	1.20	17.60			2940	4.49	9.47	23.73	286.5	0.74	1.55		
127		51.44		1.97	3192	1.94		55.93	293.9		2.96	3.29	0.40
128	1.42		2.20		2983	2.40		37.90	289.6		6.10	2.06	0.34
129		17.09			2305	20.00		33.81	259.2	0.63		5.43	
130			4.13	3.86	3782	6.25	4.02	85.89	302.7			14.06	1.16
131					2836	13.60	3.26	14.56	267.2				
132	0.98			5.26	2860	6.32	8.44	21.59	282.2	2.96	1.79		
133				3.44	2990	3.94	7.88	20.66	290.0	2.33		2.94	0.53

Table A1 continued.

Spot#	Y	Zr	Nb	Mo	Cd	In	Sn	Sb	Cs	Ba	La	Ce	Pr	Nd	Sm	Eu
151	0.21				7.05										0.97	0.48
152		0.41	0.41		13.34		1.48			0.96		0.40	0.32		2.26	
43		0.78			19.20		0.98	0.36			0.12			1.07	0.36	0.10
44	0.14		0.16			0.43						0.13			0.50	0.37
45		0.54		0.70			1.43	1.33		3.05	0.17	0.15	0.24			
46	0.13	0.53	0.24				0.61			1.31						
47				1.30				0.89	0.17	2.20						
48				0.66		0.14	0.33		0.10					1.50		0.52
49		0.56	0.39			0.22				0.99					1.52	
50	0.25			0.72		0.33			0.20							
51		0.41			24.97	0.34	1.12					0.13			1.04	
153		0.51					0.37		0.25	1.13			0.14			0.37
154				2.70	3.66		2.47			1.32			0.24		1.86	
155					20.57	0.12	2.43	1.26	0.57	2.90				1.16		
156		0.61	0.62		10.54	0.15	0.78	0.32				0.15				
157	0.19	1.70		0.58			0.38	1.75			0.07					
158	0.27				9.63	0.19			0.45			0.07				
159		0.74		0.45	8.66				0.10					0.36	1.74	
160	0.24	0.44			3.52	0.18				1.17			0.21			
161		0.34	0.62	1.19	12.79	0.39	0.90					0.11			0.38	0.30
162		0.42		1.03	14.18			0.57	0.25	1.27	0.15	0.22	0.18		1.35	0.43
163	0.21	0.57		0.81	16.10	0.14	1.31		0.26						0.35	0.45
75	0.32		0.31	1.19	11.14		0.83					0.21		0.89		
76				1.77	15.38	0.13			0.67	0.93	0.24					0.42
77	0.52	0.24	5.94		28.16		0.63	1.57	1.29		0.10	0.50				0.11
78	0.10		1.28	1.53	8.57		1.27		0.26		0.36	0.31		0.37		0.27
79	0.21				11.07		0.85	0.59	0.35						0.38	
80	0.57	0.23				0.21		0.58	0.56	1.36				1.05	2.00	
81	0.61		0.25		3.68		1.86		0.69		0.14	0.36		0.91		
82		0.93		0.54	23.83	0.18						0.12	0.05		1.06	
83	0.17		0.87	0.86	13.97			0.70	2.81			0.08		0.44	0.62	0.50
84	0.11		0.18		21.94		1.38	0.74								
85			0.37		16.88							0.10				0.11
86	0.53			1.63	22.68	0.52	0.55							1.90		
173	0.25	0.82		1.82	32.78		0.40	1.99		1.05					0.72	
174	0.39	0.52	0.35	1.69	24.16	0.13	0.72		0.38			0.30		0.62		0.12
175		0.60	0.37				1.00		0.13							0.14
176		0.80		2.09	29.92	0.49			0.36			0.30	0.06		0.37	
177					22.16	0.16	2.59				0.26	0.25		0.58		
178		0.77	0.13		42.09					1.33			0.20			
179			0.83	1.27	41.20		1.02		0.38	2.45		0.07				
180					22.46			0.90	0.15		0.07	0.19		0.34		0.30
181	0.35			1.74	14.61		0.45			1.89				1.05		
182			0.13		28.30											0.34
183		0.36	0.36		22.48	0.42		0.32	0.50	1.36			0.29	0.87		0.27
184	0.17										0.38		0.23	0.74	0.71	0.34
185			0.31		12.56		2.41			0.81	0.10	0.38	0.11	0.57		
122	0.50	3.24			7.72		1.07		0.14	1.87	0.52	0.31		0.98	0.38	
123		2.44			20.61				0.51			0.17	0.15			
124		2.72			10.73	0.23	1.90		0.58	2.04		0.33			0.58	
125	0.14	2.69			7.08				0.29	2.17	0.08	0.10				
126		0.81		0.62	17.67		1.23	0.44	0.38		0.34					
127		4.23		0.64	4.80	0.82	2.68			1.28		0.45	0.48	0.98		0.17
128		3.69	0.87		13.17			0.86	0.25		0.36	0.35	0.31	1.83		0.20
129						0.56			0.46		0.39					0.40
130	0.51	8.14	1.13	0.86		2.22			0.57	31.53		1.26	0.16	1.12	1.31	
131					11.09		0.91		0.40							
132		0.73	0.21	2.17	15.84			0.85			0.28	0.12		0.86	0.93	
133	0.19	0.23	0.47		15.22		1.06		0.24	7.74	0.30					0.53

Table A1 continued.

Spot#	Gd	Tb	Dy	Ho	Er	Tm	Yb	Lu	Hf	Ta	W	Tl	Pb	Th	U
151	2.10				1.03			0.08	0.59				0.77		
152		0.34		0.06	0.55		1.38		0.47		0.39	1.02	2.84		
43				0.16							0.35				0.29
44	0.75													0.09	0.30
45	0.97		0.93	0.16	0.39	0.05		0.30		0.07					
46	1.44		0.86		0.39					0.27	0.35	0.42		0.48	
47						0.13			0.31				0.27		
48	0.66		1.03			0.26		0.08		0.19				0.43	0.19
49		0.14	1.28		0.75		0.51	0.08						0.09	
50	0.95	0.08	0.33		0.18			0.22				0.47	0.45		0.10
51	1.20	0.16		0.20	0.28				0.49			0.26	0.39		
153	0.81			0.20	0.28	0.22				0.14	0.91			0.11	
154			0.96									0.40	1.02		0.28
155		0.14			0.24	0.08								0.11	
156	2.21			0.19			1.18		0.99						
157	0.81	0.17		0.13		0.15					0.99		0.20		0.21
158		0.08	0.77					0.21						0.21	
159			0.71		0.63	0.15				0.21	0.72	0.23		0.83	
160							0.57						0.68	0.33	
161		0.17		0.15	0.16	0.11	0.74		0.68		0.68	0.22		0.12	
162			0.75	0.13	0.38		1.21					0.20	0.20	0.09	
163	1.01				0.17	0.16						0.25	0.44	0.10	
75		0.22												0.34	0.09
76					0.65			0.17		0.07			0.52	0.15	
77	0.84				0.34	0.10	0.70		0.34	0.60		0.64		0.10	55.52
78		0.20				0.12	1.56			0.31	1.23	0.19	0.67	0.38	9.17
79	0.79	0.05	1.67	0.16	1.22					0.10				0.17	1.28
80	1.73								0.32	0.27				0.16	0.79
81	2.50				0.18	0.11				0.17		0.24		0.14	
82		0.13		0.06			0.69	0.19	0.25	0.26		0.36	2.44		
83		0.16					1.42			0.25	0.27		1.13		1.13
84	0.35	0.15		0.23			1.43	0.06	0.42			0.28			
85						0.13	1.21		0.21				0.36		
86		0.20	0.59				1.51					0.21	0.73		0.19
173						0.11		0.15		0.16	1.69			0.37	
174								0.09			0.29			0.11	
175		0.16			1.02					0.14	0.49		0.45		0.18
176			0.47		0.94	0.09	1.03			0.15		0.48	1.42		
177	1.58	0.14			0.52	0.06	1.33	0.07		0.19		1.21			0.66
178		0.26			0.81					0.08		0.37	1.11	0.10	0.49
179		0.26				0.23	1.17		0.17		0.36	0.42			
180				0.15		0.18							0.36	0.70	
181		0.10		0.05			2.02		0.21		1.45			0.21	
182				0.16	0.61							0.16	0.77		
183	0.52			0.19		0.07	0.66						0.19		
184	1.09	0.17				0.13		0.30	0.20				0.30		
185	0.70					0.15		0.13		0.09	0.46	0.19			
122	3.54		1.90	0.15	0.91	0.14	0.41		0.54		1.92	0.51	11.96		0.24
123						0.07				0.14	0.36		1.83	0.18	
124				0.08					0.14				2.19		
125						0.14			0.98	0.08	0.47	0.41	2.31		0.15
126		0.11	0.95			0.15	1.76			0.10			0.84		0.23
127		0.20				0.09			0.76				4.74		0.39
128	0.66		1.71	0.11		0.11							2.95		0.44
129	3.85		1.67		0.17		4.20	0.35	2.20			0.88	2.26		1.03
130						0.28		0.14	0.20	0.35	2.85				0.40
131							0.95				1.23	0.15			
132			1.52		0.82	0.10					0.45		0.18		0.28
133			0.30	0.13		0.11	1.24						0.76		0.10

Table A1 continued.

Location	Analysis	Spot#	Li	Na	Mg	P	Ca
Sin Nombre, Argentina	**134 GH274B Area2 160m**	**134**	91.31	1.33	697	144.76	
	135 GH274B Area2 160m	**135**	68.47	2.61	1025	153.02	
	136 GH274B Area2 160m	**136**	54.71	1.20	2669		
	137 GH274A L1 1 160m	**137**	81.97	2.24	833	294.16	312.60
	138 GH274A L1 3 160m	**138**	79.63		990		628.79
	139 GH274A L1 5 160m	**139**	70.72		784	144.84	
	140 GH274A L1 160m	**140**	78.42		633	72.01	
	141 GH274A L1 10 160m	**141**	48.47		890		
	142 GH274A L1 13 160m	**142**	85.68	1.78	923	56.18	894.82
	143 GH274A L1 16 160m	**143**	65.48		696		365.91
	144 GH274A L1 18 160m	**144**	80.04	0.71	819	122.40	
	145 GH274A L1 21 160m	**145**	79.74		1125		
	146 GH274A L1 22 160m	**146**	59.77	0.87	785		
	147 GH274A L1 24 160m	**147**	29.28	1.35	818	231.74	387.65
	148 GH274A L1 27 160m	**148**	67.64		463	168.10	
	149 GH274A L1 29 160m	**149**	70.23		713	64.83	
	150 GH274A L1 31 160m	**150**	44.38	3.20	697	104.51	
	151 GH274A L1 33 160m	**151**	76.15		766	199.83	729.61
	152 GH274A L1 35 160m	**152**	108.07	4.57	1091	89.54	
	153 GH274A L1 37 160m	**153**	56.12	3.35	880		
	154 GH274A L1 160m	**154**	53.39		757		
	155 GH274A L1 42 160m	**155**	85.62	0.70	857		351.00
	156 GH274A L1 44 160m	**156**	49.40		818		475.54
	157 GH274A L1 47 160m	**157**	81.94		713		1072.92
	158 GH274A L1 160m	**158**	48.47	0.91	1304	285.94	931.19
Spruce Pine, NC	**19 18270 T3 160m**	**19**			1597	184.74	
	20 18270 T3 160m	**20**			1721		
	21 18270 T3 160m	**21**	13.95		1739		630.36
	22 18270 T3 160m	**22**			1832	65.34	
	23 18270 T3 160m	**23**	21.00		1787		
	24 18270 T3 160m	**24**	32.17		493		
	25 18270 T3 8 160m	**25**	32.00	0.77	437		717.70
	26 18270 T3 10 160m	**26**	18.54		566	60.52	
	27 18270 T3 12 160m	**27**	20.46		573		
	28 18270 T3 14 160m	**28**	18.95		660	65.62	
	29 18270 T3 160m	**29**	7.55		664		324.54
	30 18270 T3 160m	**30**	11.05		816	212.45	
	31 18270 T3 160m	**31**	6.67	0.95	585	126.57	
	32 18270 T3 21 160m	**32**	9.72		516		
	33 18270 P4 160m	**33**			1746		462.67
	34 18270 P5 160m	**34**		2.45	1723		
	35 18270 P6 160m	**35**			1851		
	36 18270 P10 160m	**36**	16.43		1856	86.75	
	37 18270 P11 160m	**37**			1684		
Siedlimowice, Poland	**41 Sied3 A1 CrA 160m**	**41**	66.18	1.17	543	195.08	
	42 Sied3 A1 CrA 160m	**42**	68.39		365		
	43 Sied3 A1 CrA 160m	**43**	77.72		737	153.91	
	44 Sied3 A1 CrA 160m	**44**	63.22		490		
	45 Sied3 A1 CrA 160m	**45**	45.25	2.89	633		
	46 Sied3 A1 CrB 160m	**46**	57.78		643		
	47 Sied3 A1 CrC 160m	**47**	87.97		566		554.68
	48 Sied3 A1 CrC 160m	**48**	72.98		604	96.94	
	49 Sied3 A1 CrC 160m	**49**	33.48	1.08	623		
	50 Sied3 A1 CrC 160m	**50**	42.21		1144		
	51 Sied3 A1 CrC 160m	**51**	46.69		760		429.54
	52 Sied3 A1 CrD 160m	**52**	58.43	2.89	471		
	53 Sied3 A1 CrD 160m	**53**	73.17	1.54	589	89.80	
	54 Sied3 B2 CrA 160m	**54**	80.51	0.83	337		
	55 Sied3 B2 CrA 160m	**55**	70.29	0.79	409	106.35	393.86

Table A1 continued.

Spot#	Sc	Ti	V	Cr	Mn	Co	Ni	Cu	Ga	Ge	As	Rb	Sr
134	1.45	20.42			3037	1.12		14.97	290.3		3.09	2.09	
135	2.51	11.76		5.25	3093	3.55	7.82	29.04	294.5			0.70	0.37
136	3.89	48.09		1.28	2563	21.43		16.32	289.0			0.41	0.54
137	0.96	17.89	2.78	1.44	2851	2.30		22.41	292.3			1.25	0.22
138	0.83			5.38	3125	2.04		16.40	261.7			0.14	0.37
139			2.19	2.51	3139	0.45		17.06	279.1		1.59		0.39
140		8.20		1.10	3013	0.73	2.51	12.34	279.0	2.05			
141	1.76	36.36			2940	2.57		17.41	292.1	4.75		0.71	0.56
142		6.91	1.72		3103	2.41	3.95	18.22	288.7	1.01			
143			2.42		3041	0.58	7.62	21.82	276.7	4.94			0.38
144			2.51	1.65	3045	2.61		17.88	269.3			0.55	
145				3.66	3060	2.43		21.63	297.3	2.81			0.19
146	5.17		2.51		3068	1.51		19.37	284.6	0.62			
147			1.57		3113	3.37	8.65	18.32	271.9				
148			1.63		3266	1.73	2.12	21.08	279.9	0.65			0.28
149		25.29		2.85	3118	2.83	5.84	18.72	279.1	0.92		1.12	
150			2.11		3238	2.26		21.31	296.0				
151	1.84	10.99		5.12	3206	1.13		26.96	298.2				
152				1.85	3004	3.77		20.10	295.5	0.97		1.24	
153		17.94	3.88	3.04	3193	2.17	2.68	23.32	289.3	1.48	1.95		
154	1.55	14.45	3.08	1.04	3119	2.73		21.55	290.2	1.28			0.28
155		7.82		1.72	3184			21.37	283.7			0.47	
156		10.33		1.51	3119	0.89		22.00	284.0	1.58			
157		45.25			3254	4.05		20.91	289.7				
158		26.82		8.61	1716	2.14	2.10	22.63	276.0	2.90		17.03	
19			24.76	3.79	1614	7.77		24.76	183.0	2.33	8.05		
20		18.62	23.38	5.36	1346	8.76	9.78	21.17	184.5			0.58	0.28
21	1.96	6.55	27.11	1.64	1638	9.79	5.86	21.38	185.6			0.67	0.51
22	4.04		31.03	4.05	1517	8.21		16.38	202.9			0.69	
23		16.72	23.06	5.31	1550	6.57		22.66	190.6	3.82		0.18	0.28
24	1.29	10.76	7.07	4.86	3506	3.25	4.72	17.18	310.2	1.93			0.25
25			1.77		4024		2.48	21.49	321.5		4.73		
26			3.56	2.25	4027	1.27		23.33	317.1				0.50
27			1.87		3780	4.61	2.57	22.63	302.9				
28			3.35	2.63	3683			20.18	287.9	2.00	1.39		0.40
29	1.07		2.93		3760	1.20		21.35	281.1				
30		25.39	5.34	6.03	3846	3.76		19.45	294.9	1.67	7.33	0.43	
31		17.80	6.95	5.43	3658		7.24	16.93	279.9				
32			5.13		3781	2.39		21.66	286.1				
33		9.34	24.52	2.82	1493	7.98	10.94	18.99	199.9	0.96			
34			28.05	4.67	1683	6.00		23.82	180.2	1.13	3.52		0.21
35	2.13	15.38	23.84	1.56	1580	7.55		17.16	180.6				
36			20.06	4.78	1478	6.72		15.87	193.2			0.20	
37			16.14	1.95	1300	3.21	6.98	19.56	176.5	2.37			0.38
41			2.59	3.09	2565	4.72	2.53	18.37	467.7			0.46	0.35
42		13.02		2.90	2805	4.73	3.64	21.23	493.5		4.43		0.22
43		13.33		1.69	2652	2.40		15.04	482.6	2.40		0.67	
44				3.04	2563	4.12		14.45	501.1		4.58		
45			1.43	4.31	2428	3.72	4.93	19.26	473.4	1.33	3.92		0.27
46		22.39	1.95	2.78	2212	3.00		17.77	462.8	1.30	1.68	0.53	
47	2.63	16.42	5.25	1.78	2405	5.03	2.99	22.55	489.0				
48	1.40				2861	0.70		12.76	494.8	0.70	5.90		
49		27.79			2292	3.96	4.16	17.16	488.8	0.80	5.07		
50			1.59	2.42	1909	3.17	5.91	22.01	385.0	2.76			
51		35.33		5.95	2250	1.19		17.16	374.8				0.66
52				3.31	2891	3.67		17.37	498.2		2.08		0.30
53				3.63	2924	3.50	4.48	17.98	532.6	3.08			0.53
54		11.65			2040	4.47		22.68	338.3				
55	2.18	33.73		2.76	2260	1.80		20.77	345.5				0.38

Table A1 continued.

Spot#	Y	Zr	Nb	Mo	Cd	In	Sn	Sb	Cs	Ba	La	Ce	Pr	Nd	Sm	Eu
134		1.26			18.77			1.31	0.17				0.09		0.40	
135	0.20	1.95	0.29		21.77	0.19	0.48					0.31				
136		0.62			13.83	0.19	1.12		0.32			0.07	0.17	0.65	0.42	0.42
137					18.17	0.60		0.55	0.27						1.12	
138	0.22		0.70	1.11	7.06		0.34	1.54				0.22		1.61	0.54	
139					10.70		1.15	0.71	0.24			0.12	0.05	0.41	0.46	0.29
140				1.43	19.39				0.35			0.22				
141	0.15	0.46	0.42	0.66	18.59	0.12				1.23	0.58	0.14	0.11			
142			0.31		16.27			1.04		2.81	0.08		0.06		0.85	0.22
143		0.50		1.28	13.40	0.39		0.91		1.63	0.13		0.13	0.58		0.30
144			0.17	0.84	12.94	0.28	0.58	1.16	0.14		0.21	0.15		0.39	1.78	
145								0.36	1.48			0.24	0.07	1.10		
146				0.47			1.41	1.10		1.39	0.16		0.09			
147	0.40		0.22	0.43	17.03			0.98						1.23	0.65	
148					4.60	0.10	1.18	0.99			0.10		0.33		0.52	0.31
149		1.07	0.76	0.43			0.79	1.41	0.34				0.31		1.48	
150	0.18	0.27	0.28	0.44	11.03				0.18		0.41			1.54		
151	0.28			0.93	14.40		1.45				0.18			0.34	0.62	
152	0.73	1.16	0.39		12.24		0.99	0.70					0.06	1.18		
153		0.62		0.75					0.18				0.07			
154			0.20		13.79	0.37		1.53	0.36			0.28			1.64	
155	0.39		0.26		15.08	0.23	1.02			0.81	0.53		0.25	0.99	0.36	0.28
156				2.13			0.34	1.10			0.10	0.32			1.19	
157		0.42	3.11						0.23				0.07			0.15
158	0.61	9.41			3.66							0.59			1.71	
19			0.41			0.34	1.57		0.31	0.97					0.72	
20			0.30	1.06			1.67			0.60	0.15				0.46	
21		0.92			8.09		1.67					0.24		0.56		0.26
22	0.11	0.22			11.02	0.35	1.10	0.78	0.15				0.18	0.63	1.23	
23			0.16		9.11		0.82		0.11	0.61	0.15					
24					12.07	0.42	1.45	0.94	0.60				0.08	0.62		
25	0.28			0.89	13.95		1.36					0.21		1.14		
26	0.21				15.03								0.36	0.32		
27		0.29	0.12		9.59					1.03			0.22	0.87	0.45	
28					28.63	0.30	0.60								0.51	
29			0.19		12.89	0.11	1.51	0.32	0.49	1.59		0.51				
30					21.11						0.16	0.18			0.37	0.22
31			0.22		16.74							0.09	0.18			
32			0.28	0.91			0.99	1.80	0.33					0.72		
33					18.53	0.19	1.90	0.36						1.56		
34		0.86	0.14	1.27	8.44			0.48	0.18		0.07		0.15		1.52	
35			0.18	0.62	7.10	0.40	1.50				0.25					
36	0.35	0.23			18.81		1.29									0.13
37			0.61		24.73	0.19	1.35	1.11	0.29			0.09	0.23	1.92	0.78	
41		0.48	0.11		9.64		0.48				0.11	0.30			2.14	
42					12.27		0.34	0.85		0.90	0.11	0.18	0.12	0.77		0.39
43	0.41			0.72			0.94			2.37				1.07		
44					14.82		1.60					0.17			0.64	0.12
45		0.71	0.14		16.75				0.27			0.30	0.18			
46	1.12	22.20			8.25		0.91		0.37	1.77	0.25	0.11				
47				1.61		0.65				1.66	0.07					0.10
48		0.47		1.15		0.34				0.59	0.23		0.12		0.37	0.33
49		0.51	0.33	1.90	13.91	0.26	1.00	0.37					0.10			
50		0.47		1.21	11.27	0.70	1.60			0.86		0.12	0.08		1.12	
51	0.18	0.58			14.08		1.31	0.42								0.25
52					19.44		1.95			1.05	0.08	0.25	0.11			
53	0.49	0.22	0.38		24.27	0.45							0.27			
54			0.46			0.24			0.26	1.00		0.10		2.53	3.67	
55	0.28			2.23	10.64	0.52	1.39								1.25	

Table A1 continued.

Spot#	Gd	Tb	Dy	Ho	Er	Tm	Yb	Lu	Hf	Ta	W	Tl	Pb	Th	U
134		0.19	0.46				1.35		0.60			0.17	0.98		0.28
135	0.96	0.11	0.60				0.55	0.14		0.08			2.48		0.25
136		0.10	1.01			0.26			0.37		1.06	0.27	0.57		0.49
137		0.23	0.52	0.25	0.36	0.14		0.22	0.71		0.63	0.32	0.57		
138			1.92	0.24			0.96		0.76						0.29
139			0.37		0.43					0.32	0.53	0.19			
140		0.06		0.08				0.13	0.42	0.16			0.42	0.10	
141		0.11		0.15	0.18		0.32						0.34	0.23	0.10
142		0.18	0.31	0.11	0.61			0.09					3.40	0.32	
143		0.27	0.56			0.10	2.23		0.20	0.08			1.00		
144								0.11		0.08	0.34			0.28	0.40
145	0.89		1.60			0.32					0.39	0.64			0.13
146		0.15	0.66	0.26	0.31		0.60		0.86		1.63	0.49	0.30	0.47	
147			0.30			0.06	0.45	0.10				0.40	0.23		0.24
148			1.86			0.08		0.09	1.14	0.16	1.30	0.43			
149			1.05	0.14							0.91				0.25
150	0.42	0.23	1.35	0.07				0.08					0.75		0.18
151	0.94		1.25				0.52		0.61	0.14	0.52		0.22	0.18	
152				0.24			1.71				1.34	0.26	1.37		
153		0.26	0.70			0.07				0.19	0.45	0.33		0.34	0.16
154	0.93	0.08					1.72			0.13		0.38	0.83		0.38
155	1.39			0.10	0.96					0.07		0.36	0.33		0.24
156			1.08				1.51		0.38				0.55		0.12
157	0.81		1.84				0.85	0.05		0.14		0.33		0.59	
158						0.41	1.08			0.07	0.83	0.25	1.16		0.45
19	0.63					0.06		0.08	1.12	0.10	0.45	0.21	1.07		0.14
20		0.11	0.39	0.11			0.90	0.10	0.45		0.46			0.15	0.20
21	0.63	0.21		0.08			1.07	0.20				0.43	1.42	0.11	
22											0.44	0.19	0.77	0.28	0.14
23	0.76			0.15				0.09		0.19			0.93	0.12	0.21
24					0.65	0.13	1.32	0.19	0.24				0.48		0.20
25				0.17				0.11	0.23				0.54	0.36	
26			0.92		0.50					0.07	0.85				0.15
27	0.50			0.23		0.19	0.37					0.39	0.38		0.19
28		0.12		0.10	0.40	0.08		0.06		0.14	1.05	0.18			
29						0.09			0.58	0.08		0.16	0.47	0.16	
30		0.13				0.26		0.11				0.27			
31		0.15								0.23	0.33				
32		0.15	0.46					0.22				0.63	0.47		
33	0.65				0.84	0.20		0.13		0.16				0.13	0.20
34		0.18	0.78			0.09						0.65	0.66	0.15	
35					0.21		1.35	0.05	0.50	0.06					0.14
36	0.88		0.72	0.08								0.45	0.43	0.29	0.41
37		0.22	1.08						0.28			0.16		0.19	
41					0.54		0.67	0.20	0.33	0.20				0.28	
42			1.44		0.28	0.14		0.18		0.09					
43		0.18		0.43		0.22				0.19	0.46	0.44			0.12
44	1.16	0.05	0.73			0.39			0.34				0.73		0.29
45	0.65	0.11	0.89	0.19	0.38			0.06		0.26			0.38	0.16	
46			1.07	0.37		0.09	0.99		2.50	0.22			1.11	0.22	1.32
47	1.46			0.48		0.17		0.34		0.16	0.28	0.45	0.38	0.27	
48										0.11	0.45			0.15	
49	0.87	0.37	0.64	0.14		0.17		0.08	0.54						0.13
50			0.33			0.22	0.40			0.28	1.37		0.36		0.23
51		0.12		0.13	0.26			0.07							0.50
52				0.24	0.25		0.35	0.10		0.10	1.05		0.47		
53		0.16	1.49				0.47		0.43	0.13	0.47	0.97		0.14	0.36
54				0.50		0.28				0.20	0.44	0.55	1.08	0.52	
55	0.37	0.07	0.87				0.94	0.13		0.22					

Table A1 continued.

Location	Analysis	Spot#	Li	Na	Mg	P	Ca
Siedlimowice, Poland	**56 Sied3 B2 CrB 160m**	**56**	51.36		589		602.66
	57 Sied3 B2 CrB 160m	**57**	47.08	0.78	477		
	58 Sied3 B2 CrB 160m	**58**	62.15		505	125.19	
	59 Sied3 B2 CrB 160m	**59**	55.92		553		
	103 SIED1 C2 T1 CrA 160m	**103**	24.78	4.75	672		
	104 SIED1 C2 T1 CrA 160m	**104**	16.58	0.67	682		766.09
	105 SIED1 C2 T1 CrA 160m	**105**	18.35		596		895.83
	106 SIED1 C2 T1 CrA 160m	**106**	36.03	4.18	832		557.38
	107 SIED1 C2 T1 CrA 160m	**107**	61.94	2.30	782		
	108 SIED1 C2 T2 CrB 110m	**108**	49.80		528		1179.53
	109 SIED1 C2 T2 CrB 110m	**109**	52.20		503		1332.67
	110 SIED1 C2 T2 CrB 110m	**110**	21.14		296		563.72
	111 SIED1 C3 2 160m	**111**	59.90	1.18	614		485.00
	112 SIED1 C3 3 160m	**112**	62.29	2.46	638	93.40	
	113 SIED1 C3 4 160m	**113**	59.92	4.28	714		
	114 SIED1 C3 5 160m	**114**	41.50		604		
	115 SIED1 C3 6 160m	**115**	17.32		694		415.91
	116 SIED1 C3 160m	**116**	20.70		486		
	117 SIED1 C2 CrC 4 160m	**117**	29.70		395		311.80
	118 SIED1 C2 CrC 160m	**118**	38.44		685		
	119 SIED1 C2 CrC 160m	**119**	24.82		759		298.86
	120 SIED1 C2 CrC 160m	**120**	35.29	1.42	814	115.00	
	121 SIED1 C2 CrC 160m	**121**	26.96	1.86	795		636.53
	143 Sied2 B2 CrA 110m	**143**	10.29		639		
	144 Sied2 B2 CrA 110m	**144**	66.24	3.97	609	219.75	
	145 Sied2 B2 CrA 110m	**145**	31.80		878	247.27	698.97
	146 Sied2 B2 CrA 110m	**146**	11.61		593		
	147 Sied2 B2 CrA 110m	**147**	35.60	10.30	603	461.35	
	148 Sied2 B2 CrB 110m	**148**	69.86		541		750.10
	149 Sied2 B2 CrB 110m	**149**			908	211.11	
Tourmaline King Mine, CA	**75 126115 C1 T2 160m**	**75**	59.75	0.88	101	203.24	
	76 126115 C1 160m	**76**	37.17			211.30	
	77 126115 C1 T2 160m	**77**	58.02	1.14	128	408.00	
	78 126115 C1 160m	**78**	33.12		46	102.00	
	79 126115 C1 T2 160	**79**	74.33			116.58	
	80 126115 C2 T2 160	**80**	48.29				
	81 126115 C2 T2 160	**81**	53.72		79		
	82 126115 C2 T2 160	**82**	58.89	1.20		149.42	
	83 126115 C2 160m	**83**	79.56	1.34			
	84 126115 C2 160m	**84**	92.51			168.42	
Detection limits		**D.L.**	4.78	0.64	27	51.89	285.61

Table A1 continued.

Spot#	Sc	Ti	V	Cr	Mn	Co	Ni	Cu	Ga	Ge	As	Rb	Sr
56		10.97		2.54	2893	4.72		21.67	489.4		1.81		
57			1.99	3.52	2890	3.31	4.23	18.08	492.5				
58			2.01	7.86	2934	4.32		22.36	486.9	3.67	6.08		
59				4.94	2763	3.47	7.28	15.21	472.6	0.56	5.14	0.91	
103				4.04	2051	4.43	5.32	17.95	450.5	0.86	5.92	0.21	
104	1.58	16.77		1.50	2213	1.02		20.78	437.6				
105		17.53		1.30	2403	5.36		19.02	436.8			2.34	
106		62.38	1.55	1.10	2443	4.70		16.46	450.1	2.96	4.18	3.11	0.62
107		42.27	1.46	3.69	1918	1.86	5.39	18.37	448.2			32.11	0.39
108	2.03				2406	2.60		22.48	487.4			0.30	0.94
109		35.81			1994	5.95		18.64	456.7			0.52	0.84
110	4.68	17.50			2151		8.03	20.96	450.4				0.26
111		29.33		4.60	1963	3.85		20.26	485.1	3.43	5.41		
112		14.04			2430	3.83		19.89	495.0	4.89	6.80		
113		17.28			2376	6.16	6.37	16.89	474.5	1.58	1.76	0.49	
114	3.34		3.02	4.82	2034	3.17		20.94	473.2			6.61	
115				2.69	2331	5.24		15.89	459.9	0.94			0.14
116	2.33			4.26	2217	3.61		18.80	469.0				0.12
117	2.77				2278	5.54		17.85	464.4		7.58		
118		33.92		3.88	2107	4.29	5.15	20.81	476.8				0.23
119	3.15		4.20	1.42	2657			17.95	437.7		2.37		
120		15.67	1.80	1.87	2176	5.65	6.59	21.37	483.1		4.62	0.23	0.50
121		16.14	3.97	2.96	1965	3.56	3.55	21.46	431.9	1.14	4.82	0.25	
143		18.56	4.85		1847	4.95		17.58	424.6			0.66	
144		20.83		7.56	2254	6.31		18.64	423.1			0.67	0.19
145	3.03	44.21		2.46	2024	1.03		15.34	372.7				
146		10.99		5.70	1898	2.32	3.47	15.54	384.5	4.89	4.38		
147				9.48	1867	7.73		15.18	384.4	3.43	7.63		0.48
148		40.41	3.78		1969			16.53	423.8		13.15	1.27	
149				2.76	2021	4.96	3.35	18.94	382.2				
75			2.36		4197			23.53	330.9	5.18		0.82	
76				2.10	5423		5.37	21.51	373.4	3.36	13.06	3.02	
77			6.05		5339			24.19	370.6	1.20		2.61	
78	2.11	16.11	3.69	2.40	3869			23.98	332.7	1.97		0.72	
79	4.53		4.92	1.37	3780	0.58	9.43	19.84	333.5	3.01		0.57	
80	2.18	9.93	5.32		4573	1.30	5.14	19.34	317.2	3.09		0.62	0.65
81	2.09			6.44	4883		1.77	22.21	323.0	2.57			
82	4.11		7.67		5536	1.91		18.49	356.1			0.64	
83	1.46		2.58	3.03	5926	0.50	3.57	25.89	364.1	2.06			
84		6.47	5.19		5794		5.17	26.84	342.3	4.23		1.20	
D.L.	0.78	5.72	1.40	0.95	11	0.40	1.73	0.70	0.5	0.54	1.35	0.14	0.11

Table A1 continued.

Spot#	Y	Zr	Nb	Mo	Cd	In	Sn	Sb	Cs	Ba	La	Ce	Pr	Nd	Sm	Eu
56						0.17	1.56	0.65				0.21		1.01	0.53	0.17
57	0.19				7.82	0.49			0.39							
58				1.17				0.65	0.23						0.53	0.16
59	0.35	0.46	0.32	1.56		0.12	1.91	1.55			0.12	0.15				
103		0.32					0.75		0.36		0.14	0.07				
104		0.65	0.19		3.73		0.99	1.37	0.42			0.11	0.07	0.60		
105	0.27	0.47			18.80				0.78			0.31		1.58		0.30
106	0.60	3.18	0.68	1.22	20.64	0.23	1.83		0.97			0.22				
107	0.49	6.79	0.28	1.66	19.84	0.13	1.64		5.29	0.84	0.09				0.51	
108	0.50				11.75		1.08	1.34			0.14				0.96	
109	0.14		0.42		29.32	0.64									1.90	0.15
110				0.75	30.32		1.44	3.10								0.17
111					18.03					2.66			0.17	0.53		
112		1.51					0.97	1.55	0.71	0.52	0.19					0.25
113		2.55	0.24	1.04	33.27	0.15				1.35	0.12				1.41	0.34
114	0.18	2.82					2.25	0.75	1.76	1.49			0.27	1.00		
115	0.19	0.50	0.31	0.55	10.70		1.45	0.81		0.72	0.08	0.15	0.11			
116	0.33		0.15		10.72		1.20		0.17			0.21		0.66		0.15
117	0.92		0.20		11.24		1.96			0.66		0.18		1.09		0.13
118	0.10	8.77	1.10		14.70			3.01	0.22				0.11			
119	0.55	1.74	0.30			0.20							0.12		0.63	
120	0.50	0.89	0.29	2.78	13.34	0.17	2.29						0.18		0.81	
121	0.22	0.72	0.73		9.81		2.11	0.45	0.72		0.10	0.07				
143	0.37	1.08		0.86										0.79	0.93	
144	0.59	8.19							0.32	2.13		0.15	0.44	1.90		
145	0.67	7.18				0.50		1.40	0.67							0.29
146				1.37	7.12	0.55	2.79					0.43	0.22			0.20
147			0.38				2.39	0.78	0.54			0.55		1.85	0.83	
148		0.88		2.32	14.91		2.24		2.02			0.23	0.20		1.56	
149	0.43		0.21	1.28								0.23			2.24	
75	0.34		0.44		8.90	0.12	3.00	3.60	0.85	0.66	0.07		0.10	0.78	0.94	
76					12.19		0.98		2.82		0.07		0.10			
77		1.34				0.84	1.77	1.93	4.21							0.13
78	0.48		0.55		15.76			0.99	1.27	1.66	0.15	0.07	0.30			
79		0.33	0.46	1.10		0.17		3.49	0.53		0.17		0.16	1.00		
80		0.28		0.62		0.27	1.86				0.18	0.27		1.09	1.13	0.11
81		0.56			5.67		1.18	0.39	0.64						1.07	
82		0.26	0.30	2.71	24.68		2.28	4.07	0.43		0.07	0.29				
83		1.48	0.41		10.68				0.18							0.13
84	0.14	0.90				0.25	1.03	1.02	1.39		0.21			0.32		
D.L.	0.10	0.21	0.11	0.39	2.88	0.09	0.33	0.32	0.08	0.51	0.06	0.06	0.05	0.29	0.34	0.10

Table A1 continued.

Spot#	Gd	Tb	Dy	Ho	Er	Tm	Yb	Lu	Hf	Ta	W	Tl	Pb	Th	U
56	2.47	0.10			0.78			0.31				0.14		0.47	0.14
57	0.64				0.32		0.94	0.09					0.76		
58	0.36		0.47				1.39		0.30	0.13					
59			0.33	0.07		0.37		0.19		0.30		0.44		0.14	0.38
103		0.16		0.09			0.52	0.13		0.14		0.34	0.80	0.12	0.51
104		0.18	1.80	0.07		0.07					1.05			0.23	
105		0.14	0.55	0.30		0.10		0.11		0.06	0.95	0.36			
106			0.40		0.33				1.31	0.13			2.67	0.14	0.69
107			1.00			0.28		0.18	0.74	0.56	0.64	0.18	0.36	0.41	0.60
108	1.27	0.35	0.87		1.41	0.11	1.52		0.84	0.27			0.54	0.39	
109	1.91				0.32		1.14			0.13		0.72	0.85	0.53	
110	1.62	0.27	0.73		0.29	0.15	1.28			0.21	0.88	0.39			
111		0.17	0.91	0.07		0.07				0.08			0.22	0.29	
112			0.58	0.24	0.56			0.25				0.31	0.94		
113		0.11		0.34	0.57			0.13	0.13			0.19	0.71		0.31
114	0.45		0.60		0.60				0.17	0.21	0.44				0.20
115			0.68	0.27	0.50			0.06		0.17					
116	0.99	0.10	1.24	0.09	0.18			0.07					0.18		0.19
117					0.62	0.08	0.88		0.13		1.58				0.36
118	0.97					0.16	0.93	0.06	0.50	0.18					0.40
119	0.58				0.35				0.24	0.27			0.34		
120	0.57			0.11	0.20		0.29				1.84				
121		0.21		0.27	0.21	0.14				0.39			0.68	0.49	0.11
143		0.10	1.01		0.99				0.26		0.70		0.64		
144		0.33							2.83	0.99				0.67	0.48
145		0.16						0.17	1.95	0.40	1.04				
146				0.36	0.44	0.21	0.82		0.39				0.52		0.58
147	0.67	0.16		0.13				0.14				0.50	0.77	0.37	
148										0.43	0.37				
149	0.78	0.17						0.16							
75	0.43		0.78	0.12		0.10				0.08	0.43		0.82	0.42	0.16
76				0.11		0.23		0.08	0.16	0.15	1.70	0.62	0.67		
77	0.57					0.33				0.08		0.40			0.38
78		0.12	0.46	0.18				0.26					0.59		0.25
79			1.74			0.09	0.84						0.97		
80	1.27	0.23	1.59	0.05		0.32	1.28				0.33				
81		0.10		0.06			0.82		0.32		0.43				
82							0.38	0.18			0.39		4.98	0.64	
83	0.77	0.11							0.29	0.12	1.28		0.57		0.46
84		0.05					0.45		0.68		0.97		0.83		0.19
D.L.	0.35	0.05	0.28	0.05	0.16	0.05	0.28	0.05	0.13	0.05	0.25	0.13	0.18	0.09	0.07

Empty cell means value below detection limits (D.L.).
Sample analysis nomenclature as follows: Analysis "55 Sied3 B2 CrA 160m" refers to spot analysis #55, sample Sied3, area B2, CrA is crystal A, 160m means laser beam size. In some samples the third name component refers to T1 for transect 1, C1 for circle 1, and P1 for point 1.